Causes of recruitment limitation at abrupt alpine treelines

Fabian Döweler

A thesis submitted to

Auckland University of Technology

In fulfilment of the requirements for the degree of

Doctor of Philosophy (PhD)

October 2020

Supervisor: Dr Bradley Case

Second Supervisor: Assoc. Prof. Hannah Buckley

Third Supervisor: Dr Martin Bader

School of Science

Abstract

At the abrupt ecotone between the upper limit of southern beech forests in New Zealand and adjacent subalpine vegetation, ecological processes such as competition/facilitation, and species' tolerances to alpine conditions, maintain a dynamic balance between these two contrasting plant communities. While other treeline ecotones globally have responded to ongoing climatic changes there is little evidence that the position and form of the beech-subalpine ecotone has undergone similar changes over the past decades. Further, it is unknown when the beech forest-subalpine ecotone will respond to such changes in the future. Critical to predicting change is understanding the abiotic and biotic factors that limit recruitment of individual trees above the treeline. To address this, this thesis research aimed to further elucidate the role of subalpine microhabitat variability in controlling forest regeneration patterns in abrupt treeline ecotones.

As a basis to investigate the drivers of treeline recruitment patterns at the Craigieburn treeline site in New Zealand's Southern Alps, a detailed field data collection and spatial mapping campaign was undertaken to comprehensively characterise abiotic and biotic variation across this alpine treeline ecotone. This was achieved by deploying UAV operated high resolution sensors (RGB, Multispectral, LiDAR, Thermal) to spatially map and characterise the vegetation, thermal environment and topography at one treeline site. Results enabled a detailed illustration of the alpine treeline ecotone and how microhabitat heterogeneity influenced the thermal environment within the site. Further, high-resolution LiDAR point cloud data enabled the approximation of plant-height and creation of ancillary datasets such as solar radiation maps to estimate shadowing effects of individual trees. The result was a comprehensive characterisation of the alpine treeline ecotone, illustrating fine-scale information for vegetation, topography, incident radiation and thermal variability.

The environmental datasets were supplemented with three decades of seedling data from monitoring transects established by Peter Wardle in the 1990s. Modelling was used to evaluate the effects of microhabitat heterogeneity on tree seedling establishment and performance above the treeline. *Fuscospora cliffortioides* recruitment was enhanced in microhabitats which reduced exposure to macroscale-imposed limitations common at treeline (e.g. annual frost events). Successive tree colonialization of the subalpine was adversely affected by competition

with alpine vegetation and the paucity of microhabitat safe sites which limit treeline response to broad scale climate warming.

Diurnal, non-invasive chlorophyll-*a*-fluorescence measurements on exposed and canopy-sheltered seedlings at two sites in New Zealand's Southern Alps during summer and winter show no effect of an instantaneous or sustained photosystem degradation. Results reveal a remarkable level of light adaptation and contradict previous studies hinting at high light-induced photoinhibition as treeline-limiting factor. By linking low ΦPSII on winter mornings, and large, sudden temperature drops in summer, we speculate that cold-induced photoinhibition might result in lethal photo-oxidative damage. Duration and frequency of these events could diminish with global warming, which may promote treeline advance.

An agent-based model was designed to simulate emergent treeline patterns along a hypothetical mountain slope induced by a macroscale temperature gradient, intraspecific competition and facilitative thermal microclimates. Findings highlighted the sensitivity of the system to cold temperature dips and the mechanisms which enabled seedlings to escape bottleneck stressors by close associations with subalpine vegetation. When any adverse effects of a close spatial association among neighbouring plants are absent, treeline position is stabilized by increased density, but higher altitudes are only reached once avoidance of pronounced stressors is achieved.

This thesis further elucidates the complex link between biotic and abiotic limitations exposed on different temporal and spatial scales to operate as a sharpening agent in abrupt treeline phenomena.

Table of Contents

List of Figures

List of Tables

Attestation of Authorship

I hereby declare that this submission is my own work and that, to the best of my knowledge and belief, it contains no material previously published or written by another person, except where explicitly defined, nor material which to a substantial extent has been submitted for the award of any degree or diploma of a university or other institution of higher learning.

Fabian Döweler

Co-Authored Works

Chapter 4 Fabian Döweler, Bradley S. Case, Hannah L. Buckley, Martin K.-F. Bader High light-induced photoinhibition is not limiting seedling establishment at abrupt treeline ecotones in New Zealand (Submitted to Tree Physiology)	Döweler, F Bader, M Case, B Buckley, H	80 % 10 % 5 % 5 %
Contribution: FD, BC, HB and MB conceived the ideas and designed methodology; FD collected the data; FD and MB analysed the data; FD led the writing of the manuscript. All authors contributed critically to the drafts and gave final approval for publication.		
Chapter 5 Fabian Döweler, Volker Grimm, Hannah L. Buckley, Bradley S. Case Exploring the interplay of macro- and micro-scale drivers controlling treeline formation: An agent-based model (Submitted to Ecological Modelling)	Döweler, F Case, B Grimm, V Buckley, H	85 % 5 % 5 % 5 %
Contribution: FD, BC and HB conceived the ideas and designed methodology; FD designed the model; VG checked model design and revised ODD model description. FD analysed the data; FD led the writing of the manuscript. All authors contributed critically to the drafts and gave final approval for publication.		

Bradley Case	Hannah Buckley	Martin Bader	Volker Grimm

Acknowledgements

Thank you to my supervisors Brad, Hannah and Martin. Thank you, Brad, for believing in me and giving me the opportunity to work in some of the most beautiful places this world has to offer. Thank you, Hannah, for your guidance and insightful comments throughout this journey. Thank you, Martin, for your support when I needed it the most. Thank you for being such a wonderful teacher and friend - to me that made all the difference. Thank you, Graham, you made me grow confidence in my skills and did support me more than I could ever have hoped for. Thank you, Volker, for your thoughtful inputs and for being so patient und understanding with me. Thank you to all the helpers along the way, most of whom have become good friends.

Thank you, Petra, for your unconditional support for yet another crazy idea of mine. Seeing me travel further and further away from home must be hard, but I want you to know that I am living my best life, and this would have not been possible without you. Thank you to my family, you literally travelled to the other end of the world for me. I will always keep you close to my heart.

Thank you to the friendships who have stood the test of time and distance. Your words of encouragement and relentless support reach far beyond the scope of this project. Let's catch up soon.

Thank you to my flatmates, spending time with you was always something to look forward to after a long day in the office.

Thank you to all the great teachers and advisors on my way, giving me another way to look at this world. Thank you to the people who taught me to be kinder to myself and provided me the courage to face the things I am afraid of.

I would like to thank my students for these many hours we learned from each other. Being a teacher started as a necessity and turned out to be one of the most rewarding experiences of my life. Your kind words and continuous support kept me going through the most strenuous chapters of this journey. I will always go the extra mile for you.

1 General Introduction

1.1 Global treeline drivers

Ecotones are sensitive indicators of environmental change (Wasson et al., 2013) and understanding the processes currently maintaining ecosystem boundaries enables us to predict how the communities in the ecotone will respond to climatic change (Holtmeier, 2009). The formation of an alpine treeline is a global phenomenon where high biomass ecosystems give way to low stature grasses and herbaceous species within the subalpine belt. The high-elevation distribution limit of trees on a global scale can be sufficiently explained by a mean isotherm of growing season days (Körner & Paulsen, 2004). Current treeline position is a product of macroscale climatic variations controlling thermal fluctuations, rainfall patterns, incident solar radiation and the extent of the growing season (Körner, 2012). These broad scale climatic limitations gradually restrict the tree in stature and numbers until conditions become ultimately life restricting. However, if we begin to increase the resolution the task to characterise treeline position becomes far less trivial as fine scale abiotic and biotic variability is revealed.

With an enhanced resolution we begin to identify the sensitivity of the life-form tree to respond to microscale climatic variability. Individual tree position is a result of tree tolerance to biological meaningful temperature and climatic extremes (e.g. frost, intense radiation, moisture deficit). The sensitivity of the individual to critical climatic thresholds overrides the effect of macroscale-imposed limitations (Scherrer & Körner, 2010). Consequently, within this fine-scale variation we find valuable information in how to predict future ecotone shifts Global treeline position shows a heterogenous response to macroscale climatic change and some regions show a significant temporal delay in their response to prolonged growing seasons (Malanson et al., 2011). By analysing the spatial patterns in the way the tree life form approaches its altitudinal limits, we can begin to decipher the dynamics that control alpine ecotone migration (Harsch & Bader, 2011). These patterns also reflect valuable information on how the ecotone border responds to macroscale climatic changes (e.g. global warming).

1.2 Treeline patterns and responses to climatic change

In principle we distinguish between diffuse and abrupt treeline patterns, where sub-forms such as tree islands and krummholz are derivatives of these main patterns (Harsch & Bader, 2011). Diffuse treeline patterns can be observed around the globe where predominantly conifers define

the elevational boundary of forest ecosystems (Holtmeier, 2009). In the transition zone from a closed forest stand into a low stature subalpine ecosystem the life form tree gradually decreases in stature and abundance while approaching its altitudinal limits. Diffuse treeline forms are generated by a slow decrease in growing season days with altitude which gradually decreases tree proliferation and hence stature (Körner, 2012). Diffuse treeline patterns align well with the concept of a mean growing season isotherm and their response to climatic change is demonstrated by a homogenous upslope encroachment. Abrupt treeline patterns can be identified by a much more distinct, sharper transition from a high-stature forest into the herbaceous subalpine belt. Abrupt treeline ecotones are created by fine-scale ecological processes which maintain a dynamic balance between these two contrasting plant communities (Malanson et al., 2011). Local microhabitat associations override the effect of regional scale limitations dictated by mean growing days isotherm (Scherrer & Körner, 2010). The forest ecosystem facilitates the recruitment of new seedlings within established boundaries and the gradually pronounced limitation of a temperature isotherm is outside these boundaries. This leads to an enhanced tree mortality and a reinforced ecotone boundary (Wilson & Agnew, 1992). The current treeline position is therefore 'hard-wired' by beneficial feedback loops within the established ecosystem. The stronger the effect of internal climate modifications within the vegetation layer, the more independently they can operate from macroclimatic conditions (Malanson et al., 2011). Therefore, many abrupt treeline systems do not respond readily to macroscale climatic change, resulting in a temporal delay in upslope encroachment of the forest system (Harsch & Bader, 2011). However, quantifying the pace of ecosystem migration is crucial to formulate conservation efforts in the forest and subalpine vegetation communities (Ellison et al., 2005; Gunderson et al., 2012).

1.3 Mechanisms controlling abrupt treelines

In abrupt treeline ecotones, an advance of the upper forest boundary is hampered by a restricted seedling performance in the adjacent shrubland (Harsch et al., 2009). The seedling recruitment bottleneck is a result of enhanced macroscale-imposed limitations (e.g. extreme temperatures, high radiation) outside the established forest canopy (Malanson et al., 2011). The seedling can escape this limitation through close association with subalpine plants, effectively reducing stressor effects. These microclimatic 'safe sites' ideally mimic the climatic conditions under canopy. While with increasing altitude the relevance of facilitative biotic interactions increases

(Callaway, 2007), the effect is not always one-directional and beneficial (Brice et al., 2019). Tree interactions with existing vegetation can be of facilitative or adverse nature and are described as feedback switches (Wilson & Agnew, 1992). The magnitude and effect of these microhabitat responses differs between species (Loranger et al., 2017) and can be further modulated by the individual's size (Malanson & Resler, 2016) as they emerge from the internal vegetation layer (Körner, 2016). To address the complexity of microhabitat feedbacks within treeline ecotones Harsch & Bader (2011) introduced a concept of mechanistic drivers that operate across nested levels. Here macroscale-imposed limitations operate as a top-down mechanism and constrain tree performance (e.g. growth, dieback, seedling mortality) with altitude. This effect is further modulated by a species-specific response to stress mechanisms (e.g. freezing damage, desiccation, radiation) and neighbouring effects (e.g. shading, competition). These bottom-up operating mechanisms further modulate seedling mortality and therefore have the potential to locally override macroscale-imposed limitations (Harsch & Bader, 2011).

Abrupt treeline regeneration is controlled by the abundance and quality of favourable microhabitats in the subalpine. They limit the response to macroscale climatic change and serve as 'stepping-stones' for treeline advance. Once early recruits are successfully established they promote further tree recruitment and growth (Alftine & Malanson, 2004). When a clear directional facilitative feedback is established, a 'tipping point' is reached and successive tree colonialization of the subalpine is facilitated. Monitoring realised climatic niches for early recruits and their performance in subalpine microhabitats is essential to address the temporal delay in abrupt treeline ecotones. Hereby we should make use of existing records of patterns and habitat preferences (Graham et al., 2006). This process should involve a complete characterisation of potential drivers and include factors which are currently identified as weak, but could pose persistent restrictions when formulating long term trajectories (Parmesan & Yohe, 2003).

1.4 Southern Beech in New Zealand

The southern beeches (*Nothofagaceae*) belong to the order Fagales and are characterized by woody shrubs and trees with alternate, stipulate leaves, small unisexual flowers and a fruit which is a nut enclosed in an often-hardened cupule. The distribution of the southern beeches ranges from 2° south of the equator to 55° of latitude. They are entirely restricted to the

Southern Hemisphere. They occur in New Guinea, New Caledonia, South-Eastern Australia, New Zealand and in Chile. They share a set of certain ecological tolerances, able to cope well with harsh conditions and, they tend to become dominant on altitudinal gradients, forming extensive and relatively uniform forests. In most lowlands they are outcompeted by different hardwoods and softwoods and their performance at seedling stage is relatively poor (van Steenis, 1971; Wardle, 1984). The most distinctive feature of New Zealand's *Nothofagaceae* which sets them apart from relatives in the Andes is that they are evergreen. The morphology of the leaves are the main diagnostic tool for taxonomic separations and follow a guideline introduced by Allan (Allan, 1961). New Zealand's abrupt treelines are formed by two out five representatives of the genus. *Lophozonia menziesii* (silver beech, Hook.f.) and *Fuscospora cliffortioides* (mountain beech, Hook.f.) form the upper forest limits.

Fuscospora cliffortioides is the smallest representative of the genus within New Zealand. This species averages 15-20 m in height and grow on relatively fertile soils, and are less tolerant to infertile and poorly drained soils than *Lophozonia menziesii* (Smale et al., 2012). In exposed single stands they spread out crowns early and stay comparably small, where within established forest stands they show straight cylindrical trunks which are clear of branching halfway up (Wardle, 1984). Similar to silver beech, they limit their growth towards subalpine timberline. Commonly, representatives of the species can be found in the upper forest edge, reducing their growth to no more than 45 cm (J. Wardle, 1974). Snow drifts and avalanches can make them grow horizontally for several metres and establishment on ridges and spurs as well as poorly drained and infertile soils will significantly limit their growth. Along with their treeline forming conspecific, they can tolerate heavy frosts up to -13°C, which sets them apart from other representatives of the species (Smale et al., 2012)

Fuscospora cliffortioides leaves (Figure 1) are small and leathery and up to 15 mm long, pale underneath and have incurved margins. Occasionally they show light pubescent on top and with distichous branchlets. The young leaves are a bit lighter in colour and show a more ovate appearance (Allan, 1961). The bark is fibrous and fissured appearing almost black and are about 10 – 20 mm thick. Younger trees show smoother bark with a light-grey to grey colour and the branchlets show fine pubescence (Wardle, 1984).

Figure 1: Mountain beech in the subalpine belt, Mt Faust, Canterbury (Döweler, 2019)

Mountain beech vegetation ranges from 38° to 46° South latitude (Figure 2). Presence is mostly limited to montane and subalpine zones but can show up on poorly drained and infertile soils in the lowlands. It constitutes the common subalpine timberline tree in the eastern and central regions of both islands. It forms extensive single species stands in the drier east of the Southern Alps and co-dominates with silver beech towards the more humid western areas (Wardle, 1984). Mountain beech is more dominant in drier areas and shallower soils. On maritime influenced mountain ranges they reach from 900 to 1400 m, but they are able to exceed 1500 m in more continental summer warm slopes regardless of aspect and more likely to achieve these heights on steep and convex slopes with little shading (Wardle, 2008).

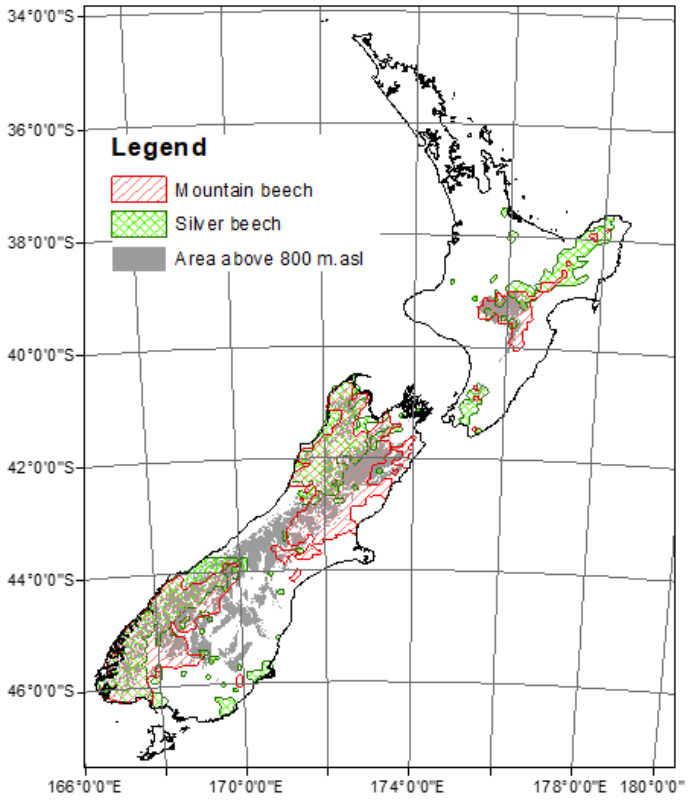

Figure 2: Distribution of mountain and silver beech across New Zealand (Bradley Case, 2017)

1.5 Drivers of treeline ecology in New Zealand

New Zealand's upper forest belt with its two dominant *Nothofagaceae* species shows characteristics which sets them apart from most other tree line forming species globally, but also from other representatives of the southern beech. The tree line formed by mountain and silver beech is remarkably abrupt (Figure 3), suggesting that the treeline is dominated by second and third level mechanisms (Harsch & Bader, 2011). Peter Wardle, a life-long treeline researcher attributed this in his last publications to a low solar radiation tolerance of young individuals, summer frost and competitions for nutrients (Wardle, 2008).

Figure 3: Abrupt treeline ecotone at the Craigieburn Valley, Canterbury (Döweler, ca. 6 am January 23rd, 2018, 43°07'31.8"S 171°42'15.2"E)

The driving forces target the more vulnerable seedling stages, where high levels of solar radiation, frequent summer frosts and competition in the adjacent tussock grassland become ultimately life restricting (Norton & Schönenberger, 1984; Wardle, 1971). This is further supported by the existence of the southern beech gap, located in central Westland of the South Island between approximately 42° to 44° latitude. The gap was created after a glacier formed in the colder Pleistocene retreated leaving wide denuded areas behind. Until today, the capability of *Nothofagaceae* to recruit beyond previously established forests was too limited to reoccupy the area (Leathwick, 1998; Mcglone et al., 2002). This raises questions of what drivers cause this regeneration bottleneck, restricting southern beech species from extending beyond their current range limits boundaries. Modelling approaches of the influence of abiotic factors on treeline position suggest that regional scale thermal influences can account for 82 % of the variation, reducing to 44 - 52 % of variation explained by a combination of thermal, physiological stress/related and disturbance related factors operating at finer scales (Case & Duncan, 2014).

1.5.1 Seeds and young seedling limitations

Facilitative microhabitat interactions at New Zealand's treeline ecotone are believed to be most relevant during early recruitment stages. If seedlings make it through their first two years, the risk of dieback decreases significantly (Wardle, 1985a). Annual seed production in New Zealand beeches averages about 1000-2000 nuts per square meter depending on local conditions and species, but can vary on a single site between 1 to 13,000 nuts per square meter (Wardle, 1984). Lack of successful seedling production can be correlated with strong frost in November just after the first flower openings or likely be influenced by heavy rain restricting the pollen dispersal (J. Wardle, 1970). The frequency of mast years for *Nothofagaceae* is 4 to 6 years and associated with above average seedling productions and event frequency is going to further increase with climate warming (Richardson et al., 2005). Dispersal is limited to 10 m beyond existing treeline (Harsch et al., 2012) and roughly a third of the seeds fall behind the forest edge (Wardle, 1984). The amount and quality of fertile seeds decrease towards higher altitudes and successful germination of seedlings have been verified for an altitude of up to 1600 m (Wardle, 1971). Even if good tree growth occurs in the area, the recruitment of young seedlings has been repeatedly reported as the bottleneck of tree line advance in the *Nothofagaceae* (Cuevas, 2000; Holtmeier, 2009; Wardle & Coleman, 1992). The decreased survivability in the very early stages of growth can be projected to most treeline forming taxa of the temperate zone of the Southern Hemisphere, which appear to operate closer to physiological limits than their northern hemisphere relatives (Körner, 2012). Reasons for seedling and early recruits limitations at treeline are often attributed to root zone competition (Holtmeier, 2009), cold temperatures and photoinhibition (Bader et al., 2007; Germino & Smith, 1999). This has been reproduced in New Zealand, where seedling germination can be adversely affected by > 27 % daylight (Wardle, 1971) and seedlings show a preference for bare, sheltered soils (Harsch, 2010). Translocation experiments with shading boxes enabled successful seedling establishment beyond current treeline position (Wardle, 1985a).

1.5.2 Temperature

New Zealand's treeline received special attention in a comparative study of treeline temperatures published by Körner & Paulsen (2004). In their global projections, the treeline position fell 200 m below their predicted values and there was no evidence that this was related to limited dispersal rates (Cullen et al., 2001). Further, global comparisons revealed the treeline

position remains relatively unresponsive to climatic change (Harsch et al., 2012). Since 1950, mountain and silver beech upper forest edges responded to a 1°C warming with less than a 10 m upslope movement (Mullan et al., 2008; Wardle & Coleman, 1992). In contrast, root zone temperature readings reveal that the current treeline position is indeed where it would be expected (Cieraad et al., 2014). In order to shed further light on the issue, treeline research is required to monitor changes with greater spatial resolution and temporal replication. One way to achieve this is to use meso-climate data derived from meteorological stations and scale them to the microclimate level (Cory & Smith, 2017) or measure temperatures with higher replication and accuracy (Körner & Hiltbrunner, 2017).

Alpine trees are most susceptible to cold damage in their acclimatization processes (dormant stages) from warm to cold temperatures and back (Sakai & Wardle, 1978; Sakai & Weiser, 1973). Newly formed leaves and flowers of European broad-leaved trees for instance can be damaged over night by temperatures as low as 1 – 3 °C already (Körner, 2012; Till, 1956). A strong susceptibility to extremely low temperatures during bud break is one of the primary dieback factors for broadleaved trees at high altitudes globally (Körner, 2012). Yet predictions for treeline advance have been primarily based on long term average means derived from weather stations (Körner, 2014). Particularly the broad-leafed and evergreen nature of New Zealand's *Nothofagaceae* led me to believe that susceptibility to frost during specific phenological stages is of higher relevance. This is further supported by comparative studies with related *Nothofagaceae* in the Andes (Wardle, 1998). Here *Nothofagus dombeyi* and *Nothofagus nitida* revealed a strong frost susceptibility during the seedlings stage (Wardle, 2008) and are particularly vulnerable in spring and summer (Reyes-Díaz et al., 2005). To escape potentially lethal frost events during early phenological stages, seedlings may occupy thermal shelter in established forest stands under canopy. This protective microhabitat shields the vulnerable recruits from extreme temperature deviations before they develop their initial frost-hardiness (Wardle, 2008). Seedling regeneration in the subalpine may therefore be limited by the availability of favorable microhabitats which mimic the benefits associated with an established forest stand. A strong association with local vegetation can provide seedlings shelter in early life stages, enabling them to escape even the worst climate warming scenarios predicted for the next century (Graham et al., 2012; Scherrer & Körner, 2010). The effect of microhabitat temperature on seedling germination has been tested in New Zealand in a prior study (Harsch, 2010) and the removal of vegetation from *Fuscospora cliffortioides* has negatively impacted seedling survivability in the subalpine. To further disentangle the role of

microhabitat variability in controlling macroscale-imposed limitations we are required to identify if a potential frost-controlled recruitment bottleneck is further modulated by other stressors.

1.5.3 Solar radiation induced photo-oxidative stress

Solar radiation levels increase exponentially with increasing elevation while water vapor levels decrease, so if there is existing susceptibility to high radiation loads the effects are amplified while the species approaches its altitudinal limits (Holtmeier, 2009). The effect of intense radiation levels controlling seedling germination, and hence sharpening the ecotone border, is often not readily identified. In fact, high light limitations at treeline are difficult to disentangle from indirect effects on the thermal environment. For instance, a closed canopy stand may indirectly restrict a temperature increase for the root zone area. This effect in turn provides sufficient explanatory value to attribute this limitation to again temperature related modifications (Körner & Hoch, 2006).

Photo-oxidative stress occurs when photosynthetically active plant tissue is exposed to high levels of solar radiation and the amount of energy absorbed exceeds the demands for electron transport and carbon fixation. Possible results are pigment bleaching, lipid peroxidation, protein oxidation or oxidative damage to nucleic acids (Wieser & Tausz, 2007). Alpine studies on *Abies lasiocarpa* and *Picea engelmanii* seedlings concluded that carbon acquisition was negatively correlated with clear sky days limiting their photosynthetic performance (Johnson et al., 2004). The sensitivity of high-altitude vegetation to high radiation loads has also been verified in the tropics, where in Northern Ecuador an abrupt treeline is reinforced by the inability of a range of tree forming genera to grow in artificially cleared sites (Bader, Geloof, et al., 2007). The effect is believed to have sharpened the abrupt ecotone transition into the subalpine *paramó*; however, anthropogenic and natural disturbances cannot be fully excluded (Bader, Geloof, et al., 2007). While the particular strength of this mechanism remains elusive, increased photodamage in the field is often linked to excess amounts of radiation amplified by other related stress factors (e.g. drought, extreme temperatures; III Adams et al., 1995). This is supported by multiple treeline studies in the Southern Hemisphere, providing evidence that the effect of photoinhibition is more pronounced when coupled with cold temperatures (Ball et al., 1991; Germino & Smith, 1999; Reyes-Díaz et al., 2005; Wardle, 1965; Wieser & Tausz, 2007). The detailed effects of photo-oxidative stress at the cellular

level, how it is mediated by the violaxanthin cycle, and how we can visualize the effects via chlorophyll fluorescence measurements are further discussed in Appendix C.

In New Zealand, the solar radiation tolerance of treeline forming *Nothofagaceae* has been discussed for a long time (Wardle, 1965) and has been particularly relevant for identifying reasons behind the inability of *Nothofagaceae* to reinvade previously established sites after the glacial period (Wardle, 1974). This hypothesis became further supported by seedling relocation experiments (Wardle, 1985a), suggesting that seedlings are capable of recruiting beyond established treeline canopy if sufficiently shaded. However, it remains to be clarified if the shading boxes used in this experiment also modulated the thermal microhabitat variability for the early recruits.

1.5.4 Peter Wardle's treeline transects

Since tree growth at high altitude is slow due to limited meristematic growth (Körner, 2012), most seedling studies at treeline lack the temporal replication to document a recruitment bottleneck mechanism (Harsch et al., 2012). In 1991 Peter Wardle established a baseline study for a permanent treeline monitoring project in New Zealand's Southern Alps. The transects span across the main divide of the mountain range, covering a range of different climatic zones. Thanks to Wardle's foresight, and the continuing contribution of colleagues, the sites have been re-measured periodically. The most recent outcome was a paper by Harsch (Harsch et al., 2012; Wardle & Coleman, 1992). Today, the study provides us invaluable information about seedling presence and performance above treeline, documenting recruitment success and growth parameters. Within the scope of this thesis, three transects have been re-measured, enabling me to look back on a record of three decades of treeline census data (Table 1). A careful implementation of this dataset into its subalpine microhabitat context can help me to shed additional light behind the drivers of limited seedling success in New Zealand's treeline ecotones.

Table 1: Treeline census periods and locations in the Southern Alps of New Zealand

Person	Measurement period	Haast	Faust	Craigieburn	Maori Saddle	Takahe
Wardle	1991	X	X	X	X	X
Wardle & Wilmhurst	2002	X	X	X	X	X
Harsch	2007	X	X	X	X	X
Döweler	2018 - 2019	X	X	X		

1.6 Research gaps in in New Zealand's abrupt treelines

Studying ecotone migration patterns in abrupt treeline phenomena faces two tremendous challenges: Research needs to address the significant temporal delay in ecotone responses to macroscale climatic change while simultaneously approximating a recruitment bottleneck effect which is 'hidden' in fine-scale seedling-microhabitat interactions. Sites unaffected by anthropogenic change are often in remote and inaccessible terrain, making it difficult to conduct labour-intensive field surveys with high spatial resolution and temporal replication to track changes in alpine plant associations. While available monitoring-plots do inherit valuable long-term census data and growth information at treeline, they lack the connection to species interactions in the subalpine. The recruitment bottleneck identified in New Zealand's *Nothofagaceae* is likely to be stimulated by intense radiation at treeline as suggested by Wardle's relocation experiments. However, we still don't know if radiation limits can be linked to long-term sustained degradation of the photosystem during periods of intense sunlight or are suddenly triggered by a temperature modulated photosystem performance (e.g. cold-induced photoinhibition).

New methodologies must be developed to address the need for a fine-scale and spatially explicit characterisation of the alpine treeline ecotone. Consequently, we will be able to quantify microhabitat heterogeneity and delineate environmental parameters most important to stimulate seedling colonialization of the subalpine. An essential step will be the implementation of long-term treeline transect information into these datasets. This will enable us to study decades of seedling regeneration patterns and approximate potential recruitment bottlenecks in abrupt treeline phenomena. In ecological modelling approaches we will then be able to isolate

these mechanisms and further investigate individual tree performance in the face of broad microclimatic stressor gradients.

1.7 Aims, research questions and objectives

The aim of this thesis is to develop a better understanding of the role of subalpine microhabitat variability in controlling upper forest limits in abrupt treeline position and identify environmental variables limiting *Nothofagaceae* regeneration in New Zealand. I have approached this by answering the following research questions via addressing their stated objectives:

(1) What microhabitat conditions modulate macroscale-imposed limitations on tree recruitment and growth above the alpine treeline?

Objective 1: To test the use of UAV-collected data to establish new workflows for monitoring microhabitat variation at treeline.

Objective 2: To determine whether seedling recruitment and growth at treeline is affected by microhabitat variation in temperature, solar radiation, slope and surrounding vegetation cover.

Objective 3: To determine how the photosynthesis of seedlings above treeline is affected by daily and seasonal variation in light conditions.

(2) What are the critical population dynamics processes that interact with temperature to cause tree spatial pattern at treeline?

Objective 1: To test how variation in neighbourhood plant interactions modify the thermal environment causing treeline formation.

Objective 2: To determine how increasing the overall site temperature alters the neighbourhood plant interactions, which in turn, cause variation in tree population spatial pattern.

The thesis is structured in the following way:

Chapter Two provides a novel workflow to monitor alpine treeline ecotones via a range of UAV operated sensors and link the dataset to an existing *Nothofagaceae* treeline census dataset. RGB and multispectral sensors were used to spatially map and identify treeline edge

and vegetation composition within the subalpine zone. LiDAR point clouds were then used to illustrate the topography and vegetation height at site. Subsequently elevation information was used to calculate a detailed solar radiation profile of the treeline ecotone. Thermal sensors monitored temperature fluctuations between morning and noon to estimate the effect of ground cover on modulating the thermal profile in the ecotone. These datasets were linked to individual seedling information extrapolated from the treeline census to put seedling performance into a spatially explicit context.

The third chapter aimed to identify seedling recruitment preferences in the subalpine and delineate environmental parameters most important to control seedling performance. The study built upon the microhabitat characterisation and seedling mapping results from the previous chapter. Thermal microhabitat loggers are used to predict a more accurate range of temperature profiles experienced on the microhabitat scale. Seedling position and performance was evaluated based on microhabitat heterogeneity in the subalpine.

In Chapter Four, a field study is described, which further investigates the role of high radiation loads in controlling New Zealand's current treeline position. Chlorophyll fluorescence measurements for summer and winter were performed to assess photosynthetic performance of early recruits within the subalpine. This non-invasive approach monitored fluorescence, leaf temperature and light environment simultaneously to assess if restricted seedling performance could be linked to sustained and/or temperature controlled photoinhibition.

For the fifth chapter, I generated a treeline ecotone along a hypothetical mountain slope using an agent-based modelling software. The model is designed to improve our understanding of how current treeline position is linked to macroscale temperature environments (top-down), further modulated by an elevational gradient, tree size and microhabitat feedback (bottom-up) for the individual tree. The model uses data from alpine weather stations and models tree response against a varying range of adverse (resource competition) and facilitative (thermal shelter) microhabitat feedbacks.

Chapter Six synthesises the results from this thesis and formulates a general conclusion and future perspectives for alpine treeline research.

2 UAV data collection methods for characterising a treeline ecotone environment

2.1 Introduction

Ecotones are transitional zones between adjacent plant communities reflecting gradual or abrupt shifts in environmental conditions and ecological processes (Gosz, 1993). Ecotones therefore provide ideal testing grounds to study responses to climate change because the occurring plant populations are operating close to their physiological limits (Wasson et al., 2013). Such populations are particularly sensitive to changes in macroscale abiotic drivers affecting growing season extent and temperature variability. An ecosystem ability to cope with sustained unfavourable climatic conditions by migration is a key features in ecosystem resilience (Gunderson et al., 2012). Thus, the characterisation of these ecotone environments and the identification of key drivers are paramount to predicting future effects of climatic change (Elliott, 2012).

Alpine treeline ecosystems (ATEs) constitute 'leading edge' tree populations in an environment where the tree life form approaches climatic stress and tolerance limits (Holtmeier, 2009). Within the alpine treeline ecotone we find species which share common traits and respond to the same fundamental climatic control and yet display fine scale variability in their response to large scale climatic patterns (Weiss, 2009). Forest ecosystem migration at treeline is coupled to early recruiter performance in the subalpine (Malanson et al., 2011). This effect is particularly pronounced in abrupt treeline phenomena, where a hampered seedling survival sharpens the ecotone transition (Harsch & Bader, 2011). Environmental variables hypothesized to govern subalpine vegetation are regionally imposed temperature limits (Scherrer & Körner, 2011) and solar radiation (Holtmeier, 2009) further modulated by local topography (e.g. aspect, slope), vegetation stature and seasonal effects controlling the extent and quality of the growing season (Körner, 2012). Therefore, understanding the role of microhabitat variability in controlling seedling regeneration in the subalpine is essential to estimate future ecotone transitions.

Current fine-scale mapping approaches of the alpine treeline ecotone are limited by the accessibility of the terrain, which has led to opportunistic data collection in the past (e.g. shallow terraces; Weiss & Walsh, 2009). Further, infrequent field studies offer a reduced perspective on the significant spatial and temporal variation in these environments (Lu & He,

2017). Remote-sensing satellite imagery has been used to address these limitations by delivering readily available, cost-efficient and repeated data with a contiguous and extensive spatial coverage (Duro et al., 2007). Space-born remote imagery sensors such as Landsat or MODIS are a widely used tool to delineate ecosystem boundaries (Lu & He, 2017) and have found frequent application for remote sensing operations in alpine treeline ecotones (J. Chen et al., 2016; Y. Chen et al., 2015; Ørka et al., 2012; Šašak et al., 2019; Weiss, 2009; Weiss & Walsh, 2009). Remotely derived multispectral imageries have been used to assess ground cover vegetation (J. Chen et al., 2016) and the high temporal value in satellite derived data can be used to map vegetation changes over decades (Y. Chen et al., 2015). Datasets consisting of multiple spectral layers can be supplemented with digital elevation models (DEM) generated by light detection and ranging (LiDAR) sensors to facilitate orthorectification, visualisation and spatial analysis (Weiss & Walsh, 2009). The combination of these sensors facilitate regional treeline monitoring procedures and enable us to quantify ecosystem migration with reduced field work components (Ørka et al., 2012). Particularly airborne LiDAR data minimizes occlusion effects typically associated with ground-based approaches (Cawood et al., 2017; Gallay et al., 2013). Further, high-resolution LiDAR information can be used to derive ancillary datasets and calculate plant height information for penetrable vegetation via the pulse difference method (Rees, 2007) or calculate the effects of topography on vegetation in controlling the solar regime in alpine environments (Weiss & Walsh, 2009).

While satellite derived information has been widely used to monitor macroscale changes at ATEs, the limited resolution of the sensors (> 1 m, Table 2) fails to address fine-scale variation in these transition zones. As a result, ground-based surveys are still required to monitor species regeneration, growth and mortality dynamics at treeline (Ørka et al., 2012). Further, available material often shows temporal distortion and high-quality data is expensive to retrieve (Candiago et al., 2015). New approaches in monitoring treeline ecotones are therefore required to fill the gap between labour intensive ground-based studies (Rhodes et al., 2015) and coarse resolution satellite imagery (Chen et al., 2016).

Over recent years, literature on unmanned aerial vehicles (UAV) has been rapidly expanding (Anderson & Gaston, 2013) and UAV-collected imagery provides a readily repeated and cost-effective solution for collecting high-resolution datasets (Candiago et al., 2015; Table 2). Consequently, the UAV data collection approach is believed to bridge the gap between ground-based surveys and satellite imagery, providing high quality imagery at high

temporal frequency (Berni et al., 2008). Recent studies revealed that centimetre resolution (5 to 10 cm) enables the identification of individual plants (Case et al., 2019; Getzin et al., 2012) and offers a future avenue to monitor heterogenous vegetation landscapes such as ATEs (Weiss, 2009). While UAV surveys can be easily repeated once the initial setup is in place, the method results in a temporal snapshot of the conditions at site and therefore offers a limited representation of slow dynamics (e.g. growth, treeline migration) and requires supplementary datasets or multiple surveys to monitor change (Chen et al., 2015).

Table 2: Resolution, usability and costs for different remote imagery applications. UAV = Unmanned aerial vehicle (adapted from Candiago et al., 2015)

	Spatial Resolution	**Field of View**	**Usability**	**Payload Mass**	**Cost for Data Acquisition**
UAV	0.5 – 10 cm	50 – 500 m	Very good/easy	Can be limited	Very low
Helicopter	5 – 50 cm	0.2 – 2 km	Pilot mandatory	Almost unlimited	Medium
Airborne	0.1 – 2 m	0.5 – 5 km	Pilot mandatory	Unlimited	High
Satellite	1 – 25 m	10 – 50 km	-	-	Very high, particularly for high-res stereo imagery

The rapid advance of UAV-data collection and the associated surge of high quality spectral datasets led to a change in image classification procedures (Blaschke et al., 2014). The interpretation of high-resolution datasets requires disentanglement of multiple layers of heterogeneous spectral information for individual species, further complicating the classification process (Hay & Castilla, 2008). While traditional pixel-based interpretation of satellite images fails to address reflectance and illumination heterogeneities (Weiss & Walsh, 2009), a paradigm shift towards object-based image analysis has been advocated to address the added dimension of the spectral information (Blaschke et al., 2014). Object-based algorithms have the advantage that they enable us to identify functional vegetation units and delineate traceable patterns (Blaschke & Strobl, 2001) which otherwise require labour-intensive ground studies (Hunsaker et al., 2001; Lang, 2008). The technological advances in image interpretation supervised by a field-trained expert enable us to derive fine-scale vegetation data (Blaschke et al., 2014) and consequently incorporate new and combined techniques into the classification procedure (e.g. vegetation indices, Weiss & Walsh, 2009), facilitating workflows required to track ecosystem migration patterns (Chen et al., 2015).

The abrupt southern beech (*Nothofagaceae*) alpine treeline ecotone in New Zealand provides a prime example of where the recruitment success of treeline species is significantly limited by the availability of fine-scale conditions that can be tolerated by young seedlings beyond the treeline edge (Wardle, 2008; Chapter 3). In fact, southern beech seedlings are known to be generally unsuccessful at recolonising previously occupied habitats even well below treeline (Leathwick, 1998; Mcglone et al., 2002). Thus, in order to expand beyond current ecosystem boundaries, one minimum requirement will likely be the availability of climatic niches within the adjacent tussock grasslands which feature similar abiotic conditions to the closed forest canopy (Batllori et al., 2009). To assess future alpine treeline ecotone dynamics in response to climate change we need to estimate the availability of microclimatic niches and how their presence is modulated by topography and vegetation (Elliott, 2011; Elliott & Kipfmueller, 2010; Harsch, 2010; Malanson et al., 2011). For a long time, treeline research was hampered by technological and logistical constraints. Ecotone migration patterns in abrupt treeline ecosystems show a significant temporal delay to climate change (Harsch & Bader, 2011) and current methodologies fail to draw a complete picture of the spatiotemporal variation at site.

Therefore, here I apply a method fusing UAV derived data of a treeline ecotone with three decades of treeline census data to create a singular multi-layered dataset and a more complete characterisation of a subalpine ecotone. The approach combines spectral (RGB, multispectral), spatial (LiDAR, thermal, solar) and temporal datasets (treeline census; Wardle, 1990-91) processed with modern workflows (object-based classification) to create a fine-scale characterisation of an alpine beech forest (*Nothofagaceae*) treeline ecotone in New Zealand. My specific aims were to i) use remotely operated sensors to establish new workflows for monitoring microhabitat variation at treeline and ii) link remotely derived information and field datasets to seedling position from long-term census data.

2.2 Material & Methods

2.2.1 Study area

This study took place at two treeline ecotone sites in the Canterbury Region on the South Island of New Zealand. Both sites are part of the treeline monitoring plot network introduced by Wardle (1991) and most recently updated by Harsch and colleagues (2012). The Craigieburn Valley site (-43.111, 171.713) is located at 1365 metres above sea level on a southeast to

southwest aspect on the east side of the South Island's Southern Alps. The site experiences frequent frost events throughout the year (135 frost days) and has an annual rainfall of *c.* 1300 mm. The Mt. Faust site (-42.505, 172.409) is located about 100 km north of the Craigieburn site on a west-to-southwest aspect, with fewer frost events than the Craigieburn site (90 annual frost days), and an annual rainfall of *c.* 2200 mm. Treelines at both sites are formed by *F. cliffortioides* (mountain beech), with trees at the treeline edge about four to seven metres in height, forming a continuous forest canopy.

At both sites, the adjoining subalpine zone is characterised by similar vegetation communities, dominated by *Chionochloa* spp. tussock grass species, *Dracophyllum uniflorum* Hook.f., *D. longifolium* (J.R.Forst et G.Forst.) and/or *Podocarpus nivalis* (Hook.) woody shrub patches, prostrate mats of *Leucopogon colensoi* (Hook), and individuals of *Hebe* spp. and *Aciphylla squarrosa* (J.R.Forst. et G.Forst) occupying some zones between tussocks and woody shrubs. Interspersed across the more arid terrain of the Craigieburn Valley are bare scree slopes; *L. colensoi* and *Hebe* spp. are the first plant species to establish in these areas. The alpine belt at Mt. Faust is comprised of a continuous low-stature vegetation mosaic dominated by tussock and woody shrubs with very little scree or other conspicuous geomorphological features.

A comprehensive data collection and processing workflow was developed for the study (Figure 4). Accurately positioned ground control point markers and vegetation type samples provided required information for image georeferencing and classification processes, respectively. The treeline seedling census data collected within the ecotone using a transect tape methodology (following Wardle 1990-91; Harsch et al., 2012) was then used subsequently to position tree seedlings occurring in the ecotone within the spatially explicit context of the drone derived imagery. Thermal and LiDAR flights were performed only for the Craigieburn site due to budget limitations.

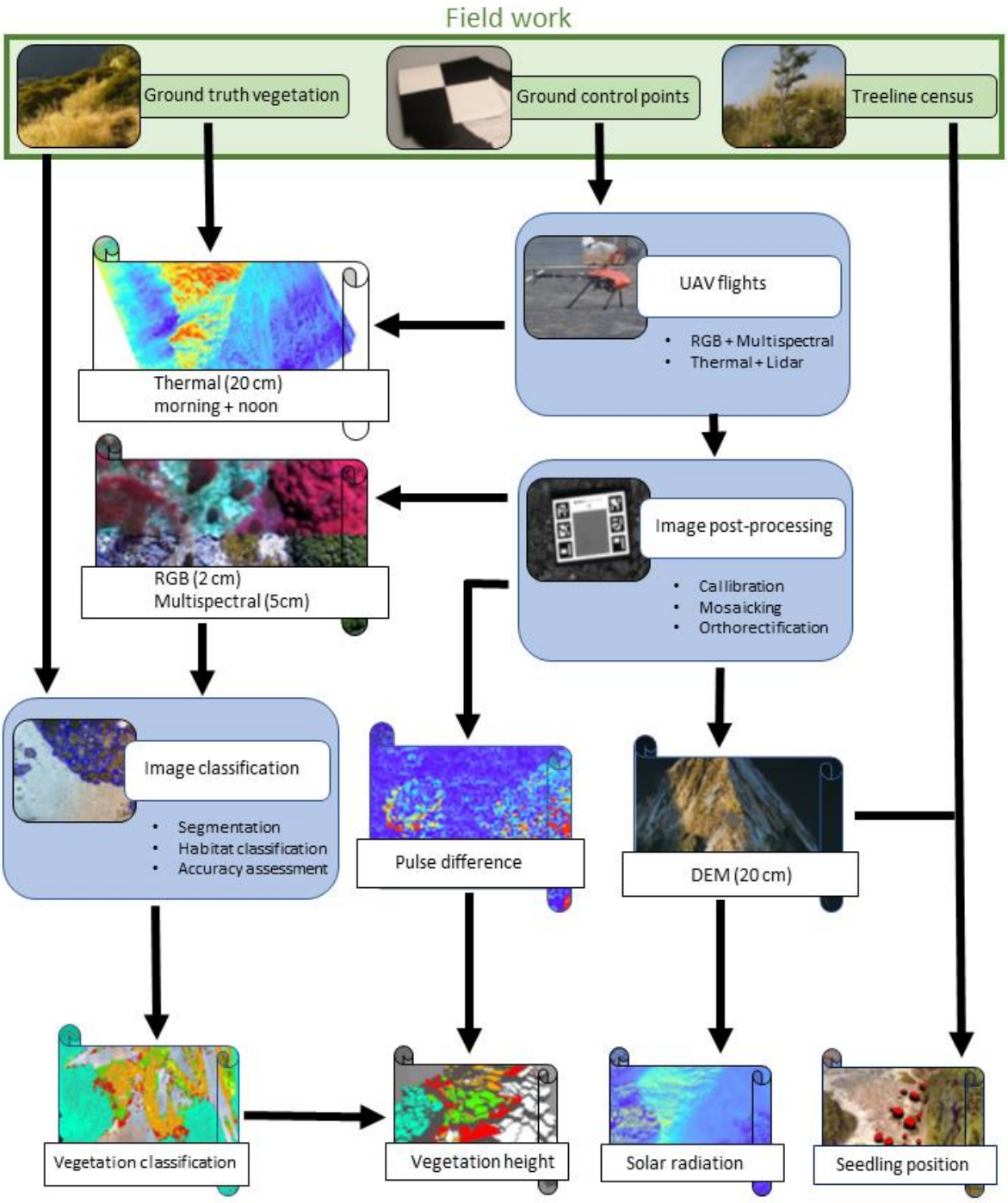

Figure 4: Overview of the technical workflow. A preliminary field study assessed vegetation at site (Craigieburn & Mt Faust), decided the scope of the UAV operation and supported georeferencing by placing ground control points. The generated images were consecutively orthorectified and post processed and the results were visualized. Combination of outputs were used to derive ancillary datasets (e.g. plant height). Thermal and LiDAR datasets were only collected for the Craigieburn site.

2.2.2 Field setup (Ground control points and vegetation ground-truth survey)

To enable the accurate georeferencing of collected drone imagery two differential GPS (Emlid, Reach RS+, Single-band real-time kinematic GNSS receiver) were used to spatially map ground control points, deployed at the site in the form of 0.5 m² chessboard structured plastic panels arranged in alignment with the planned drone flight paths. These reference points were used during the photogrammetric orthorectification process to accurately spatially co-reference the collected RGB und multispectral drone imagery. Additionally, the differential GPS was used to collect locations of plant/vegetation patch features across the study area to be used as a ground-truth dataset. A total of over 600 point-based plant identifications were carried out for each site to verify the accuracy of the remotely sensed image classification.

2.2.3 Collection of RGB colour & multispectral UAV imagery

For the RGB (red-green-blue) colour imagery, I used a DJI Phantom 4 (SZ DJI Technology Co., Ltd, China) UAV with standard equipment and 5870 mAh batteries. This UAV was also equipped with a Parrot Sequoia+ (Parrot SA, France) multispectral and sunlight sensor (Figure 5).

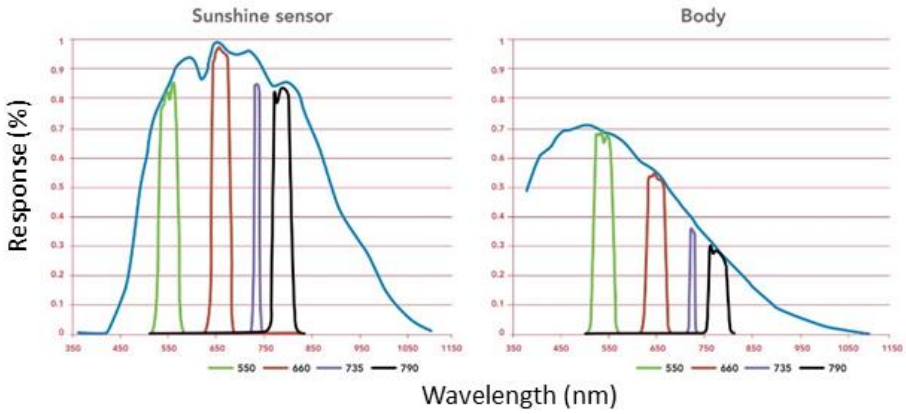

Figure 5: Relative spectral sensitivity for the Parrot Sequoia+ multispectral sunshine sensor (left) and body (right). Both sensors featured four spectral sensors with the same filters: Green (550 nm), Red (680 nm), Red-edge (734 nm) and Near-infrared (790 nm) (Parrot SA, France).

The setup incorporated an elongated antenna with the light sensor and the multispectral camera attached underneath the drone body facing downwards. Flight plans were developed using the software Universal Ground Control Station Version 3.1.817 (UgCS; SPH

Engineering, Latvia) and the compatible Android App ‘UgCS for DJI’ (SPH Engineering, Latvia). The software gives a visual presentation of the projected flight path (Figure 6). For the topographic information I used an 8 m resolution digital elevation model for New Zealand (Geographx; LINZ, 2016). To provide an approximately 1 - 2 cm resolution RGB imagery, the drone is programmed to fly 50 m above ground level, using an 8 m digital elevation model to approximate the height information. This procedure also helps to avoid obstacles (e.g. trees, boulders) which are not incorporated in the DEM. The software also provides, based on the selected drone type, an estimate for the number of way points, length of the flight and expected flight time based on the topographic heterogeneity and start and landing points. It is important to note that due to the additional weight added by the custom multispectral setup on the drone, a battery test indicated that I needed to decrease the flight time to a maximum of 12 minutes. The camera specifications provide a minimum photo interval of > 5 seconds which required me to slow down the flight speed to match the image overlap requirements for post-processing. The estimated flight path itself therefore was a result of a trade-off between area covered, topography and battery life. The projected flight time did not incorporate information related to conditions at the site; for example, on windy days the flight path would need further adjustments which cannot be made in the field. With all these limitations in mind, the setup enabled me to cover an area of approximately 200 × 200 metres (12 minutes single battery, 4 ha) while flying at 5 m/s before I was required to land the drone.

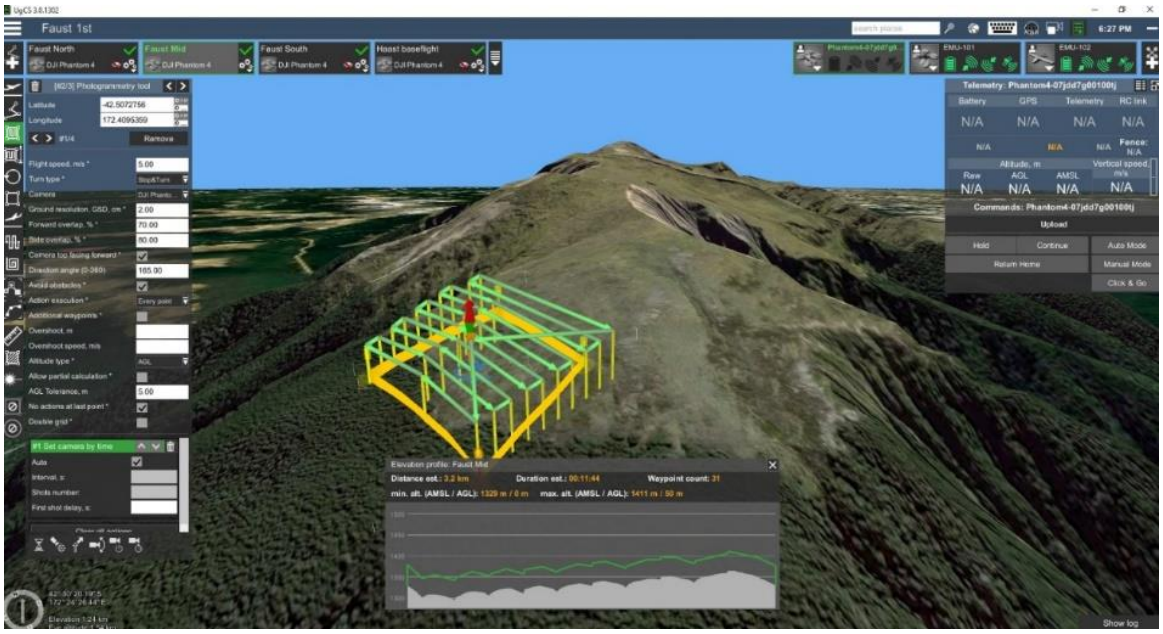

Figure 6: Planning drone flights in UgCS. The software features a 3D model of the projected flight paths and includes projections for the estimated flight time based on the UAV selected.

The built-in attachments of the multispectral and light sensors enabled the capture of colour RGB and multispectral imagery simultaneously. However, both image sensors need to be controlled separately via a Wi-Fi connection and the Sequoia+ sensor was accessed via an Android browser on the mobile phone. For the initial setup prior to departure, and along with communicating the pre-planned flight path with the UAV, the multispectral sensor had to be calibrated using a manufacturer provided calibration target plate. The calibration step was repeated post-flight. Since the multispectral camera operates independently from the RGB setup, the camera was programmed to capture footage on a 'class 10' microSD card in intervals of 4 seconds to match the velocity of the UAV and the respective overlay requirements for the photogrammetry software. To process the collected image data within the photogrammetry software, latitude and longitude information was extracted from the image metadata. For this purpose the 'ExifTool' (Harvey, 2020) was used to automate the extraction process and multispectral image coordinates were saved in a *.csv text file format to be used later within the photogrammetry software.

2.2.4 Photogrammetry post-processing

I used the photogrammetry software Pix4D (Pix4D, Switzerland) to link and georeference the UAV-collected image snapshots. To process the individual images into a single mosaicked, orthorectified image, an overall proportional overlap of > 80% was required and the ground control points were placed to span across multiple images and close to the outside margins of the area. The ground control point locations were imported from the field survey files and ground control points and imagery files were converted from the WGS 1984 geographic projection into the local New Zealand Transverse Mercator NZGD 2000 (NZTM 2000) projection. After an initial preview of the mapped area was created based on the coordinates of the individual imageries, the footage was used to link the projection information to the imported georeferenced ground control points before re-running and finalising the photogrammetry process. The procedure was re-run and optimized (manual GCP identification) until all the ground control points were correctly georeferenced to a precision of ± 5 cm. Once the orthorectified image was completed, the result was exported as a *.tif image file and further processed in the classification software. For the multispectral imagery, the above process involves the extra steps of adding the extracted coordinates via a *.csv file and the reflection panel values (Table 3) for calibration plate are entered.

Table 3: Reflectance values for the calibrated reflectance panel for the multispectral sensor.

Band	Value
Green	0.55
Red	0.55
Near-Infrared	0.49
Red-Edge	0.53

As an initial accuracy assessment step during post-processing, both results were imported into ArcGIS Pro v.2.2.3 (ESRI, 2020) to perform a visual interpretation of the overlay by using transparency and swipe tools within the software to switch between RGB and multispectral imagery (Figure 7).

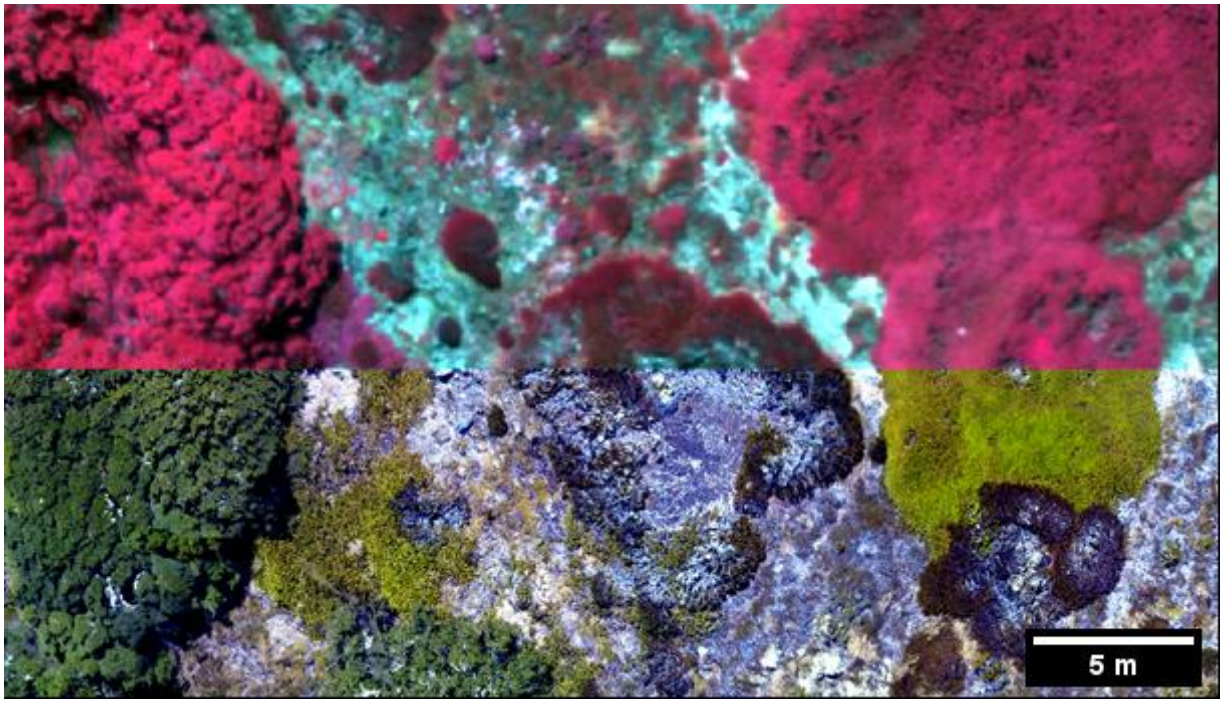

Figure 7: Overlay of RGB and multispectral output for Mt Faust. (top) 5 cm resolution output of the multispectral imagery (false colour) vs. (bottom) 1 cm resolution RGB output to estimate the accuracy of early outputs by delineating vegetation boundaries.

Once completed, the performance of the orthorectification and co-registering of both image datasets (RGB & multispectral) required evaluation. I used ground control points and distinctive features within the sites (e.g. rocks, flowers) to determine the centre of those features within both spectral layers (Figure 8). The distance between both points were then measured to assess the overall accuracy of the co-registration of both datasets.

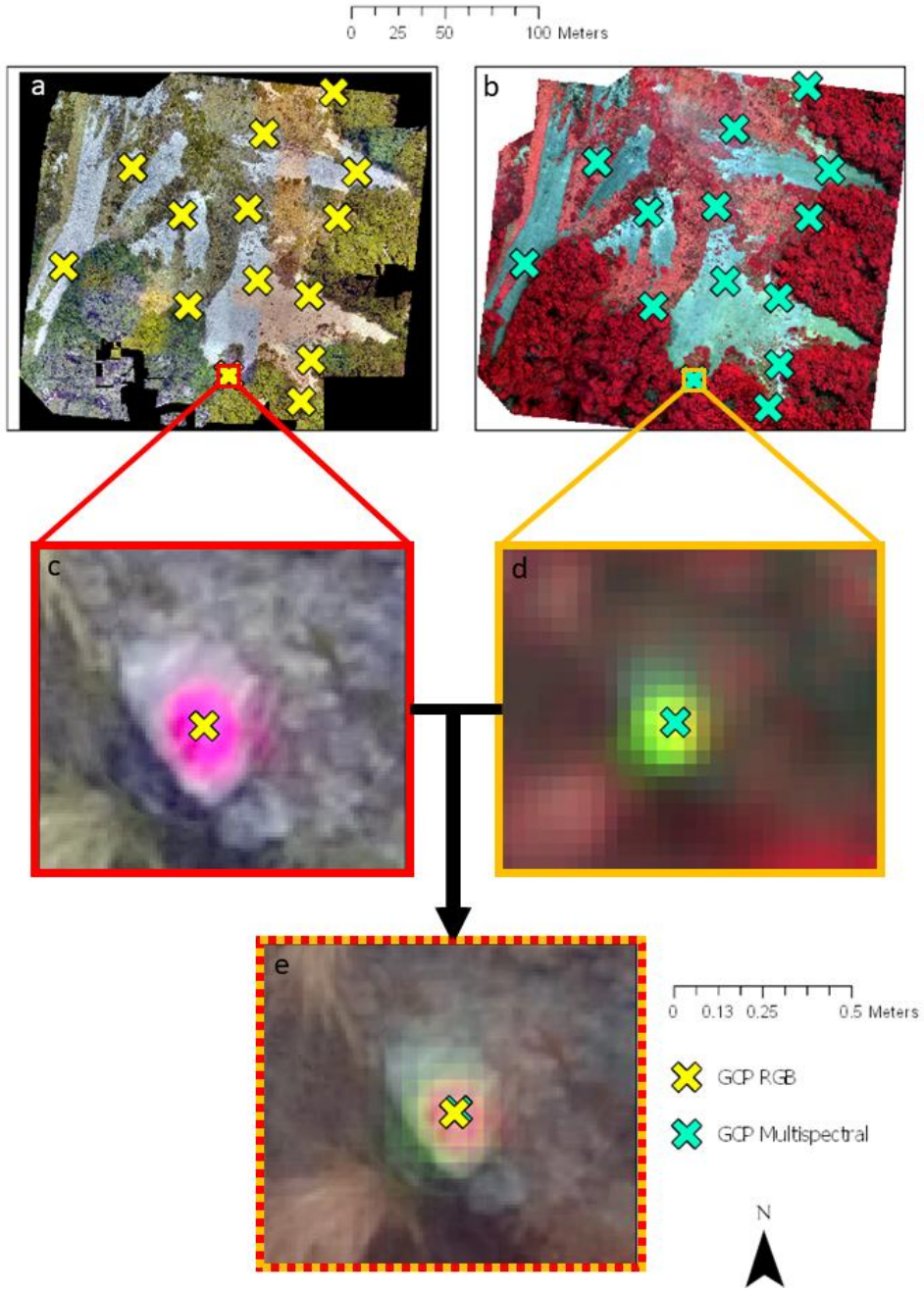

Figure 8: Accuracy assessment (RMS) of RGB vs multispectral imagery for Craigieburn Valley by manually selecting GCP centres in ArcGIS Pro. (a,c) RGB imagery and (b,d) multispectral

imagery with ground control points (GCP). (e) Overlay of both spectral layers to quantify spatial displacement.

2.2.5 Object-oriented image classification using the eCognition software

Land cover type classification of the generated imagery was conducted in eCognition Developer 9.0 software (Trimble, Germany). I used an object-based classification trained against the ground-truthed vegetation field survey data. The approach involved a segmentation procedure, followed by the application of a classification algorithm. The three colour layers (Red, Green, Blue) and four multispectral layers (Green, Red, Red Edge (RE), and Near Infrared (NIR)) formed a total of seven layers were used as the input data to this process (Table 4).

Table 4: Overview of spectral band information retrieved via drone surveys

Name	**Sensor (Imagery)**	**Resolution (cm/pixel)**
Red	Phantom 4 Camera (RGB)	1.088
Green	Phantom 4 Camera (RGB)	1.088
Blue	Phantom 4 Camera (RGB)	1.088
MS Green	Parrot Sequoia + (Multispectral)	5.646
MS Red	Parrot Sequoia + (Multispectral)	5.646
Red Edge (RE)	Parrot Sequoia + (Multispectral)	5.646
Near Infrared (NIR)	Parrot Sequoia + (Multispectral)	5.646

The ‘multiresolution segmentation’ applies an optimization procedure to minimize the average heterogeneity of the image objects based on their equally-weighted spectral values (Trimble, 2020). The result was an image segmented into objects that were relatively spectrally homogeneous (across all of the spectral input bands) in comparison to neighbouring objects (Figure 9). After a series of test runs, I used different object ‘scale’, ‘shape’ and ‘compactness’ parameter settings for the generated objects between both sites. The scale parameter defines the maximum number of pixels to be included in a single object. The shape criterion decides how much importance the algorithm assigns to the spatial structure of each putative object relative to their spectral reflectance values; the higher the shape parameter value the smaller the influence of the spectral band data in the algorithm uses in for the segmentation (Trimble, 2020). The compactness parameter controls how much weight the overall compactness (perimeter to area ratio) of the object adds into the decision process, with higher compactness

values forming objects with a smaller perimeter relative to their areas (Trimble, 2020). To account for the increased vegetation heterogeneity for the Mt Faust site I tested a range of scale and compactness criteria to verify the algorithm delineating the objects. I decided to decrease the size of the objects generated and lowered the weight of the compactness criterion since the generated objects were too large to account for the increasing vegetation heterogeneity at site (Scale: 100, Shape: 0.1, Compactness: 0.9) over the Craigieburn site (Scale: 250, Shape: 0.1, Compactness: 0.7).

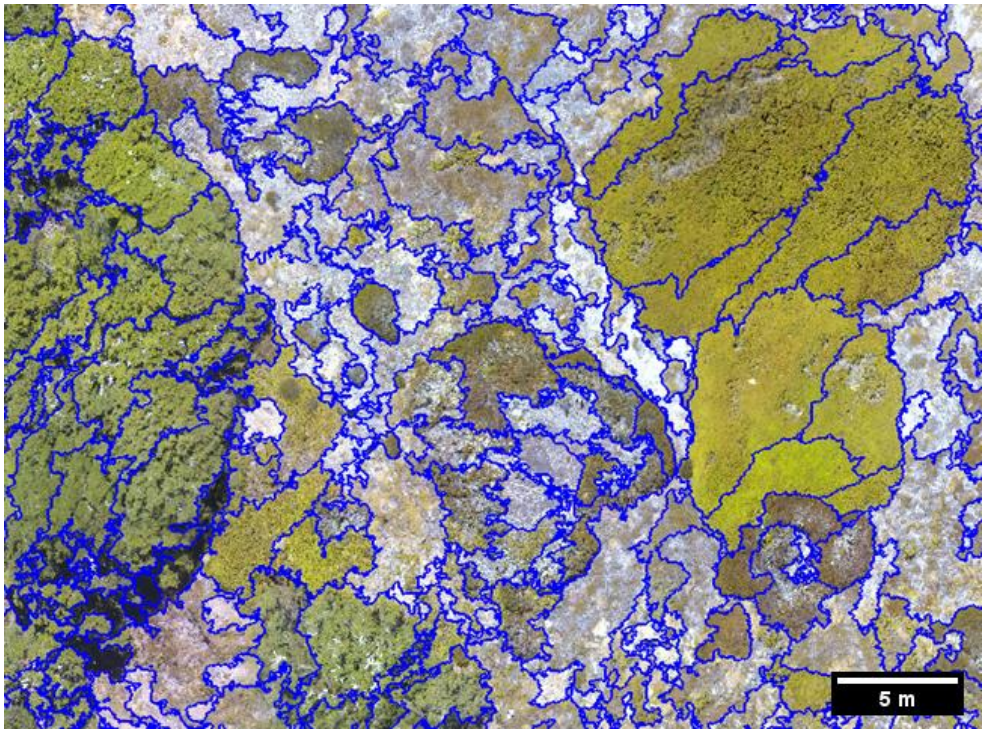

Figure 9: Example output for the segmentation process at Mt Faust (Scale: 100, Shape: 0.1, Compactness: 0.9). While only the RGB channels are illustrated, the software used all 7 UAV derived spectral bands (Table 4) for the segmentation process.

Since the Craigieburn site featured large sections of bare ground and scree, prior to the classification step, I computed and used the Normalized Difference Vegetation Index (NDVI) to clearly distinguish between objects containing vegetation and bare-ground objects. Each generated object had associated mean values for the spectral band data comprising each object; based on these mean values I calculated a mean layer value for the NDVI (1) based on the information I have from the multispectral bands:

$$NDVI = \frac{\text{NIR} - \text{MSRed}}{\text{NIR} + \text{MSRed}} \quad (1)$$

Every generated object containing any form of vegetation now had assigned for the vegetation indices. Using this information, I filtered out the scree slope zones (NDVI > 0) and performed a merge to combine the individual objects into few large scree slopes without vegetation and excluded them in the following classification (Figure 10). This concluded the segmentation process and the classification was carried out using these generated objects.

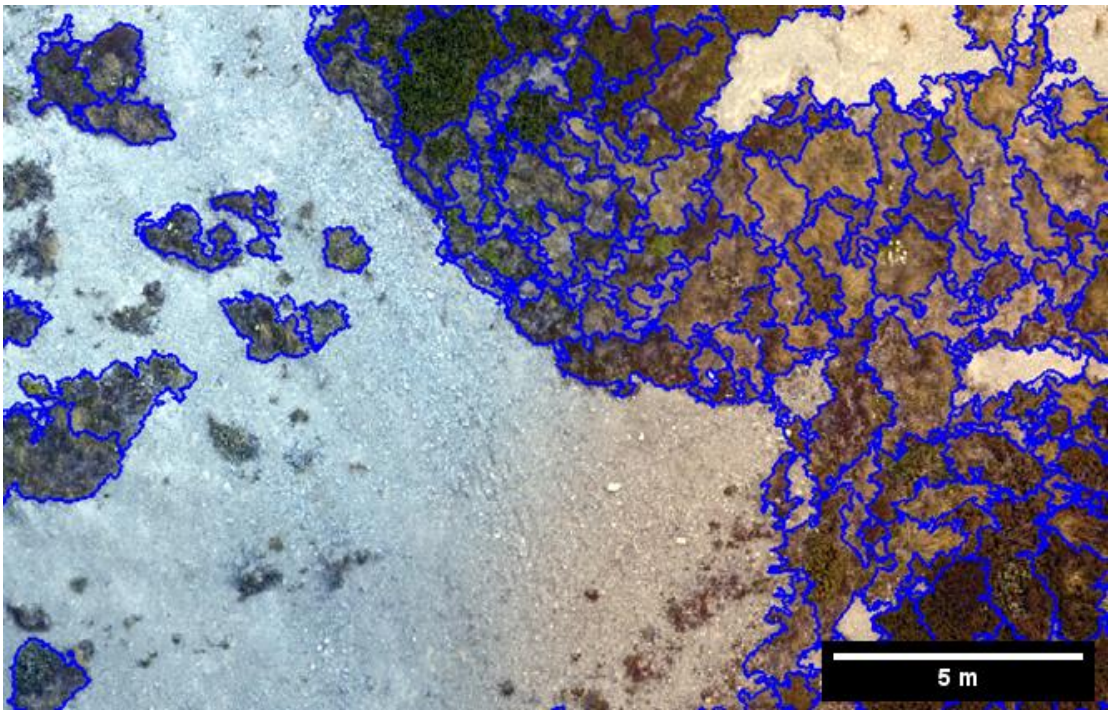

Figure 10: Example output of excluding areas without vegetation for the Craigieburn site. Unvegetated areas of the imagery have been excluded from the segmentation and classification processes by removing features which do not contain spectral information typical for vegetation initial (NDVI > 0).

Once the segmentation process was completed, all generated objects contained spectral band mean values, as well as software-calculated values for the NDVI (Figure 11). The software also automatically assigns a spectral 'brightness' criterion based on how bright the average pixels are up to a range of 254. Calculated spectral mean values within the objects were used as input to a supervised classification algorithm. Based on the results of a field survey and the initial classification output I decided to define 6 subclasses of ground cover: Bare, unvegetated ground (scree), tussock grasses (*Chionochloa* spp.), mountain beech (*Fuscospora cliffortioides*) and three types of alpine shrubs (*Dracophyllum uniflorum*, *Leucopogon colensoi*, *Podocarpus nivalis*).

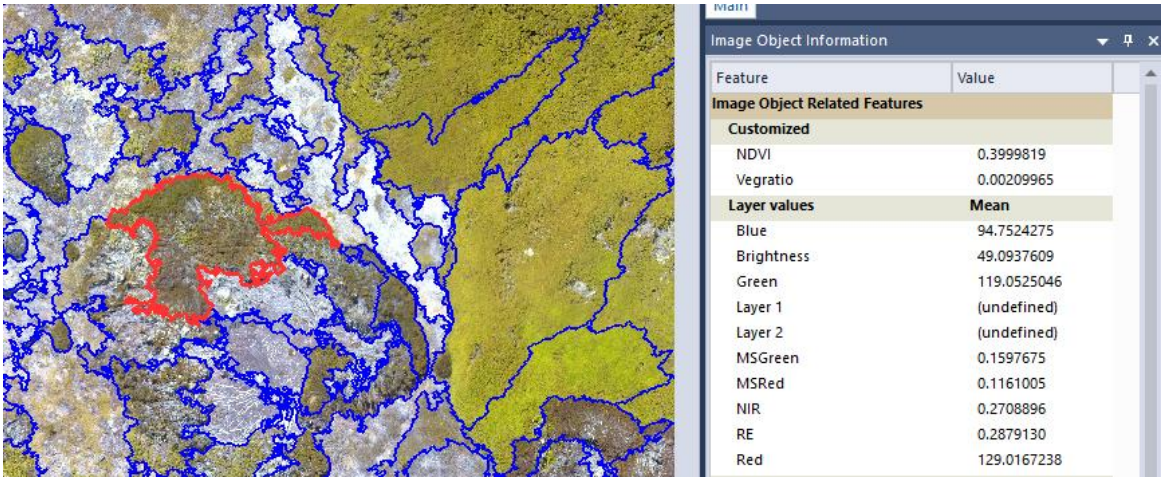

Figure 11: Mean Spectral values for individual objects within the Pix4D environment. The table within the software shows object related spectral mean values for the seven channels used plus the calculated values for the NDVI and brightness for the sample (highlighted in red).

A nearest neighbour (NN) classifier with a manual pre-selection of field-based vegetation sample locations was performed in order to train the algorithm (Figure 12).

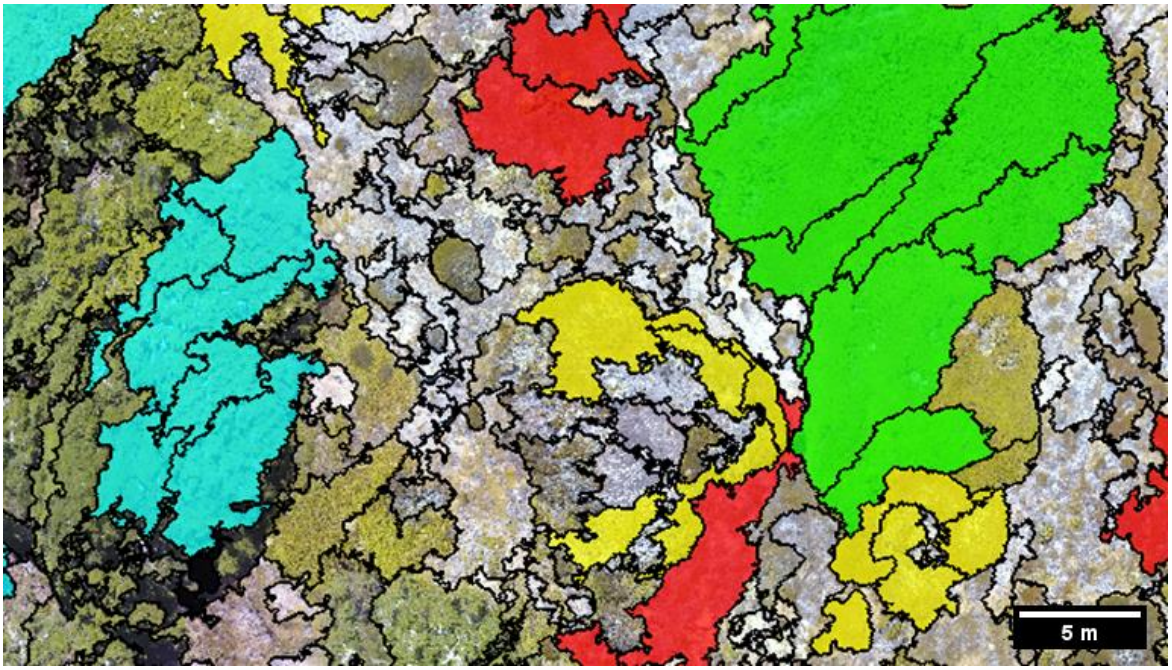

Figure 12: Selection of training samples for the supervised classification. Trained dataset for the supervised classification: *F. cliffortioides* (teal), *Dracophyllum* spp. (yellow), *Leucopogon colensoi* (red) and *Podocarpus nivalis* (green).

eCognition provided two helpful features to increase the confidence in selecting individual objects for the training sample dataset and the most effective spectral band selection to distinguish between classes. The sample editor provided an overview between different sample sets for the respective vegetation. The example below (Figure 13) shows a comparison of the spectral bands overlay for *Dracophyllum* (Draco, black) and the woody *Leucopogon colensoi* (PM, blue). Here the information in the near infrared reflectance band showed a strong overlap (20%) between both selected features, distinguishing both kinds of vegetation based on the NIR reflectance would therefore result in misclassifications. The red reflectance shows an overlap of 1% and was therefore a preferred discrimination parameter between these two classes.

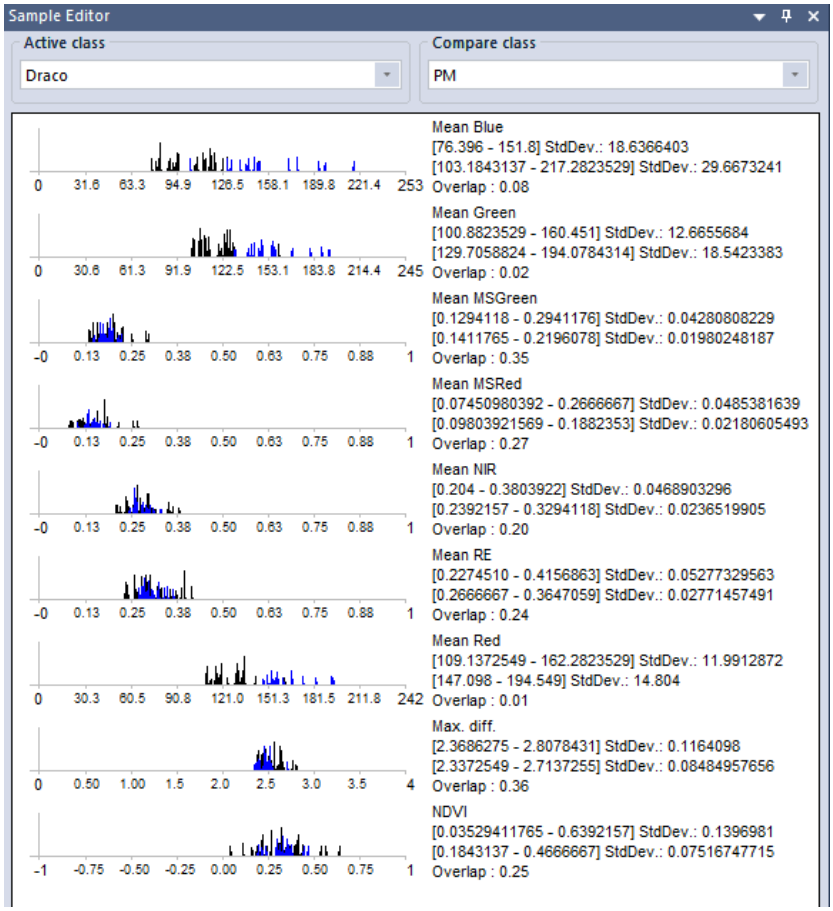

Figure 13: Mean spectral reflectance values for different vegetations within the sample editor Faust, supervised samples for *Dracophyllum* (Draco, black) and *Leucopogon colensoi* (PM, blue) for Mt Faust with derived mean reflectance for calculated objects for RGB (Red, Green, Blue) and multispectral imagery (MSGreen, MSRed, RE = Red Edge, NIR = Near Infrared, NVDI = Normalized vegetation Index).

This process enabled me to define a pre-selection of training samples and parameters that I incorporated into the classification process. Using spectral bands which share more similarities than differences can have adverse effects of the separation of features. eCognition offers a tool called 'Feature Space Optimization' to address this issue. After choosing the classes and spectral bands the software calculated the bands with highest quality and the correct quantity required to achieve the best possible separation level (Figure 14). The results of the NN supervised classification were then exported as a GIS-ready shapefile (*.shp) to be used for further analysis.

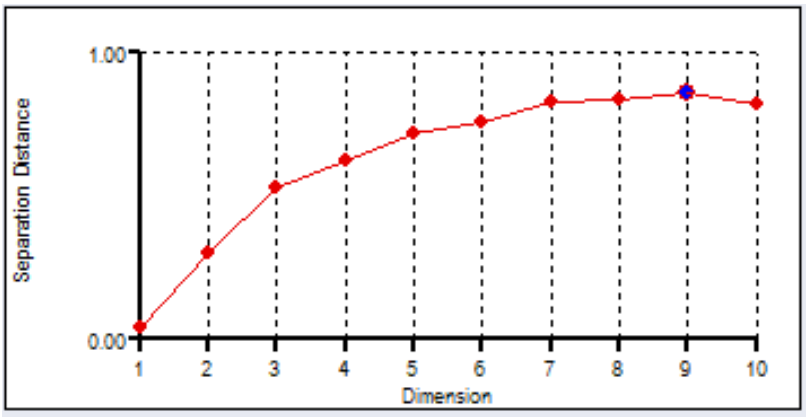

Figure 14: Separation level vs. selected number of bands. With multiple selected spectral bands (dimension) the confidence in the separation of all selected classed increases. Once a certain degree of separation has been achieved the curve flattens since additional parameters have little to no benefit in enhancing the degree of separation.

2.2.6 Classification accuracy assessment

To assess the accuracy of classifications of the Craigieburn and Mt Faust images, an error confusion matrix was created in ArcGIS Pro. The procedure involved creating 500 randomly distributed points within the classified area and assigning the value of the underlying classification to each point. The value in the field was then manually compared to the ground-truth information from the field survey. An estimate for the effectiveness of the classification process was performed using the *Kappa* single-value metric to measure agreement between classification and truth values.

2.2.7 Collection of thermal and LiDAR data

Thermal infrared and LIDAR data were collected for the Craigieburn study site. The thermal imagery flight was carried out by an external contractor with an Altus ORC2 UAV (Altus Intelligence, Hamilton, New Zealand, Figure 15). To compare thermal profiles over a diurnal course, two flights were carried out in austral winter (May 20th) in the morning and early afternoon of the same day. The thermal sensor used is a FLIR Duo Pro R, with a 640 × 512 resolution, 7.5 – 13.5 µm spectral bands, 9 Hz thermal frame rate and a 32° field of view (FLIR Systems, Wilsonville, OR, USA).

Figure 15: Helicopter drone (Altus Orc2 UAV) at Craigieburn Valley. The UAV was used to generate LiDAR and thermal imagery for the site in austral winter (May 20th, 2019).

The LiDAR data were collected using the same flight platform used for the thermal imagery (Figure 16) but on a separate flight in between the two thermal flights. The output from the LiDAR flights was a dense point cloud dataset for the entire Craigieburn site with a distance between points ranging from 0.1 to 0.5 m. A point cloud dataset was generated in ArcGIS Pro and used to create a high-resolution digital elevation model (DEM) of the Craigieburn study site. I created two versions of the DEM, one showing the vegetation surface information (e.g. top-of-vegetation canopy) and another representing a ground level DEM. To create a DEM representing just the top of the features ArcGIS Pro offers an algorithm picking the highest value within the proximity and then creates a digital surface model representing the top-of-vegetation layer for the site (‘canopy returns’). I used the pulse difference method (Rees, 2007) to separate the first and last pulse recorded for the LiDAR data. I employed an ArcGIS

Pro algorithm to estimate maximum pulse difference to generate a ground level DEM and first return information to create a top vegetation (e.g. canopy) DEM. Consecutively, I subtracted both DEM files from each other to generate a vegetation height layer (Figure 16b,c).

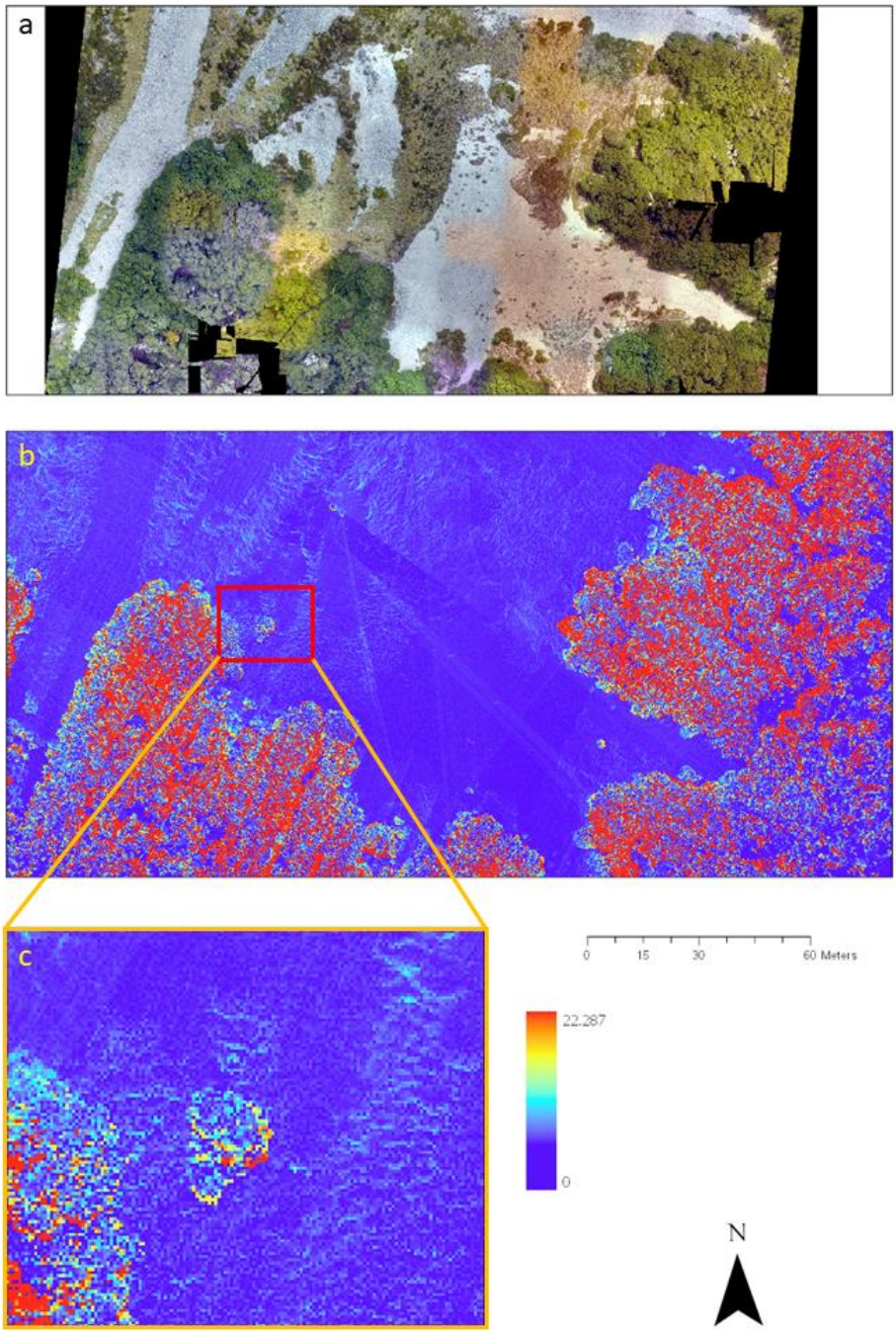

Figure 16: Digital elevation points generated from LiDAR output for the Craigieburn site. The image shows a comparison between RGB imagery (a, 2 cm resolution) and the digital elevation points (b, 20 cm) for a selected area within the Craigieburn site and highlighted individual vegetation height (c). The height information of topographic features and vegetation is derived by calculating the maximum difference between bottom and canopy digital elevation models.

2.2.8 Deriving additional environmental and topographic data

The incident solar radiation for specific days can be calculated in ArcGIS Pro using the top-of-vegetation digital surface model generated from the LiDAR dataset for the Craigieburn site (Figure 17). For the calculation of the incident radiation I compared a winter and summer day (May 20th, February 12th). The dates chosen for the winter and summer estimates match the measurement dates for the chlorophyll fluorescence survey (Chapter 4). For the microhabitat characterisation and seedling performance the LiDAR point cloud was used in the consecutive chapter to derive information about slope and solar radiation (Chapter 3). Similar to the classification accuracy assessment I used 500 random point values generated along the east facing slopes (aspect calculated within ArcGIS Pro) of the site to extract point values for solar radiation, thermal difference and identified ground cover.

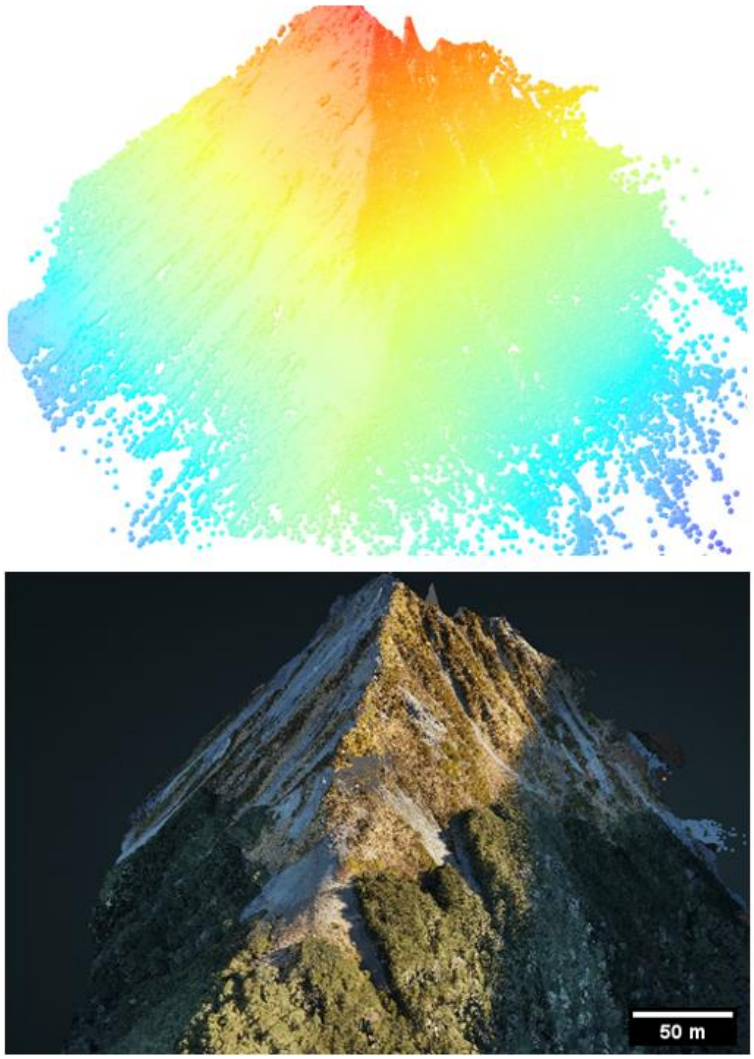

Figure 17: LiDAR dense point cloud for the Craigieburn site (top) and derived 3D model (bottom) from the LiDAR sensor UAV flight for the Craigieburn site (austral winter, 2019).

2.2.9 Spatial referencing of the monitored seedlings

The treeline seedling monitoring transects established by Peter Wardle in the austral summer of 1990-91, and remeasured three times since, have yielded information about the location of each seedling relative to a transect line running parallel to the treeline edge at a set compass bearing, seedling heights and diameters, and their tree tag numbers. Each seedling present within 20 metres beyond the treeline edge was located in the field by recording the distance along the transect at which it occurred and its perpendicular distance from transect at that location. Thus, the locations were recorded as measurements made "along" and "from" the transect tape laid out on the set bearing. The transects were resampled a fourth time (2018/19). To put the relative seedling transect location measurements into a digital GIS format, I first gathered centimetre accuracy GPS positions for the transect beginning and end poles (Figure 18, yellow points) using the same differential GPS setup as for the vegetation survey. By knowing the real-world coordinates of the transect start and end points and the bearing of the transect section, the relative seedling location information (along and from distances) were spatially referenced in the GIS to a New Zealand Transverse Mercator coordinate system. This procedure was repeated for all seedlings along each transect section. An 'offset' function was used in ArcGIS pro to place each seedling using its 'from' transect distance information at a 90 ° angle from the main transect bearing (Figure 18, teal lines).

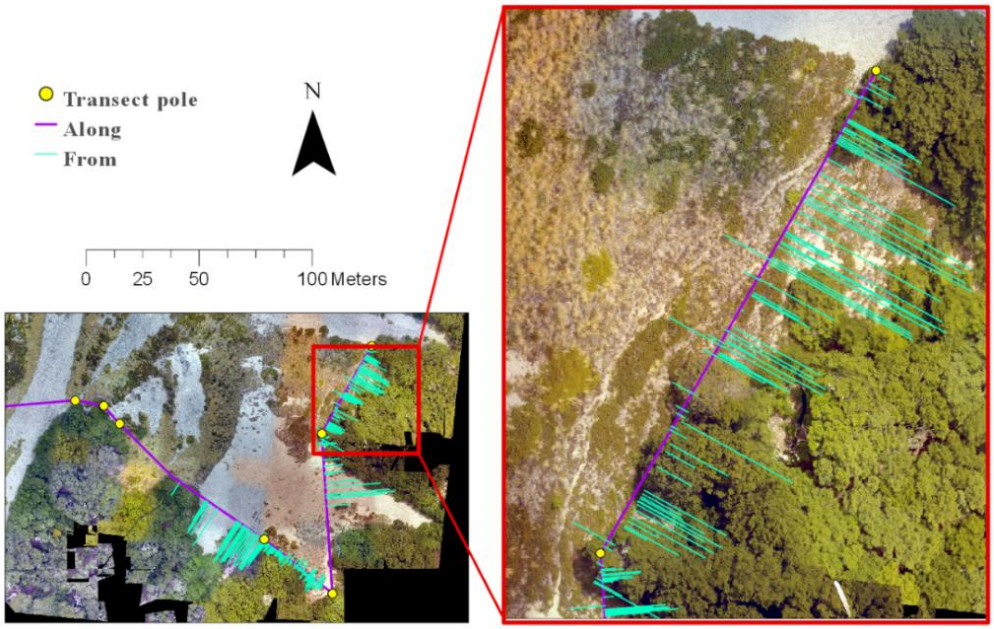

Figure 18: Wardle transect seedling data (43°06'40.6"S 171°42'53.2"E, Craigieburn Valley) converted into two-dimensional space. Seedling position along (X, purple) and from (Y, teal) the transect have been extrapolated from GPS located transect poles (yellow).

2.3 Results

The results of the Phantom drone flights (Figure 19) provided high quality RGB (2 cm) and multispectral (5 cm) imagery of the Craigieburn Valley and Mt Faust sites. The datasets enabled us to visually identify vegetation and topographic features (e.g. rocks, terrace riser) at site. The ground control points deployed during the field survey and the meta-information in the images enabled me to georeference the UAV-derived imagery with centimetre accuracy (Craigieburn: 6.14 ± 4.03 cm, Mt Faust: 5.11 ± 2.88 cm). Subsequently, I was able to use all seven spectral layers to help outline and later classify the selected microhabitat categories via an object-based classification,

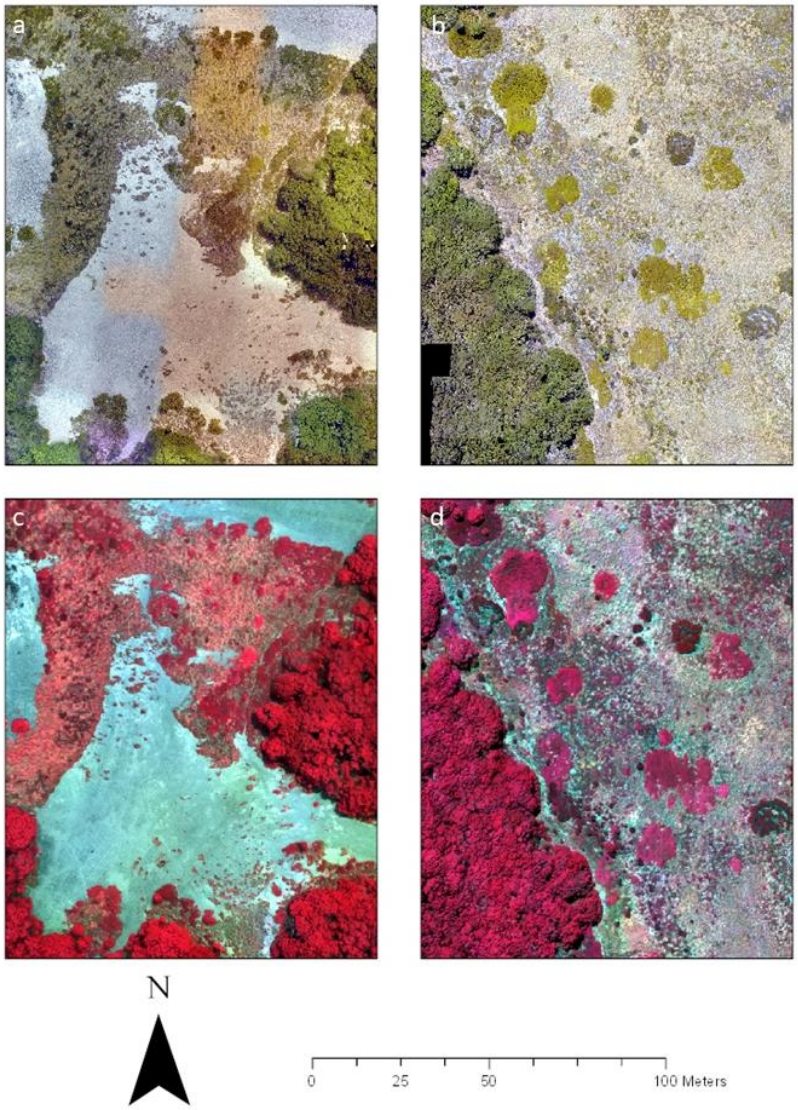

Figure 19: Results for the RGB vs multispectral imagery output for both sites. RGB images of (a) Craigieburn and (b) Mt Faust (2 cm resolution). Multispectral false colour images of (c) Craigieburn and (d) Mt Faust (5 cm).

The supervised vegetation classification (Figure 20) based on the seven spectral layers derived from the RGB and multispectral channels for the Craigieburn Valley (Figure 20c) and Mt Faust (Figure 20d) generated high-quality maps for the six most abundant ground cover types in the alpine treeline ecotone. For both sites the approach clearly delineated and classified the generated objects. The identification of vegetation based on NDVI and the delineation of the beech canopy border (teal) achieved high accuracies as supported by the cross-tabulation assessment (Table 5 & 6). Particularly the large sections of non-vegetated scree slopes at the Craigieburn valley were clearly separated from areas lacking healthy plant life using the NDVI (98 %). The evaluation of the results via a confusion matrix showed high accuracy for Craigieburn (89.7 %) and Mt Faust (71 %). For the Craigieburn site the automatic exposure settings within the RGB sensor resulted in inconsistencies in the image exposure which I then later resolved with a fixed exposure setting for Mt Faust. However, since the brightness channel had low priority within the feature space optimization procedure the resulting classification had not been adversely affected by it.

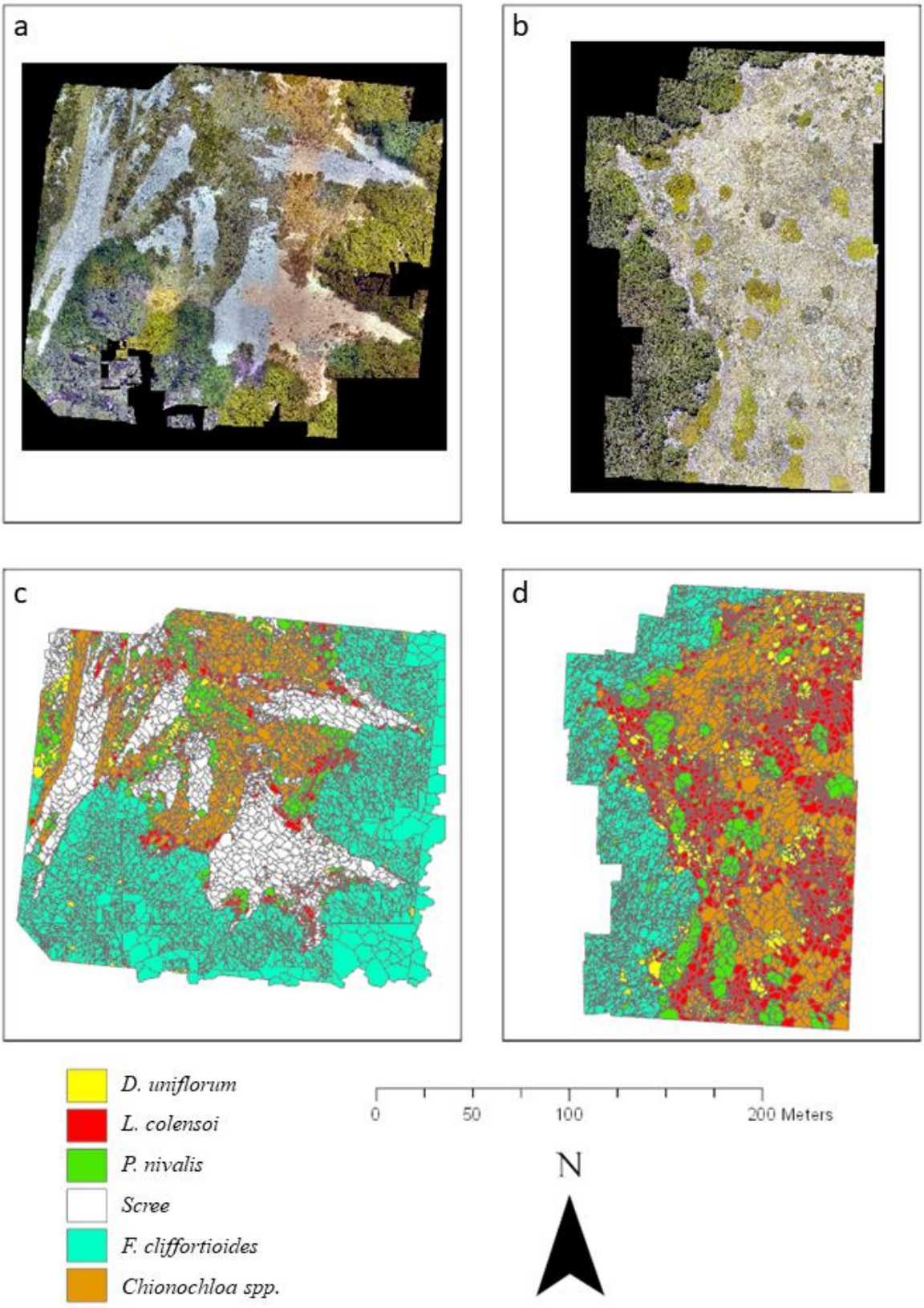

Figure 20: Results for the vegetation classification for both sites. RGB images of (a) Craigieburn and (b) Mt Faust (2 cm resolution). Vegetation classification via spectral reflectance bands of (c) Craigieburn and (d) Mt Faust. Bare, unvegetated ground (scree),

tussock grasses (*Chionochloa* spp.), mountain beech (*Fuscospora cliffortioides*) and three types of alpine shrubs (*Dracophyllum uniflorum*, *Leucopogon colensoi*, *Podocarpus nivalis*).

For the accuracy assessment in the Craigieburn Valley (Table 5) I compared six classified vegetation types (*F. cliffortioides*, Scree, *Leucopogon colensoi* (PM), *Dracophyllum* spp. (Draco), *Podocarpus nivalis* (Podo) and *Chionochloa* spp. (Tuss)) against the respective ground-truth types, across 500 validation samples for each of the sites (Table 5 & 6). The 'user's accuracy' (U columns in Table 5 & 6) reveals false positives where the classified points show incorrect presence of the given class. The 'producer's accuracy' (given in the P rows) indicates false negatives where the ground truth comparison revealed that vegetation which was actually present was not detected. The kappa statistic of agreement (Kappa) provides an overall estimate of the assessment of accuracy.

Table 5: Accuracy assessment matrix: 'confusion matrix' for the vegetation classification at the Craigieburn study site. *Kappa* single-value metric to measure agreement between classification and truth values with user's accuracy (U) and producer's accuracy (P). Beech = *F. cliffortioides*, PM = *L. colensoi*, Draco = *D. uniflorum*, Podo = *P. nivalis*, Tuss = *Chionochloa* spp.

Class	Beech	Scree	PM	Draco	Podo	Tuss	Total	U
Beech	159	0	3	0	5	0	167	95.2%
Scree	0	145	4	0	0	1	150	96.7%
PM	0	1	30	0	0	6	37	81.1%
Draco	0	0	0	19	2	0	21	90.5%
Podo	0	1	2	4	29	1	37	78.4%
Tuss	0	1	6	0	2	79	88	89.8%
Total	159	148	45	23	38	87	500	0
P	100%	98%	66.7%	82.6%	76.3%	90.8%	0	92.2%
Kappa	89.7%							

The results (Table 5) for the confusion matrix for the Craigieburn Valley show an overall Kappa statistic of agreement of 89.7%. The highest accuracies have been achieved for the classification of beech trees and tussock (< 5% misclassified), whereas data for *L. colensoi* and *Chionochloa spp*. were most frequently confused with one another and the woody *L. colensoi* and *P. nivalis* showed the highest degree of uncertainty, with 33 % and 24 % misclassification, respectively.

Table 6: Accuracy assessment matrix: 'confusion matrix' for the vegetation classification at the Faust study site. *Kappa* single-value metric to measure agreement between classification and truth values with user's accuracy (U) and producer's accuracy (P). Beech = *F. cliffortioides*, PM = *L. colensoi*, Draco = *D. uniflorum*, Podo = *P. nivalis*, Tuss = *Chionochloa* spp.

Class	Beech	PM	Draco	Podo	Tuss	Total	U
Beech	86	2	0	1	0	89	96.6%
PM	1	106	3	3	42	155	68.4%
Draco	1	10	22	1	15	49	44.9%
Podo	3	6	1	51	5	66	77.3%
Tuss	0	9	2	5	125	141	88.7%
Total	91	133	28	61	187	500	0
P	94.5%	79.7%	78.6%	83.6%	66.8%	0	78%
Kappa	71%						

The results for the confusion matrix for the Mt Faust site show only 5 classes, since scree areas were lacking. The overall *Kappa* statistic of agreement was 71 %. The highest accuracies were achieved for the classification of beech trees (< 5.5 % misclassified), whereas *Dracophyllum* spp. (55 % misclassified) and Tussock grasses (33 % misclassified) showed the highest degree of uncertainty. Particularly for larger vegetation associations which incorporate multiple spatially connected objects (e.g. *Podocarpus nivalis* and *Chionochloa* spp.), the classification procedures revealed high accuracy (up to 90%). The blue and green spectral bands (RGB), as well as the NDVI calculations (multispectral) were particularly useful for discriminating between different vegetation classes.

Calculated solar radiation maps illustrated how light regimes are controlled by the incident angle and intensity of the sun, where the local topography and particularly the aspect of the mountain face modulate the strength of this abiotic factor. The calculations were based on the top vegetation DEM (20 cm) for the Craigieburn Valley. Solar radiation regimes (Wh/m²) for different times during the year were illustrated (Figure 21).

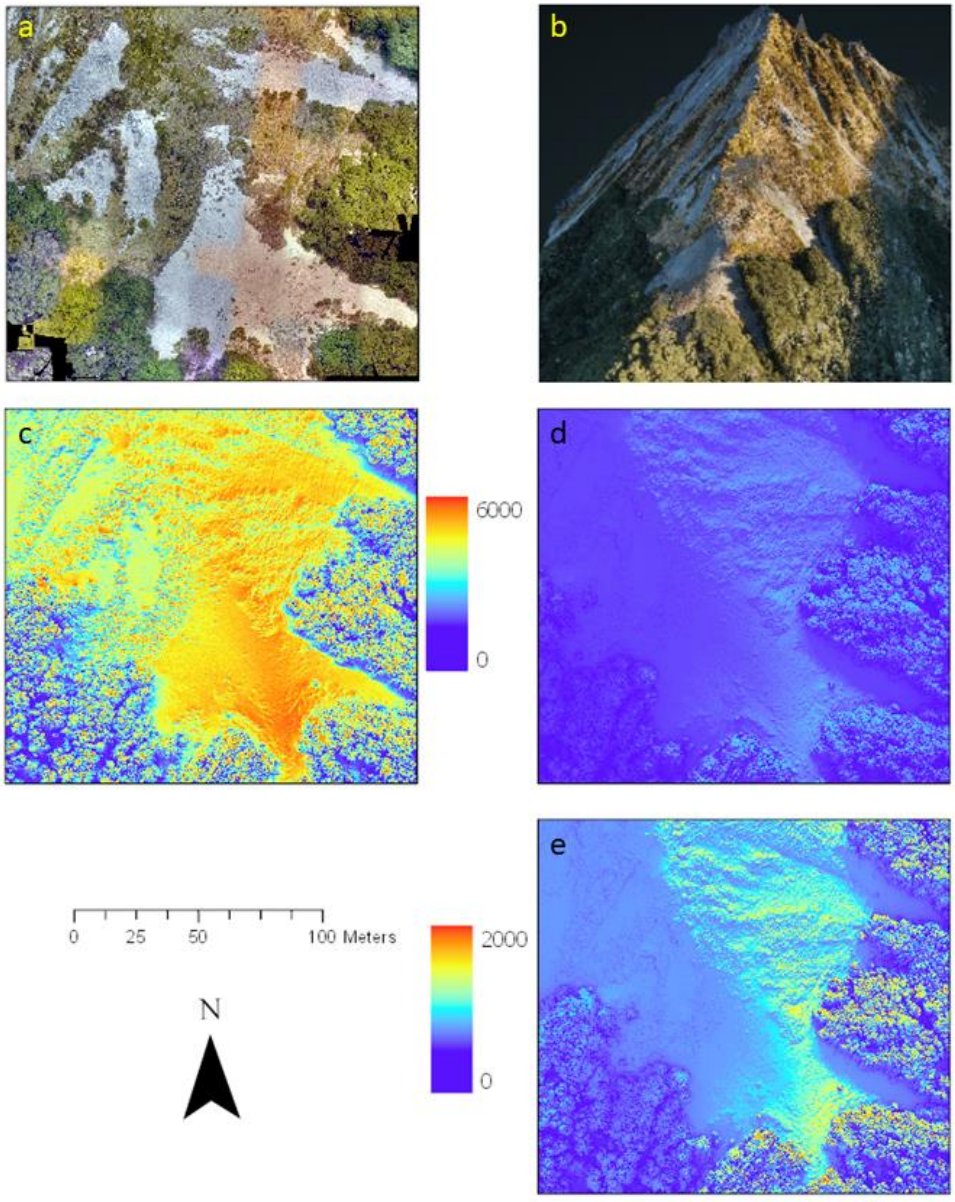

Figure 21: Calculated solar radiation environment for Craigieburn Valley (43°06'40.4"S 171°42'51.8"E). Solar radiation calculations have been performed in ArcGis Pro and are based on the top vegetation DEM generated by the LiDAR survey (May 20th 2019). RGB visualization (2 cm resolution) of the site (a) and LiDAR generated DEM (b). Predicted solar radiation in Wh/m² for a full summer (c) winter day (d) and the same winter day using a narrower colour scale to make patterns more visible (e).

Solar radiation maps based on the DEM (20 cm) generated in this study revealed clear advantages over traditionally available source material (8 m, Geographx; LINZ, 2016). The high-resolution topography information enabled me to estimate effects of slope, aspect and small-scale landscape features (e.g. boulders, trees) on the local light conditions at the Craigieburn valley. on the light regime (Figure 22).

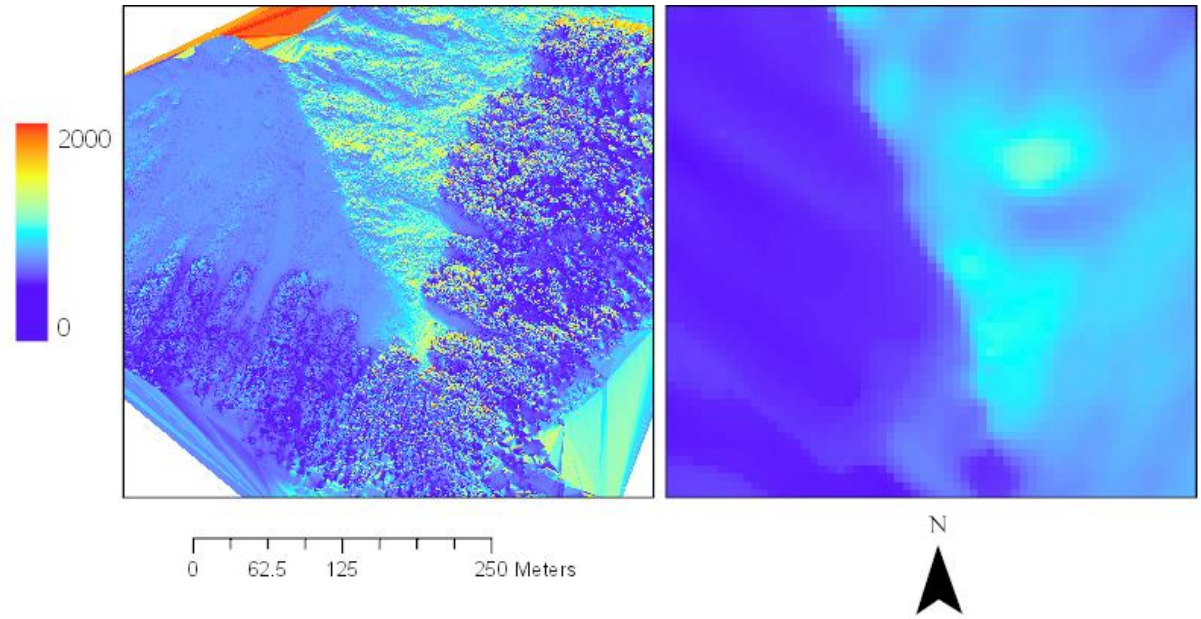

Figure 22: Effect of DEM resolution in predicting solar radiation regimes. The solar radiation map based on the airborne LiDAR DEM (left, 20 cm) is compared against traditionally available DEM (right, 8 m, LINZ, 2016) source material for the Craigieburn Valley in austral winter (May 20th).

Thermal imageries for the Craigieburn Valley provided a detailed illustration of the temperature daily temperature fluctuations in the alpine treeline ecotone for an austral winter (Figure 23). The results improved our understanding of how thermal variability is modulated by topography, vegetation and other land cover types (e.g. vegetated/non-vegetated) on the thermal environment in the subalpine belt. When comparing temperature range and ground cover type (Figure 24), I identified large differences between non-vegetated (scree) and vegetated areas. While all vegetated ground cover types largely buffered the temperature fluctuations along the eastern slope, the scree areas heated up rapidly resulting in huge temperature differences of up to 40 °C during the day.

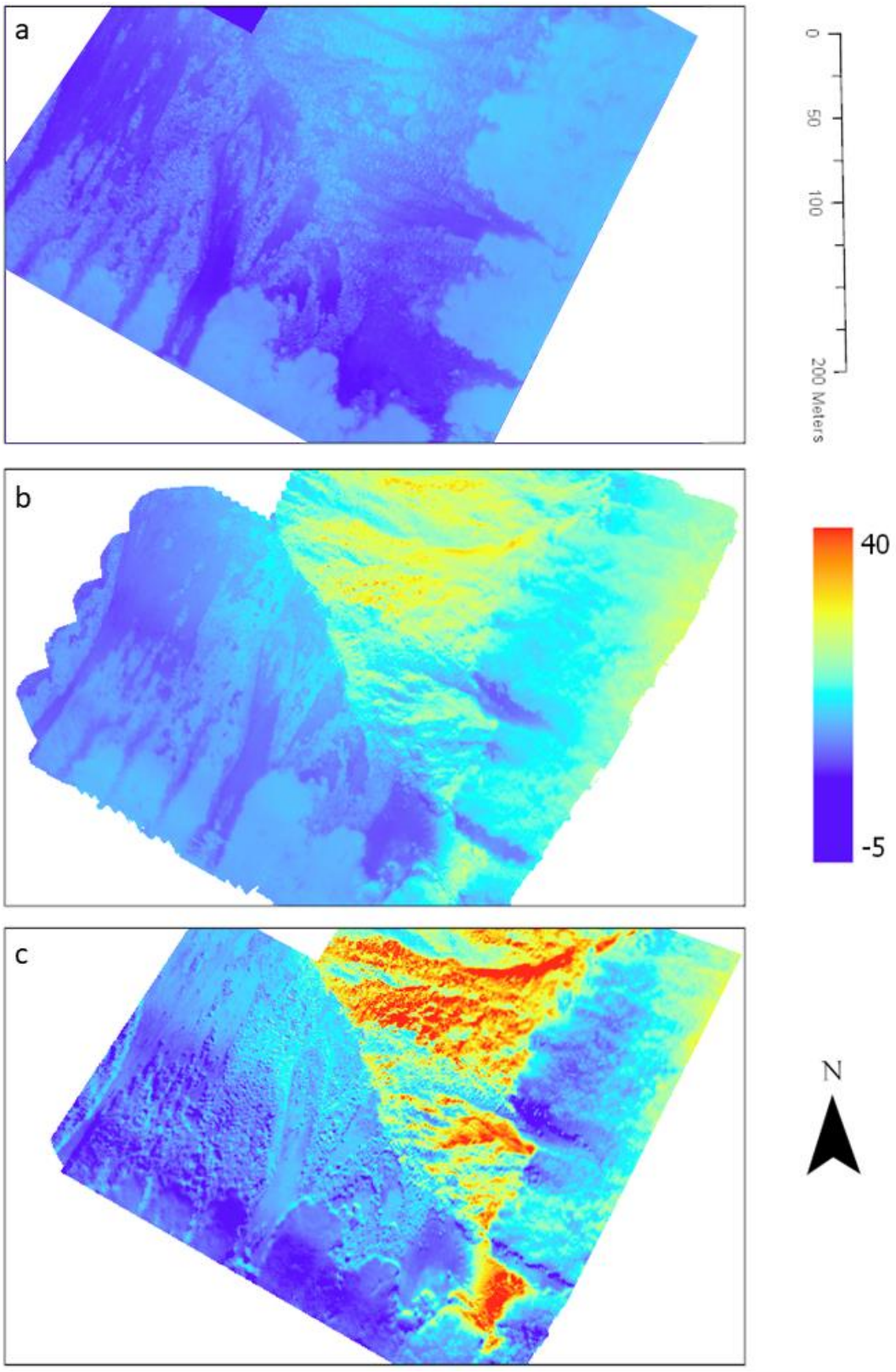

Figure 23: Results for the morning and noon thermal flights at Craigieburn (austral winter, 2019). Temperature recordings (°C) of the UAV flights on May 20, 2019 (FLIR Duo Pro R, 640x512 resolution, 7.5 – 13.5 µm) for the morning flight (top), the noon flight (centre) and the differences between both flights (bottom).

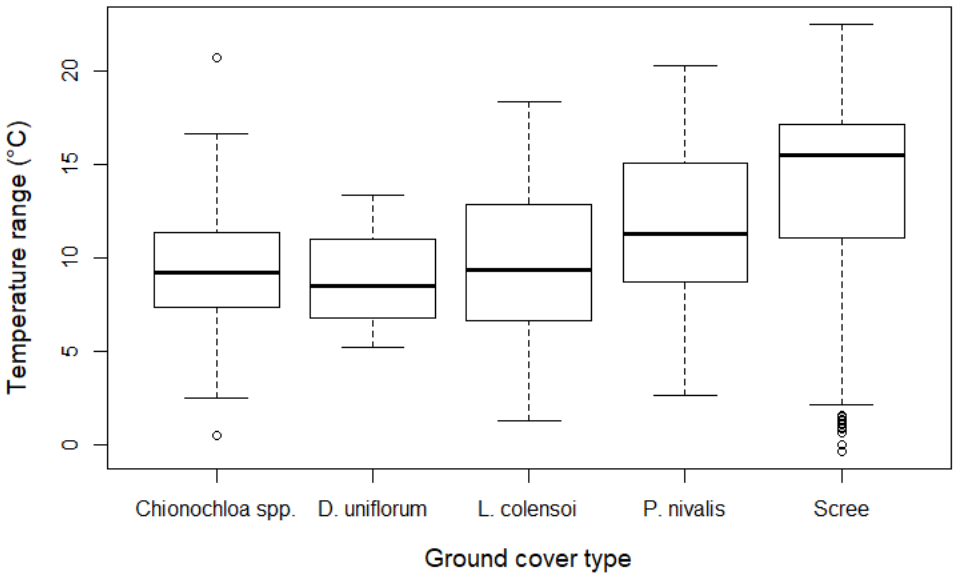

Figure 24: Diurnal temperature range by ground cover type. Median temperature difference between morning and noon UAV flights (20 May) on east facing slopes of the Craigieburn Valley.

The random point dataset was subsequently been used to illustrate the relationship between incident solar radiation and induced temperature range (Figure 25). There was a positive relationship between both climatic variables, underscoring the role of aspect and topographic heterogeneity in controlling fluctuations within the temperature regime at treeline.

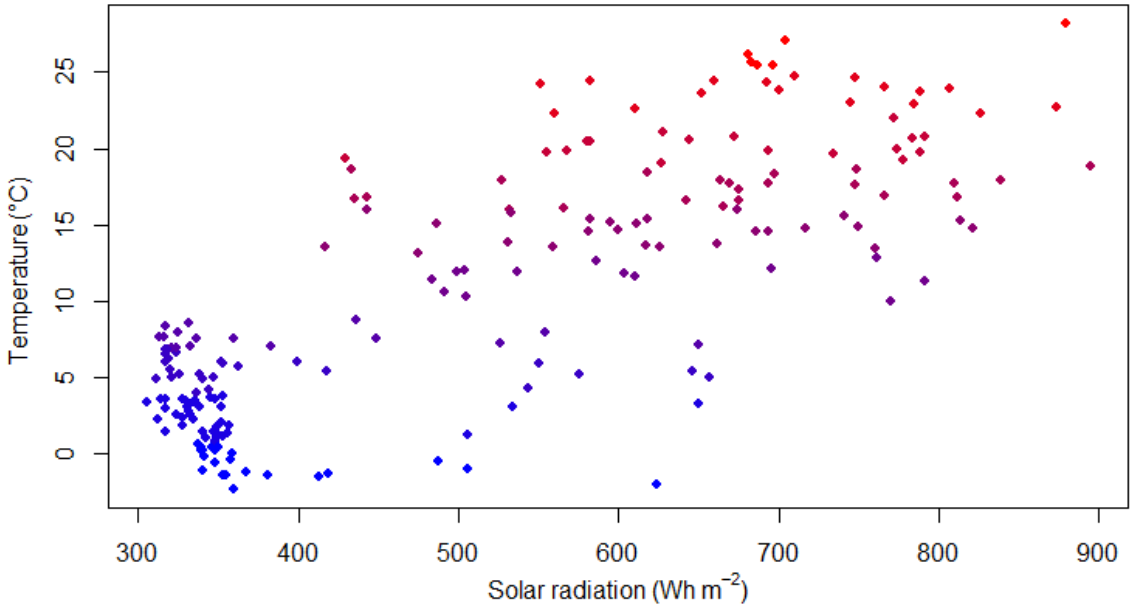

Figure 25: UAV-derived temperature profile (afternoon flight) as a function of the calculated incident solar radiation at Craigieburn on May 20, 2019.

Pulse difference methods based on ground and top-vegetation digital elevation information enabled me to generate a comprehensive height estimate of every vegetation feature at the Craigieburn site. The plant height estimates (Table 7) revealed a moderate within class variation once I filtered outliers with some assumptions based on ground-survey data. Due to technical limitations (CPU/GPU) only a subsection of the 20,000 classified vegetation polygons is displayed (Figure 26).

Table 7: Overview mean vegetation heights estimates

Name	**Colour**	**Vegetation Height (m)**	**SD**	**Assumption**
Chionochloa spp.	Orange	0.568	0.2	Below 1 m
Leucopogon colensoi	Red	0.328	0.112	Below 0.5 m
Podocarpus nivalis	Light Green	0.587	0.198	Below 1 m
Dracophyllum uniflorum	Yellow	0.559	0.197	Below 1 m
F. cliffortioides	Teal	6.603	2.521	Below 10 m, above 1 m

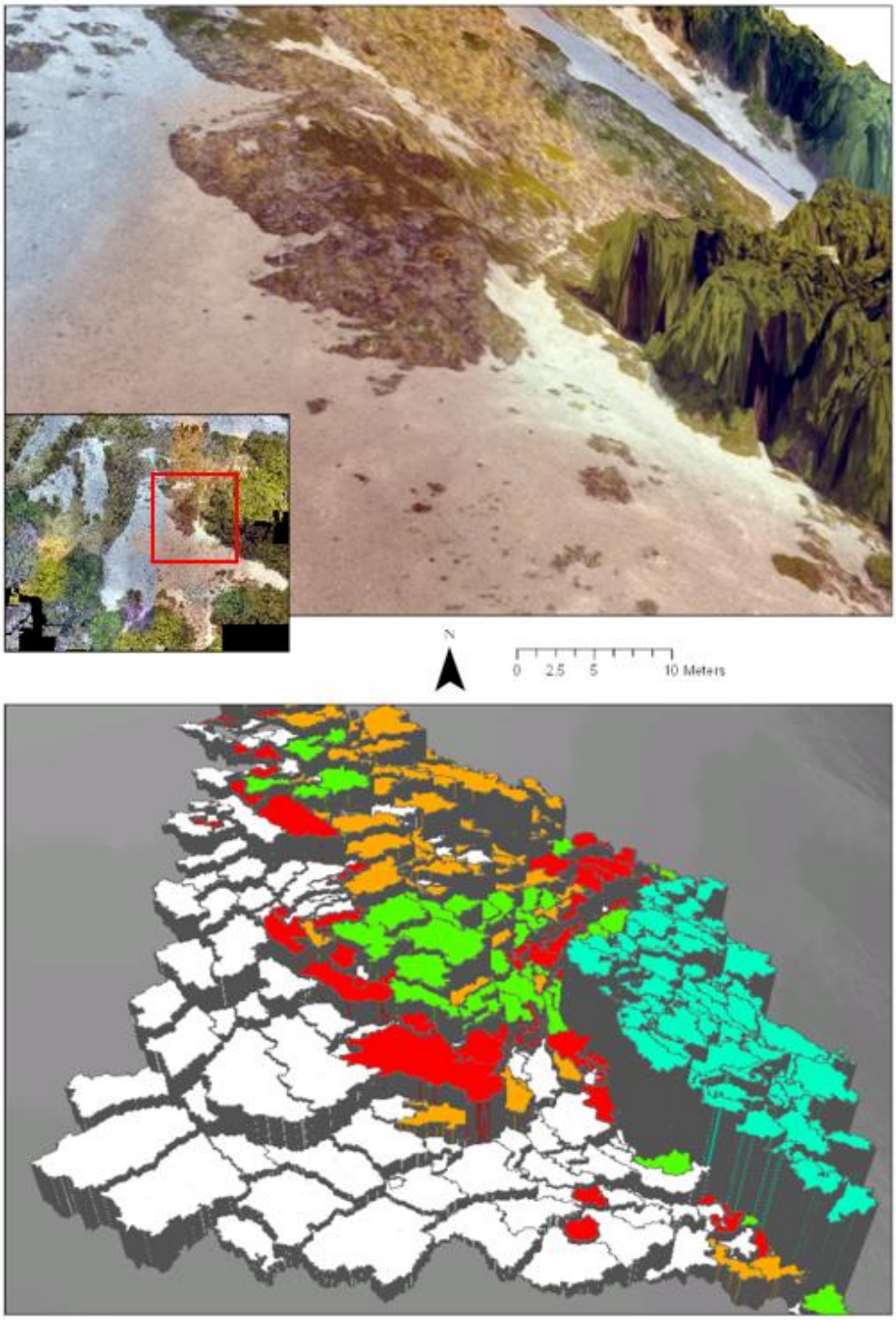

Figure 26: 3D Visualisation of selected vegetation height for identified microhabitats at Craigieburn Valley. (Top) Ground cover DEM (1 m, exposed) and canopy DEM (20 cm, forest) with RGB imagery (2 cm). (Bottom) Visualized vegetation height calculated via the pulse difference method on ground cover DEM (1 m, complete site). *F. cliffortioides* (teal), *P. nivalis* (green), *Chionochloa* spp. (orange), *L. colensoi* (red) and scree (white). Note that the displayed height is the individual height and not an averaged mean.

The combination of topography and seedling information from the transect data enabled me to illustrate three decades of seedling regeneration patterns into the subalpine (Figure 18). By selecting sub-samples of the treeline census program, I was able to readily swap between results of field studies throughout the year and display seedlings with their correct height and position in the field. I used the top- and bottom-derived DEM as a 3D mask for the drone-derived RGB, which has been draped over the topographic information acquired by the LiDAR sensor (Figure 27). The DEM beyond the canopy has been re-sampled to a coarser resolution (1 m) to reduce noise on the surface layer. Re-sampling the ground elevation model for the 3D visualisation of the seedlings is a common procedure that retains high-quality elevation information (Vaze et al., 2010) and prevents occlusion of the 3D seedling visualisation by LiDAR-sensed seedling-level data. The result was a spatial layer locating every seedling recorded in each of the four treeline census surveys at a georeferenced coordinate position within the current treeline ecotone. This enabled the information for presence/absence, growth performance and new recruitment over the four measurement periods to be linked to the results of the image classification, thermal imagery, LiDAR dataset, and associated environmental data (Chapter 3).

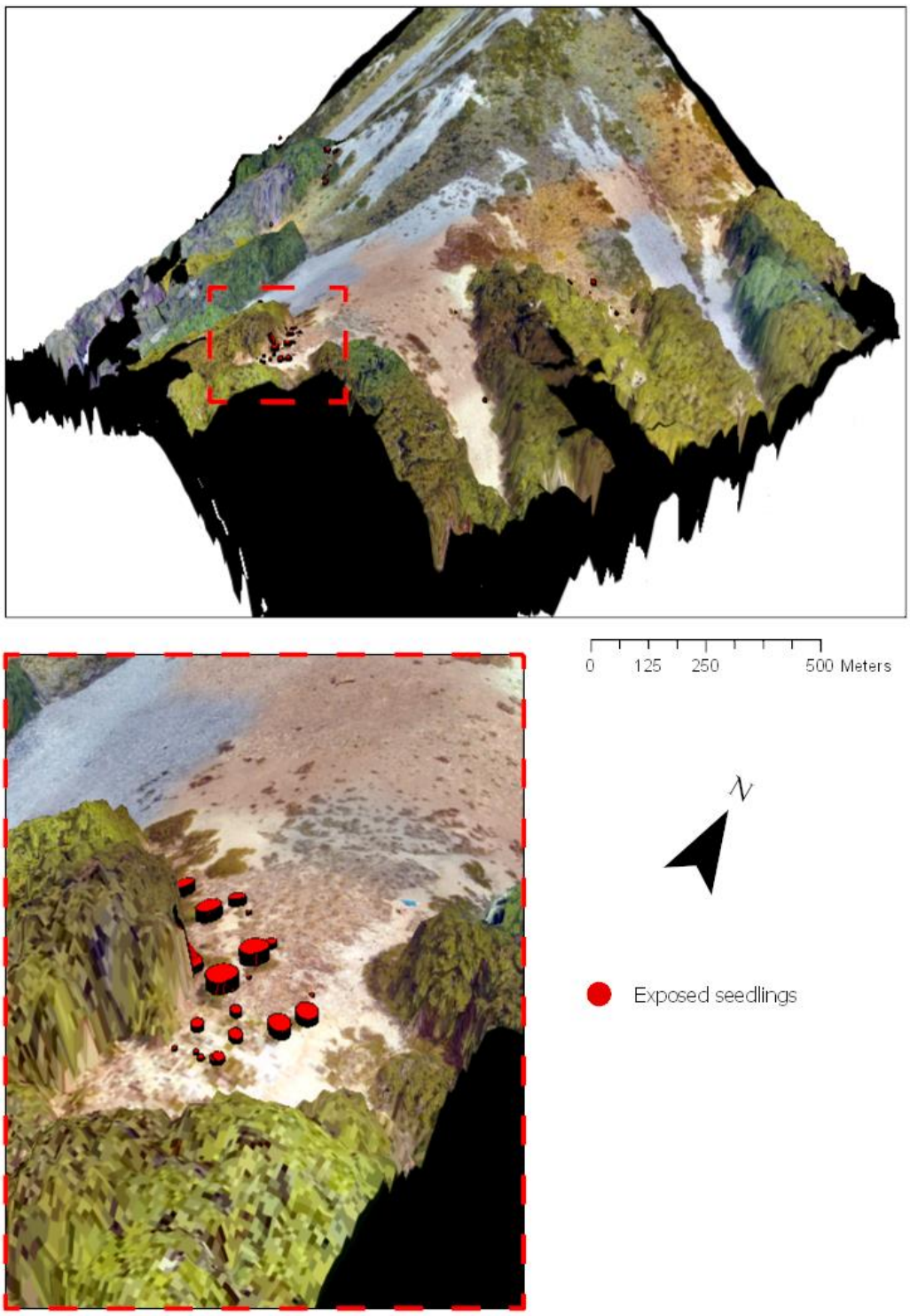

Figure 27: 3D Visualisation of the Craigieburn site with seedling position and height. The illustration uses the drone derived RGB imagery (2 cm resolution) and drapes it over the ground level DEM. The RGB information is draped over top vegetation (canopy) and the ground DEM. Seedling position from the treeline census dataset are spatially located along the transect and their recent height recordings (summer 2019) and exaggerated diameter (= height) are displayed.

The advantages of UAV-derived datasets over the traditionally available satellite DEM (8 m) for this region, become apparent in investigations of the fine-scale resolution of the topography and solar environment combined with seedling monitoring data (Figure 28). The LiDAR dataset (20 cm) enabled me to highlight the shading potential of individual trees (Figure 28c-e) and the adjacent treeline (Figure 28d,e) modulating the radiation environment at each site.

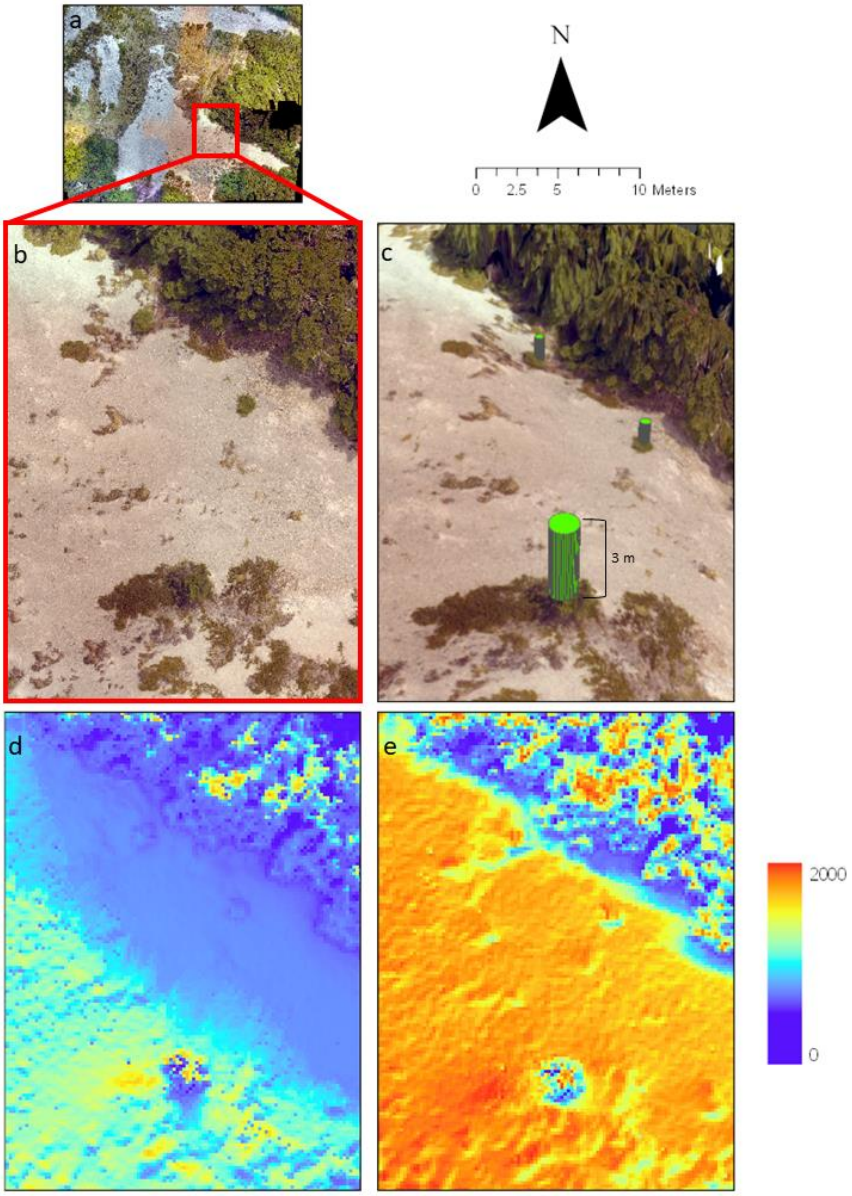

Figure 28: High DEM quality enabled shading potential of individual trees. (a) Craigieburn Valley site with (b) RGB imagery (2 cm) and (c) 3D visualization of exposed *F. cliffortioides* trees measured as part of the treeline monitoring program. (d,e) Solar radiation projections (Wh/m²) based on DEM (20 cm) in ArcGIS Pro enabled the illustration of shading potential of the treeline in (d) winter and (e) summer.

Overlaying top vegetation DEM (20 cm) with the thermal range (morning vs noon) enabled me to characterise thermal niches in the alpine treeline ecotone with remarkable precision (Figure 29). Solar information was software calculated (Figure 29b) based on the position of the sun, the thermal information was UAV derived (Figure 29a,c).

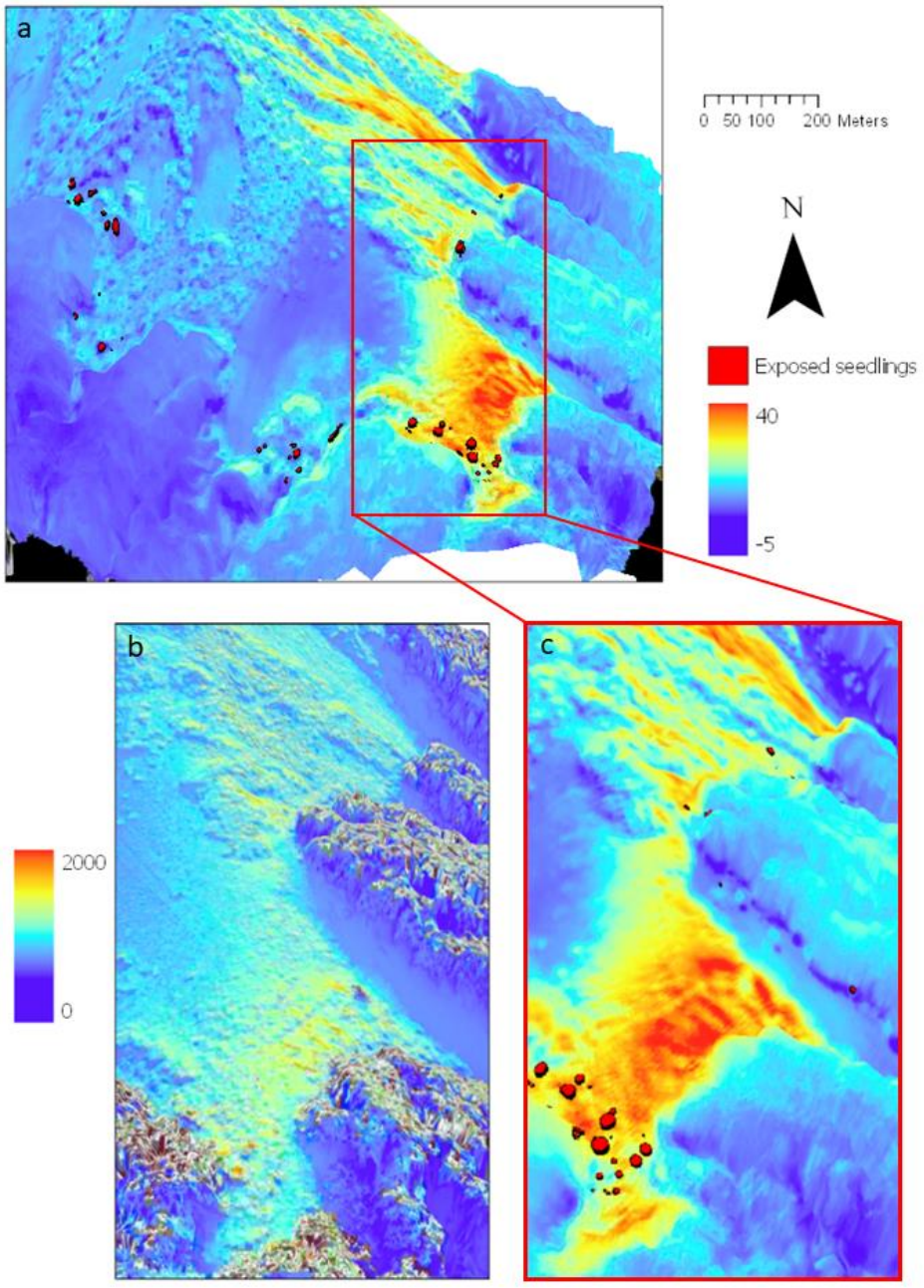

Figure 29: 3D Visualisation of the Craigieburn site with seedling position and height. The thermal difference information (20th May 2019, morning vs noon) above canopy is draped over the top vegetation DEM (a, c). Seedling position from the treeline census dataset are spatially located along the transect and their height (summer 2019) and diameter (= height) information were displayed and compared against the calculated solar radiation (b, Wh/m²) for the same winter day.

2.4 Discussion

The novel dual image capture approach harnessing the power of UAV-mounted RGB and multispectral cameras allowed me to create a detailed classification of the alpine treeline ecotone. By supplementing the datasets with topographic, thermal and radiations maps and linking the results to three decades of seedling monitoring data we can investigate the role of relevant abiotic limitations hampering current treeline advance.

Classification procedures profited immensely from the centimeter resolution datasets (Yan et al., 2019) and particularly the delineation of vegetation boundaries based on multispectral-derived NVDI data revealed remarkable accuracy (Table 5 & 6). The results highlighted the important synergy between UAV deployment, high resolution datasets and vegetation indices for mapping vegetation cover (J. Chen et al., 2016; Weiss & Walsh, 2009). Separation between vegetation types revealed inconsistencies for smaller plant associations (e.g. *Dracophyllum* spp. 60 to 90 %, *Podocarpus nivalis* 60 to 80%) due to a high overlap in the spectral bands predominantly used for the separation (> 30 %, NDVI, green (RGB)) and the minimum object size selected for the classification algorithm. The high consistency in identifying *F. cliffortioides* was probably at least partly attributable to the lack of fragmentation of the closed canopy and its abrupt transition into the subalpine belt ecotone. The selected minimum object size within the classification algorithm prevented consistent identification of individual seedlings (< 1 m) within the subalpine belt.

The recommended use of airborne LiDAR sensors (Cawood et al., 2017; Gallay et al., 2013) facilitated orthorectification procedures (Šašak et al., 2019) and helped creating ancillary datasets such as the solar radiation calculations and vegetation height (Weiss & Walsh, 2009). While limitations in the sensor resolution restricted consistent estimates of plant height, the issue is expected to be resolved with higher quality sensors and enhanced sampling rates where the laser is more likely to fully penetrate the vegetation cover. The final output revealed an estimate of microhabitat height for over 20,000 classified objects within the Craigieburn site and illustrated effects of mechanical insulation (facilitative feedback; Harsch & Bader, 2011) within the vegetation microhabitats (see Chapter 3).

Seedling regeneration patterns within the subalpine are often hampered by cold-induced photoinhibition processes. The effect of existing alpine vegetation in modulating the light environment has long been theorized in this context (Ball et al., 1991) and I was able to spatially characterise it (Figure 28). Winter solar projections revealed that seedlings which recruit close

to the existing treeline on east-facing slopes are in a state of perpetual shade close to the winter solstice (Fig. 28). This is particularly relevant for treeline sites which are believed to be limited by cold-induced photoinhibition (Ball et al., 1991; Germino et al., 2002; Reyes-Díaz et al., 2005; Sakai et al., 1981; Chapter 4). If an alpine treeline ecotone is constrained by coinciding frost and high radiation but seedlings successfully recruit within the prolonged shades in winter, we can narrow down the relevant season for this potential recruitment bottleneck. The solar radiation environment can be calculated readily for georeferenced digital elevation models and therefore provide a powerful tool in predicting light limited ecotone boundary shifts in alpine zones.

Exposed, east-facing scree slopes heated up quickly throughout the day resulting in temperature differences of up to 35 °C between morning and noon flights (Fig. 23). The detailed topography data derived with LiDAR technology facilitated the process of spatially locating the thermal profile (Boesch, 2017). The fine-scale 3D thermal profile of the subalpine belt is an important tool to help us understand how temperature is modulated by topographic features and vegetation at site. The identification of taller, exposed features of plant communities can help us understand the role of humidity, solar radiation and wind speed control the thermal variability of a species (Leinonen et al., 2006; Smigaj et al., 2015). Further, I was able to identify differences in the temperature range exposed on the predominately east-facing slope of the Craigieburn site. Randomized point values for the diurnal thermal range (morning vs noon, austral winter) revealed the effect of ground cover type on the temperature deviations experienced by the plants. Temperature fluctuations were more pronounced for non-vegetated surfaces and the classified microhabitats within the subalpine were able to buffer the temperature variability in the subalpine. This effect is discussed in more detail in the following chapter (Chapter 3).

The methodology to georeference seedling transect data to its spatial context and relevant ecological drivers revealed an immense potential in deciphering the role of microhabitat characteristics in facilitating seedling establishment (e.g. thermal/light regime) and hence future treeline migration. The workflow of georeferencing existing transect poles requires little effort and enabled me to use long-term monitoring data and put it in a spatially explicit context. This information can be visualized in the 3D space and linked to seedling performance (recruitment, growth, mortality), microhabitat features (radiation, thermal, topography) and ground cover type (for analysis see Chapter 3).

The combination of high resolution spectral, topographic and temporal data into a data generation pipeline highlights its potential to become a powerful tool for alpine treeline ecotone research. The workflows introduced within this chapter enabled me to create a detailed characterisation of the ecotone and put current research questions (seedling recruitment bottleneck) into a spatially explicit context where we can predict variation in the thermal and light regime throughout the year. Existing monitoring data for ecotone migrations benefits immensely by linking seedling position to spatially identified microhabitat features and can be used for consecutive microhabitat studies (Chapter 3). The methodology is currently only limited by the resolution of the sensors and the 'weakest link' is the poorest resolution dataset used for the interpretation (Weiss, 2009). With technological advances we will be able to employ sensors capable of further discrimination of vegetation types and even differences in phenological stages (Weiss, 2009; Weiss & Walsh, 2009). The combination of a spatially explicit characterisation of the subalpine with long-term seedling census data within an alpine treeline ecotone provide a huge step forward in understanding ecotone boundary dynamics and identifying the role of microhabitat heterogeneity and availability of climatic niches to facilitate migration patterns.

3 The role of subalpine microhabitat variability in controlling tree seedling regeneration patterns

3.1 Introduction

Disentangling the ecological factors that control species' range limits is a challenging, long-standing aim in ecology (Louthan et al., 2015). As the effects of climate change accelerate, it is critical to understand how tree populations at their high-elevation treeline boundaries are likely to respond to changes in environmental conditions, and thus whether they are likely to migrate uphill. Variations in local microhabitat conditions just beyond the treeline can have a large impact on determining the fate of dispersing tree seeds into the treeline ecotone in terms of providing 'safe sites' for seedling recruitment and survival (Elliott, 2011; Harsch & Bader, 2011; Pyatt et al., 2016; Scherrer & Körner, 2010). These safe sites typically comprise a set of conditions, often created by the shading or cooling effects from other vegetation or physical objects, that overlap the fundamental niche of dispersing tree species and thus facilitate seedling establishment and growth (Batllori et al., 2009; Resler et al., 2005). Treeline migration can be hampered by the availability of these microclimatic niches which reduce the effect of a pronounced macroclimatic stress gradient above treeline (Alftine & Malanson, 2004). 'Tipping points' for treeline advance are reached once a sufficient number of favourable microhabitats effectively suppress macroscale-imposed limitations in the open shrubland to allow a closed-canopy forest to develop. However, we currently lack fine-scale spatially explicit datasets at the treeline to characterise micro-climatic opportunities in the subalpine. To predict future treeline migration, we are required to monitor changes in vegetation community dynamics and predict their role in controlling tree regeneration in the subalpine.

Treelines which show an abrupt transition into the subalpine belt ('abrupt treelines') remain relatively unresponsive to global warming (Harsch & Bader, 2011) and vary with species and site limitations (Treml & Veblen, 2017). Such abrupt ecotone transitions are hypothesised to be the result of drivers predominantly acting on the vulnerable recruitment stage, where pronounced fine-scale stressors in the treeline ecotone cause early dieback which often leads to seedling mortality (Germino et al., 2002). Thus, seedlings recruiting successfully into the abrupt treeline ecotone frequently occur in safe sites that provide thermal conditions decoupled from ambient air temperatures (Batllori et al., 2009; Malanson et al., 2011; Scherrer & Körner, 2010). In particular, the presence of previously-established conspecific or other trees in the ecotone can promote treeline advance patterns due to snow retaining effects (Bekker,

2005), protection from abrasion (Bekker & Malanson, 2008), or the provision of a sheltering canopy (Šrůtek et al., 2002); other topographic features such as boulders and terrace risers can also serve a similar protective role (Resler et al., 2005). Thus, such features can provide stepping-stones for a species ecotone shift, allowing migrating species to escape negative effects associated with broader-scale changes in climatic stressors such as air temperature (Graham et al., 2012; Scherrer & Körner, 2010).

In New Zealand the ecotone transition from the two treeline forming beech species *N. fuscospora* and *N. lophozonia* into the subalpine belt is remarkably abrupt (Wardle, 2008). This indicates that the current altitudinal limits of the treeline are only partially restricted by gradually declining mean growing season temperatures with altitude. This finding is in line with the hampered upslope advance of these species, showing little response to macroscale drivers despite increased seed production over the last 30 years (Richardson et al., 2005) and an average temperature increase by 0.9 °C (Mullan et al., 2008). This is further supported by a 15 year long treeline census where the results show no evidence for a forest expansion and the authors attribute this to a recruitment limitation within the adjacent subalpine belt (Harsch et al., 2012). Studies suggest that the current treeline position is created by multi-scale effects, where macroscale thermal drivers at broader scales are modulated by physiological and disturbance type drivers at finer scales (Case & Duncan, 2014).

Seedling colonialisation in the subalpine can be induced by the presence of favourable climatic sites which mimic microhabitat conditions under the forest canopy and decrease the environmental gradient by clear positive directional feedbacks (Alftine & Malanson, 2004). Previous studies have indicated that the presence of adult trees protect early recruits underneath the canopy from frost and radiation, facilitating their initial establishment (Norton & Schönenberger, 1984; Wardle, 1971, 2008). Further, there is some evidence that other, low-statured vegetation in the above-treeline subalpine belt can also provide such a protective role. The vegetation in this zone is dominated by low to medium stature tussock grasses (*Chionochloa* spp.), *Dracophyllum uniflorum*, *Podocarpus nivalis* and low lying prostrate mats of *Leucopogon colensoi* (Figure 30). A previous field study revealed seedling preferences towards sheltered, bare soils, suggesting that beneficial, interspecific associations only occur if there is a balance between facilitation and competition for resources (Harsch, 2010). Thus, the probability of establishment of beech seedlings in this subalpine zone is dependent on the quality and spatial availability of these microhabitats. By studying the spatiotemporal patterns of seedlings that have recruited into the subalpine belt ecotone, we can gain insight into the

potential role of microhabitat features that might in enable new upslope recruitment in these abrupt treelines. In turn, this insight will provide a basis for predicting the pace of treeline ecotone shifts in the face of a rapidly changing climate.

Figure 30: View on subalpine vegetation classified in Chapter 2 (*Chionochloa* spp., *L. colensoi* intersected with scree), adjacent to the *F. cliffortioides* treeline at Craigieburn Valley (Döweler, ca. 1pm, January 27th, 2018, 43°06'40.4"S 171°42'51.8"E).

Our best dataset for current treeline dynamics in New Zealand is provided by the southern beech treeline monitoring transects established by P. Wardle and colleagues in the summer 1990 and 1991 at five treeline locations across the country: Several of these transects were remeasured for the fourth time over the summer of 2019, providing a record of > 0.05 m tall southern beech recruits beyond established canopy (Harsch et al., 2012). This dataset provides us detailed information about seedlings at each site, but currently has not been put in the context of subalpine microhabitat biotic and abiotic heterogeneity. At the remeasured Wardle transect at the Craigieburn treeline site, I used the UAV-based data (Chapter 2),

microhabitat temperature logger data, and three decades of seedling census data which have been spatially-referenced, to explore spatiotemporal relationships between recruiting seedlings and treeline ecotone microhabitat variation.

This study aimed to map spatial patterns in *F. cliffortioides* recruitment and growth in the subalpine and relate those patterns to microhabitat variation. I measured microhabitat variation at one treeline site encompassing multiple elevations, aspects, slopes and vegetation cover. I hypothesized that seedlings would be more likely to recruit into favourable microhabitats which reduce seedling exposure to macroscale-imposed climatic extremes (e.g. temperature, radiation) and, therefore, successful tree colonialization of the subalpine is limited by the availability of favourable microhabitats. Further, I hypothesized that favourable microhabitat effects would also be reflected in seedling growth rates, and specifically, that morning temperature, aspect, and vegetation cover would predict seedling growth.

3.2 Material & Methods

3.2.1 Study area

This study took place at the Craigieburn Valley (-43.111, 171.713) site, 1365 metres above sea level on a southeast to southwest aspect on the east side of the South Island's Southern Alps. The site shows frequent frost events throughout the year (135 frost days) and has an annual rainfall of *c.* 1300 mm. The adjoining subalpine zone is characterised by herbaceous shrub communities, dominated by *Chionochloa* spp. tussock grass species, *Dracophyllum uniflorum* Hook.f., *D. longifolium* (J.R.Forst et G.Forst.) and/or *Podocarpus nivalis* (Hook.) woody shrub patches, prostrate mats of *Leucopogon colensoi* (Hook), and individuals of *Hebe* spp. and *Aciphylla squarrosa* (J.R.Forst. et G.Forst) occupying some zones between tussocks and woody shrubs. Interspersed across the more arid terrain of the Craigieburn Valley are bare scree slopes; *Leucopogon* and *Hebe* spp. are the first plant species to establish in these areas

3.2.2 Initial parameterisation of the ecotone

The analysis in this chapter used a number of datasets representing abiotic variation, vegetation distribution, and beech seedling locations, across the Craigieburn alpine treeline ecotone (described in detail in Chapter 2) In brief, these datasets included: (1) a GIS vector polygon layer of six vegetation types which were delineated via a supervised classification using UAV-

collected colour (RGB - 2 cm) and multispectral (5 cm; Red, Green, Near-IR, Red edge) imagery; (2) high spatial resolution thermal data acquired for morning and noon flights (20th May, 2019) using a is a FLIR Duo Pro R, with a 640x512 resolution, 7.5 – 13.5 µm spectral bands, 9 Hz thermal frame rate and a 32° field of view (FLIR Systems, Wilsonville, OR, USA); (3) a digital elevation model (DEM, 20 cm) generated from UAV-collected LiDAR data; (4). seedling information (positions on the transect, survival, size) taken at three measurement times, over a 30 year period, from Wardle's (1991) Craigieburn treeline monitoring transect, which I accurately geo-positioned using a differential GPS; and (5) incident solar radiation (Wh/m²) calculated in ArcGIS Pro (2.3.3) based on the 20 cm DEM for different time periods (day of UAV flights, seasonal sums, annual sum). The five datasets were compiled as spatial layers in ArcGIS. Based on the position of the forest edge, a 40 m distance polygon was created to represent the potential recruitment zone for beech seedlings (Figure 31); beech seedlings are typically found within 10 m of the forest edge, although individual, larger beech trees occasionally occur up to 20 m or so further uphill.

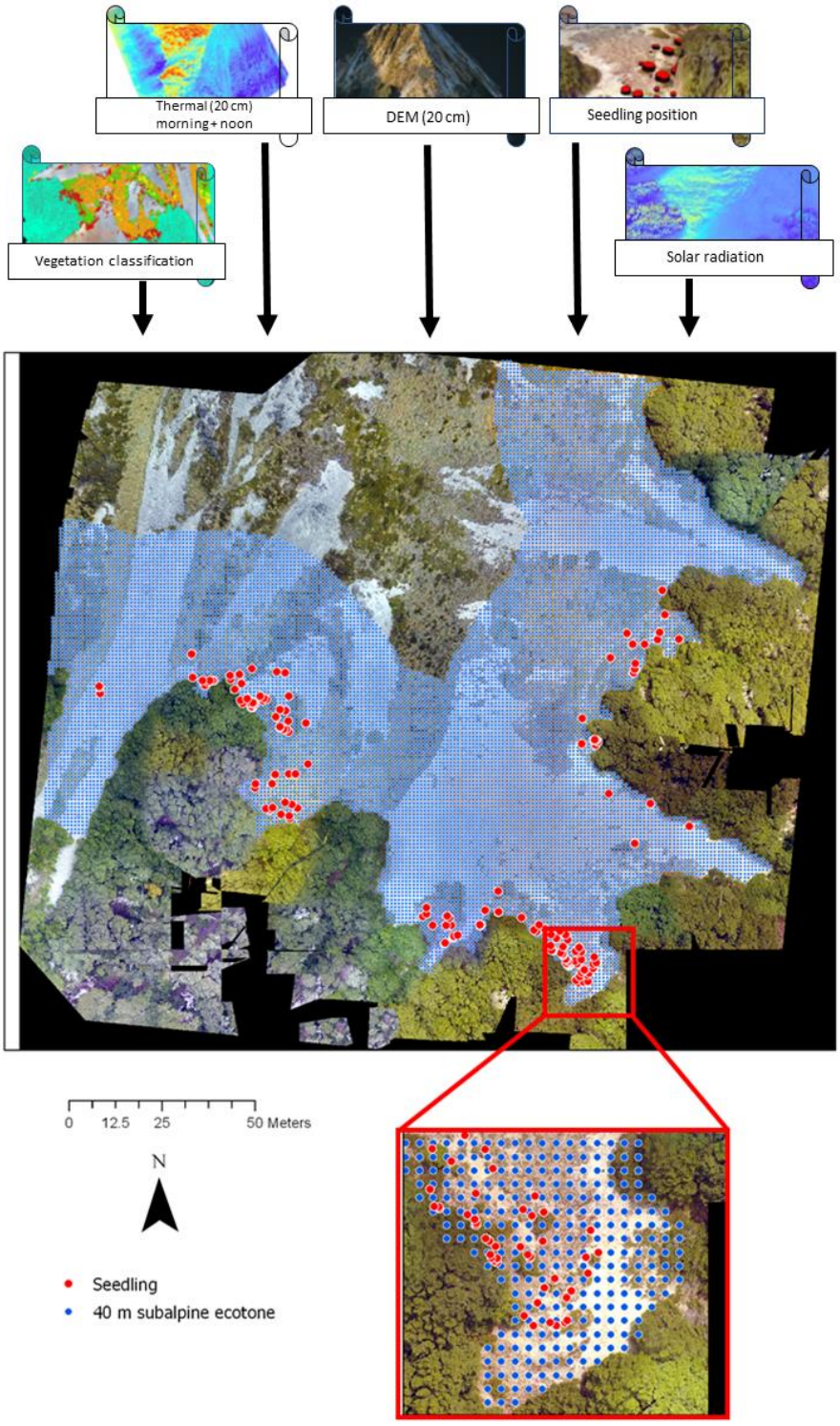

Figure 31: The main spatial datasets used for modelling microhabitats and seedling-microhabitat relationships within the 40 m treeline ecotone zone (blue) for the Craigieburn Valley. Environmental variables (incident solar radiation (year, summer/winter day, thermal information (morning, noon, difference), slope) were sampled for every m² (blue points). Seedling positions (red points) were extrapolated from Wardle's treeline transect information (Chapter 2).

3.2.3 Exploring spatial patterns of seedling recruitment

Seedling census data have been used to extrapolate position in the field from georeferenced transect poles. The study focused on seedling regeneration in the subalpine, therefore seedlings positioned below the established canopy were removed from the analysis. Each seedling contained information for the year they have been identified and height recordings for every consecutive treeline census. The seedling point data was combined with the classified ground cover dataset via a spatial join in ArcGIS Pro. The ground cover polygon contained calculated mean values for slope, received radiation, remotely sensed thermal information within the polygon which were added to the seedling dataset. To illustrate three decades of seedling regeneration patterns into the subalpine new seedlings identified in every census year were extracted and symbolized using a heatmap display within a 25 m radius (unweighted kernel density analysis). Seedling growth between 2007 and 2019 has been calculated by subtracting height information between both measurement periods.

3.2.4 Thermal microhabitat variability

To evaluate the temperature profile experienced by different microhabitats in the subalpine belt, in summer (Jan/Feb) 2019 I deployed a total of 18 temperature loggers (iButton, DS1921G-F5#, 2kB, ± 0,5 °C, −40 to +85 °C, Maxim Integrated, San José, CA, USA) along Wardle's Craigieburn treeline transect. The loggers were sealed in plastic bags and tied onto ropes close to the main stem of the seedlings sheltered from direct sun exposure, close to the center of the vegetation patch (*Dracophyllum*, *Podocarpus*, *Chionochloa*, *Leucopogon*). The remaining loggers were placed on established beech trees or 2 cm below scree/soil. For each logger, the measurement interval was set to 4 hours to enable the loggers to store data for approximately one year.

I explored the potential for using the high temporal resolution temperature data collected by the iButton sensors as a basis for modelling, predicting and mapping seedling-scale temperature conditions across the ecotone where seedlings are currently occurring. I extracted recordings from the 18 loggers at the Craigieburn site for which reliable data were available (Figure 32). The four-hourly data were summarised on a monthly basis, across all days for each month of the recorded year (2019), into monthly mean minimum, mean and mean maximum temperatures; from this dataset, annual statistics could be compiled. I used linear regression modelling to relate each of the summarised iButton annual min, mean and max temperatures to

four UAV- and GIS-derived variables at the logger locations (slope gradient, UAV morning thermal data, UAV noon thermal data, annual solar radiation sum). It was expected that the UAV/GIS-based spatial datasets, while representing different components of abiotic variation at different temporal resolutions, would be correlated with near-ground logger temperatures; previous studies have shown potential for up-scaling temperature logger data using coarser scale data (Fawcett et al., 2019; García et al., 2020; Scherrer & Körner, 2010). The "generalised linear regression" tool in ArcGIS Pro was used for the modelling. The built-in prediction functionality within the tool was then used to apply the regression model across the ecotone at a 1 × 1-m resolution to enable the spatial mapping of logger-based temperatures; this provided a means to relate seedling occurrence and growth to putative fine-scale temperature variation at the seedling scale.

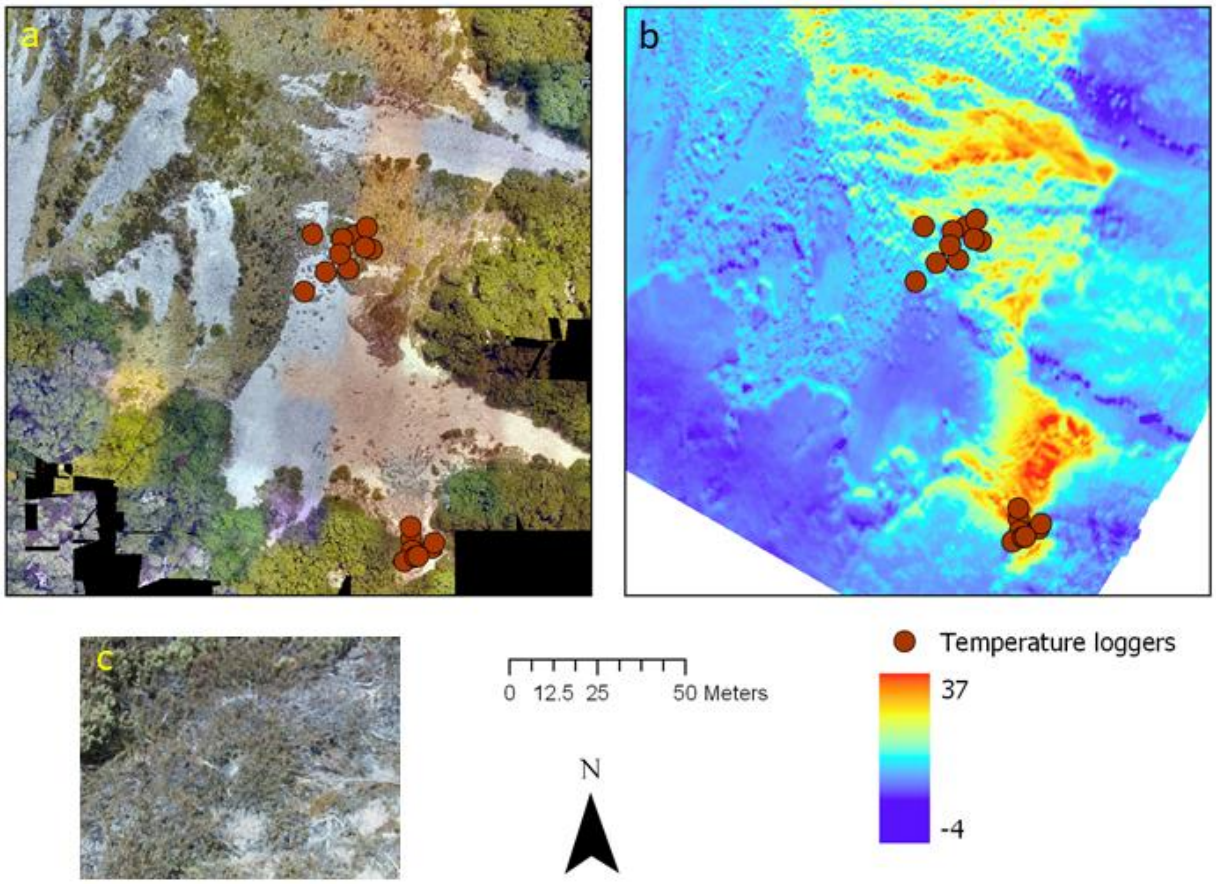

Figure 32: Microhabitat temperature logger position at the Craigieburn Valley treeline ecotone for the remotely derived RGB (a, 2 cm) and thermal difference datasets (b, morning vs noon). (c) Loggers were buried 2 cm below-ground or placed within the centre of subalpine vegetation.

3.2.5 Analysing seedling occurrence relative to microhabitat availability

I used three different approaches to characterise microhabitat variability occurring across the 40-m ecotone zone. First, I used the ground cover layer (*F. cliffortioides*, *Dracophyllum*, *Podocarpus*, *Chionochloa*, *Leucopogon*, scree) classified from the multispectral UAV image analysis (Chapter 2) as an initial way to represent microhabitat variation, assuming that these different vegetation types would reflect variation in possible safe site locations for recruiting seedlings.

Second, I used a multivariate analysis approach to explore if UAV- and GIS-derived thermal and solar radiation variables (see Fig. 38) cluster statistically into distinct thermal microhabitat types and whether these types also show clear spatial patterns across the ecotone. For this analysis, I applied the "multivariate clustering" tool within the ArcGIS Pro (2.2.3) software into a total of six feature clusters. The datasets (incident solar radiation (year, summer/winter day), thermal information (morning, noon, difference), slope) were standardised using a z-transformation to reduce impact of outliers and optimized seed locations. R^2 values reflect total variation retained from the source ranking the features which was able to discriminate best in the datasets (Jain, 2008). The data input to this tool comprised point 14,742 values representing grid cell centre points for a 1×1-m resolution vector grid laid over the ecotone zone (see Fig. 38). After clustering, the cluster classes could then be mapped back onto those points to enable a visualisation of the spatial pattern of the cluster analysis output.

Third, I used the three spatial layers predicting mean thermal environment in the subalpine and expected minimum and maximum temperature deviations throughout the year. I binned the values for each modelled temperature layer into six zones of equal size (16.7 %) using quantile symbolisation in ArcGIS Pro, giving a category centred on the mean and several standard deviation categories on either side of the mean.

I analysed whether seedlings surveyed within the ecotone at the time of the 2019 census were statistically more or less likely to be associated with specific microhabitats, standardised by the relative availability of the different microhabitats across the ecotone. This analysis was limited to the ecotone defined by the most distant seedling, which comprised a zone delimited by a 15-m distance from the treeline. To do this, each seedling was spatially intersected with, and assigned to, a microhabitat category as defined by the three methods outlined above (ie., cluster class, thermal quantile, and vegetation type). A test for given proportions was carried out in R ('prop.test', package *stats*, R Core Team, 2019). For each microhabitat type identified I tested if there was significant difference between relative microsite availability and actual

seedling occupancy. The resulting *P*-values were adjusted for multiple testing using a false discovery rate method (Benjamini & Hochberg, 1995).

3.2.6 Modelling seedling height growth against environmental variables

I used a forest-based classification and regression analysis within ArcGIS Pro to model the total height increment of censused seedlings in the ecotone that were present between the 2007 and 2019 measurement times (Figure 33). The algorithm operated as a machine-learning procedure and uses categorical and continuous variables (Table 8) to validate and rank explanatory variables in predicting the variability in the growth performance. Relative importance ranks the explanatory variables according to their predictive power. It is calculated using Gini coefficients which identify the number of splits made by individual trees relative to the forest. The forest based algorithm uses thousands of decision trees which individually act as a predictors relative to the entire 'forest' (Breiman, 2001, 2017).

Table 8: Overview of the twelve explanatory variables (Relative North/East, Slope, Solar radiation (winter, summer, year), thermal microhabitat (morning, noon, difference), NDVI, vegetation type, Cluster ID) used to predict exposed seedling growth between 2007 and 2019 at the Craigieburn Valley.

Explanatory training variable (unit)	**Subclasses (Min/Max)**	**Source**
Aspect (-1 to 1)	Relative North/East	Reclassified DEM (20 cm)
Slope* (°)	(7.2 / 50)	Reclassified DEM (20 cm)
Solar radiation* (Wh/m²)	Winter (62 /1863) Summer (749/5185) Annual (211k / 1321k)	Software calculated incident radiation based on georeferenced DEM
Thermal microhabitat* (°C)	Morning (-4.6/3.07) Noon (-0.6/17.73) Difference (-0.8/21.4)	Results for the two thermal flights
NDVI*	-	Calculated mean for vegetation patch based on multispectral data (Chapter Two)
Vegetation type	Categorical	Vegetation classification output (Chapter Two)
Cluster ID	Categorical	Multivariate cluster analysis output (1 m)

*Calculated mean within vegetation segment classified

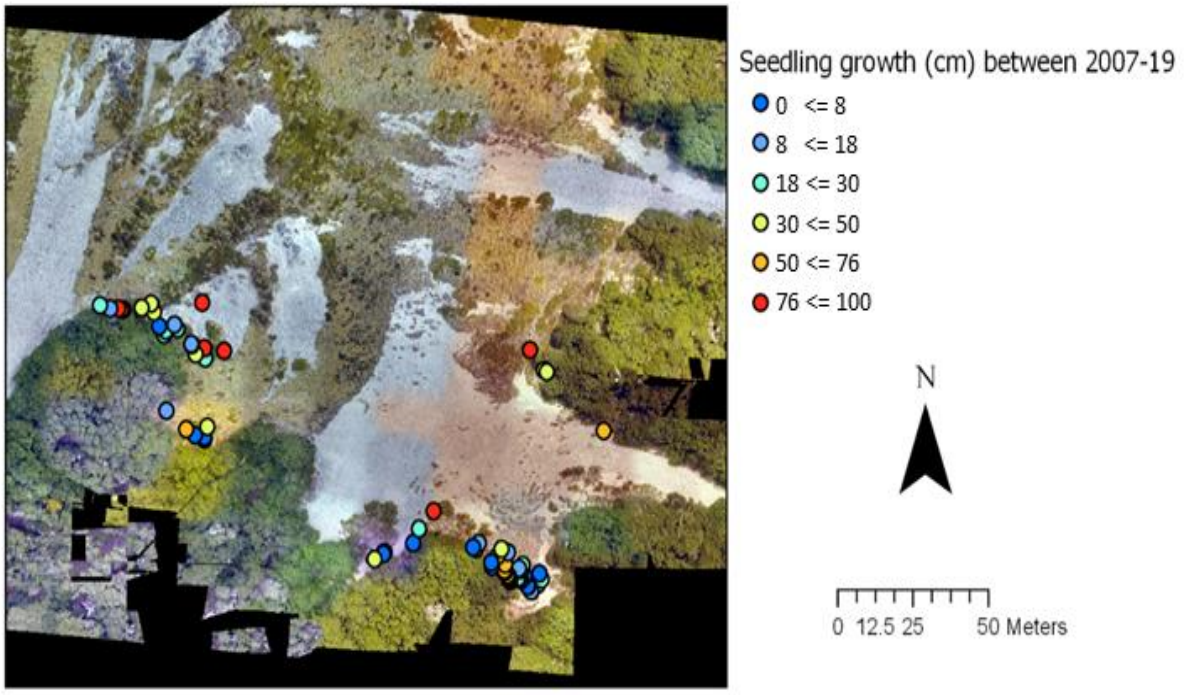

Figure 33: Seedling height growth (cm) as observed for 79 seedlings present in both the latest (2019) and previous (2007) measurement surveys along the Craigieburn Valley transect.

3.3 Results

3.3.1 Exploring spatial patterns of seedling recruitment

Extrapolating treeline transect data into a two-dimensional RGB layer of the subalpine treeline ecotone provided a spatial visualisation of seedling regeneration patterns into the subalpine (Figure 34). Seedling recruitment mapping showed three consistent recruitment hotspots over the three measurement periods; conversely, there are sections of the treeline transects that have shown no recruitment to date. New seedlings were concentrated on vegetated east and western slopes and the sparsely vegetated shallow plateau at the southern tip of the ecotone. Recruitment between 2002 and 2007 (383) was much higher than the other measurement times, where approximately three times as many new recruits were identified compared to 2002 (108) or 2019 (130). In the most recent census (2019) the predominant recruitment hotspots shifted towards the eastern facing slopes (Figure 34d).

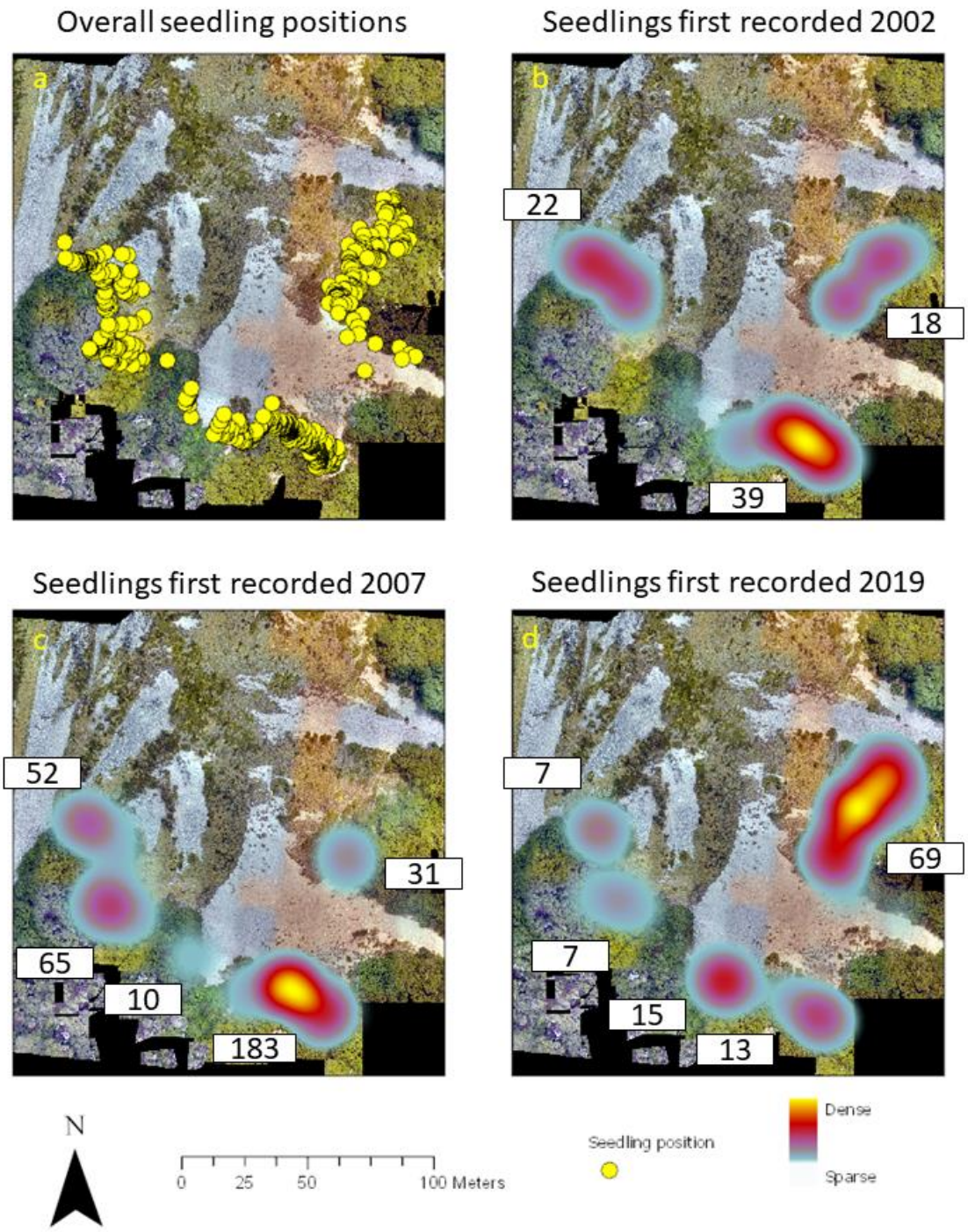

Figure 34: (a) Overall *F. cliffortioides* seedling position recorded as part of the treeline census in the Craigieburn Valley. (b-d) A kernel hotspot heatmap generated based on the densities of recruited seedlings identified in the respective census years. The numbers of seedlings recruiting in each time period and each hotspot zone are provided.

3.3.2 Thermal microhabitat variability

Thermal logger recordings for the Craigieburn Valley (Figure 35) revealed strong microhabitat temperature variability throughout the year. Microhabitat temperatures frequently exceeded 30 °C for bare ground, tussock grasses (*Chionochloa* spp.) and *Leucopogon* (austral summer, November to April). Winter periods of limited temperature variability can be used to approximate snow events. First annual snowfall in June and sustained periods of snow cover from July to September buffered daily thermal variability for all microhabitats (< 5 °C). Beech seedlings experience more frequent frost events throughout the winter due to their elevated logger placement (~ 10 cm aboveground) close to the base. Cold temperatures dips (< 2 °C) can be observed throughout the year.

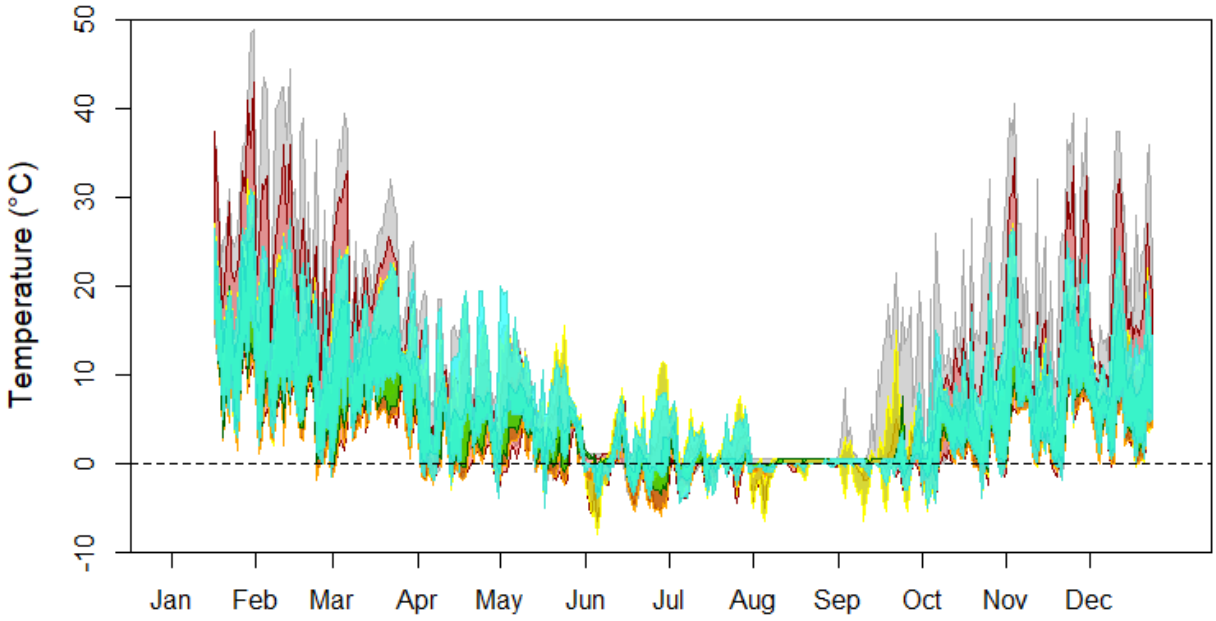

Figure 35: Diurnal temperature fluctuations for the alpine treeline ecotone at Craigieburn Valley. Fuscospora cliffortioides (teal), *Dracophyllum* spp. (yellow), *Podocarpus nivalis* (green), *Chionochloa* spp. (orange), *Leucopogon* (red), scree/bare soil (grey). Data sampled 6 times per day using thermal microhabitat loggers (iButton), for a measurement period of 11 months (2019).

Daily temperature variability for microhabitat types (Figure 36) showed significant differences between all microhabitats (multiple site comparison see Appendix A,
Table 24 & Figure 56). Microhabitat temperature range decreased throughout the winter period (< 10 °C, July to mid-September). Temperature variability increased towards the summer months and frequently exceeded 15 °C. Highest variability was identified in the scree and low-density prostrate mat *Leucopogon* which frequently experienced temperature ranges above 25

°C throughout the summer. The presence of vegetated ground cover confined temperature variability for every scenario tested.

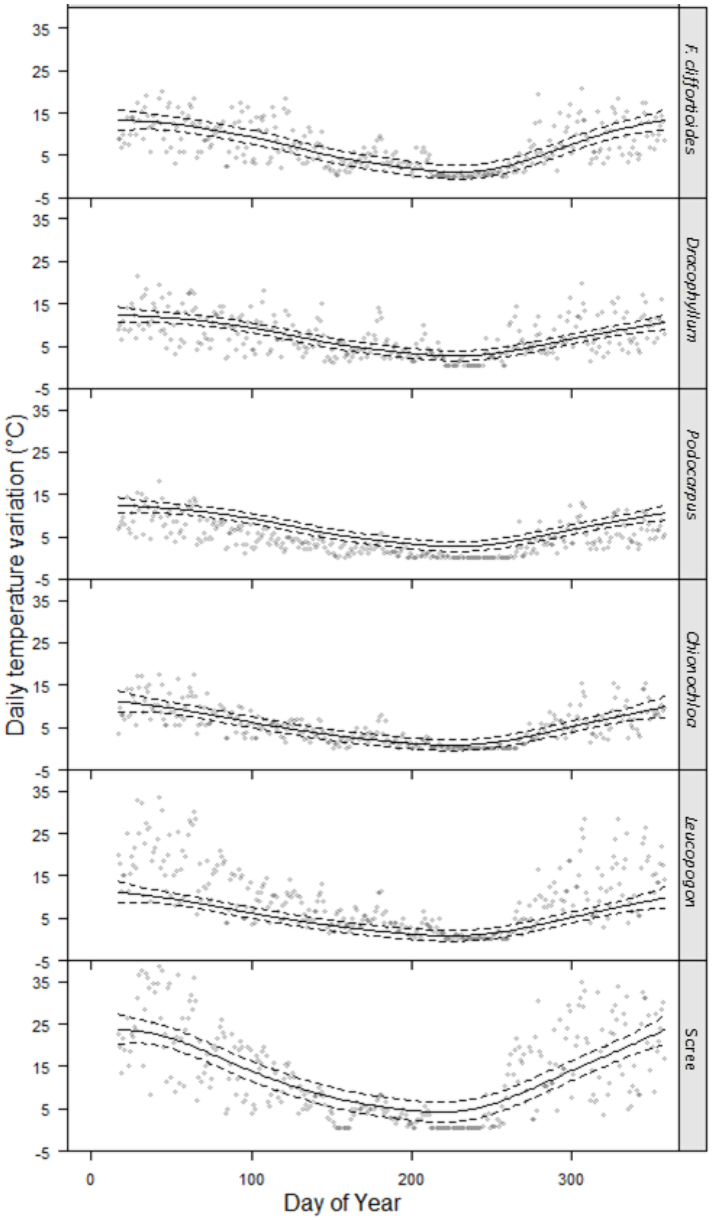

Figure 36: Diurnal temperature variation (range) from lowest to highest recording. From top to bottom row, microhabitats sorted by height: *Fuscospora cliffortioides*, *Dracophyllum* spp., *Podocarpus* spp., *Chionochloa* spp., *Leucopogon*, scree. Data sampled six times per day, for a measurement period of 11 months (2019).

Predicted thermal zones (Figure 37 b-d; min, mean, max) derived from the thermal microhabitat loggers show extreme temperature deviations in similar patterns as the UAV

derived thermal imagery (Figure 37a). Particularly in non-vegetated areas and the shallow or east-facing slopes warmer temperature deviations can be identified. This consistent with the seedling recruitment heatmaps which showed seedling regeneration patterns in the east-facing and shallow slopes (Figure 34). Cold temperature deviations are primarily observed at steeper, east facing aspects, where the abrupt canopy is casting perpetual shade during winter.

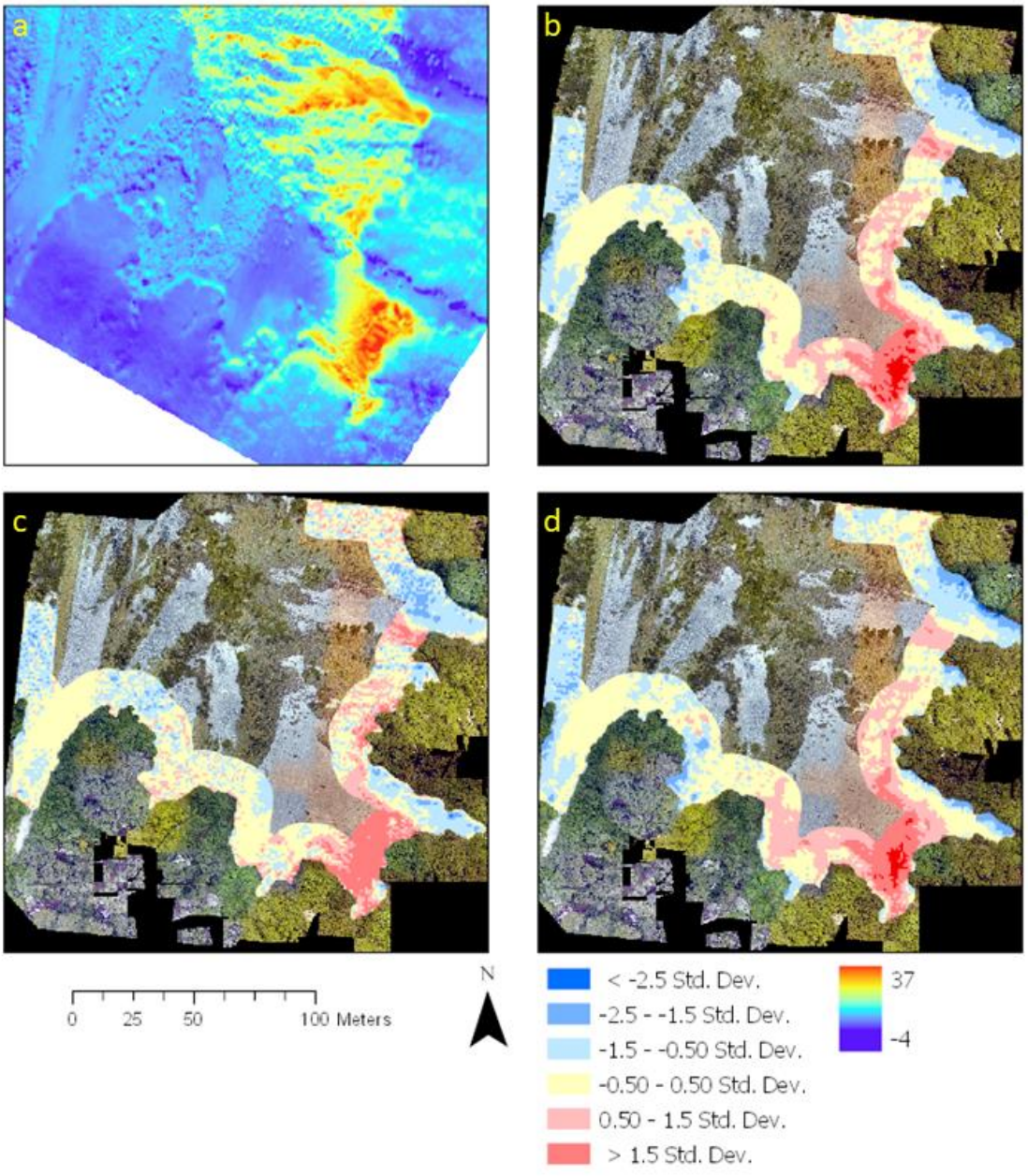

Figure 37: Thermal difference profile between morning and noon during winter for the Craigieburn Valley (a). Temperature anomalies in predicted clusters, for mean (b), minimum (c) and maximum (d) temperatures within a 15 m treeline ecotone.

3.3.3 Analysing seedling occurrence relative to microhabitat availability

For the three temperature polygons (Figure 38; min, mean, max) predicted with the microhabitat logger information clear trends can be identified. Seedlings in the minimum temperature zones show a significant preference for the warmest quantile, where 43.8 % of all seedlings recruited in a zone showing above 2.82 °C annual minimum temperature. This trend is continued with annual mean temperatures zones, where 32.8 % of the seedlings showed spatial association with the warmest class and significantly lower individuals were identified for the two lowest mean temperature zones (10.5 % and 7.6 %). For absolute maximum temperatures the trend is consistent but less pronounced at the higher temperature end. For the warmest class I identified 26.2 % of seedlings and for the lowest maximum temperature classes 12.3 % and 9.7 %.

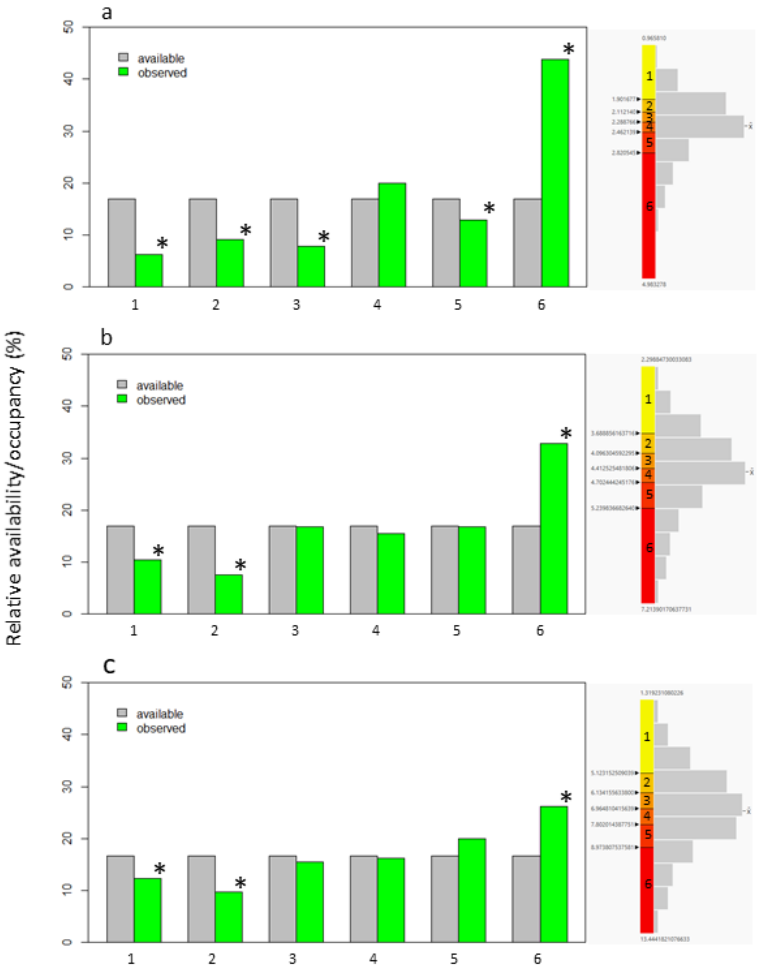

Figure 38: Relative thermal microhabitat availability (light grey bars) vs seedling occupancy (light green bars) for the minimum (a), mean (b) and maximum (c) thermal zones predicted within 15 m of the established treeline canopy. Significant difference (*) in expected proportions are displayed, detailed results for the analysis can be found in Appendix A.

The multivariate cluster analysis (Table 20, Appendix A) identified six clusters (Figure 55, Appendix A) using UAV- and GIS-derived variables compiled at a 1-m^2 grid resolution across the 40-m ecotone zone at the Craigieburn Valley site (Figure 39). Boxplot graphs showing the relative contribution of each of the input variables in characterising each of the clusters (Figure 40) indicate that there were typically one or two variables that contributed primarily to defining cluster types and enabling a general characterisation of the meaning of each cluster (Table 9). Cluster parameterisation was non-spatial so zones identified in the visualization (Figure 39) can be attributed to identified ranges dominant in the area. A mapping of the cluster classes spatially across the ecotone zone suggested that the multivariate input data were useful in defining distinct spatial zones that characterised differences across the site related to patterns of variation in thermal, radiation, and slope characteristics (Fig. 42).

Table 9: Description of identified clusters using seven environmental variables (slope, solar radiation (winter, summer, year), temperature (morning, noon, difference)) for n = cluster points derived for the Craigieburn Valley

Cluster ID	**Key pattern metrics (relevance)**	**Interpretation**
1, n = 2,690	High: Slope, Temperature difference	Steep, vegetated slopes
2, n = 1,157	High: Slope, Winter radiation Low: Temperature morning	Shallower sites, sparsely vegetated
3, n = 3,729	High: Slope, Temperature difference	West facing scree slopes
4, n = 2,418	High: Winter radiation, Slope	Vegetated east facing slopes
5, n = 2,878	High: Slope Low: Winter radiation	Shallow south-west facing scree slopes
6, n = 1,870	High: Radiation, Temperature morning Low: Temperature difference	Vegetated slopes in directional shading from canopy or shrubs

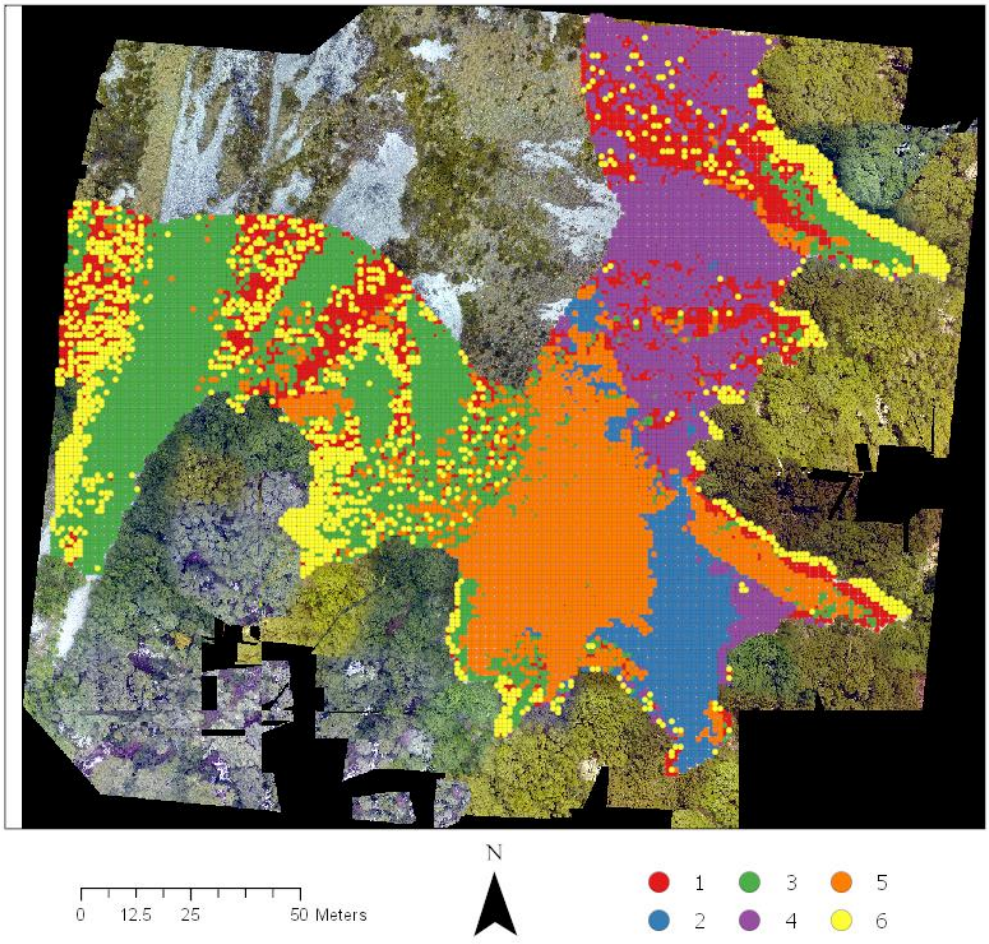

Figure 39: Results of the multivariate cluster analysis within ArcGIS Pro for the Craigieburn Valley. Six clusters were identified that represent distinct combinations of slope gradient (degrees), solar radiation (Wh/m²) and remotely sensed thermal information (°C).

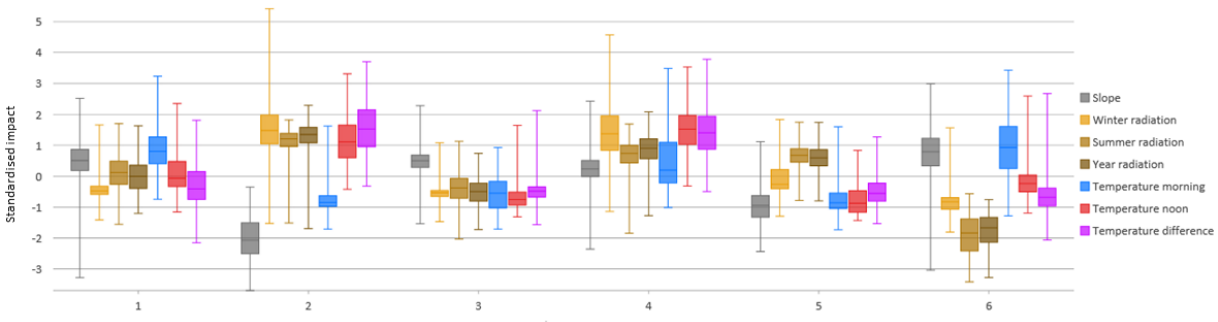

Figure 40: Illustration of the seven environmental variables and their impact (z-transformation, 0 = no impact) on discriminating the six spatial cluster identified at the Craigieburn Valley. Information about slope, received solar radiation and remotely sensed thermal information have been processed in the multivariate analysis.

A comparison of the vegetation microhabitats and cluster classes (Figure 41) in which seedlings are occurring against the relative availability of these microhabitats across the 15-m ecotone showed clear preferences for seedling-microhabitat associations. The test for given proportions (Table 21 & 22, Appendix A) revealed enhanced recruitment in prostrate mats (*Leucopogon*), where they are 1.8 times more likely to occur; 33.4 % of all seedlings recruited within these low stature shrub mats, making up 17.7 % of the available microsites. Only 2% of established seedlings were associated with alpine tussock grasses (*Chionochloa* spp.) despite tussock zones occupying 16.7 % of the 15 m subalpine belt. Bare ground cover (scree) made up 34.3 % of the available area, but only 23.5 % of seedlings occupied these zones. Seedlings were significantly over-represented in the second cluster where 30.3 % of all seedlings can be found, representing only 10.1 % of the available area. This effect is compensated within the first and fourth cluster, where 16.7 % and 16.3% of the total available area only host 6.8 % and 8.4 % of all seedling respectively.

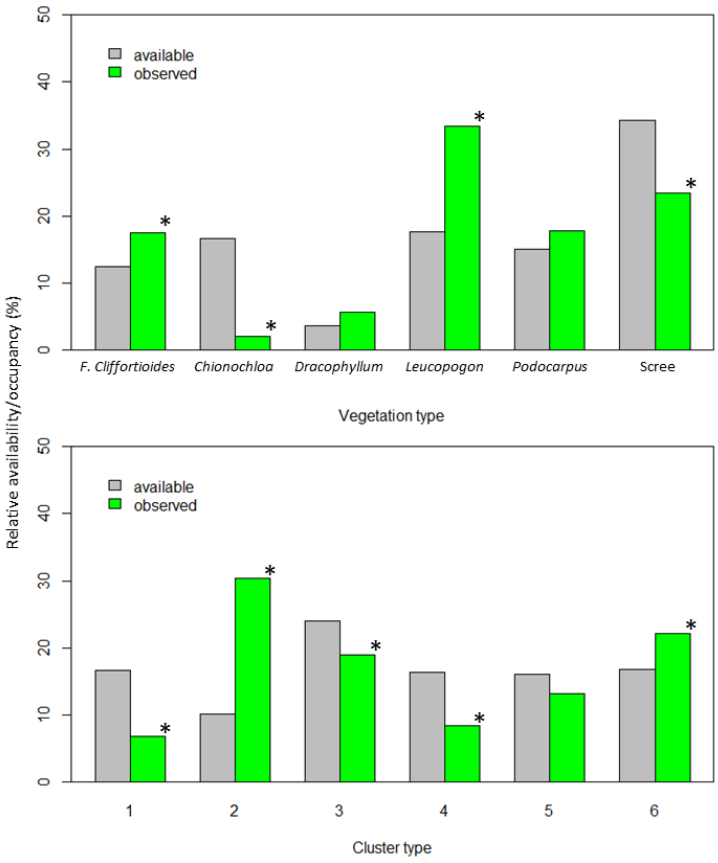

Figure 41: Relative microhabitat availability (light grey bars) vs seedling occupancy (light green bars) by vegetation type (top) and identified clusters (bottom) within 15 m of the established treeline canopy. Significant difference (*) in expected proportions are displayed, detailed results for the analysis can be found in Appendix A.

3.3.4 Modelling seedling height growth against environmental variables

Results for the forest-based classification and regression analysis (Table 10) showed high confidence (R^2 = 0.893, P < 0.000, Std Dev = 0.025, 10 % of training data exclude for validation, 4 variables selected randomly) for the training data used to perform the regression. Explanatory variables are ranked to estimate their influence to drive the results, R^2 indicates prediction accuracy. The ground cover classification showed highest importance (16 %) is the most influential explanatory variable to predict tree growth. Incident solar radiation in winter, an east facing aspect and early morning temperatures (10 % each) were ranked the next highest, and equal, in relevance. Lowest rank variables are the thermal difference between morning and noon, the cluster ID and the temperature recordings at noon (6 % each).

Table 10: Variable importance in explaining subalpine seedling growth between 2007 and 2019 for the Craigieburn Valley generated by the forest-based classification and regression.

Explanatory variable	**Importance (%)**
Vegetation type	16
Solar radiation winter day	10
Eastness	10
Thermal morning	10
NDVI	8
Slope	8
Northness	8
Solar radiation summer	7
Solar radiation year	7
Thermal difference	6
Cluster ID	6
Thermal noon	6

3.4 Discussion

The fine-scale dataset from an alpine treeline ecotone enabled me to delineate the environmental microhabitats that were beneficial for seedling regeneration above treeline, but also highlighted potential species-specific recruitment limitations within subalpine vegetation. As anticipated, *F. cliffortioides* recruitment was enhanced in microhabitats which reduced exposure to macroscale-imposed limitations common at treeline (e.g. annual frost events). However results indicate, successive tree colonialization of the subalpine is hampered by the adverse effects of competition and the paucity of microhabitat safe sites which limit treeline response to broad scale climate warming.

F. cliffortioides recruitment heatmaps for the Craigieburn Valley showed spatial pattern in three decades of treeline regeneration in the subalpine. The dataset indicated steady recruitment hotspots within the subalpine, suggesting favourable microclimatic habitats to be spatially explicit and prominent at the east-facing slopes and shallow southern plateau. Enhanced recruitment between the 2002 and 2007 census can potentially be linked to a preceded masting year (2004 & 06; DOC, 2014). However, frequency and richness of masting years bear no implications for treeline advance in *Nothofagaceae* (Harsch et al., 2012). Further, correlation of masting years and census data is limited, since I was not able to non-invasively date seedlings due to their small stature and restricted growth. The cause of an observed recruitment shift from the shallow southern plateau (until 2007) towards the east facing slopes (2019) remained elusive. Drivers can potentially be attributed to seasonal climatic variability which resulted in a temporarily weakened microclimate gradient (Hohnwald et al., 2020). This effect can be induced by wind (Holtmeier & Broll, 2010) or growing season extent and snowpack duration (Bader et al., 2018; Davis & Gedalof, 2018) but will require extended research at other transects.

Microhabitat temperature regimes are subject to strong thermal variability throughout the year. Existing alpine vegetation reduces the thermal range locally and this effect is pronounced in dense tussocks grasses (*Chionochloa* spp.) or *Podocarpus*, while temperature fluctuated unrestrictedly on non-vegetated scree (Ball et al., 1991). While all vegetation microhabitats suppressed extreme heat deviations during summer, none effectively reduced the frequency of low temperature dips throughout the year (< 2 °C). Seedling recruitment was significantly reduced in coldest minimum temperature zones, while simultaneously favouring recruitment in warmer ends of the spatial projections. Increased recruitment in warmer

microhabitats was less pronounced but still significant in the mean and maximum predicted temperature zones, suggesting frost-controlled recruitment limitations prominent in *Nothofagaceae* (Reyes-Díaz et al., 2005; Wardle, 2008) and a high tolerance to heat-modulated limitations (e.g. moisture deficiency; Holtmeier & Broll, 2017; Sigdel et al., 2018).

F. cliffortioides recruitment related significantly to the spatial patterns in microhabitats represented by the vegetation and clusters. Contrary to expectations, seedling regeneration was greatly reduced in alpine vegetation which most efficiently reduced temperature variability in the subalpine (*Chionochloa* spp, 1/6 of subalpine area, 2 % of seedlings found), but significantly enhanced in low-stature herbaceous shrubs (*Leucopogon*, 1/6 area, 33.4 % seedlings) and shallow, sparsely-vegetated microhabitats (1/10 area, 30.3 % seedlings). This suggested directional facilitative feedbacks for *F. cliffortioides* to be species-specific and limited by competitive interactions within tussock grasses and the herbaceous subalpine (Loranger et al., 2017). As anticipated, characterised environmental variables deemed most influential in this context were also most important in controlling seedling performance. *F. cliffortioides* growth was modulated strongest by the ground-cover type, followed by morning temperature (e.g. low-temperature susceptibility). Interestingly also aspect ('eastness') and winter radiation influenced seedling colonialization, suggesting a combined effect of low-temperature and light (e.g. cold-induced photoinhibition, Ball et al., 1991; Germino & Smith, 1999; Sakai et al., 1981). Light-induced seedling dieback has been observed in previous studies of *F. cliffortioides* (Norton & Schönenberger, 1984; Wardle, 1985b, 2008a), but has never been discussed in a temperature modulated context.

Seedling-microhabitat interaction in the subalpine vegetation are complex and ambiguous and a clear directional facilitative feedback that promotes successive colonialization is not always established (Alftine & Malanson, 2004; Callaway & Walker, 1997; Holmgren et al., 1997). They can be modulated by the seedlings ontogenetic stage and size (Körner, 2016; Loranger et al., 2017; Malanson & Resler, 2016) and the interacting alpine species (Gómez-Aparicio et al., 2005; Rose et al., 2020). Since *Nothofagaceae* showed evidence for frost and high-light susceptibility in earlier studies (Norton & Schönenberger, 1984; Reyes-Díaz et al., 2005; Wardle, 1985a, 2008) it is particular useful to study size modulated emergence effects where seedlings gradually decouple from the microclimate established by the subalpine shrub layer (Chapter 4, Körner, 2016). Further, favourable microhabitats have been associated with reduced exposure to frost and sparsely vegetated scree slopes with low-stature/-density prostrate mats *Leucopogon colensoi*. However, these

microhabitat safe sites for *F. cliffortioides* represented only a small proportion of the subalpine shrubland. I therefore speculate, that treeline advance in *F. cliffortioides* is currently limited by the paucity of favourable micro-climatic conditions in the subalpine which can shelter seedlings from macroscale-imposed frost while simultaneously giving them enough space to grow. Further studies of belowground biotic interactions are required to elucidate adverse effects of subalpine vegetation (Bader et al., 2018; Hagedorn et al., 2019; Hasselquist et al., 2005) particularly how the facilitative nature of this feedback can be size modulated (Malanson & Resler, 2016). I therefore suggest isolating key mechanics believed to control current treeline advance (temperature & competition) and discuss their interplay to establish a climatic niche strong enough to induce successive seedling regeneration as 'tipping points' for ecosystem migration at treeline (Chapter 5).

A combination of high-quality spatial (drone operated sensors, extrapolated thermal logger data) and temporal information (treeline census data) proved to be ideal datasets to address the temporal lag in a response of abrupt treeline phenomena to broad scale climatic warming. I have used these datasets to study how macroscale-imposed climatic limitations are ameliorated by local microhabitats and to identify how directed facilitative feedbacks for early recruits in the subalpine are established. This allows us to hypothesise the mechanisms leading to current recruitment bottlenecks and formulate more directed research to elucidate their role in hampering treeline advance. The significant temporal lag of abrupt treeline position in the face of global warming can therefore only be predicted if we continue to monitor fine-scale changes in subalpine plant communities and further disentangle species-specific shrub-seedling interactions.

4 High light-induced photoinhibition is not limiting seedling establishment at abrupt treeline ecotones in New Zealand

4.1 Introduction

There is general consensus that a decreasing mean temperature with increasing elevation can limit tree growth and play a critical role in determining the upper elevational limits of tree species' ranges (Körner, 2012; Malanson et al., 2011). However, there are often additional environmental conditions and biological factors that can interact with temperature gradients to inhibit tree establishment and growth at high elevation tree population boundaries. Accordingly, treeline formation and spatial patterns have been hypothesised to be driven by factors acting on three hierarchical, mechanistic levels (Harsch & Bader, 2011). The 'first-level mechanisms' of tree growth, mortality, and dieback are proximal mechanisms controlling whether a treeline displays a gradual, abrupt, island, or krummholz spatial structure. These first-level mechanisms are modulated by a number of site-specific stressors ('second-level mechanisms'), including, but not limited to, growing season length (Cieraad, 2011; Körner, 2012), seasonal desiccation effects (Cairns, 2001; Cuevas, 2000), frequency of frost and ice-particle abrasion (Holtmeier, 2009), high solar radiation (Bader, van Geloof, et al., 2007), moisture limitations (Loranger et al., 2016), invasive plant pathogens (Tomback et al., 2016) and reductions in seed production and viability (Wardle, 2008). Second-level mechanisms can be further modulated by ecological interactions with plant neighbours ('third-level mechanisms') to ultimately determine the emergent treeline form at a given location. Thus, this hierarchical framework provides a useful context for developing and testing hypotheses regarding the treeline-forming processes at different regions.

Treelines dominated by first-level growth limitation processes tend to result in a diffuse (or gradual) treeline form (Harsch & Bader, 2011). Diffuse treelines represent the most common treeline pattern globally and, because they are limited mainly by temperature, show the greatest response to climatic change (Harsch et al., 2009). In contrast to diffuse treelines, abrupt treelines are hypothesised to be maintained primarily by second- and third-level mechanisms that exert a threshold-type control on the ability of new tree seedlings to establish and survive beyond the treeline edge (Harsch & Bader, 2011). Consequently, the majority of abrupt treelines have not shown responses to increased warming that are similar to diffuse treelines (Harsch et al., 2009). Thus, research into potential underlying mechanisms limiting seedling establishment characteristic of abrupt treelines is urgently required to predict the

future conditions under which these treelines are likely to respond and start shifting uphill (Malanson et al., 2011).

Figure 42: View of an abrupt *Fuscospora cliffortioides* treeline, Craigieburn Valley, New Zealand. Photo: Döweler.

Abrupt treelines show a rapid ecotone transition from a continuous forest stand into low-stature alpine vegetation (e.g., Figure 42), suggesting that this treeline pattern is being reinforced by positive feedback processes on both sides of the treeline boundary (Wilson & Agnew, 1992). Thus, for a tree seedling to establish and grow beyond the forest edge, it must overcome the effect(s) of critical stressors causing highly limited seedling recruitment and performance. For some tree species, there is evidence that recruitment limitations beyond abrupt treeline boundaries are associated with the deleterious impacts of incident sunlight (Bader et al., 2007; Germino et al., 2002). Insufficient tolerance to excessive levels of sunlight to already pronounced radiation levels in high altitude environments can lead to an over-excitation of leaf tissues and is commonly linked to restricted photosystem functionality (Demmig-Adams & Adams, 2006). Susceptibility to radiation can be further modified by the thermal regime experienced by the leaves. At high temperatures, plants may reduce stomatal conductance resulting in a downregulation of photosynthetic electron transport, which in turn

may cause photo-oxidative damage and photoinhibition under strong sunlight (high light-induced photoinhibition; Takahashi & Murata, 2008). By contrast, low temperatures slow down biochemical processes (reduced electron sink activity) and together with high light intensities this can also result in photo-oxidative damage and photoinhibition (low-temperature photoinhibition, Germino & Smith, 1999; Zarter et al., 2006a,b,c).

Hence, photoinhibition effects can be modulated by the temperature regime the leaves are experiencing. The projection of future upward shifts of abrupt treelines, requires a deeper understanding of the abiotic drivers and the period of greatest seedling susceptibility, which together cause the recruitment bottleneck (Danby & Hik, 2007). For treelines believed to be limited by radiative effects, this includes determining if the cause is a cumulative effect leading to sustained suppression of photosynthetic performance over the course of multiple intense days, or whether a single event where one or more multiple stressors produce lethal conditions for pioneering recruits.

In New Zealand, treelines formed by the evergreen "southern beech" species *Fuscospora cliffortioides* (Nothofagaceae) provide an ideal context for examining the mechanisms driving the formation and maintenance of the abrupt treeline form. A handful of previous studies at these treelines provide insight into possible mechanisms. For instance, since 1950, these beech forest treelines have responded very little to a *c.* 1 °C warming, with new recruitment occurring predominately within 10 m of the forest edge (Harsch et al., 2012; Mullan et al., 2008; Wardle & Coleman, 1992). Available evidence suggests a restricted upward movement is not likely related to short dispersal distances (Cullen et al., 2004), variability of seed fall patterns towards the timberline (Allen & Platt, 1990), seed viability (Wardle, 1985b), or the winter frost hardiness of seedlings (Sun & Sweet, 1996). Wardle (1985a) compared germination, growth, and survival of *F. cliffortioides* with those of several exotic tree species (*Pinus* and *Eucalyptus*), both sown and transplanted, in plots up to 300 m above the beech treeline subjected to differing levels of shading. Transplanted seedlings at 150 m above the treeline showed better performance and survival at the highest shade treatment, with individuals surviving under, but not beyond, the shade screen 35 years later (Wardle, 2008). Observations of seedlings growing disproportionately more frequently in more highly shaded microsites above the beech treeline (Harsch, 2010) is also consistent with Wardle's (1985a) experimental results. While these findings suggest a strong negative correlation between seedling performance and direct exposure to open-sky conditions, the specific role of photoinhibition as a mechanism for low seedling recruitment remains to be confirmed by direct physiological measurements. Within the scope of this study we will use the 'seedlings'

terminology to refer to low stature individuals within the subalpine belt, since their age cannot readily be determined. In fact, some seedlings < 15 cm have been part of long-term monitoring campaigns and are older than a decade.

In this study, we hypothesise that photoinhibition, coupled with extreme temperatures experienced by southern beech tree seedlings in the exposed treeline ecotone, impairs photosynthetic functioning and thus may result in a survival bottleneck that hinders establishment. To test this hypothesis, we: i) measured the photosystem II performance of seedlings using non-invasive chlorophyll fluorescence measurements on exposed seedlings in summer and early winter, at two spatially independent sites with similar climatic regimes. We expected to see cumulative effects inducing photoinhibition where high radiation loads translate into a sustained or even lethal photosystem degradation. We also anticipated similar patterns among the two sites, ii) generated light curves to compare microhabitat differences between exposed and canopy-sheltered individuals and expected no significant microhabitat-related differences in light curve parameters, and iii) characterised the intra-annual temperature fluctuation at the microsite level associated with seedlings, facilitating the interpretation of the physiological data in the context of the range of temperatures experienced by seedlings throughout the course of a year.

4.2 Material & Methods

Study sites

This study took place at two treeline ecotone sites in the Canterbury Region in the South Island of New Zealand, most recently described by Harsch and colleagues (2012). The Craigieburn Valley (-43.111, 171.713) site is located at 1365 metres above sea level and on a southeast to southwest aspect on the east side of the South Island's Southern Alps. The site shows frequent frost events throughout the year (135 frost days) and has an annual rainfall of *c.* 1300 mm. The Mt. Faust (-42.505, 172.409) site is located about 100 km north of the Craigieburn site on a west-to-southwest aspect, with fewer frost events than the Craigieburn site (90 annual frost days), and an annual rainfall of *c.* 2200 mm. Treelines at both sites are formed by *F. cliffortioides* (mountain beech), with trees at the treeline edge about four to seven metres in height, forming a continuous forest canopy. As is typical of abrupt beech treelines in New Zealand, the majority of seedlings in the subalpine ecotone occur in close vicinity to the forest canopy (within 5 m) and few individuals are found in 5 to 30 metres distance to the canopy edge.

Figure 43: Craigieburn Valley transect (left) with scree slopes cutting across the subalpine vegetation belt. Mount Faust transect (right) with continuous low alpine shrub vegetation. Photo: Döweler.

At both sites, the adjoining subalpine zone is characterised by similar vegetation communities, dominated by *Chionochloa* spp. tussock grass species, *Dracophyllum uniflorum* Hook.f., *D. longifolium* (J.R.Forst et G.Forst.) and/or *Podocarpus nivalis* (Hook.) woody shrub patches, prostrate mats of *Leucopogon colensoi* (Hook), and individuals of *Hebe* spp. and *Aciphylla squarrosa* (J.R.Forst. et G.Forst) occupying some zones between tussocks and woody shrubs. Interspersed across the more arid terrain of the Craigieburn Valley are bare scree slopes; *Leucopogon colensoi* and *Hebe* spp. are the first plant species to establish in these areas. The alpine belt at Mt. Faust is comprised of a continuous low-stature vegetation mosaic dominated by tussock and woody shrubs with very little scree or other conspicuous erosion landforms (Figure 43).

Data collection

We characterised the diurnal variability in chlorophyll fluorescence signals of seedling foliage at the two sites and simultaneously recorded the leaf-level temperature and light environment during one typical day during summer and again during early winter. Fluorescence measurements were carried out on seedlings at each site located in the sun-exposed alpine belt. Since treeline ecotone seedlings had been previously monitored over a 30-year timeframe at these sites (see Harsch et al., 2012), we were able to select seedlings that showed highest radiation exposure in the ecotone, ensuring that seedlings included in our sampling were comparable. In the austral summer (February 2019), chlorophyll-*a*-fluorescence recordings

were taken on five leaves from each of 16 seedlings at each site over a full diurnal course at 2-hourly intervals using a Mini-PAM fluorometer (Walz, Effeltrich, Germany). At the Craigieburn Valley, early austral winter (late May 2019) fluorescence recordings were also carried out using the same individuals to test effects of low temperatures combined with radiation.

One of the five sampled leaves of every plant was shaded 30 minutes before the measurement using a dark leaf clip with sliding shutter (DLC-8, Walz, Effeltrich, Germany) to calculate the optimal quantum yield (F_v/F_m) allowing us to evaluate the effective quantum yield (ΦPSII) recovery throughout the day. Simultaneously, temperature and photosynthetic photon flux density (PPFD) were measured for each leaf using the thermocouple temperature probe and the miniature light sensor built into the leaf clip holder of the fluorometer device (leaf clip 2030-B, Walz, Effeltrich, Germany). The daily courses of non-photochemical quenching (NPQ) and ΦPSII were analysed using generalized additive mixed models (GAMM, package *mgcv*, Wood, 2011) with gaussian or beta (log link) error distribution, respectively. The beta error distribution was chosen for the ΦPSII data because it is bound by 0 and 1. For the summer data smoothing functions with 8 knots provided appropriate fits as judged by the Akaike Information Criterion (AIC) and for the winter period, smoothers with 3 knots were sufficient. Model diagnostic plots showed variance heterogeneity, which was modelled using a fixed variance structure with 'time' as variance covariate (Pinheiro et al., 2019).

To test the influence of the strongly varying light regime among the two microhabitats (exposed versus crown-shaded microsites) on seedling physiology we recorded rapid light curves on a separate set of seedlings (ten individuals and five leaves per treatment) growing under the canopy and in the open. This supplementary experiment aimed to characterize the maximum photosynthetic rate of seedlings based on their position within and beyond the established canopy to account for potential microhabitat-induced performance differences. Light response curves were recorded with the same Mini-PAM fluorometer device as described above. The illumination provided by the fluorometer's internal halogen lamp was increased in seven increments from 100 µmol m^{-2} s^{-1} up to 2300 µmol m^{-2} s^{-1} using 30 s intervals. The electron transport rate (ETR) was derived from the equation (Genty et al., 1989; Krall & Edwards, 1992; Maxwell & Johnson, 2000):

$$ETR = \Phi PSII \times PPFD \times 0.5 \times 0.84 \quad (1)$$

Generalised non-linear least squares models (R package *nlme*, Pinheiro et al., 2019) were used to analysed ETR as a function of PPFD based on the following exponential regression equation (modified after Lobo et al., 2013):

$$ETR = ETR_{max}\left(1 - e^{-\alpha\, PPFD/ETR_{max}}\right) \quad (2)$$

where, ETR_{max} is the maximal electron transport rate of PSII, PPFD is the photosynthetic photon flux density, and α is the quantum yield (initial slope). A nonlinear model, assuming common parameter estimates for the two microhabitats, represented the null hypothesis of similar ETR_{max} and α values for both microhabitats. The alternative hypothesis was implemented by a nonlinear model allowing separate parameter estimates for each microhabitat assuming a statistically significant, microhabitat-related difference in ETR_{max} and α. A likelihood ratio test was used to compare the two models. Graphical model validation tools were used to check the underlying assumptions of variance homogeneity (plots of the normalized residuals against the fitted values and versus the predictor values) and normality (quantile-quantile plots). We did not detect gross deviations from normality but the diagnostic plots indicated variance heterogeneity, which was dealt with in both models using a variance function with fixed variances using the photosynthetic photon flux density (PPFD) as variance covariate (R function *varFixed*() in package *nlme*).

To assess the temperature variation throughout the year, we deployed two temperature loggers at each site (iButton, DS1921G-F5#, 2kB, ± 0.5 °C, −40 to +85 °C, Maxim Integrated, San José, CA, USA), sealed them in plastic bags and tied onto ropes close to the main stem of the seedlings and another seven loggers were placed at both sites 2 cm below the scree to prevent direct sunlight exposure (Figure 44). Logging started at the end of January at 4-hourly intervals.

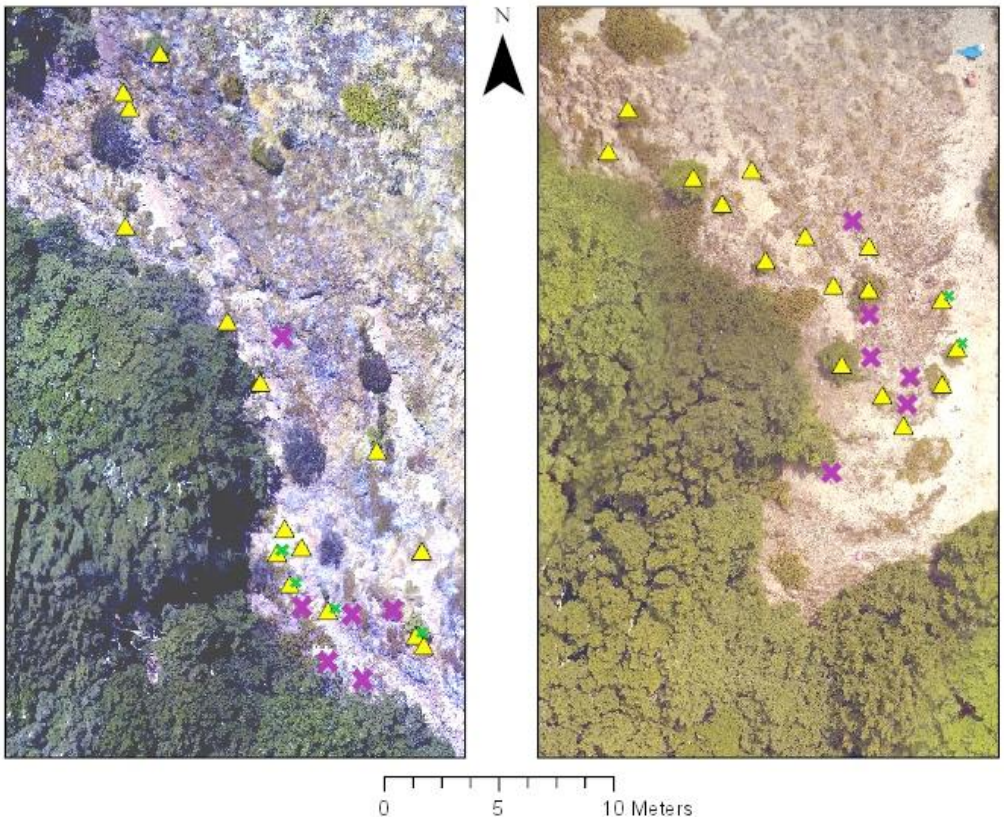

Figure 44: RGB image (DJI Phantom 4, 2 cm resolution) of the study sites Mt. Faust (left) and Craigieburn Valley (right) in the Southern Alps of New Zealand. Symbols indicate seedling locations (yellow triangles) and temperature loggers (purple: scree; green: beech).

4.3 Results

At both sites, PPFD reached up to 2000 µmol m^{-2} s^{-1} around noon in summer (Figure 45). At the south-easterly facing slope at the Craigieburn Valley, PPFD increased and declined earlier compared to the more west-facing Mt. Faust site, where sunlight hours extend into the evening (Figure 45). During winter, the time window for measurements at the Craigieburn Valley was restricted by shorter daylight hours but proved sufficiently long to capture the largest variation in the diurnal pattern. The maximum PPFD values reached approximately 1000 µmol m^{-2} s^{-1} in winter (Figure 45). In summer, leaf temperatures reached 35 °C at Mt. Faust, and 30 °C at Craigieburn Valley. In winter, the initial measurements (8 am) coincided with temperatures as low as 2 to 4 °C before the first sunlight hit the seedlings.

Sun-exposed seedlings at the Mt. Faust site showed the typical U-shaped diurnal course of the effective quantum yield of PSII (ΦPSII) on a clear-sky day (Figure 45). The ΦPSII showed rapid recovery; 1 hour after sunset ΦPSII values (0.794 ± 0.025, mean ± SE) had nearly returned to pre-dawn values (0.805 ± 0.024). A very similar pattern was seen at the Craigieburn

Valley site where the recovery of ΦPSII to pre-dawn values also occurred within two hours after sunset (10 pm, 0.780 ± 0.031). The quick recovery potential of *F. cliffortioides* was further supported by the dark-recovery experiment. Irrespective of site and season, quantum yield of PSII returned to pre-dawn values during 30 minutes dark-recovery at all times of the day, even at noon when PPFD reached peak values of 2000 µmol m^{-2} s^{-1} (Figure 45, bottom row). Based on the light curve analysis, ETR_{max} and α in sun-exposed seedlings were 12% and 43% higher compared to the individuals growing beneath canopy (L = 7.24, df = 2, P = 0.027; Figure 46).

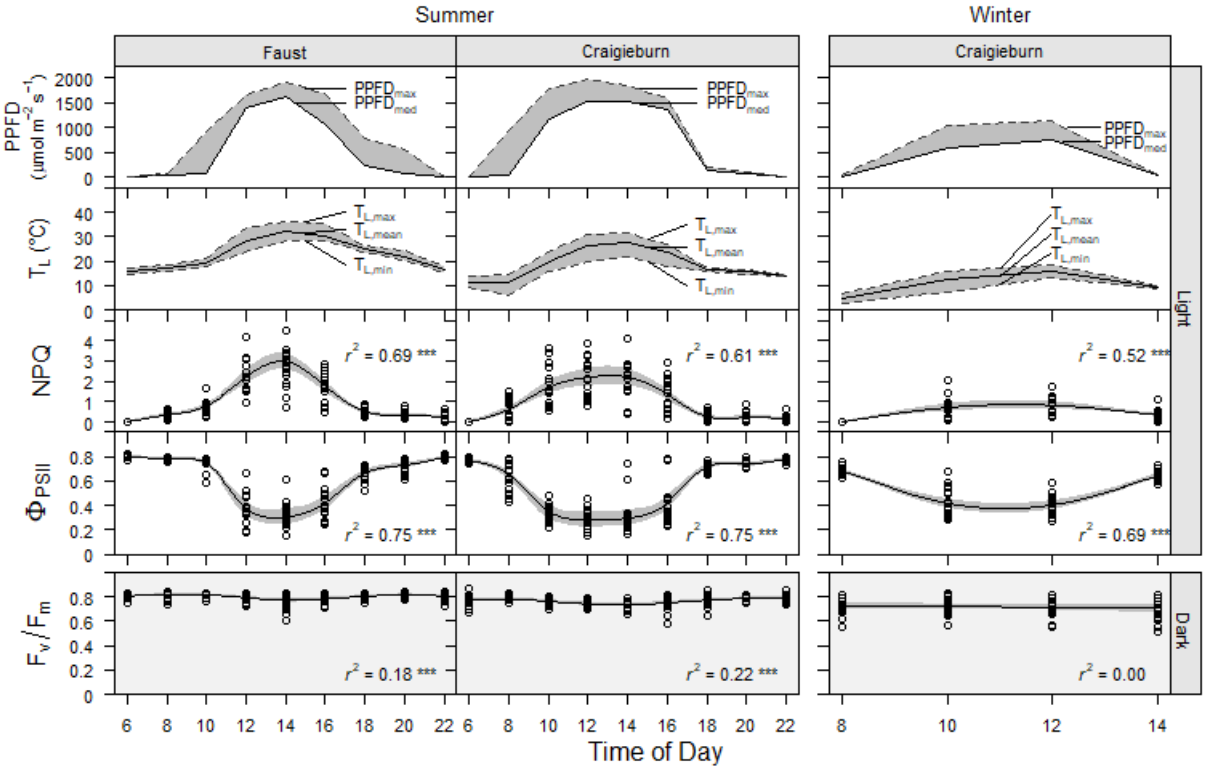

Figure 45: From top to bottom row: Diurnal changes in light intensity (PPFD = photosynthetic photon flux density), leaf temperature (T_L), non-photochemical quenching (NPQ), effective quantum yield of photosystem II in the light-adapted state (ΦPSII) and optimal quantum yield in the dark-adapted state (F_v/F_m) (see vertical indicator strips on the right) of *Fuscospora cliffortioides* seedlings on a summer day at Mt. Faust (left panels, January 2019) and Craigieburn Valley (middle panels, February 12th 2019), and a winter day at Craigieburn Valley (right panels, May 20th 2019). We displayed the maximum and the median leaf-level PPFD but omitted the strongly varying minimum values (due to intermittent shading). Due to shorter daylight hours and associated health and safety reasons there are fewer time points in winter compared to summer.

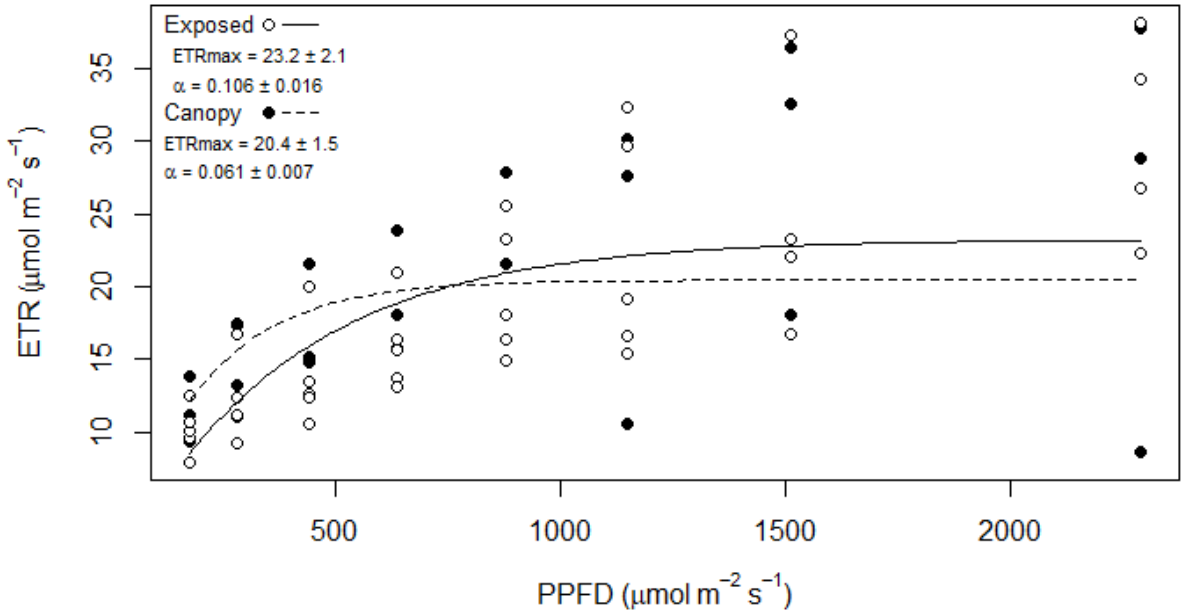

Figure 46: Rapid light curves created from data collected for canopy-shaded and exposed seedlings in the Craigieburn Valley. PPFD (photosynthetic photon flux density) levels were manually increased in seven increments from 100 µmol m^{-2} s^{-1} up to 2300 µmol m^{-2} s^{-1} using 30 second illumination intervals.

Throughout the entire year, scree and seedling temperature varied strongly with maximum daily amplitudes in summer of 37.5 °C in the scree and 17.5 °C for the beech seedlings at the Craigieburn site, and of 58.5 °C and 31°C for the Mt. Faust site, for scree and beech seedling microenvironments, respectively (Figure 47). Early morning temperature experienced by seedlings in late spring and summer (late November to February) dropped multiple times below 2 °C (Craigieburn: 16, Faust: 12) and sometimes even below freezing (Craigieburn: 3, Faust: 2) down to -2 °C. The temperature around seedlings in this period ranged between 26.5 °C and -2 °C and in the scree between 60.5 °C and -0.5 °C. The variability in daily scree and seedling temperature decreased markedly following the onset of winter and became minimal after snowfall starting on 1st June shortly after the chlorophyll fluorescence measurements (20th May) had been conducted.

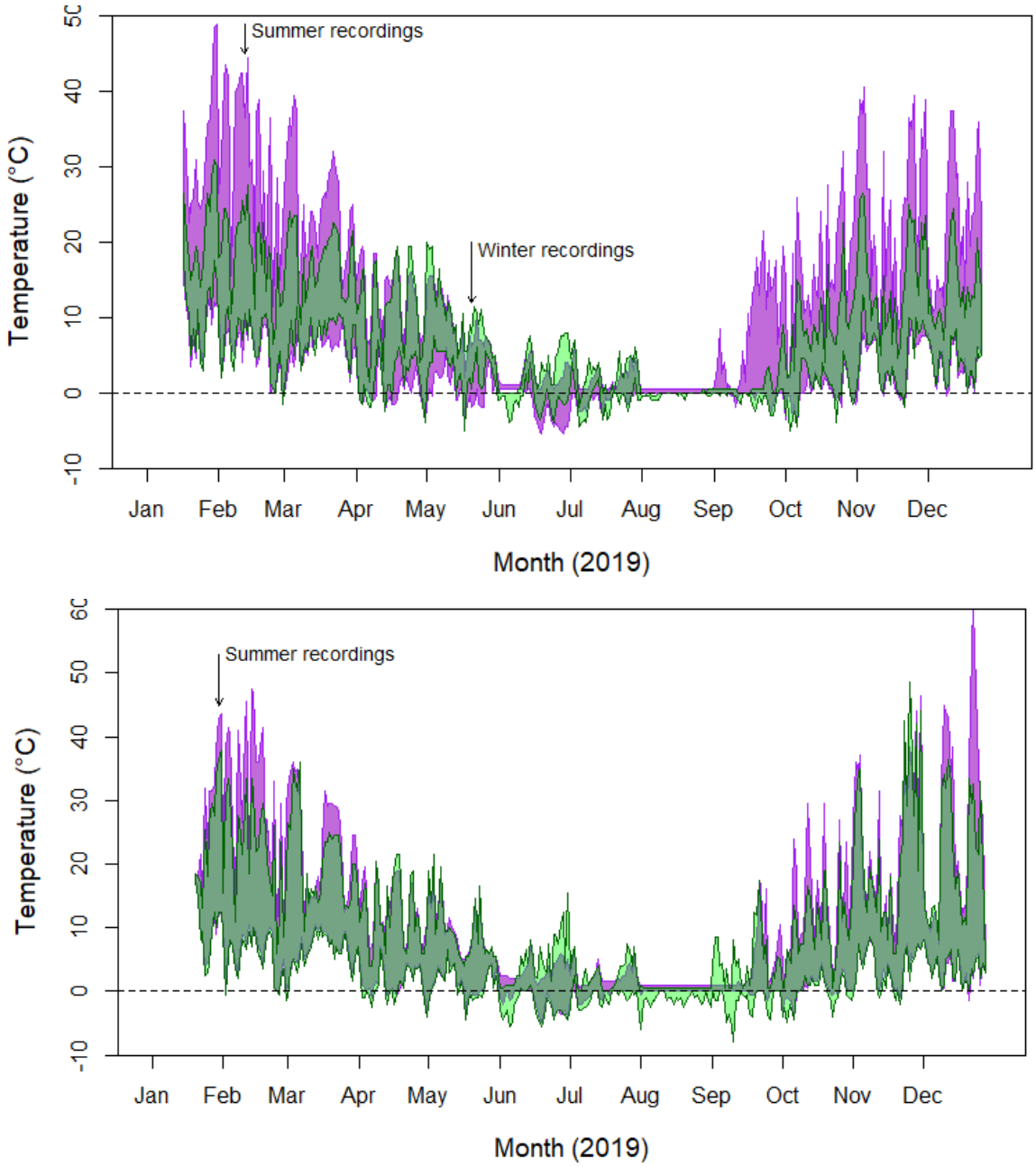

Figure 47: Intra-annual variation of temperature bound by daily minimum and maximum values (lower and upper polygon boundaries) at the treeline (1350 m a.s.l.) at the Craigieburn Valley (top) Mount Faust (bottom) from mid-January to late December 2019. Purple = scree microhabitats (7 loggers); green = beech seedlings (2 loggers).

4.4 Discussion

The framework presented by Harsch and Bader (2011) lays a foundation for conceptualising how local-scale physiological stressors may result in a recruitment bottleneck just beyond the edge of the closed-canopy treeline, thus enabling a positive feedback loop that maintains an abrupt treeline ecotone boundary form. Within this concept, the 'second-level' stressors responsible for the sharp transition characteristic of abrupt treelines remain elusive' but their identity is essential for predicting how climatic changes may trigger the 'release' of this feedback mechanism and the future migration of these tree populations uphill (Harsch & Bader, 2011). Given evidence that photoinhibition may be a strong contributor to seedling mortality for some species at a variety of abrupt treeline ecotones globally (Bader et al., 2007; Close et al., 2002; Germino et al., 2002; Zarter, 2006a) we investigated the degree to which the negative impacts of photoinhibition on its own, or in combination with extreme temperatures, is limiting the establishment of southern beech seedlings at New Zealand's abrupt treelines.

Results from chlorophyll fluorescence measurements indicate that severe physiological impairment is not occurring to the extent that seedling survival is threatened. Southern beech seedlings showed a remarkable potential to recover from exposure to high PPFD, clearly refuting early suggestions in the literature that photoinhibition alone might hinder seedling establishment (Wardle 1985a,b; Wardle, 2008; Norton & Schönenberger, 1984). Our results suggest that the photosynthetic apparatus of beech seedlings is well adapted to the high-light alpine environment. The virtual lack of photoinhibition at very high light levels experienced over short periods (light curves) or longer time frames (clear-sky days) implies that photochemical and non-photochemical processes operate at levels sufficient to prevent severe photo-oxidative damage in these beech seedlings. Even when high solar radiation coincided with extreme temperatures, ΦPSII showed rapid recovery to pre-drawn values within half an hour of shading or, under non-dark-adapted conditions, at the latest by the end of the day on clear-sky days. Neither the high levels of solar radiation in summer (> 2000 µmol m^{-2} s^{-1}) together with high summer leaf temperatures (e.g. > 33 °C at Mt. Faust) nor the combination of low temperatures (< 3 °C) and high winter light intensity at dawn (> 800 µmol m^{-2} s^{-1}) experienced by the seedlings caused sustained stress levels that would overtax the photoprotective and regeneration capabilities of the seedlings. The light curves have been designed to scale beyond the light levels experienced in summer (2300 µmol m^{-2} s^{-1}) and exposed beech seedlings showed 12 % higher ETR_{max} and a 1.74-fold larger α value compared to canopy-sheltered individuals. However, neither beneath the forest canopy nor in the exposed

subalpine belt did beech seedlings show a consistent decline in ETR with increasing PPFD, which would indicate photoinhibition.

For the early winter measurement carried out at Craigieburn, there was a slight down-regulation of ΦPSII; this may reflect a mechanistic effect of sustained photoprotection found for evergreen species in winter, where adjustments in the xanthophyll cycle and reduction in light-harvesting performance resulted in sustained NPQ. For instance, work by Zarter and colleagues (2006a,b,c) on photosynthetically winter-active evergreen tree and shrub species in Colorado's high-elevation environments revealed zeaxanthin retention and decreases in oxygen evolution capacity and light-harvesting pigments which correlated with a depression in ΦPSII efficiency until the early spring. Sustained down-regulation of PSII performance is a particularly evident photoprotection mechanism in extreme environments (Demmig-Adams & Adams, 2006) and the environmental factors triggering it are believed to be coupled to air and soil temperatures as well as moisture availability (Strand et al., 2002; Zarter et al., 2006c). However, regardless of this down-regulation of light harvesting efficiency, *F. cliffortioides*' rapid recovery of PSII was also observed during winter indicating that the underlying biochemical processes have the potential to fully regenerate to pre-dawn conditions, suggesting no evidence for sustained photosynthetic stress regardless of seasonal mean temperatures.

Temperature sensor data suggest that late austral spring and summertime below-freezing temperatures are not infrequent at these treeline sites, occurring 12-16 times from early November to late February. While the temperatures experienced by the seedlings were limited to a maximum of 26.5 °C during the hottest summer periods, the air temperature around the established seedlings in the subalpine belt can drop as low as the temperature of the surrounding scree (-2 °C). Of particular note are the occurrences of sub-zero temperatures in summer, when the seedlings are not winter-hardened. Previous work has also suggested that actively growing seedlings of *F. cliffortioides* can incur severe frost injury at temperatures of -2 to -3 °C (Sun & Sweet, 1996). Winter ΦPSII values recorded at dawn in the Craigieburn Valley indicate potential performance limits when high PPFD and cold temperatures coincide. Throughout the entire experiment, the strongest leaf-level decline in ΦPSII was seen when the first sunlight hit the leaves during winter. Under these circumstances, relatively high early-morning light intensities coincided with minimal seedling temperatures and ΦPSII values were as low as 0.04. These observed reductions in ΦPSII suggest that photoinhibition may occur under low temperature regimes. This so-called cold-induced photoinhibition has been identified in a range of studies, leading to leaf-loss in the broad-leaved *Aristotelia serrata* in New Zealand (Dungan

et al., 2003), severe degradation of PSII performance resulting in limited regeneration of *Eucalyptus pauciflora* seedlings at the treeline (Ball et al., 1991), and has played a key role in shaping *Eucalyptus globulus* distribution boundaries in Australia (Close et al., 2000). Evidence for enhanced frost susceptibility can be traced back to related *Nothofagaceae* in Chile, where *Nothofagus dombeyi* and *Nothofagus nitida* show good photochemical efficiency (in terms of ΦPSII) in high alpine environments, but lack frost tolerance in spring and summer (Reyes-Díaz et al., 2005).

We therefore suggest that isolated weather events during the spring-summer period such as radiative frost conditions during clear nights combined with high light intensities shortly after dawn may become lethal for exposed individual leaves. The susceptibility to cold-induced dieback is influenced by the respective size/age, the number of leaves, the degree of nearby protection (e.g., from adjacent vegetation) and the number of occurrences of such conditions relative to recovery time. Certainly, this supports the results of Wardle's seedling transplantation and shading experiment (Wardle, 1985a) where the roofs of the seedling shelter boxes act as a barrier preventing radiation from escaping directly into outer space. Instead the radiation emitted from the leaves at night is partially reflected back onto the leaves and some of the heat that is absorbed by the roof is partially radiated back to the foliage. Under these conditions, leaf temperature at night will be higher compared to unsheltered individuals and radiation frost is less likely to occur.

Overall, our results indicate that *F. cliffortioides* is able to physiologically cope with the subalpine high-light environment but occasional occurrences of sub-zero temperatures and high light intensities during the growing season might result in severe cold-induced photoinhibition hindering regeneration and encroachment upslope. Soil temperature data collected by Cieraad & Mcglone (2014) suggest that New Zealand beech treelines are occurring, on average, 100 or more metres below the potential limit indicated by global treeline data (Körner and Paulsen, 2004) and other country-scale analyses (Case and Buckley, 2015). The lower-than-anticipated New Zealand treeline is also highlighted by the occurrence of exotic conifer trees (e.g., *Pinus contorta*) growing 100 m or more above the current beech treeline (Wardle, 2008).

A pressing research challenge is to identify the meteorological conditions allowing enhanced seedling establishment and treeline advance. Abrupt treelines are of particular interest, since their drivers are not readily identified and a delayed response to global warming effects can be compensated by rapid uphill encroachment once the bottleneck limitations are

gone (Harsch & Bader, 2011). Further experimental approaches are required to disentangle how climatic extremes interact with several key stressors that contribute to seedling mortality. For example, winter temperatures at our sites indicate that the surrounding scree was frozen, rendering soil moisture unavailable for root uptake. This might suggest that, at least for the winter period, soil moisture availability may be co-limiting *F. cliffortioides* seedling survival. Likewise, beyond-treeline seedling survival has been shown to be facilitated by sheltered microhabitats near existing subalpine plants (Batllori et al., 2009). This suggests that microhabitat variability can play a vital facilitative role by modulating the impact of stressful events associated with extreme temperatures, low soil moisture availability, periods of intense solar radiation or combinations of these (Körner, 2014; Körner et al., 2016; Körner & Hiltbrunner, 2017). Automated microclimate weather stations with soil moisture sensors, combined with a long-term monitoring fluorometer or a leaf spectrometer to assess the photochemical reflectance index, could be used to evaluate the impacts of microclimatic extreme events on seedling physiology across a range of local environmental conditions.

In conclusion, we found no evidence that high light-induced photoinhibition impairs *F. cliffortioides* vitality and thus hampers subalpine forest advancement uphill in the New Zealand Alps. In many respects *F. cliffortioides* shows remarkable adaptation to the high-light conditions in subalpine environments despite New Zealand's limited genetic repertoire of treeline forming genera. However, we have observed that sudden increases in light intensity combined with low leaf temperatures (< 2 °C) coincide with a drastic, but not sustained ΦPSII decline. Thermal logger readings identified radiative frost experienced by the seedlings throughout the entire year, suggesting that particularly in summer, when seedlings are not cold-hardened, the combination of frosty conditions and high light intensity at dawn is likely to result in photochemical overexcitation and radical-mediated oxidative damage. This could have detrimental effects on overall plant health and even pose a significant dieback risk (Germino & Smith, 1999). Therefore, we believe that intermittent cold-induced photoinhibition events act as the bottleneck hampering *F. cliffortioides* treeline advance in New Zealand.

5 Exploring the interplay of macro- and micro-scale drivers controlling treeline formation: An agent-based model

5.1 Introduction

Following global warming trends, current ecosystem distribution ranges are expected to expand towards their cooler boundaries (Le Roux & McGeoch, 2008). The pace and extent of these ecosystem regime shifts are primarily dictated by broad scale abiotic limitations which define a species' current spatial extent. With ongoing global warming, our ecosystems are subjected to unprecedented rates of change (Brooker, 2006; Parmesan & Yohe, 2003) and the ability to adapt is controlled by the climatic range and spatial connectivity of these systems (Ellison et al., 2005). In particular, species which modify their ecosystem to make it more suitable for their own community (Wilson & Agnew, 2006) reveal a restricted ability to migrate due to their co-dependence and self-induced microclimates (Lustenhouwer et al., 2012). This effect may lead to a delayed ecosystem response to global climate trends (Harsch & Bader, 2011) involving greater risks to further perturbations and greater danger to become fragmented or absorbed by other ecosystems (Oliver et al., 2015).

Alpine forest ecosystems are a prominent example of these ecotone boundaries, where a high-biomass forest ecosystem transitions into low-stature vegetation (Holtmeier, 2009). Absolute treeline altitude is predominately linked to macroscale climatic effects dictating current elevational limits for the life form tree (Körner & Paulsen, 2004). With ongoing global warming trends we expect extended growing seasons to induce forest encroachment beyond current elevation limits (Körner & Paulsen, 2004) at the expense of subalpine and alpine species (Rehfeldt et al., 2006). While abiotic forest limitations are gradually approached with altitude, the relevance of facilitative biotic interactions for the tree species increases (Stress gradient hypothesis (SGH), Bertness & Callaway, 1994; Callaway, 2007). This effect is pronounced in abrupt treeline phenomena, where tree species require positive feedbacks to establish, facilitating their own microclimate within current ecosystem boundaries (Malanson et al., 2011). As a result, their response to top-down macroscale abiotic effects is limited, resulting in a temporal lag in their migration response (Harsch & Bader, 2011).

Abrupt treeline regeneration is recruitment-, rather than growth-limited (Elliott, 2011) and early recruits require microclimatic shelter (bottom-up) to dampen the impact from top-down operating abiotic stressors (Harsch, 2010). Beneficial microhabitats can be created by

existing trees (Batllori et al., 2009; Harsch, 2010), alpine vegetation (Gómez-Aparicio et al., 2005; Loranger et al., 2017), or other topographic features mimicking this effect (Butler et al., 1994; Germino et al., 2002; Resler, 2006). Recruitment success is therefore linked to the availability of climatic 'opportunities' in the subalpine (Scherrer & Körner, 2011). If favourable conditions in the subalpine are absent, existing top-down limitations control seedling performance, resulting in a sharpened ecotone transition and limiting the response to global warming (Harsch & Bader, 2011; Malanson et al., 2011). Facilitative interactions among alpine biota are complex and poorly studied, but once beneficial vegetation associations are identified, nurse plants can be used to enable forest regeneration to occur beyond current boundaries (Pyatt et al., 2016; Rose et al., 2020). While some treeline genera require specific seedling-shrub associations to reach maximum altitudes (Akhalkatsi et al., 2006) others are recruitment limited by alpine vegetation resulting from strong competition for nutrients and space (Grau et al., 2012; Sullivan & Sveinbjörnsson, 2010).

The influence of bottom-up controlled seedling performance is further modulated by the individual's size, as they begin to emerge from the subalpine layer and increase exposure to broad-scale (top-down) climatic variability (Körner, 2016). In this context a size gradient hypothesis for treeline species has been formulated, where trees are required to increase size relative to a neighbouring focal plant to reduce stress exposure (e.g. mechanical shelter, Malanson & Resler, 2016). Biotic seedling facilitation processes via the amelioration of abiotic stress are therefore highly context dependent and are a product of bottleneck limitations modulated on the macro and micro-scale (Butterfield & Callaway, 2013). The complexity of these microhabitat feedbacks requires alpine researchers to focus studies towards the individual (Körner & Hiltbrunner, 2017) and infer microclimatic conditions from mesoclimatic data (Cory & Smith, 2017). Only with a thorough understanding of individual tree performance at the ecotone level, mediated by both top-down (climatic variability) and bottom-up effects (biotic interactions, climatic shelter), will we begin to decipher relevant recruitment bottlenecks and tipping points for plant interactions.

Existing modelling approaches have been used to generate treeline forms along a smooth stressor gradient describing growth, mortality and facilitative interactions as dynamic processes (Wiegand et al., 2006) and use historical photographs to predict the pace of ecotone migration (Wallentin et al., 2008). While the relevance of bottom-up effects and the response down to the individual has been repeatedly emphasized (Malanson & Resler, 2016; Smith-McKenna et al., 2014), current approaches do not assess size-mediated performance under

variable stress gradients. Within the scope of this study, I propose a model to explore the interplay of broad-scale abiotic gradients and size-modulated microclimatic limitations and opportunities and their implications on treeline position. I draw from the theoretical framework of Harsch & Bader (2011) to distinguish between top-down, macroclimatic drivers and finer-scale, bottom-up drivers which modulate the role of abiotic stressors locally.

Here, I develop and apply an agent-based model (ABM) of a treeline ecotone occurring along an elevational gradient. In this hypothetical landscape, mean air temperature (top-down driver) undergoes monthly cycles and decreases gradually with increasing elevation based on a set lapse rate. This temperature gradient, as experienced by the individual tree, is locally modified by microclimatic temperature regimes (bottom-up factors) that are modulated by facilitative seedling interactions (Harsch & Bader, 2011). Adverse effects of close spatial associations among neighbours are incorporated as competition for space and resources following a zone of influence model (ZOI, Lin et al., 2012). Lower temperatures experienced by the individual leads to reduced plant growth and enhanced mortality and height-mediated performance of individual trees dictates the facilitative/competitive nature of tree interactions (Malanson & Resler, 2016) and the availability of thermal shelter (Scherrer & Körner, 2011).

Using this model, the objectives of this study were to: (1) Develop, describe, and evaluate an agent-based model to simulate emergent treeline patterns along a hypothetical mountain slope induced by a macroscale temperature gradient, intraspecific competition and facilitative thermal microclimates, (2) Use existing data from alpine meteorological stations within New Zealand to generate alpine beech treeline ecotone scenarios, (3) Identify thermal threshold values expressed on the microscale level (bottom-up) which enable successful tree recruitment beyond current treeline population boundaries, (4) Explore the role of competitive/facilitative plant-plant interactions in dictating treeline ecotone population dynamics along the stress gradient, and (5) Manipulate the model's top-down temperature regime to explore beech treeline population responses to a global warming scenario.

5.2 Material & Methods

5.2.1 Model overview

The hypothetical mountain treeline ecotone developed within the Netlogo modelling environment (6.0.4, Wilensky, 1999) drew loosely on a hierarchical conceptual model of

treeline pattern development outlined by Harsch & Bader (2011) where sets of nested mechanistic drivers act to impose elevational limits on tree recruitment, mortality and growth at the treeline ecotone. In my model, a macroscale thermal gradient exerted top-down control on the thermal environment along the gradient, which was then locally modulated at finer scales by existing trees and subalpine vegetation. Thus, the performance of newly recruiting seedlings, in terms of survival and growth, resulted from both top-down effects of mean temperature and bottom-up effects of neighbourhood interactions that controlled fine-scale variations in seedling thermal microhabitat (facilitative effect, shelter) and competition for resources (adverse effect).

Microclimatic shelter had the form of intraspecific associations between putative seedlings and existing trees, where taller neighbours provide thermal benefits for smaller successors; alternately, in the above-treeline subalpine zone, existing alpine vegetation provided sheltered 'safe sites' for seedlings by buffering them from stressful conditions (Malanson et al., 2011). Within the context of this model, these alpine vegetation features were referred to as 'subalpine tussock grasses', but climatic niches in the subalpine can occur in a variety of forms of physical shelter (e.g. dead trees, geomorphological features; Resler, 2006; Batllori et al., 2009). Close intraspecific associations among trees introduced adverse effects of competition of space and resources in their zone of influence (ZOI, adapted after Lin et al. 2012). Hence, pioneering recruits in bare, non-vegetated areas operated free from resource competition but were still subject to abiotic stress. Without the presence of surrounding vegetation (absence of thermal shelter) these seedlings were entirely exposed to decreasing ambient air temperatures (and radiation) with increasing elevation, which eventually lead to carbon sink limitations and enhanced mortality (Case & Duncan, 2014). The model comprised a 2-dimensional area with the y-axis oriented parallel to the mountain slope gradient. With every timestep the system updated a cycle of monthly updated mean temperatures which were further modulated by the elevation gradient (Figure 48). With increasing elevation, the grid temperature gradually declined based on a lapse rate of 0.6 °C/100 m of elevation (Nigrelli et al., 2018). Therefore, the coldest temperatures were more likely to be experienced by the trees at higher elevations during the winter months. The response of seedlings to this thermal gradient was then further modulated at a finer scale by interactions with adjacent vegetation and the local environmental conditions (Figure 48a-c). The interaction among neighbouring trees were able to produce facilitative thermal microclimates for the smaller individuals (b) or limited nutrient uptake by increased competition for space (c). For final model evaluation the

mountain slope was divided into 100 m long elevation zones to quantify treeline position changes for different model treatments.

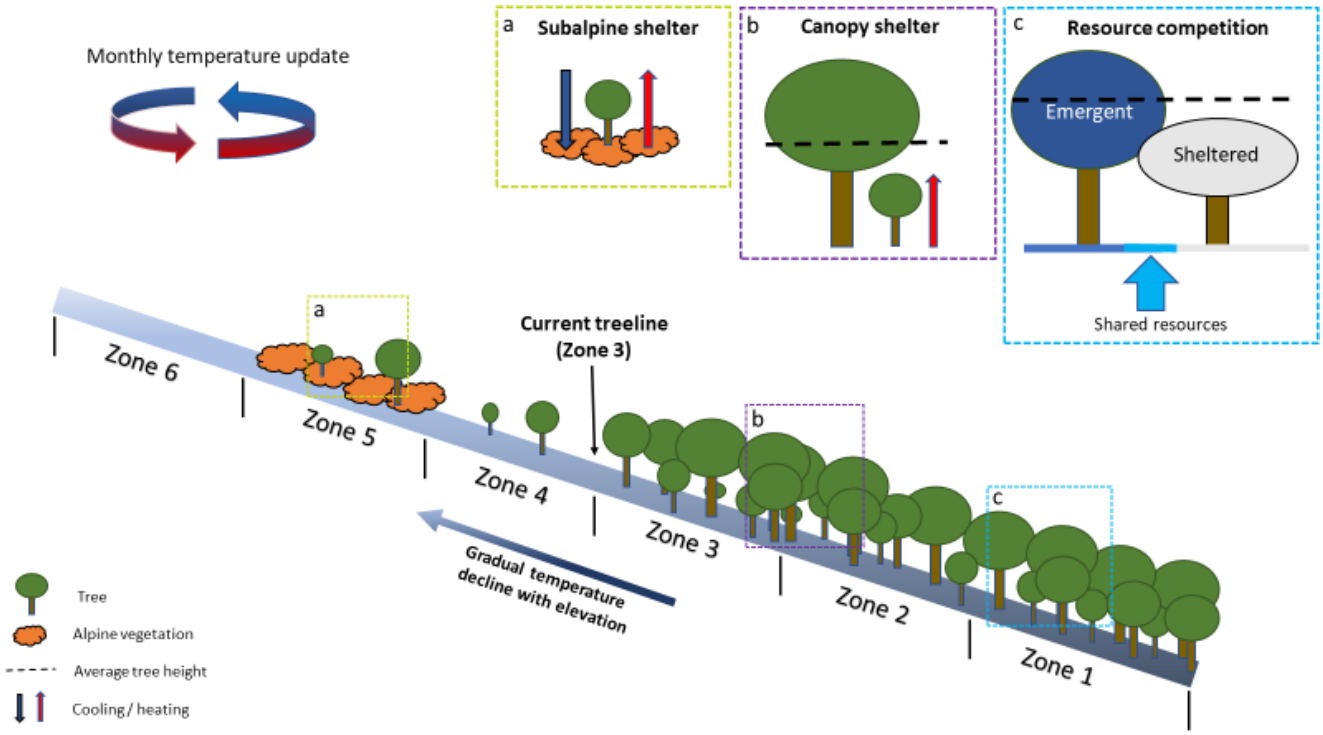

Figure 48: Hypothetical mountain slope within the NetLogo environment. The slope was subject to a smooth temperature gradient, decreasing with elevation (a) Temperature extremes were reduced if a seedling grew in existing alpine vegetation. (b) Smaller than average neighbouring trees gained thermal benefit from association with taller individuals. (c) Neighbouring trees shared resources if their area overlapped based on selected interaction modes and got classified depending on average size of neighbours.

The temperature 'sensed' by an individual tree was a result of the mean monthly temperature modified by local microhabitat conditions based on the following process rules: (a) If a seedling recruited into existing alpine vegetation (e.g. tussock grasses), as opposed to bare, non-vegetated areas, the individual was protected from extreme temperature deviations (e.g. heat/frost) and the temperature sensed by the individual was based on a buffering effect of the tussock vegetation within a finite distance. (b) In locations with multiple trees nearby, the height of each tree was evaluated with respect to the average height of itself and its neighbours. If an individual was shorter than the average it received thermal benefits by protection of surrounding individuals (Figure 48b). (c) If neighbouring trees overlapped in their spatial extent, they shared the resources in this area. The sharing process followed a zone of influence

(ZOI) effect (Figure 48c - turquoise) and resources were allocated based on the selected competition mode (Section 5.2.5.3) which distributed resources based on physical parameters of the individual.

5.2.2 Purpose

The purpose of this model was to explore how changes in annual mean temperature variation and biotic tree interactions (bottom-up) affected treeline position and may induced facilitative associations among agents to escape broad-scale (top-down) thermal limitations.

5.2.3 Model entities, state variables, and scales

The following entities were included in the model: The *global environment* represented a climatic treeline ecotone (i.e. monthly mean temperatures), the *grid cells* corresponded to the elevation gradient within this ecotone (i.e. mountain slope) and the *agents* represented individual trees in different growth stages (i.e. emergent trees, sheltered trees). Table 11 provides an overview of the entities' state variables.

Table 11: Overview of state variables used within the treeline model

Environment		
Climate data	Sets mean air temperature for every month for calculating within the cell context	[°C]
Time	Plant performance parameters are updated with every step on a monthly resolution	[Month]
Agents (trees)		
Growth factor (a)	Constant growth factor, representing genetically fixed intraspecific trait variation (ITV).	1 ± 0.1 [kg m^{-2} time $step^{-1}$]
$B_{init,}$ Bmax, B	Initial Biomass (ITV) Maximum biomass (ITV) biomass	2 ± 0.2 [kg] $2\times10^{6} \pm 2\times10^{5}$ [kg] [kg]
Grid cells		
Elevation	Represents assigned altitude of the patch	[m]

The environment represented a hypothetical treeline ecotone where the temperature sensed by the agents was dictated by annual mean temperatures changing in monthly intervals (Table 11).

Agents represented individual trees with different biomass and height and their physiological performance was modified by state variables ranging within a defined intraspecific trait variation (ITV, Table 11). *Grid cells* represented a mountain slope, where agents aimed to successfully establish. Each cell represented its own microclimate derived from the elevation position (y-axis) on the mountain slope. With an increasing y-axis value, the temperature of the cells decreased. The *global environment* (i.e. treeline ecotone) was the only entity on the system level and defined the monthly temperature variations to which the mountain slope was exposed to.

The model's spatial extent was a rectangular grid of 400 × 600 square cells (Figure 49), each 1 m² in size. The mountain slope therefore extended over 600 m in elevation and the environment was wrapped horizontally to avoid edging effects. The resolution of 1 m² was considered suitable to account for regional and local effects while enabling the model to run practically. In this regard, table 2 provides an overview of selected initialisation parameters and growth processes.

Table 12: Overview of initialisation settings and growth processes used in the model

Variable	Meaning	Value	Source
Initialisation parameters			
Initial trees	Places a starting number of agents randomly distributed in the environment	500	Static value*
Existing vegetation	If activated, places an existing vegetation belt above treeline in elevation zone 5	Default: deactivated	Site dependent
Mortality	If the tree growth rate (gr) falls below this value, it has a stochastic chance to die.	0.095	Static value*
Recruitment	Stochastic chance to spawn seedlings on the entire mountain slope	0.002	Static value*
Abiotic stress	Limits the relative resource quality for the individual (energy intake) and lowers plant growth	0.7	(Chu et al., 2008; Lambers et al., 2008; Travis et al., 2006)
Height to radius	The height of an individual tree is calculated based on the ratio of height to width and can be chosen by the modeller. Factor 2: An individual with a 1.5 m radius now has a height of 3 m.	2	-
Competition mode	Resource-mediated competition for shared areas between individuals (Section 5.2.5.3)	Complete asymmetry	(Lin et al., 2012)
Shelter	Increases the experienced temperature of a tree classified as sheltered (only warming, Figure 48b,c)	3 °C	Tested**
Growth and resources allocation			
gr	Growth rate modified by experienced temperature, growth factor (ITV), maximum biomass (ITV), abiotic stress and competition index (added to biomass)	Section 5.2.5.5	(Lin et al., 2012)
fc	Competition index, share of resources available for trees within their ZOI.	$fc = \frac{\text{n of shared patches}}{n\ of\ total\ patches}$	(Schwinning & Weiner, 1998)
Ae	Effective area an agent occupied modified by biomass and fc	$Ae = B^{3/4} \times fc$	(Enquist & Niklas, 2001)
ITV	Intraspecific genetic trait variation, to account for performance variation within the genetic pool	± 10 %	(Bolnick et al., 2011)

*Initial number of agents, recruitment and mortality were not parameterised against real data. Setup was tested to create stable population numbers for model executions. **Initial response threshold of a warming effect identified in the alpine vegetation treatment.

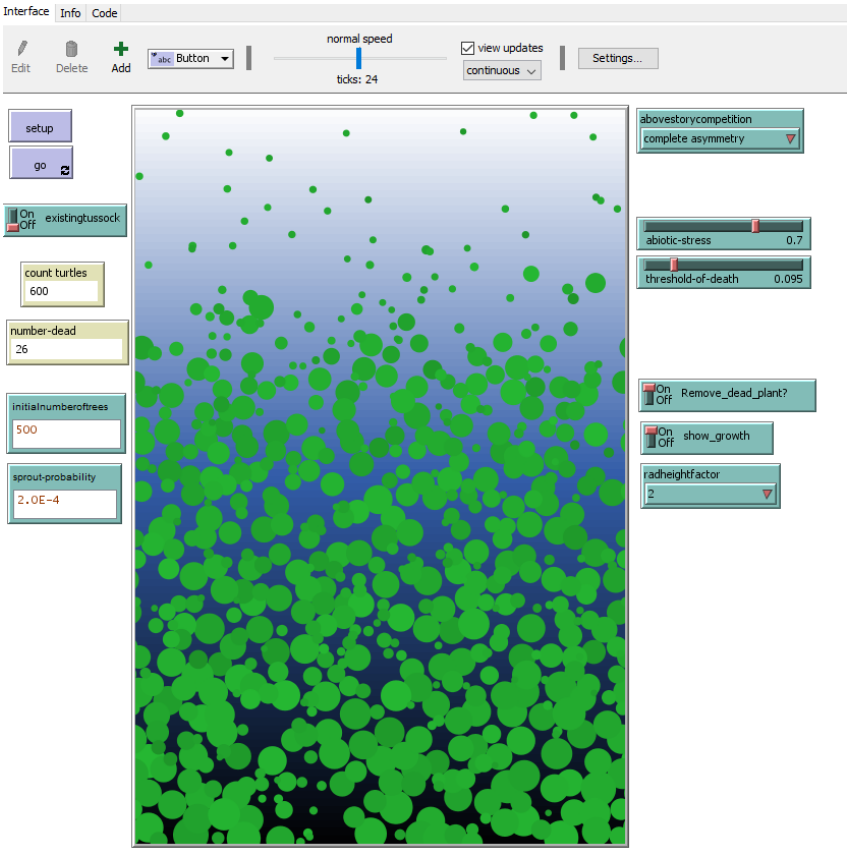

Figure 49: Netlogo (6.0.4) modelling environment. Example output after 24 timesteps (e.g. 24 months). Elevation increased along the y-axis (600 m) (blue – white). Individual trees (green dots) were scaled with their current height.

5.2.4 Process overview and scheduling

A conceptual flowchart of the model processes and scheduling is presented in Figure 50. At each time step, the monthly temperature update triggered a calculation of the temperature sensed by the agents as the sum of the monthly temperature and the temperature assigned to the current elevation grid modified by the thermal gradient. If the agent recruited into existing alpine vegetation (here, subalpine tussock), the agent's temperature was buffered from extreme temperature deviations (Section 5.2.5.4). The tree 'sensed' the average height of neighbouring trees and, dependent on its height, classified itself as a 'sheltered' or 'emergent' tree (Figure 1c). The individual tree then calculated its available resources based on the selected competition mode (Section 5.2.5.3), the quality of the patch (*abiotic stress*) and the spatial overlap among neighbours (ZOI, *Ae*). The trees then calculated their growth rate (*gr*) and if it fell below a certain threshold value the tree dies (Section 5.2.5.5). Next, the trees updated their height information. Finally, recruitment took place, new agents spawned with a predefined probability (Section 5.2.5.2) and got their state variables (ITV) assigned (Figure 50).

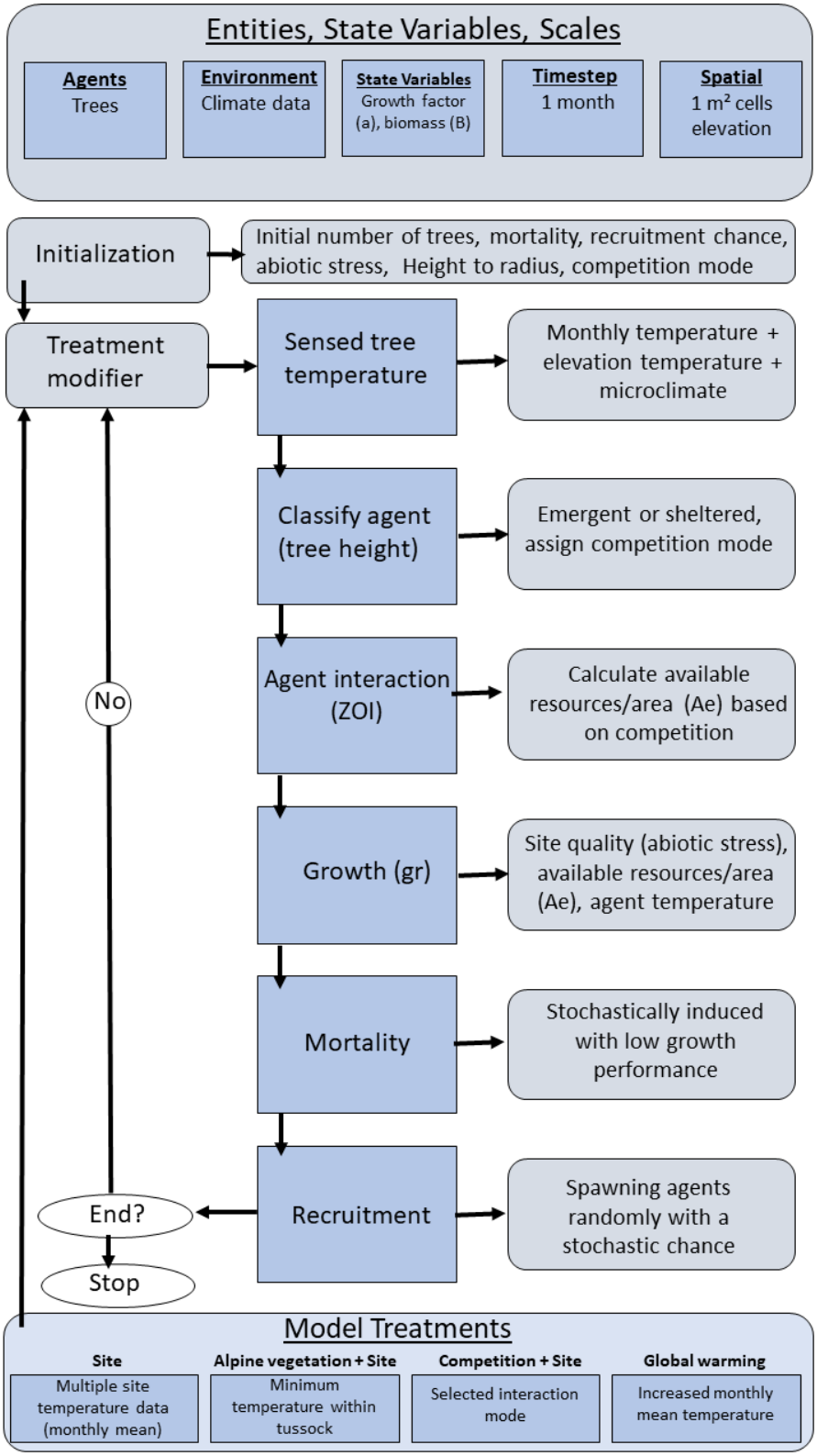

Figure 50: Conceptual flow diagram of the treeline model illustrating the hierarchy of operation structures within the model.

5.2.5 Design concepts

5.2.5.1 Basic principles

Model parameterisation was selected to create generic treeline transitions by decreasing numbers with altitude within the 600 m gradient. Model treatments (broad & fine-scale effects) were designed to observe outlining drivers behind the nature of treeline transitions (diffuse, abrupt) along the hypothetical mountain slope. Trees approached the physiological limitations as the climatic stressors became more pronounced with increasing elevation, meaning that there was an increased benefit of positive plant interactions (Callaway et al., 2002) at treeline which is being investigated within this model. These positive associations of trees with existing vegetation had the potential to overrule macroscale stressors, highlighting the importance of microhabitat heterogeneity for recruitment success (Scherrer & Körner, 2011). Within the concept of this model, a predominant top-down operating driver of monthly mean temperatures was gradually more pronounced towards higher altitude (*sensu* Harsch & Bader, 2011). Fine-scale, bottom-up mechanistic drivers further modulated this effect and were based on individual tree biotic interactions (plant-plant) with neighbours (intraspecific) (Batllori et. al. 2009) or other vegetation (plant-environment) in the subalpine belt (interspecific) (Harsch, 2010). The model aimed to shed some light onto the interplay of these mechanistic drivers, illustrating how a gradual decrease in mean temperature towards higher altitudes (top-down) combined with close microhabitat associations (bottom-up) lead to the formation of a treeline ecotone.

The intraspecific interaction was based on resource competition among neighbouring trees, where they competed for equally distributed resources, they were able to allocate towards growth. If seedlings spatially overlapped, they shared resources within this area based on the selected interaction mode (Section 5.2.5.3). The model offered a range of competitive interaction modes which were based on the zone of influence (ZOI) models developed by Lin et al. (2012). While trees competed for resources, they also showed facilitative interactions with their neighbours, where a close association of smaller trees to taller neighbours provided mechanic shelter. This effect increased the temperature sensed by the individual, dampening the impact of the top-down limitation. An additional opportunity for the trees to realise an interspecific facilitative association was presented by thermal shelter in the environment, which was represented in this model as existing vegetation (alpine tussock). Within the scope of this work, the concept of top-down and bottom-up operating drivers was simplified to address relevant expression of thermal regimes and identify critical temperature threshold values.

The response of individual trees to changing conditions was imposed via probabilistic rules without adaptive decision making (e.g. learning). However, trees were assumed to sense their ambient temperature, their own height, and the average height of neighbouring trees. Existing taller trees (emergent) created warmer thermal microhabitats for smaller neighbours (sheltered), while at the same time competed for resources if their zones of influence overlapped. Based on their competition mode, the trees actively competed for space to increase available resources they were able to allocate towards growth. The interactions among neighbouring trees were therefore of both facilitative (thermal benefit) and competitive nature (resource allocation).

There were two randomised mechanisms within the model: the chance to spawn in any given patch on the field and the intraspecific genetic trait differences (ITV) which has been advocated as an important factor in the modelling of community dynamics (Bolnick et al., 2011). When new trees spawn, they were assigned a growth rate (a) and an initial and maximum biomass (B, B_{max}) randomly selected within their ITV range (Table 11). The growth performance on the individual level therefore was slightly altered by the genetic diversity of the tree species. Tree mortality was induced if tree growth (*gr*) is constrained by the amount of resources they can actively use and the temperature they were currently experiencing.

5.2.5.2 Initialisation

The model was designed to be generally applicable to multiple sites, I therefore provided different options to account for different conditions on a hypothetical mountain slope. Since the model was designed to simulate general treeline emergence patterns along a hypothetical stress gradient, the initialisation parameters were selected and tested (Table 12 & Section 5.2.6) to verify the replicability of the output.

5.2.5.3 Competition

I distinguished between five different modes (Table 13) for resource-mediated competition adapted after the ZOI model proposed by Lin. et al (2012). Modes ranged from complete asymmetry (the bigger individual takes all contested resources) to complete symmetric competition (even allocation of resources in their effective area independent of size) (Schwinning & Weiner, 1998). The different competition modes were indexed in the model using the *fc* parameter. This value in turn modulated the effective area (*Ae*) which was used by the tree to allocate its resources towards growth.

Table 13: Overview of competition modes and their respective effects (adapted after Lin et al., 2012). The value of the shared area for the individual was distributed discretely or was based on their current biomass (size symmetry, allometric interactions). Equations in Appendix B.

Competition mode	Effect
Complete Symmetry	All plants receive the same amount of benefit from each other, irrespective of their species or sizes
Size symmetry	Benefit is proportional to benefactor's size (equal gain per unit size)
Allometric symmetry	Benefit increases with benefactor's size, but less than proportionally
Complete asymmetry	The beneficiary plant receives all benefits, with no advantage to the benefactor plants. Bigger takes it all.
Allometric asymmetry	Benefit increases with benefactor's size super-linearly

The competition index (*fc*) identified the share of resources available for the tree within their respective ZOI (Schwinning & Weiner 1998):

fc Index for competition $\mathrm{fc} = \frac{\text{n of shared patches}}{n\ of\ total\ patches}$

The effective area (*Ae*) scaled allometrically with the tree's biomass (Enquist & Niklas, 2001) and was further modified by the competition index:

Ae Effective Area $Ae = B^{3/4} \times fc$

5.2.5.4 Temperature

The model took the mean temperature of the respective month derived from the provided climatic table (Section 5.2.7) and the temperature assigned to the patch the tree was located on which was modulated by the altitudinal temperature lapse rate (0.6 °C / 100 m, Nigrelli et al., 2018). The model started at zero elevation (T_{Tree} = air-temperature-mean) and the temperature sensed by the individual tree was the sum of both values.

T_{Tree} = air-temperature-mean + altitudinal temperature

The temperature was then further modified if a tree showed close spatial association (temperature increase/buffering) with neighbouring individuals by a value later identified to

generate warming effects in alpine vegetation simulations (+ 3 °C). If a tree recruited within existing alpine vegetation the temperature was buffered and did not exceed 20 °C or falls below a predefined minimum temperature (Section 5.2.8).

5.2.5.5 Growth

Plant growth was modified by current biomass, available space and grid quality and was added to the biomass after each timestep. It followed the concept of growth under competition and abiotic stress proposed by Lin. et al. (2012). The growth rate (*gr*, kg m^{-2} time $step^{-1}$) was a product of temperature sensed by the tree (T_{Tree}), a growth factor (*a*), accounting for the ITV (± 10 %), effective area (*Ae*), biomass (*B*, $B_{\max}$) and competition index (*fc*). Abiotic stress adversely and linearly affected resource uptake and was modified by the shared area and limited by the maximum achievable biomass. The result was added to the current biomass (*B*) of the tree. Tree temperature was adjusted by a scaling factor (*s*) which represented the annual mean temperature across all sites tested (Section 5.2.7) to limit the impact on growth performance.

$$gr = \frac{T_{Tree}}{\mathrm{S}} \times a \times Ae \times \left(1 - \frac{(\frac{B}{Bmax})^{1/4}}{\left(1 - \frac{abiotic\ stress}{1}\right) \times fc}\right) \times (1 - \frac{abiotic\ stress}{1})$$

with

fc Index for competition $fc = \frac{\text{n of shared patches}}{n\ of\ total\ patches}$

If tree growth fell under a critical threshold (*gr* < (*B* ^ 0.75) * Mortality) the tree died and got removed. Successful tree performance is therefore associated with higher temperatures and by minimising resource competition with neighbours.

A detailed model description follows the ODD (Overview, Design concepts, Details) protocol for describing individual- and agent-based models (Grimm et al., 2006, as updated by Grimm et al., 2020). This is designed to enable model reproducibility (see Appendix B).

5.2.6 Sensitivity

Initialisation parameters were selected based on previous studies but population dynamics (initial number, spawn, mortality) were not parameterised against real data. They were selected based on preliminary simulations to assure tree pool numbers did not collapse within the observed timeframe (24 timesteps). To test the model performance, I ran the model within a 10% range (+/-) for the initialisation parameters and observed the relative change in tree numbers at the end of simulation compared to the unchanged baseline scenario (Table 14). This procedure was designed to test the stability of the model and the impact of initialisation parameters for the final output. I tested the initial number of trees, the stochastic probability to die (Mortality), the relation between radius to height, the germination chance of new trees (Spawn rate) and the impact of abiotic stress. For every scenario I ran 50 model simulations and 24 timesteps (months). The model showed highest sensitivity to increases in abiotic stress (site quality) and increased mortality (+ 10%) where the total numbers of trees decreased by 12 % and 5 % respectively. The model revealed high stability, and this can probably be attributed to the high degree of self-organization in alpine forest ecosystems (Smith-McKenna et al., 2014).

Table 14: Relative change in tree population after 24 months for changing initialisation parameters (+/- 10%)

Parameter [Initial value]	**-10%**	**+10%**
Initial trees [500]	1.01	0.99
Mortality [0.095]	1.05	0.94
Radius to height [2]	1.00	1.00
Spawn rate [0.002]	0.95	1.03
Abiotic stress [0.7]	1.03	0.88

5.2.7 Model application for New Zealand beech treelines

I tested the simulation with average mean temperatures for four *Nothofagaceae* treeline sites at different locations within New Zealand's North and South Islands. The climatic data used for the model were sourced from four available mountain weather stations (> 700 m a.s.l., Table

10) from the Cliflo online database (CliFlo, 2020). I used monthly mean temperature averaged from 1981 to 2010 (Tables 16 & 17).

5.2.8 Simulation treatments

To test the impact of variation in aspects of the broad temperature regime and microscale interactions, I designed a range of four model treatments (Table 15). Final treatment outputs were compared for each of 50 replicates at the end of the 24-month period. Population dynamics where quantified in their respective elevation zones and were plotted within R (R Core Team, 2019). If not explicitly stated, initialisation parameters where kept constant.

Table 15: Four tested modelling scenarios and their objectives

Model Treatment	**Modified Parameter**	**Reference**
Objective: Use existing data from alpine meteorological stations within New Zealand to generate alpine beech treeline ecotone scenarios		
Variation in macroscale temperature gradient	Annual mean temperature modified by datasets from four meteorological stations	Körner & Paulsen, 2004
Objective: Identify thermal threshold values expressed on the microscale level (bottom-up) which enable successful tree recruitment beyond current treeline population boundaries		
Climatic shelter in subalpine vegetation	Annual mean temperature + minimum temperature experienced by seedlings within alpine vegetation (Zone 5)	Scherrer & Körner, 2011 Batllori, 2011
Objective: Explore the role of competitive/facilitative plant-plant interactions in dictating treeline ecotone population dynamics along the stress gradient		
Macroscale gradient and fine scale agent interaction	Annual mean temperature + five different interaction modes	Malanson & Resler, 2016
Objective: Manipulate the model's top-down temperature regime to explore beech treeline population responses to a global warming scenario.		
Global warming	Spatially homogenous increase in elevation temperature	Elliott 2011; 2012

For the first treatment, I tested the influence of variation in the top-down, macroscale temperature gradient on treeline position. This treatment was introduced to test how variations within annual mean temperatures affect treeline shape (e.g. diffuse, abrupt) and treeline zone position (Körner & Paulsen, 2004) and served as a baseline for other scenarios tested.

The second treatment introduces subalpine vegetation just beyond the current treeline edge identified in the first scenario. The vegetation belt represents a microclimatic niche within the tree-environment interaction and buffers the temperature range within defined limits. This scenario was designed to assess thermal threshold values within microclimatic feedbacks (bottom-up) which enabled trees to dampen the impact of top-down operating macroscale temperature gradient manipulated within the initial treatment (Malanson et al., 2011). While the maximum temperature sensed by an agent within alpine vegetation is 20 °C and remains unchanged, I tested a range of absolute minimum temperatures which trees can experience if they establish within the alpine vegetation (Zone 5) and verify if the presence of this thermal buffer facilitates treeline recruitment beyond ecotone borders identified without alpine vegetation. I used the mean temperature data from all four previously used weather stations and tested a range of -2 to 5 °C (0.5 °C intervals) absolute minimum temperatures.

The third treatment tested the hypothesis that variations in tree interactions (competition) within their ZOI would lead to different treeline forms (diffuse, abrupt) and/or changes maximum treeline elevation zone. I modelled variations in interaction modes and macroscale temperature simultaneously. This way I was able to test the influence of symmetric (size, allometric, complete) and asymmetric (allometric, complete) resource allocation principles (Table 13) for the agent interaction and their role in dictating species populations (Chu et al. 2008). It has been hypothesised that with an elevated stress gradient the relevance for tree interaction with their environment increases (Bertness & Callaway, 1994; Callaway, 2007), which might affect population abundance in higher elevations.

The fourth treatment simulates a warming scenario, where the top-down temperature gradient (monthly mean temperature) is homogenously elevated by up to 3 °C in increments of 0.5 °C (elevation temperature). This scenario was designed to estimate the effect of climate warming on the position and pattern of alpine treeline ecotones (Elliott, 2011, 2012) and was tested for the Craigieburn valley climate dataset, the site which has been most intensively studied within this thesis.

Table 16: Position of meteorological stations in New Zealand used within this study

Station	Latitude	Longitude	Elevation (m.a.s.l.)	Observing Authority
Arthurs Pass	-42.94152	171.56285	745	NIWA*
Craigieburn Forest	-43.154	171.714	914	N/A
Mt Cook	-42.736	170.096	730	NIWA*
Mt Ruapehu	-39.19589	175.54504	1097	NIWA*/DOC**

* National Institute of Water and Atmospheric Research ** Department of Conservation

Table 17: Annual monthly mean temperatures (°C) for four meteorological stations in New Zealand (> 700 m a.s.l.) from 1981 to 2010.

Arthurs Pass												
Jan	Feb	Mar	Apr	May	Jun	Jul	Aug	Sep	Oct	Nov	Dec	Year
13.3	13.5	11.1	8.3	5.4	2.8	1.7	3.1	5.2	7.0	9.5	11.5	7.7
Craigieburn Forest												
Jan	Feb	Mar	Apr	May	Jun	Jul	Aug	Sep	Oct	Nov	Dec	Year
13.9	13.9	11.8	8.7	5.8	3.1	2.5	3.7	5.9	7.8	9.9	12	8.3
Mt Cook												
Jan	Feb	Mar	Apr	May	Jun	Jul	Aug	Sep	Oct	Nov	Dec	Year
14.6	14.6	12.3	9.4	6.2	3.3	2.2	4.0	6.8	8.6	10.9	12.7	8.8
Mt Ruapehu												
Jan	Feb	Mar	Apr	May	Jun	Jul	Aug	Sep	Oct	Nov	Dec	Year
12.4	12.6	10.7	8.3	5.9	3.6	3.1	3.3	4.9	6.4	8.4	10.6	7.5

5.3 Results

The model results were displayed as tree abundance per elevational zone (Figure 51) and were designed to estimate the impact of macroscale temperature variations on treeline position (Körner & Paulsen, 2004). Three sites (Arthurs Pass, Craigieburn, Mt Cook) exhibited a more gradual population decline starting from the fourth elevation zone just beyond the current treeline. This decline was more pronounced for Arthur's Pass (40.5 % decrease in zonal tree abundance compared to the previous zone) than for Craigieburn or Mt Cook (12.4 to 19.4 % decrease in zonal tree abundance). Mt Ruapehu generated a higher treeline and an initial population decline can be observed starting from the fifth elevation zone and shows a more

rapid decline than the other sites (- 81.4 %). Population numbers within established forest (Zones 1 - 3) revealed no clear differences between sites and the same can be observed for the highest zones tested (5 - 6), where tree abundance was only half of that found within the forest zones. Tree abundance differences induced by top-down control via monthly mean temperatures can therefore only be observed in higher elevation zones (Zones 4 & 5). The mildest winter scenario tested (Mt Ruapehu) generated the highest treeline position before an initial population decline became evident. Climate datasets used within this conceptual model were used to study emergence of different treeline forms and are merely indicative for absolute treeline position as identified in the field.

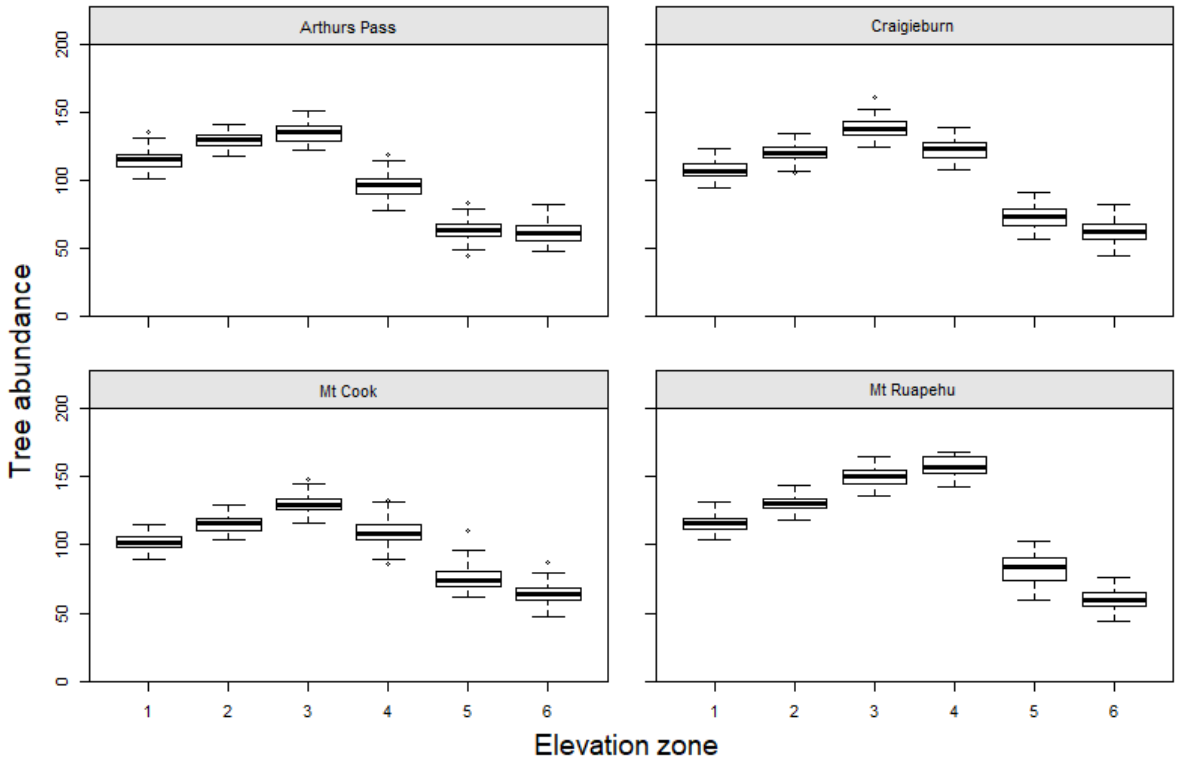

Figure 51: Effect of variation in annual mean temperature on emerging treeline patterns. Tree abundance per elevation zone for four different annual monthly mean temperature treatments (site data). Temperatures derived from meteorological stations (> 700 m a.s.l.) in New Zealand. 24 timesteps (2 year), 50 model runs per site treatment.

For the comparison of minimum temperature within the alpine vegetation (Figure 52), I used the same initialisation parameters as in the site comparison (Figure 51), but introduced a vegetation belt within the subalpine just above current treeline limits (Zone 5). The existing

alpine vegetation had the potential to buffer cold temperature dips (e.g. frost) within the alpine belt. All four tested sites generated consistent tree abundance within the vegetation belt down to a minimum low temperature threshold of 2.5 °C. However, for minimum local temperatures above 3 °C, the model generated an abrupt increase in tree numbers in this zone of 63 to 80 % of initial abundance (Figure 5). The population increased further with 3.5 °C (99 to 120 %) and levelled off at 4 °C at 112 to 130 % of the initial population size. The effect of temperature was similar across all four sites.

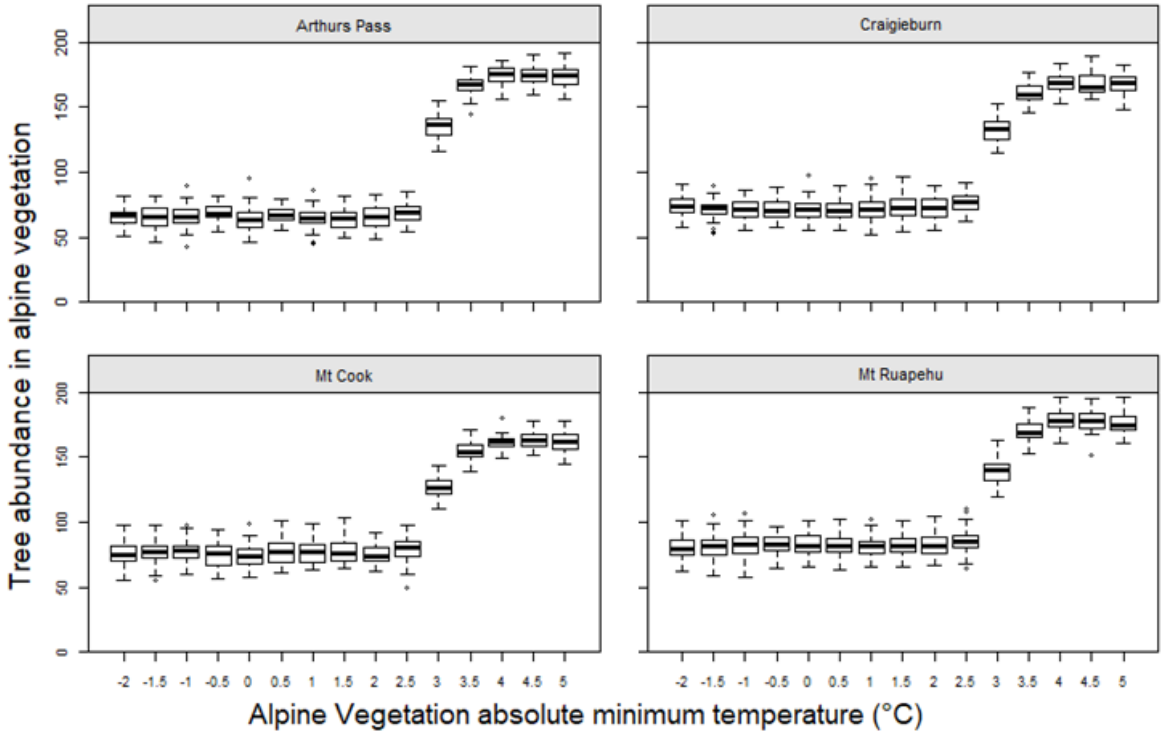

Figure 52: Effect of subalpine shelter and site on tree abundance in the alpine vegetation belt (zone 5). Seedling abundance vs buffered absolute minimum temperature experienced by the individual. The model has been run multiple times (50x), per temperature threshold tested for a total of four different sites (700 model runs per graph, 24 months).

For the third treatment, I compared a range of biotic resource competition scenarios among seedlings sharing their ZOI (Figure 53). When assuming complete symmetry resource allocation, tree abundance was highest within the treeline limit (zone 1 - 3), where all trees receive the same amount of benefit from each other, irrespective of their size. For this scenario, tree abundance declined sharply in the adjacent subalpine by -37 % and -81% in zones 4 and

5, respectively. For Arthurs Pass, Craigieburn and Mount Cook, population size started to decline from elevation zone 4 onwards, regardless of the underlying interaction model (Figure 6). For a given site, the remaining 4 competition modes generated similar treeline patterns mirroring the trend seen in the purely temperature-driven model output (Figure 51). By contrast, for Mount Ruapehu all competition modes predicted maximum tree abundance at elevation zone 4, indicating higher treeline levels, followed by a sharp decline in population size starting from the fifth elevational zone (Figure 53).

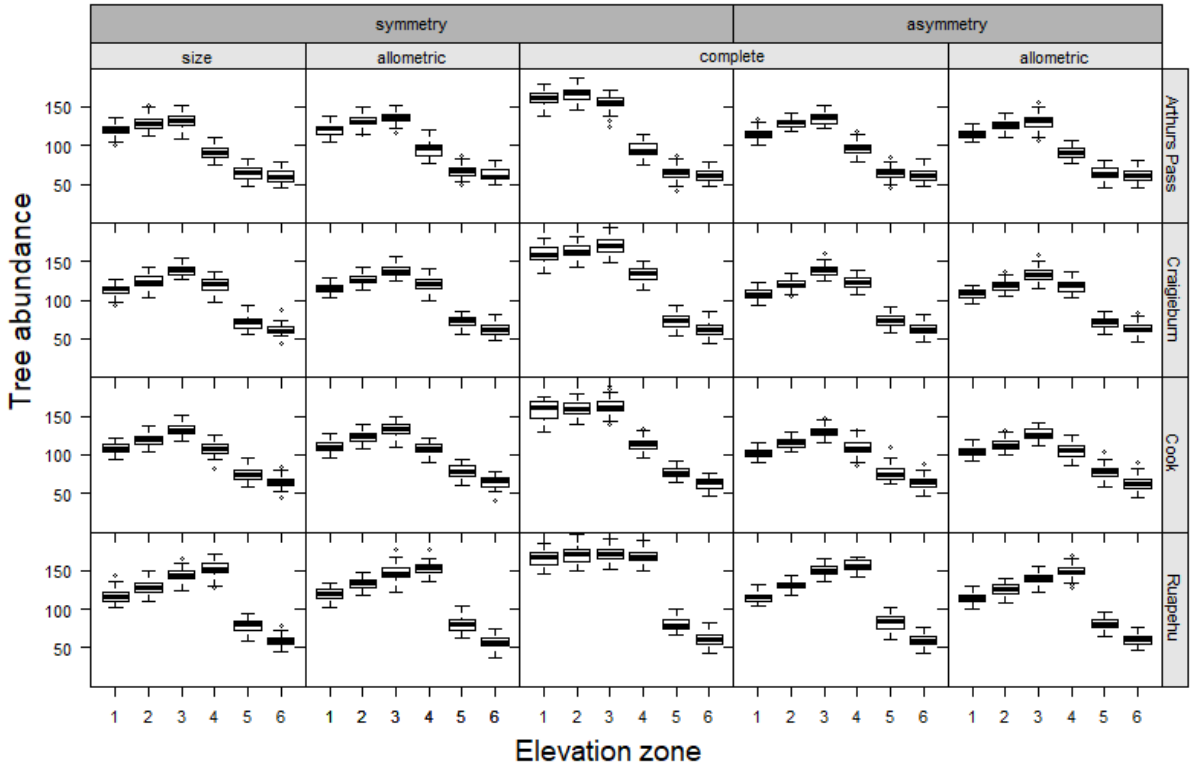

Figure 53: Comparison of resource allocation scenarios (competition modes) for trees interacting within their zone of influence. Columns from left to right: Symmetric and asymmetric interaction modes with sub-modes. Panels show tree abundance estimates as a function of elevation zone for 50 model runs. Each competition mode is tested for all four climate datasets (= 200 runs/competition mode, 24 months).

I designed a global warming scenario for the Craigieburn valley site where a homogenous warming of the mountain slope has been simulated (Figure 54). The grid temperature in every scenario has been increased to approximate future warming scenarios (0 °C to 3 °C) and relative

increases in tree abundance are compared to the ‘no warming’ scenario. The results revealed a strong sensitivity to even moderate warming, shifting the onset of population declines towards the fourth (+13.5 % population increase, +0.5 °C warming) or fifth (+85.8 %, + 1.5 °C) elevation zone followed by abrupt populations declines in the subsequent elevation zones (-37.7 % / -42.2 %). Further warming scenarios showed no effect on tree abundance within the expanded forest boundary spanning elevation zones 1 – 4, but while a 1 °C increase only resulted in a more gradual transition into the subalpine zone, the fifth zone became fully part of the existing forest boundary in all following warming scenarios (+1.5 °C). This process was then stepwise repeated, where the highest elevation zone (6) approaches current treeline quantities (+89.5 %, +2.5 °C) and ultimately extends the forest limit towards the highest zone simulated (+115.3 %, +3 °C).

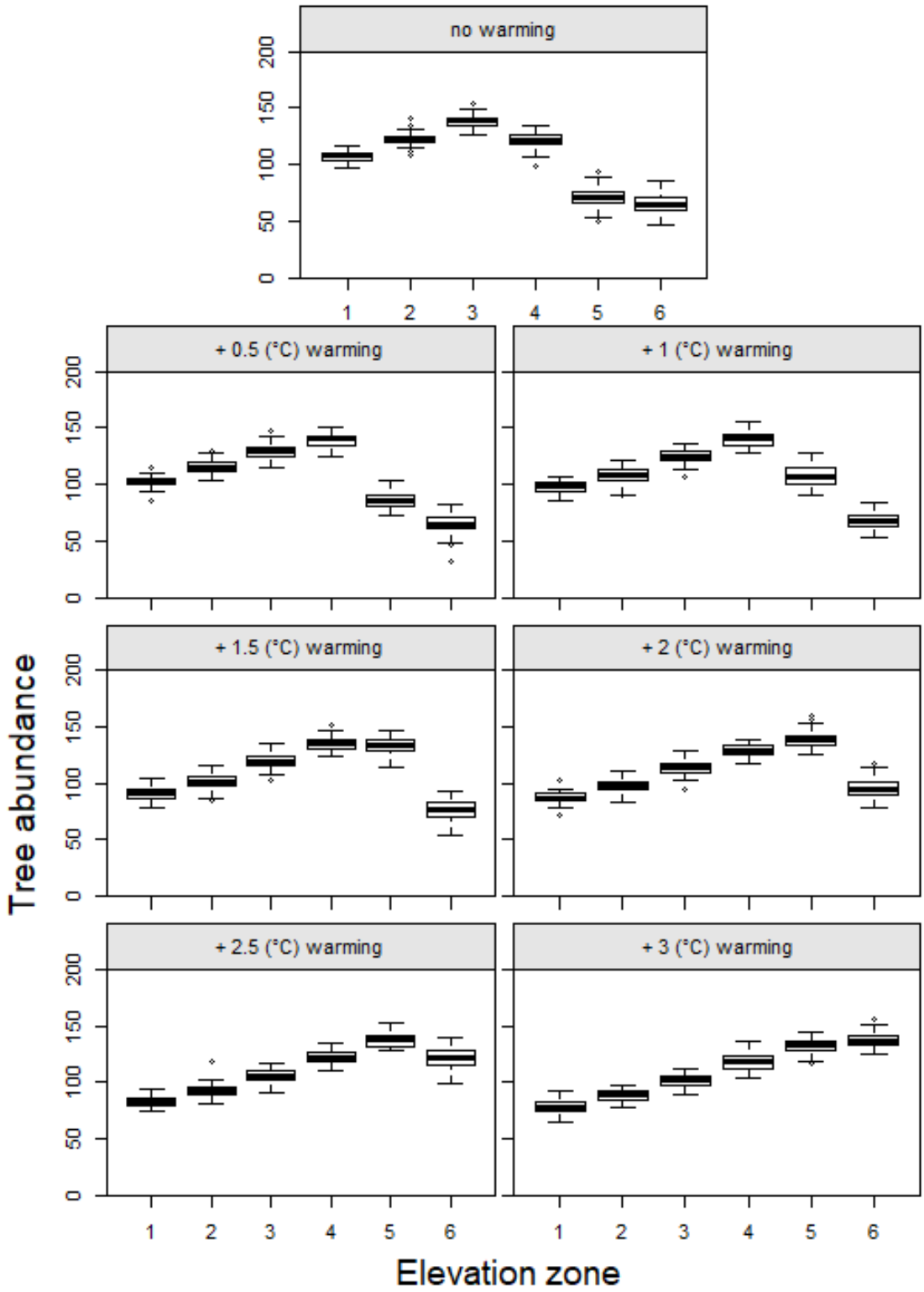

Figure 54: Effect of global warming scenarios on tree abundance. Tree abundance per elevation zone for seven warming scenarios, where elevation temperature is raised incrementally (24 months, 50 runs per graph).

5.4 Discussion

The agent-based model was able to consistently generate realistic treeline patterns based on the thermal regimes imposed on the hypothetical mountain slope. As anticipated, broad-scale, top-down operating temperature levels declined with elevation and adversely affected tree growth, leading to increased tree mortality in higher elevation zones. Trees are therefore more likely to establish within warmer, lower elevational zones, but variation in the monthly mean temperature influenced the sharpness of the tree abundance decline towards higher altitudes. The treeline position is further controlled by bottom-up drivers which influence biotic interactions of seedlings with neighbouring conspecific individuals or existing alpine vegetation. By introducing an absolute minimum temperature threshold facilitated by existing subalpine vegetation I was able to consistently increase population numbers for all tested sites. Further, when the adverse impacts of resource competition among neighbouring trees were smallest (complete symmetry), tree numbers increased within lower zones (1 - 3), increasing ecosystem stability. The implemented global warming scenarios resulted in a gradual increase in tree abundance in subalpine zones (4 - 6) with every warmer increment.

The model results for variation in the top-down thermal variation (site comparison) indicated a higher sensitivity of the treeline position towards cold temperature extremes, which enhanced mortality rates, rather than an adverse effect of low annual mean temperature and hence a potentially restricted growing season. The positioning of the upper forest edge in this model can therefore be best explained by the severity of winter cooling events and associated low tree growth rates rather than a mean growing season isotherm (Körner & Paulsen, 2004). Population numbers within lower elevation zones are kept within confined limits due to adverse effect resource competition (Chu et al., 2008; Lin et al., 2012).

The sensitivity of individuals towards low temperature thresholds is consistent with the results for the model runs which incorporated the alpine vegetation belt just beyond treeline. Once cold temperature extremes are buffered within existing subalpine vegetation, temperature has less of an effect on tree abundance within this zone. This underscores the significance of shifting the treeline research focus towards microclimate regimes, which have the potential to overrule macroclimate effects (Scherrer & Körner, 2011). Further, this finding is consistent with a range of treeline studies, advocating for the importance of thermal niches in the subalpine in determining tree recruitment success and ultimately successful upslope migration of the forest ecotone (Elliott, 2012; Malanson et al., 2011). While the thermal shelter in this

model is represented by existing alpine vegetation, thermal opportunities are not necessarily limited to intraspecific interactions, but can also be established by nurse plants (Pyatt et al., 2016; Rose et al., 2020) or mimicked by topographic terrain features (Cieraad, 2011; Resler, 2006). Although the successful establishment of early recruits benefits from the availability of thermal shelter within the subalpine vegetation, consecutive tree establishment is expected to improve physical shelter and hence availability of thermal niches for successors (Harsch & Bader, 2011). The total number of trees generated within this zone is once again limited by the adverse effect of competition, keeping population numbers within confined limits.

A comparison for competition scenarios where trees are exposed to different mechanism of resource allocation was designed to enhance our understanding of the balance between fine scale thermal shelter and resource competition effects among tree individuals within the leading edge of their ecosystem boundaries. Regardless of site and competition mode, all tested scenarios produce consistently low population numbers for the highest elevation zones (5 – 6), suggesting strong top-down temperature control. A comparison among biotic resource allocation modes revealed no site-related differences in the onset of tree abundance declines and resulted in similar treeline patterns, regardless of the nature of adverse effects of competition among neighbours. Only the 'size symmetry' scenarios which shifted biotic interaction towards a predominately facilitative component resulted in a clear increase in tree populations within the lower elevation zones (1-3). Further, it sharpened the commencement of population decline since it had no impact on areas where tree interaction was limited due to smaller numbers imposed by the top-down operating driver. This mechanism illustrates the drivers behind abrupt treeline phenomena (Harsch & Bader, 2011), which rely heavily on strong positive feedbacks to enhance beneficial microclimates (here: thermal shelter) within their existing ecosystem boundaries (Bekker, 2005; Malanson et al., 2011; Wilson & Agnew, 1992). It is worth noting that the facilitative effect of thermal shelter for smaller individuals within this model only affected the populations dynamics within the lower elevational zones where we would see a denser forest stand regardless of competition mode, suggesting this scenario has only significant implications for the resistance of the current ecosystem boundaries towards change, but has no bearing on future treeline migration (Harsch, 2010).

The simulated warming scenarios had virtually no effect on population abundance at the current forest limits but enabled treeline advance. The initial warming scenario (+ 0.5 °C) increased tree abundance in the upper treeline zone and therefore sharpened the population line

beyond. The result is a treeline pattern similar to the Ruapehu scenario (Figure 51), where this effect can be attributed to milder previous winter periods. Abrupt treeline patterns created in this warming scenario indicate that these treeline forming genera (e.g. *Nothofagaceae*) are potentially at the brink of a significant upslope advance, but will remain stagnant as long as the current bottleneck limitations imposed by cold winters remain in effect (Harsch & Bader, 2011). Remarkably, at higher altitudes the number of trees within a zone increased with elevation – an effect which has not been observed in natural treelines controlled by a macroscale temperature gradient. However, within this model there is a simplified correlation between milder temperatures and a decreased mortality of seedlings, resulting in more trees with smaller biomass at higher altitudes. Hence, their ZOI is less likely to overlap and more smaller individuals can successfully recruit towards higher altitudes. Agent-based modelling scenarios revealed the sensitivity of treeline systems to thresholds values, advocating for research to focus on biologically meaningful temperature regimes for the individual and the implications for the phenological stage (Körner & Hiltbrunner, 2017; Loranger et al., 2017). Treeline migration patterns are primarily controlled by early recruiter performance and mortality (Batllori et al., 2009; Harsch & Bader, 2011), suggesting research to be targeted towards bottleneck effects during regeneration stages. The role of microhabitat feedbacks remains ambiguous (Loranger et al., 2017), size (Malanson & Resler, 2016) and context dependent (e.g. seasonality, Butterfield & Callaway, 2013), hidden in belowground biota (Hagedorn et al., 2019) or resource competition (Chen et al., 2015; Gómez-Aparicio et al., 2005). Future studies on abrupt treelines should aim to further disentangle the role of mechanical shelter within vegetation layers (Bråthen & Lortie, 2016) and how these effects are modified by plant size (Körner, 2016) and species-specific interactions within subalpine zones (Pyatt et al., 2016; Rose et al., 2020). Ecological modelling provides a powerful tool to isolate relevant abiotic limitations highlight their role in top-down and bottom-up drivers. Particularly, agent-based models take a step into the right direction, focusing the research on microscale associations and extrapolate findings into larger scale functional stress gradients (Callaway, 1997; Harsch & Bader, 2011; Malanson & Resler, 2016). Only with a thorough understanding of growth inhibition, mortality and facilitation at treeline (Wiegand et al., 2006) we begin to understand ‘tipping points’ in plant interactions and temporal lags in migration responses of sharp boundary ecosystem (Davis & Gedalof, 2018) in the face of a rapidly changing climate (Michalet & Pugnaire, 2016)

6 General Discussion

The aim of this study was to improve our understanding of the role of subalpine microhabitat variability in controlling upper forest limits in abrupt treeline position and identify environmental variables limiting *Nothofagaceae* regeneration in New Zealand. Results of this study have revealed novel insights into abrupt alpine treelines dynamics where subalpine regeneration is limited by cold-induced photoinhibition and the paucity of favourable microhabitats. The findings elucidate the complex link between biotic and abiotic limitations exposed on different temporal and spatial scales to operate as a sharpening agent in abrupt treeline ecotones.

I investigated i) the role of microhabitat conditions in modulating macroscale-imposed limitation on tree recruitment and growth above treeline and ii) described critical population dynamics processes that interact with temperature to control tree regeneration in the subalpine. I showed the potential for drone technologies to gather meaningful ecological datasets that we can readily combine with existing monitoring plots to help us decipher abrupt ecotone dynamics. We can use these datasets to approximate current bottleneck effects and isolate specific mechanics in modelling approaches to put individual species performance in the context of macroscale- imposed stress gradients.

6.1 Temperature

Fuscospora cliffortioides regeneration patterns in the subalpine revealed a preference for seedlings to recruit in warmer zones with a reduced risk to experience low minimum temperatures. Exposure to high temperature fluctuations was reduced in subalpine vegetation and revealed species-specific differences. Periodic low-temperature dips are observed throughout the year. Modelling suggested enhanced seedling regeneration above treeline if suitable thermal microclimates limited the expression of macroscale-imposed low temperature dips. A similar directional positive feedback was observed in the projected global warming scenarios.

Susceptibility to frost poses a regeneration bottleneck in many treeline phenomena globally and sharpens the ecotone transition (Bader et al., 2007; Ball et al., 1991; Batllori et al., 2009; Cuevas, 2000; Germino et al., 2002). The effect of frost is a bottom-up mechanism working at the microhabitat level and operates as a stress factor enhancing seedling mortality

(Harsch & Bader, 2011). The role of facilitative thermal microhabitat plays a crucial role in generating favourable climatic niches to escape this limitation (Scherrer & Körner, 2010). If a recruitment niche is realised, the seedlings receives thermal protection during the vulnerable early growth stages (Körner, 2016). Once a tree escapes the recruitment bottleneck and successfully establishes in the subalpine it can then ameliorate site conditions for successors, decreasing the stress gradient (Malanson et al., 2011). Successive improvement of site conditions generates directional positive feedback (Alftine & Malanson, 2004) for seedling establishment. This cascade of facilitative feedback promotes further tree regeneration above treeline and can be observed as long as the recruitment bottleneck is confined. For a frost limited treeline this is achieved if macroscale-imposed change (global warming) reduces the overall frequency of low temperature dips or a fundamental climatic niche is presented in the subalpine, which overrides the recruitment bottleneck until initial frost-hardening is achieved.

With ongoing macroscale climatic warming, the role of a temperature-controlled regeneration bottleneck will change. Extended growing seasons (Graham et al., 2012) and a reduced/flattened environmental gradient into the subalpine (Elliott, 2012; Hohnwald et al., 2020) will decrease the stress gradient. Hence, the role of suitable microhabitat to buffer increasingly scarce frost events (Scherrer & Körner, 2010) in the subalpine will decline while the nutrient availability due to warmer root zones will increase (Fetzer et al., 2019). This, in turn, promotes directional positive feedbacks such as the availability of thermal niches in the subalpine (Elliott, 2011) which successively enhance tree establishment beyond current limits. In contrast, global warming shifts the period of frost sensitive ontogenetic stages for pioneering recruits (e.g. bud break; Körner, 2012; Poikolainen et al., 2016), enhances radiative frost due to shorter periods of insulating snow pack in winter (Bader et al., 2018; Davis & Gedalof, 2018) and introduces new limitations such as heat induced desiccation stress during the growing season. The response of treeline forming genera to global warming remains species-specific (Treml & Veblen, 2017) and limited by the genetic repertoire at site (southern beech in New Zealand; Cieraad, 2011) and a resulting limited phenological plasticity (Donnelly et al., 2012) to respond to variations in the sharpened stress gradient.

The role of microhabitat vegetation heterogeneity in ameliorating the effect of macroscale-imposed temperature limitations is a robust feature throughout projected meteorological variability and is likely to play an important role in the future (Rydsaa et al., 2016). The temporal lag in a responsiveness to climatic change in abrupt treeline ecotones can only be sufficiently addressed if the true nature of a recruitment bottleneck is identified. For

southern beech forming tree species these means deciphering the role of a temperature modulated photoinhibition effect.

6.2 Light

Results of the fourth chapter clearly refuted the hypothesis that New Zealand's treeline is hampered by photoinhibition alone (Norton & Schönenberger, 1984; Wardle, 1985a, 2008). The photosynthetic apparatus of *F. cliffortioides* is well adapted to the high-light environment and revealed no evidence of periodic or sustained photodamage. However, early morning temperature and winter solar radiation indicated to be important factors in predicting seedling growth in the subalpine (Chapter 3). By linking low ΦPSII on winter mornings, and large, sudden temperature drops in summer, I was able to conclude that cold-induced photoinhibition might result in lethal photo-oxidative damage in *N. cliffortioides*.

Solar radiation stress at treeline operates on the microhabitat levels and is a microsite limitation expressed on the seedling stage (Harsch & Bader, 2011) sharpening the treeline ecotone. A solar induced recruitment bottleneck in abrupt treelines is poorly understood and only few studies have addressed this phenomena (Bader, van Geloof, et al., 2007; Ball et al., 1991; Close et al., 2000, 2002; Reyes-Díaz et al., 2005).The study design for the seedling chlorophyll measurements was influenced by an observed effect deemed to be relevant in controlling related *Nothofagaceae* treeline forming species (*N. dombeyi* and *N. pumilio*) of the Southern Hemisphere. Findings in the Andes revealed the relevance of frost modulated seedling performance (Piper et al., 2005; Reyes-Díaz et al., 2005) and light limited carbohydrate acquisition (Piper et al., 2009). I hypothesised this effect to be even be more pronounced in the evergreen *Nothofagaceae* of New Zealand.

The role of light in constituting a potential recruitment bottleneck in abrupt treeline phenomena globally is an area which remains elusive. While chlorophyll measurements provide an ideal tool to study microhabitat variations in light and temperature simultaneously, the role of a down-regulated photosystem performance as a stress response requires further research. Plants may reduce photosystem activity to decrease the risk of photo-oxidative damage (Demmig-Adams & Adams, 2006). This can be achieved via a reduced carbon-sink activity through adjustments in the violaxanthin cycle (Jahns et al., 2009). Yet, only a few studies described a down-regulated photosynthetic yield during winter as a mechanism to respond to lower levels of incident light (III Adams et al., 1995; Reyes-Díaz et al., 2005; Zarter

et al., 2006a,b,c). This form of an adaptive stress response was not pronounced in *F. cliffortioides*, indicating that the species may lack the plasticity to respond to cold-induced photoinhibition effects. Therefore, I hypothesise that a limited down-regulated yield during periods of expected reduced carbon sink activity (e.g. winter) enhances exposure to a cold-induced photoinhibition bottleneck. This effect might be further influenced by the topography of the site, suggesting a more pronounced effect on East-facing slopes which receive earlier sunlight. Further research is required to disentangle the role of high radiation levels to function as a sharpening agent in treeline ecotones. In order to address this issue, we required further research to build our understanding of how shrub-seedling interactions control the light and temperature environment in the ecotone.

6.3 Microhabitat interactions

Microhabitat heterogeneity modulated macroscale-imposed limitations relevant for *F. cliffortioides* recruitment patterns in the subalpine. Seedling presence in *Leucopogon colensoi* was significantly higher than the spatial availability of these sites. Recruitment was severely limited amongst tussock grasses (*Chionochloa* spp.), despite its superior ability to buffer temperature deviations. Findings suggested that their dense arrangement does not leave seedlings enough space to establish. The ground-cover vegetation was the dominant explanatory variable stimulating growth in exposed seedlings. Modelling outputs suggested that adverse effects of competition only played a major role in controlling stability of current forest boundaries.

Neighbourhood effects in the subalpine modulate the effect of microhabitat conditions expressed on the seedling stage (Harsch & Bader, 2011). While a treeline forming species approaches its physiological limits with altitude, the role of favourable biotic interactions increases (Callaway, 2007). Fundamental climatic niches for seedling establishment are generated when shrub-seedling interactions ameliorate macroscale-imposed limitations and mimic microclimates present under the forest canopy (Malanson et al., 2011b). While the climatic benefits of these associations in the subalpine have been repeatedly underscored (Pyatt et al., 2016; Scherrer & Körner, 2010a), the biotic interactions are not exclusively facilitative. The realisation of the climatic niche is hampered by adverse effects of competition for space and resources (Chu et al., 2008). The role of shrub-seedling interactions is ambiguous

(Butterfield & Callaway, 2013; Loranger et al., 2017) and research is required to disentangle species and site-specific links (Bader et al., 2018).

A pivotal shift in abrupt treeline migration is reached once the shrub-seedling relationship triggers successive forest regeneration patterns. This 'tipping point' is reached when the quantity of nurse objects is sufficient to facilitate treeline community development in the subalpine (Batllori et al., 2009; Pyatt et al., 2016; Rose et al., 2020). Future global warming is expected to modify microhabitat temperature and competition regimes in the subalpine (Klanderud & Totland, 2005) and alter seedling-shrub responses by the effects of homogenised shrub communities at the ecotone border (Kitagawa et al., 2020). Therefore, ecotones require fine-scale monitoring approaches to predict the pace of ecosystem migration.

6.4 Spatial characterisation and future directions

I deployed a wide array of tools and techniques to address the need for an increasing demand to characterise microhabitat heterogeneity in the subalpine treeline ecotone (Chapter Two). This methodology enabled me to derive fine-scale information for vegetation communities, topography and thermal range at treeline, representing the most comprehensive characterisation of a subalpine treeline ecotone to-date. The combination of fine-scale spatial information with seedling transect data (temporal) elucidated the role of facilitative microhabitat responses in promoting species distributions along the ecotone gradient (Fortin, 1993; Palmer & Dixon, 1990)

With global warming, the realised niche of the forest is shifting in elevation and current limitations imposed on tree performance and reproduction are reduced (Brown et al., 2019). While macroscale-imposed limitations are still effective, a successful colonialization of the subalpine is coupled to the quantity and quality of favourable microhabitats. To detect ecotone dynamics and responses to change a detailed classification of subalpine vegetation is required. These datasets can then be used to approximate bottleneck effects in abrupt treelines by combining topographic and vegetation features at site and study their impact on ameliorating macroscale-imposed limitations (Chapter 2 & 3). Detailed studies of the spatial characterisation of the treeline ecotone can be used for preliminary studies of the site and formulate initial research questions. For instance, photoinhibition experiments can be conducted in areas where extreme temperature deviations coincide with high radiation levels. Further, measurement periods for field studies can be specified my identifying a potential seasonality of a recruitment

limitation. For example, a cold-induced photoinhibition bottleneck can be disregarded in winter if seedlings successfully establish in areas where the software predicted areas of perpetual shade.

To further elucidate the effect of sudden coinciding abiotic extremes (e.g. frost and radiation), I suggest the setup of a long-term monitoring station in the subalpine. The station would periodically record microhabitat variability in the temperature and light regime and plant-health based parameters such as NDVI and chlorophyll fluorescence measurements. Permanent photo points retaken at regular intervals should be used to monitor dieback and effects of invasive animals prominent in the area (e.g. deer). Where possible, the role of below-ground biota (e.g. competition, mycorrhiza) and nutrient availability (e.g. frost limited water uptake) should be monitored, as they may be additional parameters driving subalpine forest regeneration (Hagedorn et al., 2019; Hasselquist et al., 2005). Location of these monitoring stations can be identified using the 3D maps created in the fine-scale characterisation of the alpine treeline ecotone (Chapter 2).

6.5 Combining techniques to monitor abrupt ecotone systems

The research conducted within this thesis establishes three different techniques and ultimately three different perspectives on seedling recruitment in an abrupt treeline ecotone: Geospatial techniques for mapping and analysis, field-based observations of environmental conditions and plant physiology, and agent-based simulation modelling. While all three methodologies may function as independent observations of an abrupt ecosystem border, the combination of techniques helps to stepwise approach the recruitment bottleneck and estimate the strength of drivers in the future.

The 3D model (Chapter Two) provides the baseline for the conducted research, it introduces a ‘playground’ to plan future study designs and enables a pre-analysis of the field condition. Cold-induced photoinhibition experiments can be conducted in areas where cold temperatures and high radiation levels coincide, avoiding areas of perpetual winter shade. The next step would be to attach hyperspectral sensors to the UAV systems to allow us to further discriminate between subalpine vegetation and ideally identify new beech seedlings via remote sensing techniques. A combination with higher resolution LiDAR sensors could enable us to measure seedling growth without the need of additional field surveys, allowing us to monitor seedling transects at higher frequency. Repeating field surveys more often could provide

valuable information about annual variation in seedling regeneration patterns we do not fully understand yet (see hotspot visualisations). Seedling performance evaluations based on the transect data and remotely derived information (Chapter Three) are an ideal tool to test a hypothesis with a wealth of independent variables. The interpretation of these datasets with machine learning algorithms provides an unbiased interpretation of the 'raw data' and helps further elucidate relevant drivers. The chlorophyll fluorescence measurements (Chapter Four) and their respective study design are ideally an outcome of the perspectives granted from the previous chapters. The methodology has proven particularly useful for slow ecosystem transformations as documented within this study. With more time at hands, I recommend conducting these techniques in chronological order, to allow a more targeted approximation of relevant drivers. The modelling chapter was designed to illustrate regeneration patterns into the subalpine and further elucidate the role of micro-scale effects between neighbours and adjacent vegetation. While the model in the current state allows the 'personalisation' to local treelines using data from nearby weather stations, the next logical step would be to incorporate seedling transect information (agent position/size) and link the information to the seedling performance studies in Chapter Three. Hereby the subalpine environment could be modified to reflect the field data for subalpine vegetation and seedling performance within could be adjusted accordingly. Therefore, with additional site-specific modification based on previous studies the model can provide a powerful tool to predict the pace of future treeline response to global warming.

6.6 Conclusion

The temporal lag in a response of abrupt treeline phenomena suggests that the current macroscale-imposed limitations are not necessarily at climatic equilibrium. Underlying drivers do not reveal clear directional facilitative feedbacks into the subalpine which we can correlate with predicted warming events. Successful treeline advance is hampered by a *F. cliffortioides* recruitment bottleneck in the subalpine. To further elucidate the nature of the current limitations, we can deploy new technologies in remote imagery to fulfil the higher demand for high-quality spatial datasets. Within this thesis I provided new workflows to extract meaningful ecological datasets at treeline. Such detailed spatial information on the alpine treeline ecotone will allow future treeline research to deliver greater spatial and temporal replication at fine scales to monitor changes. These datasets can be combined readily with long-term treeline census information. The combination of methodologies can be used to study forest migration patterns into the subalpine and approximate potential bottleneck effects sharpening the ecotone gradient.

This research shows that for the *Nothofagaceae* treeline in New Zealand, the current treeline position is constrained by cold-induced photoinhibition effects linked to the surprising occurrence of frequent summer frosts at treeline. As *F. cliffortioides* is otherwise well-adapted for high altitude environments, suggesting that we will observe a rapid uphill encroachment once current limitations diminish in the face of global warming. Such empirical results, combined with greater use of agent-based modelling that incorporates fine-scale topographic maps and microhabitat heterogeneity will assist us to put individual tree performance in the context of large scale abiotic functional stress gradients and improve our understanding of alpine ecotone formation and maintenance.

7 References

Adams, W., Demmig-Adams, B., Winter, K., & Schreiber, U. (1990). The ratio of variable to maximum chlorophyll fluorescence from photosystem II, measured in leaves at ambient temperature and at 77K, as an indicator of the photon yield of photosynthesis. *Planta*, *180*, 166–174. https://doi.org/10.1007/BF00193991

Akhalkatsi, M., Abdaladze, O., Nakhutsrishvili, G., & Smith, W. K. (2006). Facilitation of Seedling Microsites by *Rhododendron Caucasicum* Extends the *Betula Litwinowii* Alpine Treeline, Caucasus Mountains, Republic of Georgia. *Arctic, Antarctic, and Alpine Research*, *38*(4), 481–488. https://doi.org/10.1657/1523-0430(2006)38[481:FOSMBR]2.0.CO;2

Alftine, K. J., & Malanson, G. P. (2004). Directional positive feedback and pattern at an alpine tree line. *Journal of Vegetation Science*, *15*(1), 3–12. https://doi.org/10.1111/j.1654-1103.2004.tb02231.x

Allan, H. H. (1961). Flora of New Zealand. Volume I. *Flora of New Zealand. Volume I., 8 x 5 1/2*. https://www.cabdirect.org/cabdirect/abstract/19620300145

Allen, R. B., & Platt, K. H. (1990). Annual Seedfall Variation in *Nothofagus solandri* (*Fagaceae*), Canterbury, New Zealand. *Oikos*, *57*(2), 199–206. https://doi.org/10.2307/3565940

Anderson, K., & Gaston, K. J. (2013). Lightweight unmanned aerial vehicles will revolutionize spatial ecology. *Frontiers in Ecology and the Environment*, *11*(3), 138–146. https://doi.org/10.1890/120150

Asada, K. (1999). The water-water cycle in chloroplasts: Scavenging of active oxygens and dissipation of excess photons. *Annual Review of Plant Physiology and Plant Molecular Biology*, *50*, 601–639. https://doi.org/10.1146/annurev.arplant.50.1.601

Bader, M. Y., Geloof, I. van, & Rietkerk, M. (2007). High solar radiation hinders tree regeneration above the alpine treeline in northern Ecuador. *Plant Ecology*, *191*(1), 33–45. https://doi.org/10.1007/s11258-006-9212-6

Bader, M. Y., Loranger, H., Zotz, G., & Mendieta-Leiva, G. (2018). Responses of Tree Seedlings near the Alpine Treeline to Delayed Snowmelt and Reduced Sky Exposure. *Forests*, *9*(1), 12. https://doi.org/10.3390/f9010012

Ball, M. C., Hodges, V. S., & Laughlin, G. P. (1991). Cold-Induced Photoinhibition Limits Regeneration of Snow Gum at Tree-Line. *Functional Ecology*, *5*(5), 663–668. https://doi.org/10.2307/2389486

Batllori, E., Camarero, J. J., Ninot, J. M., & Gutiérrez, E. (2009). Seedling recruitment, survival and facilitation in alpine *Pinus uncinata* tree line ecotones. Implications and potential responses to climate warming. *Global Ecology and Biogeography*, *18*(4), 460–472. https://doi.org/10.1111/j.1466-8238.2009.00464.x

Bekker, M. F. (2005). Positive Feedback Between Tree Establishment and Patterns of Subalpine Forest Advancement, Glacier National Park, Montana, U.S.A. *Arctic, Antarctic, and Alpine Research*, *37*(1), 97–107. https://doi.org/10.1657/1523-0430(2005)037[0097:PFBTEA]2.0.CO;2

Bekker, M., & Malanson, G. (2008). Linear forest patterns in subalpine environments. *Progress in Physical Geography*. *32*, 635–653. https://doi.org/10.1177/0309133308101384

Benjamini, Y., & Hochberg, Y. (1995). Controlling the False Discovery Rate: A Practical and Powerful Approach to Multiple Testing. *Journal of the Royal Statistical Society. Series B (Methodological)*, *57*(1), 289–300.

Bertness, M. D., & Callaway, R. (1994). Positive interactions in communities. *Trends in Ecology & Evolution*, *9*(5), 191–193. https://doi.org/10.1016/0169-5347(94)90088-4

Björkman, O., & Demmig, B. (1987). Photon yield of O_2 evolution and chlorophyll fluorescence characteristics at 77 K among vascular plants of diverse origins. *Planta*, *170*(4), 489–504. https://doi.org/10.1007/BF00402983

Björkman, O., & Demmig-Adams, B. (1995). Regulation of Photosynthetic Light Energy Capture, Conversion, and Dissipation in Leaves of Higher Plants. *Ecophysiology of Photosynthesis*, 17–47. https://doi.org/10.1007/978-3-642-79354-7_2

Blaschke, T., Hay, G. J., Kelly, M., Lang, S., Hofmann, P., Addink, E., Queiroz Feitosa, R., van der Meer, F., van der Werff, H., van Coillie, F., & Tiede, D. (2014). Geographic Object-Based Image Analysis – Towards a new paradigm. *Journal of Photogrammetry and Remote Sensing*, *87*, 180–191. https://doi.org/10.1016/j.isprsjprs.2013.09.014

Blaschke, T., & Strobl, J. (2001). What's wrong with pixels? Some recent developments interfacing remote sensing and GIS. *GIS – Zeitschrift Für Geoinformationssysteme*, *14*, 12–17.

Boesch, R. (2017). Thermal remote sensind with UAV-based workflows. *International Archives of the Photogrammetry, Remote Sensing and Spatial Information Sciences*, *XLII-2/W6*, 41–46. https://doi.org/10.5194/isprs-archives-XLII-2-W6-41-2017

Bolnick, D. I., Amarasekare, P., Araújo, M. S., Bürger, R., Levine, J. M., Novak, M., Rudolf, V. H. W., Schreiber, S. J., Urban, M. C., & Vasseur, D. A. (2011). Why intraspecific trait variation matters in community ecology. *Trends in Ecology & Evolution*, *26*(4), 183–192. https://doi.org/10.1016/j.tree.2011.01.009

Bråthen, K. A., & Lortie, C. (2016). A portfolio effect of shrub canopy height on species richness in both stressful and competitive environments. *Functional Ecology*, *30*(1), 60–69. https://doi.org/10.1111/1365-2435.12458

Breiman, L. (2001). Random Forests. *Machine Learning*, *45*(1), 5–32. https://doi.org/10.1023/A:1010933404324

Breiman, L. (2017). *Classification and Regression Trees*. Routledge. https://doi.org/10.1201/9781315139470

Brice, M.-H., Cazelles, K., Legendre, P., & Fortin, M.-J. (2019). Disturbances amplify tree community responses to climate change in the temperate–boreal ecotone. *Global Ecology and Biogeography*, *28*(11), 1668–1681. https://doi.org/10.1111/geb.12971

Brooker, R. W. (2006). Plant–plant interactions and environmental change. *New Phytologist*, *171*(2), 271–284. https://doi.org/10.1111/j.1469-8137.2006.01752.x

Brown, C. D., Dufour-Tremblay, G., Jameson, R. G., Mamet, S. D., Trant, A. J., Walker, X. J., Boudreau, S., Harper, K. A., Henry, G. H. R., Hermanutz, L., Hofgaard, A., Isaeva, L., Kershaw, G. P., & Johnstone, J. F. (2019). Reproduction as a bottleneck to treeline advance across the circumarctic forest tundra ecotone. *Ecography*, *42*(1), 137–147. https://doi.org/10.1111/ecog.03733

Butler, D. R., Malanson, G. P., & Cairns, D. M. (1994). Stability of alpine treeline in Glacier National Park, Montana, U.S.A. *Phytocoenologia*, 485–500. https://doi.org/10.1127/phyto/22/1994/485

Butterfield, B. J., & Callaway, R. M. (2013). A functional comparative approach to facilitation and its context dependence. *Functional Ecology*, *27*(4), 907–917. https://doi.org/10.1111/1365-2435.12019

Cairns, D. (2001). Patterns of Winter Desiccation in Krummholz Forms of *Abies Lasiocarpa* at Treeline Sites in Glacier National Park, Montana, USA. *Geografiska Annaler*, *83*(3), 157–168. https://doi.org/10.1111/j.0435-3676.2001.00151.x

Callaway, R. (2007). *Positive Interactions and Interdependence in Plant Communities*. Springer.

Callaway, R. M. (1997). Positive interactions in plant communities and the individualistic-continuum concept. *Oecologia*, *112*(2), 143–149. https://doi.org/10.1007/s004420050293

Callaway, R. M., Brooker, R. W., Choler, P., Kikvidze, Z., Lortie, C. J., Michalet, R., Paolini, L., Pugnaire, F. I., Newingham, B., Aschehoug, E. T., Armas, C., Kikodze, D., & Cook, B. J. (2002). Positive interactions among alpine plants increase with stress. *Nature*, *417*(6891), 844–848. https://doi.org/10.1038/nature00812

Callaway, R. M., & Walker, L. R. (1997). Competition and Facilitation: A Synthetic Approach to Interactions in Plant Communities. *Ecology*, *78*(7), 1958–1965. https://doi.org/10.1890/0012-9658(1997)078[1958:CAFASA]2.0.CO;2

Candiago, S., Remondino, F., De Giglio, M., Dubbini, M., & Gattelli, M. (2015). Evaluating Multispectral Images and Vegetation Indices for Precision Farming Applications from UAV Images. *Remote Sensing*, *7*(4), 4026–4047. https://doi.org/10.3390/rs70404026

Case, B.S., & Duncan, R. P. (2014). A novel framework for disentangling the scale-dependent influences of abiotic factors on alpine treeline position. *Ecography*, *37*(9), 838–851. https://doi.org/10.1111/ecog.00280

Case, B.S., Buckley, H. L., Fake, M., Bryan, S., Bilkey, J., & Griffiths, J. (2019). *Assessing the use of UAV-collected data for characterising the distributions and frequencies of sand dune vegetation cover types at Kaitorete Spit, Canterbury. New Zealand.* Department of Conservation Research and Development Series.

Cawood, A. J., Bond, C. E., Howell, J. A., Butler, R. W. H., & Totake, Y. (2017). LiDAR, UAV or compass-clinometer? Accuracy, coverage and the effects on structural models. *Journal of Structural Geology*, *98*, 67–82. https://doi.org/10.1016/j.jsg.2017.04.004

Chen, Jianguo, Yang, Y., Stöcklin, J., Cavieres, L. A., Peng, D., Li, Z., & Sun, H. (2015). Soil nutrient availability determines the facilitative effects of cushion plants on other plant species at high elevations in the south-eastern Himalayas. *Plant Ecology & Diversity*, *8*(2), 199–210. https://doi.org/10.1080/17550874.2013.872206

Chen, Jianjun, Yi, S., Qin, Y., & Wang, X. (2016). Improving estimates of fractional vegetation cover based on UAV in alpine grassland on the Qinghai–Tibetan Plateau. *International Journal of Remote Sensing*, *37*(8), 1922–1936. https://doi.org/10.1080/01431161.2016.1165884

Chen, Y., Lu, D., Luo, G., & Huang, J. (2015). Detection of vegetation abundance change in the alpine tree line using multitemporal Landsat Thematic Mapper imagery. *International Journal of Remote Sensing*, 36(18), 4683-4701. https://doi.org/10.1080/01431161.2015.1088675

Chu, C.-J., Maestre, F. T., Xiao, S., Weiner, J., Wang, Y.-S., Duan, Z.-H., & Wang, G. (2008). Balance between facilitation and resource competition determines biomass-density relationships in plant populations. *Ecology Letters*, *11*(11), 1189–1197. https://doi.org/10.1111/j.1461-0248.2008.01228.x

Cieraad, E. (2011). Temperate oceanic treelines—Low temperature effects on photosynthesis and growth. Doctoral dissertation, Durham University.

Cieraad, E., & Mcglone, M. (2014). Thermal environment of New Zealand's gradual and abrupt treeline ecotones. *New Zealand Journal of Ecology*, *38*, 12–25.

Close, D. C., Beadle, C. L., Brown, P. H., & Holz, G. K. (2000). Cold-induced photoinhibition affects establishment of *Eucalyptus nitens* (Deane and Maiden) Maiden and *Eucalyptusglobulus* Labill. *Trees*, *15*(1), 32–41. https://doi.org/10.1007/s004680000070

Close, D. C., Beadle, C. L., Holz, G. K., & Brown, P. H. (2002). Effect of shadecloth tree shelters on cold-induced photoinhibition, foliar anthocyanin and growth of *Eucalyptus globulus* and *E. nitens* seedlings during establishment. *Australian Journal of Botany*, 50(1), 15-20. https://doi.org/10.1071/BT01038

Cory, S. T., & Smith, W. K. (2017). Predicting the size and elevation of future mountain forests: Scaling macroclimate to microclimate. *AGU Fall Meeting Abstracts, 24*. http://adsabs.harvard.edu/abs/2017AGUFMGC24G..07C

Cuevas, J. G. (2000). Tree Recruitment at the *Nothofagus pumilio* Alpine Timberline in Tierra del Fuego, Chile. *Journal of Ecology*, *88*(5), 840–855. JSTOR.

Cullen, L. E., Stewart, G. H., Duncan, R. P., & Palmer, J. G. (2001). Disturbance and climate warming influences on New Zealand *Nothofagus* tree-line population dynamics. *Journal of Ecology*, *89*(6), 1061–1071. https://doi.org/10.1111/j.1365-2745.2001.00628.x

Danby, R. K., & Hik, D. S. (2007). Variability, contingency and rapid change in recent subarctic alpine tree line dynamics. *Journal of Ecology*, 95(2), 352-363. https://doi.org/10.1111/j.1365-2745.2006.01200.x

Davis, E. L., & Gedalof, Z. (2018). Limited prospects for future alpine treeline advance in the Canadian Rocky Mountains. *Global Change Biology*, *24*(10), 4489–4504. https://doi.org/10.1111/gcb.14338

Demmig-Adams, B. (2005). Linking the xanthophyll cycle with thermal energy dissipation. In *Discoveries in Photosynthesis*, 923–930. https://doi.org/10.1007/1-4020-3324-9_83

Demmig-Adams, B., & Adams, W. W. (1996). The role of xanthophyll cycle carotenoids in the protection of photosynthesis. *Trends in Plant Science*, *1*(1), 21–26. https://doi.org/10.1016/S1360-1385(96)80019-7

Demmig-Adams, B., & Adams, W. W. (2006). Photoprotection in an ecological context: The remarkable complexity of thermal energy dissipation. *New Phytologist*, *172*(1), 11–21. https://doi.org/10.1111/j.1469-8137.2006.01835.x

DOC. 2014. The science behind the Department of Conservation's beech mast response and predator control. Department of Conservation (DOC). https://www.osnz.org.nz/sites/osnz.org.nz/files/DOC%20brochure%20battle%20for%20our%20birds.pdf

Donnelly, A., Caffarra, A., Kelleher, C., O'Neill, B., Diskin, E., Pletsers, A., Proctor, H., Stirnemann, R., O'Halloran, J., Penuelas, J., Hodkinson, T., & Sparks, T. (2012). Surviving in a warmer world: Environmental and genetic responses. *Climate Research*, 245–262. https://doi.org/10.3354/cr01102

Dowdle, J., Ishikawa, T., Gatzek, S., Rolinski, S., & Smirnoff, N. (2007). Two genes in *Arabidopsis thaliana* encoding GDP-L-galactose phosphorylase are required for ascorbate biosynthesis and seedling viability. *The Plant Journal: For Cell and Molecular Biology*, *52*(4), 673–689. https://doi.org/10.1111/j.1365-313X.2007.03266.x

Dungan, R. J., Whitehead, D., McGlone, M. S., Richard P, D., & Allen, R. B. (2003). Cold-induced photoinhibition and winter leaf-loss in the broad-leaved tree *Aristotelia serrata (Elaeocarpaceae)*. *Functional plant biology*, 30(5), 543-550. https://doi.org/10.1071/FP02190

Duro, D., Coops, N., Wulder, M., & Han, T. (2007). Development of a large area biodiversity monitoring driven by remote sensing. *Progress in Physical Geography, 31*, 235–260. https://doi.org/10.1177/0309133307079054

Elliott, G. P. (2011). Influences of 20th-century warming at the upper tree line contingent on local-scale interactions: Evidence from a latitudinal gradient in the Rocky Mountains,

USA. *Global Ecology and Biogeography*, *20*(1), 46–57. https://doi.org/10.1111/j.1466-8238.2010.00588.x

Elliott, G. P. (2012). Extrinsic regime shifts drive abrupt changes in regeneration dynamics at upper treeline in the Rocky Mountains, USA. *Ecology*, *93*(7), 1614–1625. https://doi.org/10.1890/11-1220.1

Elliott, G. P., & Kipfmueller, K. F. (2010). Multi-scale Influences of Slope Aspect and Spatial Pattern on Ecotonal Dynamics at Upper Treeline in the Southern Rocky Mountains, U.S.A. *Arctic, Antarctic, and Alpine Research*, *42*(1), 45–56. https://doi.org/10.1657/1938-4246-42.1.45

Ellison, A. M., Bank, M. S., Clinton, B. D., Colburn, E. A., Elliott, K., Ford, C. R., Foster, D. R., Kloeppel, B. D., Knoepp, J. D., Lovett, G. M., Mohan, J., Orwig, D. A., Rodenhouse, N. L., Sobczak, W. V., Stinson, K. A., Stone, J. K., Swan, C. M., Thompson, J., Von Holle, B., & Webster, J. R. (2005). Loss of Foundation Species: Consequences for the Structure and Dynamics of Forested Ecosystems. *Frontiers in Ecology and the Environment*, *3*(9), 479–486. JSTOR. https://doi.org/10.2307/3868635

Elstner, E. F., & Osswald, W. (1994). Mechanisms of oxygen activation during plant stress. *Proceedings of the Royal Society of Edinburgh, Section B: Biological Sciences*, *102*, 131–154. https://doi.org/10.1017/S0269727000014068

Enquist, B. J., & Niklas, K. J. (2001). Invariant scaling relations across tree-dominated communities. *Nature*, *410*(6829), 655–660. https://doi.org/10.1038/35070500

Fawcett, S., Sistla, S., Dacosta-Calheiros, M., Kahraman, A., Reznicek, A. A., Rosenberg, R., & Wettberg, E. J. B. von. (2019). Tracking microhabitat temperature variation with iButton data loggers. *Applications in Plant Sciences*, *7*(4), e01237. https://doi.org/10.1002/aps3.1237

Fetzer, J., Frossard, E., Moiseev, P., & Hagedorn, F. (2019). Climate change driven treeline shifts in Northern Russia are fostered by an improving nutrient availability. *Geophysical Research Abstracts, 21*, 2452.

Fortin, M. (1993). Detection of ecotones: Definition and scaling factors. Doctoral dissertation, State University of New York.

Foyer, C. H., & Noctor, G. (2000). Oxygen processing in photosynthesis: Regulation and signalling. *New Phytologist*, *146*(3), 359–388. https://doi.org/10.1046/j.1469-8137.2000.00667.x

Foyer, C. H., & Noctor, G. (2011). Ascorbate and Glutathione: The Heart of the Redox Hub. *Plant Physiology*, *155*(1), 2–18. https://doi.org/10.1104/pp.110.167569

Gallay, M., Lloyd, C. D., McKinley, J., & Barry, L. (2013). Assessing modern ground survey methods and airborne laser scanning for digital terrain modelling: A case study from the Lake District, England. *Computers & Geosciences, 51*, 216–227. https://doi.org/10.1016/j.cageo.2012.08.015

García, M. B., Domingo, D., Pizarro, M., Font, X., Gómez, D., & Ehrlén, J. (2020). Rocky habitats as microclimatic refuges for biodiversity. A close-up thermal approach. *Environmental and Experimental Botany, 170*, 103886. https://doi.org/10.1016/j.envexpbot.2019.103886

Genty, B., Briantais, J.-M., & Baker, N. R. (1989). The relationship between the quantum yield of photosynthetic electron transport and quenching of chlorophyll fluorescence. *Biochimica et Biophysica Acta - General Subjects, 990*(1), 87–92. https://doi.org/10.1016/S0304-4165(89)80016-9

Germino, M. J., & Smith, W. K. (1999). Sky exposure, crown architecture, and low-temperature photoinhibition in conifer seedlings at alpine treeline. *Plant, Cell & Environment, 22*(4), 407–415. https://doi.org/10.1046/j.1365-3040.1999.00426.x

Germino, Matthew J., Smith, W. K., & Resor, A. C. (2002). Conifer seedling distribution and survival in an alpine-treeline ecotone. *Plant Ecology*, *162*(2), 157–168. https://doi.org/10.1023/A:1020385320738

Getzin, S., Wiegand, K., & Schöning, I. (2012). Assessing biodiversity in forests using very high-resolution images and unmanned aerial vehicles. *Methods in Ecology and Evolution*, *3*(2), 397–404. https://doi.org/10.1111/j.2041-210X.2011.00158.x

Gómez-Aparicio, L., Valladares, F., Zamora, R., & Quero, J. L. (2005). Response of tree seedlings to the abiotic heterogeneity generated by nurse shrubs: An experimental approach at different scales. *Ecography*, *28*(6), 757–768. https://doi.org/10.1111/j.2005.0906-7590.04337.x

Gosz, J. R. (1993). Ecotone Hierarchies. *Ecological Applications*, *3*(3), 369–376. https://doi.org/10.2307/1941905

Graham, C., Moritz, C., & Williams, S. (2006). Habitat history improves prediction of biodiversity in rainforest fauna. *Proceedings of the National Academy of Sciences of the United States of America*, *103*, 632–636. https://doi.org/10.1073/pnas.0505754103

Graham, E. A., Rundel, P. W., Kaiser, W., Lam, Y., Stealey, M., & Yuen, E. M. (2012). Fine-Scale Patterns of Soil and Plant Surface Temperatures in an Alpine Fellfield Habitat, White Mountains, California. *Arctic, Antarctic, and Alpine Research*, *44*(3), 288–295. https://doi.org/10.1657/1938-4246-44.3.288

Grau, O., Ninot, J. M., Blanco-Moreno, J. M., Logtestijn, R. S. P. van, Cornelissen, J. H. C., & Callaghan, T. V. (2012). Shrub–tree interactions and environmental changes drive treeline dynamics in the Subarctic. *Oikos*, *121*(10), 1680–1690. https://doi.org/10.1111/j.1600-0706.2011.20032.x

Grill, D., Tausz, M., & de Kok, L. J. (2001). *Significance of Glutathione to Plant Adaptation to the Environment*. http://www.springer.com/de/book/9781402001789

Grimm, V., Berger, U., Bastiansen, F., Eliassen, S., Ginot, V., Giske, J., Goss-Custard, J., Grand, T., Heinz, S. K., Huse, G., Huth, A., Jepsen, J. U., Jørgensen, C., Mooij, W. M., Müller, B., Pe'er, G., Piou, C., Railsback, S. F., Robbins, A. M., DeAngelis, D. L. (2006). A standard protocol for describing individual-based and agent-based models. *Ecological Modelling*, *198*(1), 115–126. https://doi.org/10.1016/j.ecolmodel.2006.04.023

Grimm, V., Railsback, S. F., Vincenot, C. E., Berger, U., Gallagher, C., DeAngelis, D. L., Edmonds, B., Ge, J., Giske, J., Groeneveld, J., Johnston, A. S. A., Milles, A., Nabe-Nielsen, J., Polhill, J. G., Radchuk, V., Rohwäder, M.-S., Stillman, R. A., Thiele, J. C., & Ayllón, D. (2020). The ODD Protocol for Describing Agent-Based and Other Simulation Models: A Second Update to Improve Clarity, Replication, and Structural Realism. *Journal of Artificial Societies and Social Simulation*, *23*(2), 7. https://doi.org/10.18564/jasss.4259

Gunderson, L. H., Allen, C. R., & Holling, C. S. (2012). Foundations of Ecological Resilience.

Hagedorn, F., Gavazov, K., & Alexander, J. M. (2019). Above- and belowground linkages shape responses of mountain vegetation to climate change. *Science*, *365*(6458), 1119–1123. https://doi.org/10.1126/science.aax4737

Harsch, M., Hulme, P., Mcglone, M., & Duncan, R. (2009). Are treelines advancing? A global meta-analysis of treeline response to climate warming. *Ecology Letters*, *12*, 1040–1049. https://doi.org/10.1111/j.1461-0248.2009.01355.x

Harsch, M. A., & Bader, M. Y. (2011a). Treeline form – a potential key to understanding treeline dynamics. *Global Ecology and Biogeography*, *20*(4), 582–596. https://doi.org/10.1111/j.1466-8238.2010.00622.x

Harsch, M.A., Buxton, R., Duncan, R. P., Hulme, P. E., Wardle, P., & Wilmshurst, J. (2012). Causes of tree line stability: Stem growth, recruitment and mortality rates over 15 years at New Zealand *Nothofagus* tree lines. *Journal of Biogeography*, *39*(11), 2061–2071. https://doi.org/10.1111/j.1365-2699.2012.02763.x

Harsch, M. A. (2010). Treeline dynamics: Pattern and process at multiple spatial scales. Doctoral dissertation, Durham University.

Harvey, P. (2020). *ExifTool*. https://exiftool.org/

Hasselquist, N., Germino, M. J., McGonigle, T., & Smith, W. K. (2005). Variability of *Cenococcum* colonization and its ecophysiological significance for young conifers at alpine–treeline. *New Phytologist*, *165*(3), 867–873. https://doi.org/10.1111/j.1469-8137.2005.01275.x

Hay, G. J., & Castilla, G. (2008). Geographic Object-Based Image Analysis (GEOBIA): A new name for a new discipline. In T. Blaschke, S. Lang, & G. J. Hay (Eds.), *Object-Based Image Analysis: Spatial Concepts for Knowledge-Driven Remote Sensing Applications* (pp. 75–89). Springer. https://doi.org/10.1007/978-3-540-77058-9_4

Hohnwald, S., Indreica, A., Walentowski, H., & Leuschner, C. (2020). Microclimatic Tipping Points at the Beech–Oak Ecotone in the Western Romanian Carpathians. *Forests*, *11*(9), 919. https://doi.org/10.3390/f11090919

Holmgren, M., Scheffer, M., & Huston, M. A. (1997). The Interplay of Facilitation and Competition in Plant Communities. *Ecology*, *78*(7), 1966–1975. https://doi.org/10.1890/0012-9658(1997)078[1966:TIOFAC]2.0.CO;2

Holtmeier, F.-K. (2009). Mountain Timberlines: Ecology, Patchiness, and Dynamics.

Holtmeier, F.-K., & Broll, G. (2017). Treelines - Approaches at Different Scales. *Sustainability*, *9*(5), 808. https://doi.org/10.3390/su9050808

Hunsaker, C. T., Goodchild, M. F., Friedl, M. A., & Case, T. J. (2001). Spatial Uncertainty in Ecology: Implications for Remote Sensing and GIS Applications.

III Adams, W., Demmig-Adams, B., Verhoeven, A., & Barker, D. (1995). "Photoinhibition" During Winter Stress: Involvement of Sustained Xanthophyll Cycle-Dependent Energy Dissipation. *Functional Plant Biology*, *22*, 261–276. https://doi.org/10.1071/PP9950261

J. Berni, J. A., Suárez, L., & Fereres, E. (2008). Remote sensing of vegetation from UAV platforms using lightweight multispectral and thermal imaging sensors. *Int. Arch. Photogramm. Remote Sens. Spatial Inform. Sci*, 38(6), 6.

Jahns, P., & Holzwarth, A. R. (2012). The role of the xanthophyll cycle and of lutein in photoprotection of photosystem II. *Biochimica et Biophysica Acta (BBA) - Bioenergetics*, *1817*(1), 182–193. https://doi.org/10.1016/j.bbabio.2011.04.012

Jahns, P., Latowski, D., & Strzalka, K. (2009). Mechanism and regulation of the violaxanthin cycle: The role of antenna proteins and membrane lipids. *Biochimica et Biophysica Acta (BBA) - Bioenergetics*, *1787*(1), 3–14. https://doi.org/10.1016/j.bbabio.2008.09.013

Jain, A. K. (2008). Data Clustering: 50 Years Beyond K-means. *Machine Learning and Knowledge Discovery in Databases*. https://doi.org/10.1007/978-3-540-87479-9_3

Johnson, D. M., Germino, M. J., & Smith, W. K. (2004). Abiotic factors limiting photosynthesis in *Abies lasiocarpa* and *Picea engelmannii* seedlings below and above the alpine timberline. *Tree Physiology*, *24*(4), 377–386. https://doi.org/10.1093/treephys/24.4.377

Kitagawa, R., Masumoto, S., Nishizawa, K., Kaneko, R., Osono, T., Hasegawa, M., Uchida, M., & Mori, A. S. (2020). Positive interaction facilitates landscape homogenization

by shrub expansion in the forest–tundra ecotone. *Journal of Vegetation Science*, *31*(2), 234–244. https://doi.org/10.1111/jvs.12818

Klanderud, K., & Totland, Ø. (2005). The Relative Importance of Neighbours and Abiotic Environmental Conditions for Population Dynamic Parameters of Two Alpine Plant Species. *Journal of Ecology*, *93*(3), 493–501. https://doi.org/10.1111/j.1365-2745.2005.01000.x

Körner, C. (2012). Alpine Treelines—Functional Ecology of the Global High Elevation Tree Limits.

Körner, C. (2014). Mountain ecosystems in a changing environment. *Journal on Protected Mountain Areas Research and Management*, *6*(1), 71–77. https://doi.org/10.1553/ecomont-6-1s71

Körner, C. (2016). When it gets cold, plant size matters – a comment on treeline. *Journal of Vegetation Science*, *27*(1), 6–7. https://doi.org/10.1111/jvs.12366

Körner, C., Basler, D., Hoch, G., Kollas, C., Lenz, A., Randin, C. F., Vitasse, Y., & Zimmermann, N. E. (2016). Where, why and how? Explaining the low-temperature range limits of temperate tree species. *Journal of Ecology*, *104*(4), 1076–1088. https://doi.org/10.1111/1365-2745.12574

Körner, C., & Hiltbrunner, E. (2017). The 90 ways to describe plant temperature. *Perspectives in Plant Ecology, Evolution and Systematics*. https://doi.org/10.1016/j.ppees.2017.04.004

Körner, C., & Hoch, G. (2006). A Test of Treeline Theory on a Montane Permafrost Island. *Arctic, Antarctic, and Alpine Research*, *38*(1), 113–119. https://doi.org/10.1657/1523-0430(2006)038[0113:ATOTTO]2.0.CO;2

Körner, C., & Paulsen, J. (2004). A World-Wide Study of High Altitude Treeline Temperatures. *Journal of Biogeography*, *31*(5), 713–732. https://doi.org/10.1111/j.1365-2699.2003.01043.x

Krall, J. P., & Edwards, G. E. (1992). Relationship between photosystem II activity and CO_2 fixation in leaves. *Physiologia Plantarum*, *86*(1), 180–187. https://doi.org/10.1111/j.1399-3054.1992.tb01328.x

Kranner, I., Birtić, S., Anderson, K. M., & Pritchard, H. W. (2006). Glutathione half-cell reduction potential: A universal stress marker and modulator of programmed cell death? *Free Radical Biology and Medicine*, *40*(12), 2155–2165. https://doi.org/10.1016/j.freeradbiomed.2006.02.013

Krause, G. H., & Weis, E. (1991). Chlorophyll Fluorescence and Photosynthesis: The Basics. *Annual Review of Plant Physiology and Plant Molecular Biology*, *42*(1), 313–349. https://doi.org/10.1146/annurev.pp.42.060191.001525

Lambers, H., III, F. S. C., & Pons, T. L. (2008). Plant Physiological Ecology (2nd ed.). https://doi.org/10.1007/978-0-387-78341-3

Lang, S. (2008). Object-based image analysis for remote sensing applications: Modeling reality – dealing with complexity. In T. Blaschke, S. Lang, & G. J. Hay (Eds.), *Object-Based Image Analysis: Spatial Concepts for Knowledge-Driven Remote Sensing Applications* (pp. 3–27). https://doi.org/10.1007/978-3-540-77058-9_1

Leathwick, J. R. (1998). Are New Zealand's *Nothofagus* Species in Equilibrium with Their Environment? *Journal of Vegetation Science*, *9*(5), 719–732. https://doi.org/10.2307/3237290

Leinonen, I., Grant, O. M., Tagliavia, C. P. P., Chaves, M. M., & Jones, H. G. (2006). Estimating stomatal conductance with thermal imagery. *Plant, Cell & Environment*, *29*(8), 1508–1518. https://doi.org/10.1111/j.1365-3040.2006.01528.x

Liedschulte, V., Wachter, A., Zhigang, A., & Rausch, T. (2010). Exploiting plants for glutathione (GSH) production: Uncoupling GSH synthesis from cellular controls results in unprecedented GSH accumulation. *Plant Biotechnology Journal*, *8*(7), 807–820. https://doi.org/10.1111/j.1467-7652.2010.00510.x

Lin, Y., Berger, U., Grimm, V., & Ji, Q.-R. (2012). Differences between symmetric and asymmetric facilitation matter: Exploring the interplay between modes of positive and negative plant interactions. *Journal of Ecology*, *100*(6), 1482–1491. https://doi.org/10.1111/j.1365-2745.2012.02019.x

LINZ. (2016). *NZ 8m Digital Elevation Model*. Land Information New Zealand (LINZ). https://data.linz.govt.nz/layer/51768-nz-8m-digital-elevation-model-2012/metadata/

Lobo, F. de A., de Barros, M. P., Dalmagro, H. J., Dalmolin, Â. C., Pereira, W. E., de Souza, É. C., Vourlitis, G. L., & Rodríguez Ortíz, C. E. (2013). Fitting net photosynthetic light-response curves with Microsoft Excel - A critical look at the models. *Photosynthetica*, *51*(3), 445–456. https://doi.org/10.1007/s11099-013-0045-y

Loranger, H., Zotz, G., & Bader, M. (2016). Early establishment of trees at the alpine treeline: Idiosyncratic species responses to temperature-moisture interactions. *AoB Plants*, *8*. https://doi.org/10.1093/aobpla/plw053

Loranger, H., Zotz, G., & Bader, M. (2017). Competitor or facilitator? The ambiguous role of alpine grassland for the early establishment of tree seedlings at treeline. *Oikos*. https://doi.org/10.1111/oik.04377

Louthan, A. M., Doak, D. F., & Angert, A. L. (2015). Where and When do Species Interactions Set Range Limits? *Trends in Ecology & Evolution*, *30*(12), 780–792. https://doi.org/10.1016/j.tree.2015.09.011

Lu, B., & He, Y. (2017). Species classification using Unmanned Aerial Vehicle (UAV)-acquired high spatial resolution imagery in a heterogeneous grassland. *ISPRS Journal*

of Photogrammetry and Remote Sensing, *128*, 73–85. https://doi.org/10.1016/j.isprsjprs.2017.03.011

Lustenhouwer, M. N., Nicoll, L., & Ellison, A. M. (2012). Microclimatic effects of the loss of a foundation species from New England forests. *Ecosphere*, *3*(3), art26. https://doi.org/10.1890/ES12-00019.1

Malanson, G. P., & Resler, L. M. (2016). A size-gradient hypothesis for alpine treeline ecotones. *Journal of Mountain Science*, *13*(7), 1154–1161. https://doi.org/10.1007/s11629-016-3984-5

Malanson, G. P., Resler, L. M., Bader, M. Y., Holtmeier, F.-K., Butler, D. R., Weiss, D. J., Daniels, L. D., & Fagre, D. B. (2011). Mountain treelines: A roadmap for research orientation. *Arctic, Antarctic, and Alpine Research*, *43*(2), 11. https://doi.org/10.1657/1938-4246-43.2.167

Maxwell, K., & Johnson, G. N. (2000). Chlorophyll fluorescence—A practical guide. *Journal of Experimental Botany*, *51*(345), 659–668. https://doi.org/10.1093/jexbot/51.345.659

Mcglone, M., Duncan, R., & Heenan, P. (2002). Endemism, species selection and the origin and distribution of the vascular plant flora of New Zealand. *Journal of Biogeography*, *28*, 199–216. https://doi.org/10.1046/j.1365-2699.2001.00525.x

Michalet, R., & Pugnaire, F. I. (2016). Facilitation in communities: Underlying mechanisms, community and ecosystem implications. *Functional Ecology*, *30*(1), 3–9. https://doi.org/10.1111/1365-2435.12602

Mullan, Brett, Allan, S., Wratt, D., Dean, S., Hollis, M., Williams, T., & Kenny, G. (2008). Climate change effects and impacts assessment: A guidance manual for local government in New Zealand. *Ministry for the Environment*. https://www.mfe.govt.nz/publications/climate-change/climate-change-effects-and-impacts-assessment-guidance-manual-local-6

Munné-Bosch, S., & Alegre, L. (2002). The Function of Tocopherols and Tocotrienols in Plants. *Critical Reviews in Plant Sciences*, *21*(1), 31–57. https://doi.org/10.1080/0735-260291044179

Nigrelli, G., Fratianni, S., Zampollo, A., Turconi, L., & Chiarle, M. (2018). The altitudinal temperature lapse rates applied to high elevation rockfalls studies in the Western European Alps. *Theoretical and Applied Climatology*, *131*(3), 1479–1491. https://doi.org/10.1007/s00704-017-2066-0

Niyogi, K. K. (2000). Safety valves for photosynthesis. *Current Opinion in Plant Biology*, *3*(6), 455–460. https://doi.org/10.1016/S1369-5266(00)00113-8

Norton, D. A., & Schönenberger, W. (1984). The Growth Forms and Ecology of *Nothofagus Solandri* at the Alpine Timberline, Craigieburn Range, New Zealand. *Arctic and Alpine Research*, *16*(3), 361–370. https://doi.org/10.1080/00040851.1984.12004425

Oliver, T. H., Heard, M. S., Isaac, N. J. B., Roy, D. B., Procter, D., Eigenbrod, F., Freckleton, R., Hector, A., Orme, C. D. L., Petchey, O. L., Proença, V., Raffaelli, D., Suttle, K. B., Mace, G. M., Martín-López, B., Woodcock, B. A., & Bullock, J. M. (2015). Biodiversity and Resilience of Ecosystem Functions. *Trends in Ecology & Evolution*, *30*(11), 673–684. https://doi.org/10.1016/j.tree.2015.08.009

Ørka, H. O., Wulder, M. A., Gobakken, T., & Næsset, E. (2012). Subalpine zone delineation using LiDAR and Landsat imagery. *Remote Sensing of Environment*, *119*, 11–20. https://doi.org/10.1016/j.rse.2011.11.023

Palmer, M. W., & Dixon, P. M. (1990). Small-scale environmental heterogeneity and the analysis of species distributions along gradients. *Journal of Vegetation Science*, *1*(1), 57–65. https://doi.org/10.2307/3236053

Parmesan, C., & Yohe, G. (2003). A globally coherent fingerprint of climate change impacts across natural systems. *Nature, 421*(6918), 37–42. https://doi.org/10.1038/nature01286

Pinheiro, J., Bates, D., DebRoy, S., & Sarkar, D. (2019). *Linear and Nonlinear Mixed Effects Models*. https://CRAN.R-project.org/package=nlme

Piper, F. I., Reyes-Díaz, M., Corcuera, L. J., & Lusk, C. H. (2009). Carbohydrate storage, survival, and growth of two evergreen Nothofagus species in two contrasting light environments. *Ecological Research*, *24*(6), 1233–1241. https://doi.org/10.1007/s11284-009-0606-5

Piper, F. I., Cavieres, L. A., Reyes-Díaz, M., & Corcuera, L. J. (2005). Carbon sink limitation and frost tolerance control performance of the tree Kageneckia angustifolia D. Don (Rosaceae) at the treeline in central Chile. *Plant Ecology*, *185*(1), 29. https://doi.org/10.1007/s11258-005-9081-4

Poikolainen, J., Tolvanen, A., Karhu, J., & Kubin, E. (2016). Seventeen-year trends in spring and autumn phenophases of Betula pubescens in a boreal environment. *International Journal of Biometeorology*, *60*(8), 1227–1236. https://doi.org/10.1007/s00484-015-1118-3

Pyatt, J. C., Tomback, D. F., Blakeslee, S. C., Wunder, M. B., Resler, L. M., Boggs, L. A., & Bevency, H. D. (2016). The Importance of Conifers for Facilitation at Treeline: Comparing Biophysical Characteristics of Leeward Microsites in Whitebark Pine Communities. *Arctic, Antarctic, and Alpine Research*, *48*(2), 427–444. https://doi.org/10.1657/AAAR0015-055

R Core Team. (2019). R: A language and environment for statistical computing. https://www.R-project.org/

Rees, W. G. (2007). Characterisation of Arctic treelines by LiDAR and multispectral imagery. *Polar Record*, *43*(4), 345–352. https://doi.org/10.1017/S0032247407006511

Rehfeldt, G. E., Crookston, N. L., Warwell, M. V., & Evans, J. S. (2006). Empirical Analyses of Plant-Climate Relationships for the Western United States. *International Journal of Plant Sciences*, *167*(6), 1123–1150. https://doi.org/10.1086/507711

Resler, L. M. (2006). Geomorphic Controls of Spatial Pattern and Process at Alpine Treeline. *The Professional Geographer*, *58*(2), 124–138. https://doi.org/10.1111/j.1467-9272.2006.00520.x

Resler, L. M., Butler, D. R., & Malanson, G. P. (2005). Topographic Shelter and Conifer Establishment and Mortality in an Alpine Environment, Glacier National Park, Montana. *Physical Geography*, *26*(2), 112–125. https://doi.org/10.2747/0272-3646.26.2.112

Reyes-Díaz, M., Alberdi, M., Piper, F., Bravo, L., & Corcuera, L. (2005). Low temperature responses of Nothofagus dombeyi and Nothofagus nitida, two evergreen species from south central Chile. *Tree Physiology*, *25*, 1389–1398. https://doi.org/10.1093/treephys/25.11.1389

Rhodes, C. J., Henrys, P., Siriwardena, G. M., Whittingham, M. J., & Norton, L. R. (2015). The relative value of field survey and remote sensing for biodiversity assessment. *Methods in Ecology and Evolution*, *6*(7), 772–781. https://doi.org/10.1111/2041-210X.12385

Richardson, S. J., Allen, R. B., Whitehead, D., Carswell, F. E., Ruscoe, W. A., & Platt, K. H. (2005). Climate and Net Carbon Availability Determine Temporal Patterns of Seed Production by *Nothofagus*. *Ecology*, *86*(4), 972–981. https://doi.org/10.1890/04-0863

Rose, K. M., Friday, J. B., Oliet, J. A., & Jacobs, D. F. (2020). Canopy openness affects microclimate and performance of underplanted trees in restoration of high-elevation

tropical pasturelands. *Agricultural and Forest Meteorology*, *292–293*, 108105. https://doi.org/10.1016/j.agrformet.2020.108105

Rydsaa, J., Stordal, F., Bryn, A., & Tallaksen, L. M. (2016). Effects of shrub cover increase on the near surface atmosphere in northern Fennoscand. *Biogeosciences Discussions*, 1–32. https://doi.org/10.5194/bg-2016-373

Sakai, A., & Wardle, P. (1978). Freezing resistance of New Zealand trees and shrubs. *New Zealand journal of ecology*, 1, 51-61.

Sakai, A., & Weiser, C. J. (1973). Freezing Resistance of Trees in North America with Reference to Tree Regions. *Ecology*, *54*(1), 118–126. https://doi.org/10.2307/1934380

Sakai, Akira, Paton, D. M., & Wardle, P. (1981). Freezing Resistance of Trees of the South Temperate Zone, Especially Subalpine Species of Australasia. *Ecology*, *62*(3), 563–570. https://doi.org/10.2307/1937722

Šašak, J., Gallay, M., Kaňuk, J., Hofierka, J., & Minár, J. (2019). Combined Use of Terrestrial Laser Scanning and UAV Photogrammetry in Mapping Alpine Terrain. *Remote Sensing*, *11*(18), 2154. https://doi.org/10.3390/rs11182154

Scherrer, D., & Körner, C. (2010). Infra-red thermometry of alpine landscapes challenges climatic warming projections. *Global Change Biology*, *16*(9), 2602–2613. https://doi.org/10.1111/j.1365-2486.2009.02122.x

Scherrer, D., & Körner, C. (2011). Topographically controlled thermal-habitat differentiation buffers alpine plant diversity against climate warming. *Journal of Biogeography*, *38*(2), 406–416. https://doi.org/10.1111/j.1365-2699.2010.02407.x

Schreiber, U. (2004). Pulse-Amplitude-Modulation (PAM) Fluorometry and Saturation Pulse Method: An Overview. *Chlorophyll a Fluorescence: A Signature of Photosynthesis* (pp. 279–319). https://doi.org/10.1007/978-1-4020-3218-9_11

Schwinning, S., & Weiner, J. (1998). Mechanisms determining the degree of size asymmetry in competition among plants. *Oecologia*, *113*(4), 447–455. https://doi.org/10.1007/s004420050397

Sigdel, S. R., Wang, Y., Camarero, J. J., Zhu, H., Liang, E., & Peñuelas, J. (2018). Moisture-mediated responsiveness of treeline shifts to global warming in the Himalayas. *Global Change Biology*, *24*(11), 5549–5559. https://doi.org/10.1111/gcb.14428

Smale, M. C., Bergin, D. O., Steward, G. A., & Scion (Organization : N.Z.). (2012). The New Zealand beeches: Establishment, growth, and management.

Smigaj, M., Gaulton, R., Barr, S., & Suarez Minguez, J. (2015). UAV-borne thermal imaging for forest health monitoring: Detection of disease-induced canopy temperature increase. *International Archives of the Photogrammetry, Remote Sensing and Spatial Information Sciences*, *XL-3/W3*, 349–354. https://doi.org/10.5194/isprsarchives-XL-3-W3-349-2015

Smirnoff, N. (2000). Ascorbic acid: Metabolism and functions of a multi-facetted molecule. *Current Opinion in Plant Biology*, *3*(3), 229–235. https://doi.org/10.1016/S1369-5266(00)80070-9

Smith-McKenna, E. K., Malanson, G. P., Resler, L. M., Carstensen, L. W., Prisley, S. P., & Tomback, D. F. (2014). Cascading effects of feedbacks, disease, and climate change on alpine treeline dynamics. *Environmental Modelling & Software*, *62*, 85–96. https://doi.org/10.1016/j.envsoft.2014.08.019

Šrůtek, M., Doležal, J., & Hara, T. (2002). Spatial Structure and Associations in a Pinus canariensis Population at the Treeline, Pico del Teide, Tenerife, Canary Islands. *Arctic, Antarctic, and Alpine Research*, *34*(2), 201–210. https://doi.org/10.1080/15230430.2002.12003485

Strand, M., Lundmark, T., Söderbergh, I., & Mellander, P.-E. (2002). Impacts of seasonal air and soil temperatures on photosynthesis in Scots pine trees. *Tree Physiology*, *22*(12), 839–847. https://doi.org/10.1093/treephys/22.12.839

Sullivan, P. F., & Sveinbjörnsson, B. (2010). Microtopographic Control of Treeline Advance in Noatak National Preserve, Northwest Alaska. *Ecosystems*, *13*(2), 275–285. https://doi.org/10.1007/s10021-010-9318-5

Sun, O. J., & Sweet, G. B. (1996). Comparison of frost tolerance of *Nothofagus solandri var. Cliffortioides* (Hook.f.) Poole and *Nothofagus menziesii* (Hook.f.) Oerst. *New Zealand Journal of Botany*, *34*(2), 273–278. https://doi.org/10.1080/0028825X.1996.10410691

Takahashi, S., & Murata, N. (2008). How do environmental stresses accelerate photoinhibition? *Trends in Plant Science*, *13*(4), 178–182. https://doi.org/10.1016/j.tplants.2008.01.005

Till, O. (1956). Über die Frosthärte von Pflanzen sommergrüner Laubwälder. *Flora Oder Allgemeine Botanische Zeitung*, *143*(4), 499–542. https://doi.org/10.1016/S0367-1615(17)33134-8

Tomback, D. F., Blakeslee, S. C., Wagner, A. C., Wunder, M. B., Resler, L. M., Pyatt, J. C., & Diaz, S. (2016). Whitebark pine facilitation at treeline: Potential interactions for disruption by an invasive pathogen. *Ecology and Evolution*, *6*(15), 5144–5157. https://doi.org/10.1002/ece3.2198

Travis, J. M. J., Brooker, R. W., Clark, E. J., & Dytham, C. (2006). The distribution of positive and negative species interactions across environmental gradients on a dual-lattice model. *Journal of Theoretical Biology*, *241*(4), 896–902. https://doi.org/10.1016/j.jtbi.2006.01.025

Treml, V., & Veblen, T. T. (2017). Does tree growth sensitivity to warming trends vary according to treeline form? *Journal of Biogeography*, *44*(7), 1469–1480. https://doi.org/10.1111/jbi.12996

Trimble. (2020). *ECognition* (9.5.0). Computer software. https://docs.ecognition.com/v9.5.0/Page%20collection/eCognition%20Suite%20Dev%20RB.htm

Vacca, R. A., Valenti, D., Bobba, A., de Pinto, M. C., Merafina, R. S., De Gara, L., Passarella, S., & Marra, E. (2007). Proteasome function is required for activation of programmed cell death in heat shocked tobacco Bright-Yellow 2 cells. *FEBS Letters*, *581*(5), 917–922. https://doi.org/10.1016/j.febslet.2007.01.071

van Steenis, C. G. G. J. (1971). *Nothofagus*, key genus of plant geography, in time and space, living and fossil, ecology and phylogeny. *Blumea - Biodiversity, Evolution and Biogeography of Plants*, *19*, 65–98.

Vaze, J., Teng, J., & Spencer, G. (2010). Impact of DEM accuracy and resolution on topographic indices. *Environmental Modelling & Software*, *25*(10), 1086–1098. https://doi.org/10.1016/j.envsoft.2010.03.014

Wallentin, G., Tappeiner, U., Strobl, J., & Tasser, E. (2008). Understanding alpine tree line dynamics: An individual-based model. *Ecological Modelling*, *218*(3), 235–246. https://doi.org/10.1016/j.ecolmodel.2008.07.005

Wardle, J. (1970). The ecology of Nothofagus solandri. *New Zealand Journal of Botany*, *8*(4), 494–531. https://doi.org/10.1080/0028825X.1970.10430159

Wardle, J. (1974). The life story of mountain beech (*Nothofagus solandri var. Cliffortiodes*. *Proceedings (New Zealand Ecological Society)*, *21*, 21–26.

Wardle, P. (1965). A Comparison of Alpine Timber Lines in New Zealand and North America. *New Zealand Journal of Botany*, 3:2, 113-135.

https://doi.org/10.1080/0028825X.1965.10876989

Wardle, P. (1971). An explanation for alpine timberline. *New Zealand Journal of Botany*, *9*(3), 371–402. https://doi.org/10.1080/0028825X.1971.10430192

Wardle, P. (1984). The New Zealand beeches: Ecology, utilisation and management.

Wardle, P. (1985a). New Zealand timberlines. 1. Growth and survival of native and introduced tree species in the Craigieburn Range, Canterbury. *New Zealand Journal of Botany, 23*(2), 219–234. https://doi.org/10.1080/0028825X.1985.10425328

Wardle, P. (1985b). New Zealand timberlines. 2. A study of forest limits in the Crow Valley near Arthur's Pass, Canterbury. *New Zealand Journal of Botany*, *23*(2), 235–261. https://doi.org/10.1080/0028825X.1985.10425329

Wardle, P. (1998). Comparison of alpine timberlines in New Zealand and the Southern Andes. *Royal Society of New Zealand Miscellaneous Publications*, *48,* 69–90.

Wardle, P. (2008). New Zealand Forest to Alpine Transitions in Global Context. *Arctic, Antarctic, and Alpine Research*, *40*(1), 240–249.

Wardle, P., & Coleman, M. (1992). Evidence for rising upper limits of four native New Zealand forest trees. *New Zealand Journal of Botany*, *30*, 303–314. https://doi.org/10.1080/0028825X.1992.10412909

Wasson, K., Woolfolk, A., & Fresquez, C. (2013). Ecotones as Indicators of Changing Environmental Conditions: Rapid Migration of Salt Marsh–Upland Boundaries. *Estuaries and Coasts*, *36*(3), 654–664. https://doi.org/10.1007/s12237-013-9601-8

Weiss, D. (2009). Alpine treeline ecotones in the western United States: A multi-scale comparative analysis of environmental factors influencing pattern-process relations. Doctoral dissertation, University of North Carolina. https://doi.org/10.17615/1b92-ak21

Weiss, D. J., & Walsh, S. J. (2009). Remote Sensing of Mountain Environments. *Geography Compass*, *3*(1), 1–21. https://doi.org/10.1111/j.1749-8198.2008.00200.x

Wiegand, T., Camarero, J. J., Rüger, N., & Gutiérrez, E. (2006). Abrupt population changes in treeline ecotones along smooth gradients. *Journal of Ecology*, *94*(4), 880–892. https://doi.org/10.1111/j.1365-2745.2006.01135.x

Wieser, G., & Tausz, M. (Eds.). (2007a). Trees at their Upper Limit: Treelife Limitation at the Alpine Timberline (Vol. 5). https://doi.org/10.1007/1-4020-5074-7

Wilensky, U. (1999). NetLogo. http://ccl.northwestern.edu/netlogo/

Wilson, J. B., & Agnew, A. D. Q. (1992). Positive-feedback Switches in Plant Communities. In M. Begon & A. H. Fitter (Eds.), *Advances in Ecological Research*, 23, 263–336. https://doi.org/10.1016/S0065-2504(08)60149-X

Wood, S. N. (2011). Fast stable restricted maximum likelihood and marginal likelihood estimation of semiparametric generalized linear models. *Journal of the Royal Statistical Society: Series B (Statistical Methodology)*, *73*(1), 3–36. https://doi.org/10.1111/j.1467-9868.2010.00749.x

Yan, Y., Deng, L., Liu, X., & Zhu, L. (2019). Application of UAV-Based Multi-angle Hyperspectral Remote Sensing in Fine Vegetation Classification. *Remote Sensing*, *11*(23), 2753. https://doi.org/10.3390/rs11232753

Zarter, C. R., Adams, W. W., Ebbert, V., Adamska, I., Jansson, S., & Demmig-Adams, B. (2006). Winter acclimation of PsbS and related proteins in the evergreen *Arctostaphylos uva-ursi* as influenced by altitude and light environment. *Plant, Cell & Environment*, *29*(5), 869–878. https://doi.org/10.1111/j.1365-3040.2005.01466.x

Zarter, C. R., Adams, W. W., Ebbert, V., Cuthbertson, D. J., Adamska, I., & Demmig-Adams, B. (2006a). Winter down-regulation of intrinsic photosynthetic capacity coupled with up-regulation of Elip-like proteins and persistent energy dissipation in a

subalpine forest. *The New Phytologist*, *172*(2), 272–282. https://doi.org/10.1111/j.1469-8137.2006.01815.x

Zarter, C. R., Adams, W. W., Ebbert, V., Cuthbertson, D. J., Adamska, I., & Demmig-Adams, B. (2006b). Winter down-regulation of intrinsic photosynthetic capacity coupled with up-regulation of Elip-like proteins and persistent energy dissipation in a subalpine forest. *The New Phytologist*, *172*(2), 272–282. https://doi.org/10.1111/j.1469-8137.2006.01815.x

Zarter, C. R., Demmig-Adams, B., Ebbert, V., Adamska, I., & Adams, W. W. (2006). Photosynthetic capacity and light harvesting efficiency during the winter-to-spring transition in subalpine conifers. *The New Phytologist*, *172*(2), 283–292. https://doi.org/10.1111/j.1469-8137.2006.01816.x

Appendix

A) Cluster, seedling preference and microhabitat thermal logger statistics

Multivariate cluster analysis

Results for the multivariate clustering analysis used within the ArcGIS Pro (2.2.3) software to delineate a total of six unique feature clusters (Table 18). Numbers of clusters were decided on using a K-mean clustering algorithm in R ('kmeans', package *stats*, R Core Team, 2019). Variables used for the separation were plotted as an ordination plot (Figure 55, Principal component analysis of all variables used for the clustering algorithm). I agreed on six clusters to be sufficient to define distinct portions of the space while separating well into their cluster groups. The datasets (incident solar radiation (year, summer/winter day, thermal information (morning, noon, difference), slope) were standardised using a z-transformation to reduce impact of outliers and optimized seed locations. R^2 values reflect total variation retained from the source ranking the variables according to their ability to discriminate among features (Jain, 2008).

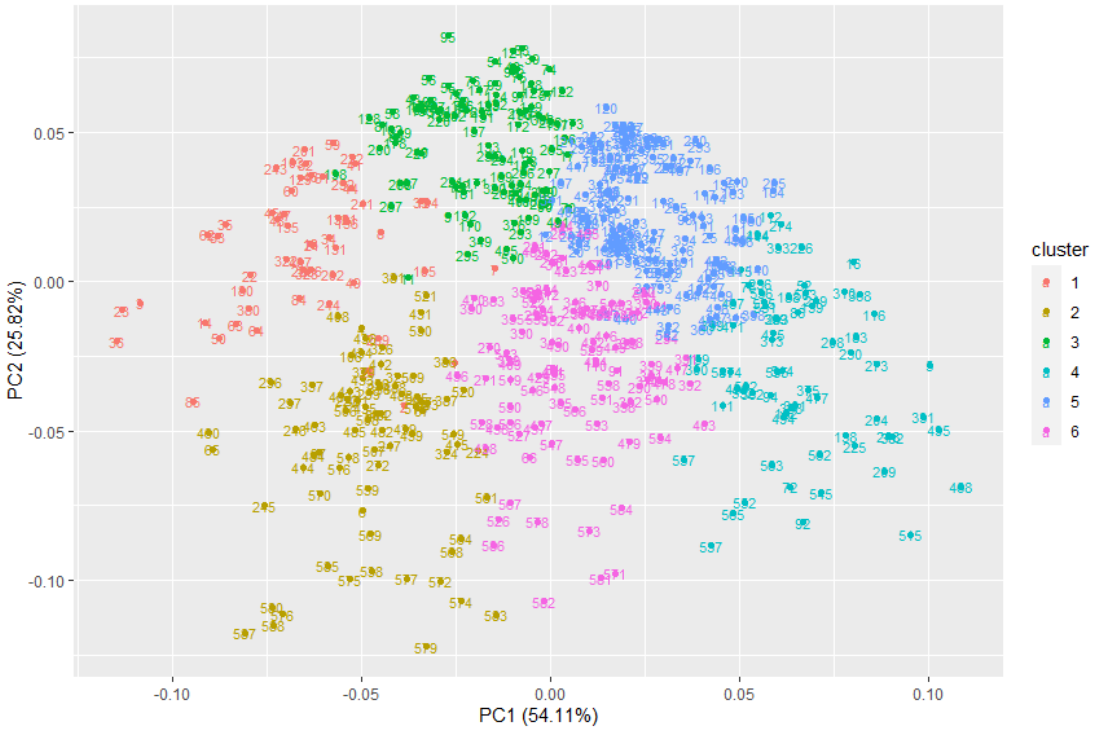

Figure 55: Principal component analysis used for agreeing on the numbers of clusters for the multivariate analysis at Craigieburn Valley. Principal components (PC) with their explained variation for environmental variables (Table 18) are plotted along the axes.

Table 18: Results for the multivariate cluster analysis in ArcGIS Pro

Variable	Mean	Std. Dev.	Min	Max	R^2
Solar Year (Wh/m²)	846981.59	258036.18	616.91	1437580.00	0.78
Solar Summer (Wh/m²)	3729.75	1089.46	2.36	5710.50	0.76
Solar Winter (Wh/m²)	466.59	257.48	0.73	1863.00	0.73
Thermal Noon (°C)	5.09	5.21	-2.37	23.54	0.72
Slope	31.19	8.37	0.20	56.20	0.68
Thermal Difference (°C)	6.59	4.85	-3.86	24.95	0.67
Thermal Morning (°C)	-1.49	2.18	-5.28	6.10	0.54

Seedling preference analysis

Results for the seedling preference analysis for identified clusters, ground cover and three thermal layers extrapolated from microhabitat loggers (Table 19 – 23). Each seedling was spatially intersected with, and assigned to, a microhabitat category as defined by the three methods outlined in Chapter Three (ie., cluster class, thermal quantile, and vegetation type). A test for given proportions was carried out in R ('prop.test', package *stats*, R Core Team, 2019). For each microhabitat type identified I tested if there was significant difference between relative microsite availability and actual seedling occupancy. The resulting P-values were adjusted for multiple testing using a false discovery rate method (Benjamini & Hochberg 1995).

Table 19: Seedling preference results for the vegetation classification (Overall significance: $X^2 = 157.14$, df = 6, $p < 0.001$)

Vegetation	Relative area available (%)	Occupied	X^2	Adjusted p
Dracophyllum	3.7	22	2.5969	1.2852e-01
Leucopogon	17.7	128	60.662	4.0590e-14
Podocarpus	15.1	68	2.0683	1.5040e-01
Scree	34.3	90	18.357	3.6640e-05
F. cliffortioides	12.4	67	10.431	1.8585e-03
Chionochloa	16.7	8	59.301	4.0590e-14

Table 20: Seedling preference results for the multivariate clusters (Overall significance: $X^2 = 232.58$, df = 6, $p < 0.001$)

Cluster	Relative area available (%)	Occupied	X^2	Adjusted p
1	16.7	26	26.903	6.4170e-07
2	10.1	115	172.02	1.3200e-15
3	24.0	73	4.9295	3.1680e-02
4	16.3	32	15.546	1.6108e-04
5	16	50	2.0185	1.5540e-01
6	16.8	84	6.8004	1.3671e-02

Table 21: Seedling preference results for the minimum mean temperature predictions (Overall significance: $X^2 = 271.27$, df = 6, $p < 0.001$)

Minimum temperature range	Relative area available (%)	Occupied	X^2	Adjusted p
1	16.7	24	30.166	1.1901e-07
2	16.7	35	15.937	9.8250e-05
3	16.7	30	21.846	5.9080e-06
4	16.7	76	2.1416	1.4330e-01
5	16.7	49	4.3374	4.4736e-02
6	16.7	169	192.51	1.3200e-15

Table 22: Seedling preference results for the mean temperature predictions (Overall significance: $X^2 = 103.33$, df = 6, p-value < 2.2e-16)

Mean temperature range	Relative area available (%)	Occupied	X^2	Adjusted p
1	16.7	40	30.166	1.8652e-03
2	16.7	29	15.937	4.5180e-06
3	16.7	64	21.846	9.7060e-01
4	16.7	59	2.1416	7.0845e-01
5	16.7	64	4.3374	9.7060e-01
6	16.7	125	192.51	2.2494e-15

Table 23: Seedling preference results for the maximum mean temperature predictions (Overall significance: $X^2 = 46.414$, df = 6, p-value = 2.449e-08)

Maximum temperature range	Relative area available (%)	Occupied	X^2	Adjusted p
1	16.7	47	5.548	3.7000e-02
2	16.7	37	13.833	5.9940e-04
3	16.7	59	0.51662	5.6676e-01
4	16.7	62	0.095852	7.5690e-01
5	16.7	76	2.1416	2.1495e-01
6	16.7	100	22.437	1.3032e-05

Microhabitat logger analysis

Site and vegetation comparison (Table 24, Figure 56) for microhabitat thermal loggers in the Craigieburn Valley (C), Mt Faust (F) and Mt Haast (H). The annual daily temperature variation was analysed using generalised additive mixed models (GAMM, package mgcv, Wood, 2011) with an auto regressive moving average auto-correlation structure (ARMA), whose parameters *P*, indicating the auto regressive correlation to *n* previous measurements and *Q*, specifying the moving average order were estimated using an auto-correlation function (acf, Venables & Ripley, 2002). The GAM smoothing functions were run with 20 knots as judged by comparisons of models with varying number of knots based on the Akaike Information

Criterion (AIC). The grey shaded fields give the overall significance of the vegetation type × site interaction, while the white fields indicate the results of a *post-hoc* procedure based on a likelihood ratio tests comparing the most complex GAMM with separate smoothers for each site to simpler GAMMs where two of the three sites were lumped in turn. The resulting P-values were adjusted for multiple testing using a false discovery rate method (Benjamini & Hochberg 1995).

Table 24: Statistical output for the thermal range comparison for six microhabitats at three sites (Craigieburn Valley, Mt Faust, Mt Haast) for 11 months in 2019.

Fuscospora cliffortioides (ARMA parameters: Q = 1, P = 1), Overall significance: L = 7.67, p = 0.0067 df = 2		
C vs F	C vs H	F vs H
L = 25.73 p = <.0001 df = 1	L = 25.06 p = <.0001 df = 1	L = 28.54 p = <.0001 df = 1
Dracophyllum spp. (ARMA parameters: Q = 1, P = 1) Overall significance: L = 183.99 p = <.0002 df = 1		
C vs F	C vs H	F vs H
L = 8.44 p = 0.0147 df = 2	L = 1.82 p = 0.4021 df = 2	L = 5.27 p = 0.0717 df = 2
Podocarpus nivalis (ARMA parameters: Q = 2, P = 2) Overall significance: L = 27.00 p = <.0002 df = 1		
C vs F	C vs H	F vs H
L = 6.27 p = 0.0123 df = 1	NA*	NA*
Chionochloa spp. (ARMA parameters: Q = 2, P = 2) Overall significance: L = 3.29 p = 0.0696 df = 1		
C vs F	C vs H	F vs H
L = 93.28 p = <.0001 df = 3	L = 88.96 p = <.0001 df = 3	L = 106.46 p = <.0001 df = 3
Leucopogon colensoi (ARMA parameters: Q = 2, P = 2) Overall significance: L = 19.99 p = <.0002 df = 1		
C vs F	C vs H	F vs H
L = 11.39 p = 0.0007 df = 1	NA*	NA*
Bare ground/scree (ARMA parameters: Q = 2, P = 2) Overall significance: L = 18.56 p = 1e-04 df = 2		
C vs F	C vs H	F vs H
L = 6.98 p = 0.0082 df = 1	L = 11.83 p = 6e-04 df = 1	L = 5.70 p = 0.017 df = 1

*no information for Haast available

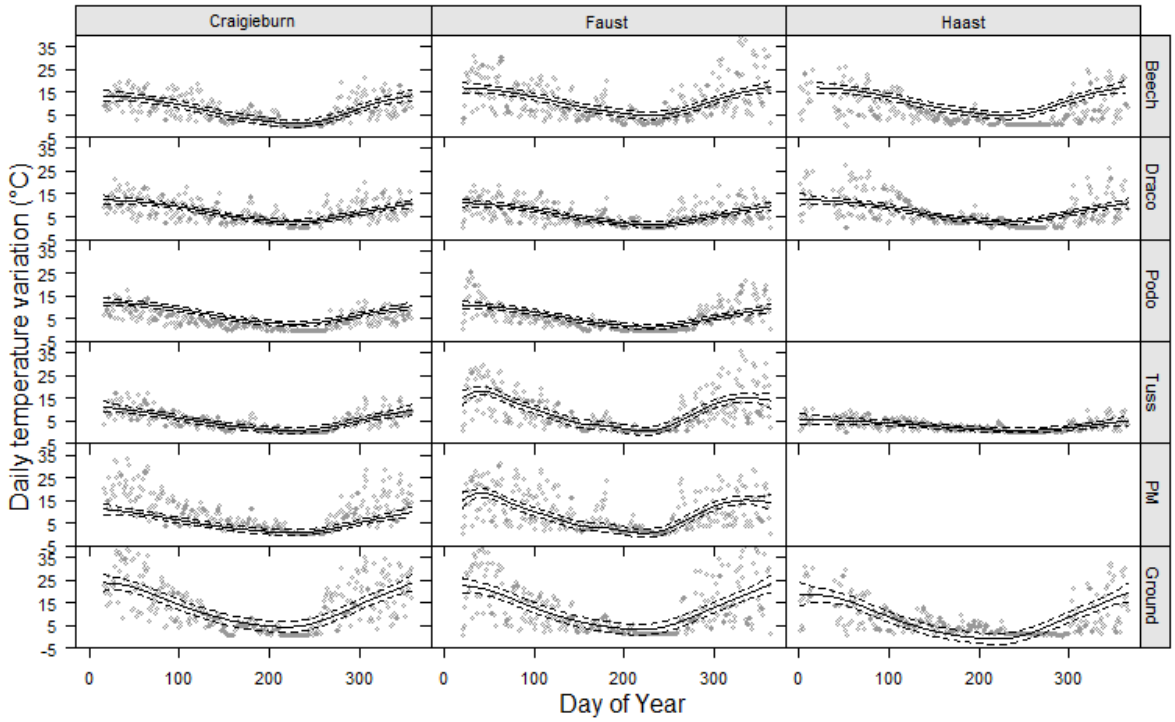

Figure 56: Diurnal temperature variation (range) from lowest to highest recording. From top to bottom row, microhabitats sorted by height: Fuscospora cliffortioides (Beech), *Dracophyllum* spp. (Draco), *Podocarpus* spp., *Chionochloa* spp. (Tuss), *L. colensoi* (PM), scree/bare soil (Ground). Data sampled 6 times per day, for a measurement period of 11 months per site (2019). Haast loggers were deployed later and feature the first two weeks of 2020. Day 1 corresponds to January 1st.

B) Treeline model ODD

The model description follows the ODD (Overview, Design concepts, Details) protocol for describing individual- and agent-based models (Grimm et al., 2006, 2020).

1. Purpose and patterns

The model is designed to explore how treeline formation and position is controlled by fine-scale mechanistic associations among trees and the response to an outlining temperature gradient. In this model we place tree agents on a hypothetical mountain slope which gradually decreases the agents sensed temperature with elevation. The agents receive thermal benefits by close associations with taller individuals or finding thermal shelter within the grid cells. The mountain slope environment goes through a cycle of monthly mean temperatures and the experienced temperature by the agents is then further modified by the cells and agents.

The overall purpose is to explore how changes in annual mean temperature variation affect treeline position and induce facilitative associations among agents to escape thermal limitations. I evaluate the model by its ability to illustrate patterns in tree formation reaching its upper elevational limits.

2. Entities, state variables, and scales

Since global treeline patterns can vastly be explained by temperature regimes expressed on macroscale-imposed mean isotherm (top-down, (Körner & Paulsen, 2004) or micro-scale modified heterogeneities within the alpine ecotone (bottom-up, Harsch & Bader, 2011), I decided to restrict the generation of treeline patterns to different tiered expressions of the thermal environment.

The following entities are included in the model: The *global environment* represents a climatic treeline ecotone (i.e. monthly mean temperatures), the *grid cells* correspond to the elevation gradient within this ecotone (i.e. mountain slope) and the *agents* represent individual trees in different growth stages (i.e. emergent trees, sheltered trees). Table 25 provides an overview of the entities state variables.

Table 25: Overview of state variables used in the model

Environment		
Climate data	Sets mean air temperature for every month for calculating within the cell context	[°C]
Time	Plant performance parameters are updated with every step on a monthly resolution	[Month]
Agents (trees)		
Growth factor (a)	Constant growth factor, representing genetically fixed intraspecific trait variation (ITV).	1 ± 0.1 [kg m^{-2} time $step^{-1}$]
$B_{init,}$ Bmax, B	Initial Biomass (ITV) Maximum biomass (ITV) biomass	2 ± 0.2 [kg] $2\times10^6 \pm 2\times10^5$ [kg] [kg]
elevation	Represents assigned altitude of the patch	[m]
Grid cells		
elevation	Represents assigned altitude of the patch	[m]

The environment represents a hypothetical treeline ecotone where the temperature sensed by the agents is dictated by annual mean temperatures changing in monthly intervals (Table 25). Agents represent individual trees with different biomass and height and their physiological performance is modified by state variables ranging within a defined intraspecific trait variation (ITV, Table 25). The trees height is calculated from their biomass via a certain conversion factor. Trees can further be distinguished into *emergent trees*, which thermally decouple from existing vegetation due to their height. They are taller than their surrounding and therefore exposed to climatic limitations imposed by the global and local environment (referred to as top-down mechanism). *Sheltered trees* are smaller than their surrounding agents, the imposed temperature limitation (top-down) is thermally decoupled by surrounding sheltering individuals (referred to as bottom-up mechanisms).

Grid cells represent a mountain slope, where agents aim to successfully establish. Each cell represents its own microclimate derived from the elevation position (ordinate) on the mountain slope. With an increasing ordinate, the temperature of the cells decreases. The *global environment* (i.e. treeline ecotone) is the only entity on the system level, defining the monthly temperature variation the mountain slope is exposed to.

The model's spatial extent is a rectangular grid of 400 x 600 square cells, each 1 m² in size. The chosen resolution is a compromise to account for regional and local effects likewise.

We want to identify how treeline formation is gradually pronounced by overarching climate drivers (top-down) while at the same time being able to account for local heterogeneities such as existing vegetation (bottom-up) to modulate the response to the regional drivers. The model runs with monthly time steps for five years. Climate data is updated monthly according to mean temperature readings of the tested site.

3. Process overview and scheduling

In each time step, after the monthly temperature has been updated, first the agents calculate their sensed temperature based on the patch they are on (treetempupdate). If the agent is in existing tussock vegetation, extreme temperature gets buffered (existingtussock). The agent counts the number of neighbouring trees (count-trees-in-radius) and uses this information to calculate the average height of neighbouring trees (thresholdemergingvegetation). If the trees fall below this threshold they are classified as sheltered, their sensed temperature gets increased by 3 °C and the competition mode gets assigned (competitionsmall). Trees taller than this threshold thermally decouple from the shelter, so their competition mode gets assigned (competitionbig). The trees then update their effective area (*Ae*) based on the competition mode. Trees died in the previous time step are removed (remove_dead_plant) and the remaining agents are growing (growth). If the growth rate (gr) falls below a certain threshold value, the tree has a stochastic chance to die (threshold-of-death). The trees update their height (updatetreeheight) and data will get plotted (plotting). Finally, recruitment takes place (sproutall).

4. Design concepts

Basic principles:

This model addresses the difficulties to describe current treeline position towards multiple drivers exposed on different spatial scales. Once the life-form tree approaches the physiological limitations the climatic stressors are more pronounced, leading to an increasing benefit of positive plant interactions (Callaway et al., 2002) at treeline. These positive associations of trees with existing vegetation have the potential to overrule macroscale stressors, highlighting the importance of microhabitat heterogeneity towards recruitment success (Scherrer & Körner, 2011). However, the detailed tree-line patterns emerging remain elusive as the because the interplay between physical limitations and facilitative thermal associations are poorly understood (Elliott, 2011). The outlining drivers and their varying strength have been discussed

proposing a concept of three mechanistic levels (Harsch & Bader, 2011). Where the overarching first level driver of mean average temperature days is gradually more pronounced towards higher altitude (top-down). Bottom-up mechanistic drivers are based on the interaction with neighbouring trees (intraspecific) other existing vegetation in the subalpine belt (interspecific).

Our model aims to shed some light onto the delicate interplay on these mechanistic drivers, illustrating how a gradual pronounced isotherm towards higher altitudes (top-down) combined with close plant associations (bottom-up) lead to the formation of a treeline ecotone. The intraspecific interaction is based on resource competition among neighbouring trees, where they compete for resources which are equally distributed in the model. The competitive interaction modes are based off the ZOI (Zone of Influence) models developed by Lin et al. (2012). Trees therefore compete for resources, but also show facilitative interactions with their neighbours, where a close association to neighbouring individuals will increase the temperature, dampening the impact of the top-down limitation. An opportunity for the trees to realize an interspecific facilitative association is presented by providing thermal shelter in the form of an alpine tussock belt. As stated earlier the concept of hierarchical mechanistic is hereby simplified within the context of the model to help us understand the benefit of thermal associations.

Emergence:

The behaviour or the trees is imposed via probabilistic rules, it is thus not emergent as it does not include adaptive decision making.

Sensing:

The trees are assumed to sense their ambient temperature, their own height, and the average height of their neighbouring trees.

Interaction:

Existing emergent trees create warmer thermal environments for smaller neighbours (sheltered), while at the same time compete for resources if their zones of influence overlap. Based on their competition mode (Table 26), the trees actively compete for space to increase available resources they can allocate towards growth. The interactions among neighbouring agents is therefore of facilitative (thermal benefit) and competitive nature (resource allocation).

Stochasticity:

There are two randomized mechanism within the model. The chance to spawn in any given patch on the field and the probability to die. When new trees spawn, they get assigned a growth rage randomly choose from a certain interval to account for intraspecific genetic trait differences (ITV, Table 25). The growth performance on the individual level therefore is slightly altered by the genetic diversity of the tree species. The probability to die is enhanced if tree growth is constrained by the amount of resources they can actively use and the temperature they are currently experiencing.

Observation:

Graphical output on the model interface shows the spatial distribution of trees in six different 100-grid cell wide zones. The model counts absolute numbers of trees currently present and visualizes monthly changes in a plotting environment. By summarizing the numbers of trees within a zone and agreeing on a specific number of required individuals form a treeline, we can observe absolute changes in the treeline position. Here, a given tree abundance at the end of the measurement period (2 years) will decide which zone the treeline has reached under the present climatic conditions. The rest of the observations remains of descriptive nature and tries to identify mechanisms oh how trees establish beyond the current treeline position.

5. Initialization

The model is designed to be generally applicable to multiple sites, I therefore provide different options to account for different conditions in our hypothetical mountain slope.

Landscape initialization: The initial state of the model at t = 0 is a hypothetical mountain slope environment of 400x600 cells of 1x1 m with a linear increase in altitude. The ordinate reflects the elevational gradient, where one grid cell corresponds to 1 m elevation gain (Fig. 57). The temperature of the grid cell is modulated by its altitude and decreases gradually towards higher altitudes (elevationtemp). The modeller also has the option to incorporate a tussock belt (Table 27, existingtussock) as a vegetational strip above treeline into the mountain slope. Agent initialization: Simulations start with a selected number of trees (initialnumberoftrees) which are randomly distributed over the grid cells and assigned their starting ITV (Table 25). Within the alpine ecotone we can select the option of an existing treeline (Table 27, existingtreeline) with a selected number of trees (treelinedensity) towards this elevation segment. We can then assign the probability for agents to die (threshold-of-death), the ratio of height to diameter

(Table 26 & 27, radheightfactor) and competition modes (Table 26). Growth performance is limited by abiotic stress and linear proportionally constraints an agents' energy intake (adapted after Lin et al. 2012).

The selected competition mode can be selected for sheltered/exposed agents separately and changes dynamically according to their sensed height. The selected mode decides the amount of resources an agent can use for growth if their areas overlap on grid cells.

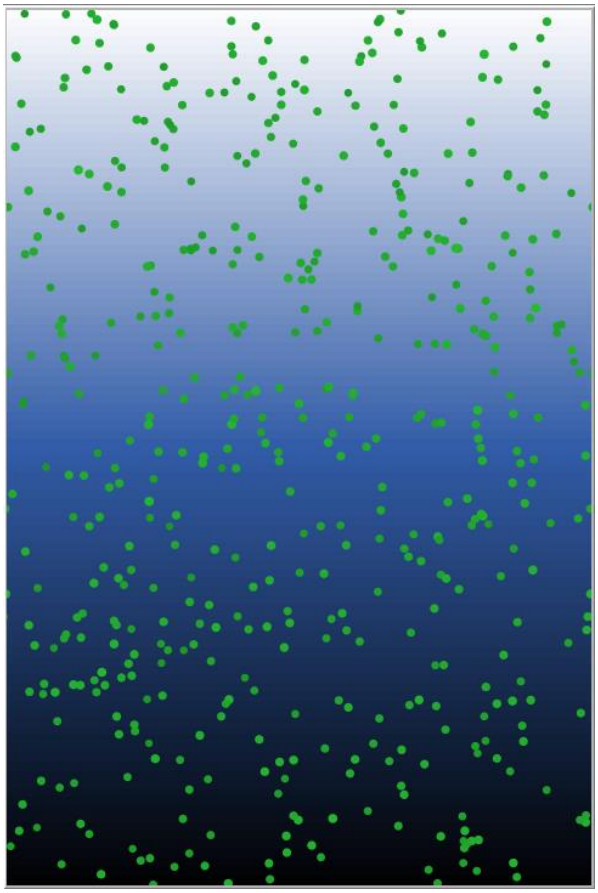

Figure 57: Netlogo (6.0.4) modelling environment. Visualisation of the starting conditions. Elevation increased along the y-axis (600 m) (blue – white). Individual trees (green dots) were scaled with their current height.

Table 26: Overview competition modes (adapted after Lin et al., 2012), their respective effect and how it is implemented as a modifier into the plant growth calculations. The value of the shared area for the individual is distributed discretely or is based on their current biomass (size symmetry, allometric interactions).

Competition mode	Effect
Complete Symmetry	All plants receive the same amount of benefit from each other, irrespective of their species or sizes
Size symmetry	Benefit is proportional to benefactor's size (equal gain per unit size)
Allometric symmetry	Benefit increases with benefactor's size, but less than proportionally
Complete asymmetry	The beneficiary plant receives all benefits, with no advantage to the benefactor plants. Bigger takes it all.
Allometric asymmetry	Benefit increases with benefactor's size super-linearly

Table 27: Overview of initialization parameters with defined limits. Parameters functions explained, maximum range (brackets) and grid positioning

Variable	Meaning	Initial value [Range]
Radheightcorrelation (Auxiliary variable) ($Radh_{corr}$)	The height of an individual tree is calculated based on the ratio of height to width and can be chosen by the modeller. Factor 2: An individual with a 1.5 m radius now has a height of 3 m.	[1,3]
Threshold-of-death (%death)	If the tree growth rate (gr) falls below this value, it has a stochastic chance to die.	[0, 0.5]
Abiotic-stress	Individual agents energy intake restriction, limits growth performance	[0, 1]
existingtreeline	Places an existing treeline ecotone into the environment	< 200 m elevation
existingtussock	Places an existing vegetation belt above treeline	400 to 500 m elevation

6. Input data

The monthly temperature variation is based on real life climate data derived from weather stations around the world. The modeller can use information from their respective sites and make global comparisons.

7. Submodels

The submodels provide a detailed overview how growth, competition and sensed temperature are calculated and processed within the agent-sets. A baseline for all submodel calculations is the elevation temperature value derived from the grid cells the agent is growing on.

Agent sensed temperature calculations (Treetempupdate)

Updates the temperature sensed by the tree for the next timestep. The model takes the mean temperature of the respective month derived from the provided climatic table and the temperature assigned to the patch the agent is located on. The temperature sensed by the individual tree is the sum of both values. This temperature can be modified due to sheltering (see below).

T_{Tree} = air-temperature-mean + elevationtemp

Calculating the number of neighbouring trees (count-trees-in-radius)

Counts total number of trees a trees zone of influence (see below) is overlapping with, in a radius of my current height expanded by 80%.

Treesinradius = Count trees in radius (treeheight * 1.8)

Calculate average tree height of neighbouring agents (Thresholdemergingvegetation, (%emerge))

Calculates the average tree height (treeheightlocal) the agent needs to exceed in order to be classified as an emergent tree which will change its assigned competition mode Once a tree is classified as emergent, it does not receive a temperature increase from shelter anymore. The threshold value is calculated for each individual and is based on the average height of the surrounding trees in each radius. The temperature benefit for trees classified as sheltered gets incorporated during resource allocation calculations.

Threshold height is the average height of trees in a radius (current tree height * 1.8 patch lengths)

$$\%\text{emerge} = \frac{\sum H_{Tree} \times 1.8}{n\ of\ Treesinradius}$$

Calculate tree growth (Growth)

Calculates growth rate (*gr*), while accounting for abiotic stress level and adds result to the current biomass (*B*) of the tree. Tree temperature is divided by a tested scaling factor to limit the effect on growth performance.

$$gr = \frac{T_{Tree}}{8} \times a \times Ae \times \left(1 - \frac{(\frac{B}{Bmax})^{1/4}}{\left(1 - \frac{abiotic\ stress}{1}\right) \times fc}\right) \times (1 - \frac{abiotic\ stress}{1})$$

with…

fc Index for competition $fc = \frac{\text{n of shared patches}}{n\ of\ total\ patches}$

Calculate allocated resources based on direct neighbour interaction (Competitionsmall/-big)

Calculates the assigned competition index (*fc*), based on the selected competition (Table 26, for calc. see below) for trees which are below the threshold value (%emerge). Trees below have an additional increase in temperature by 3 °C [T_{Tree}]. For the remaining taller agents, a different competition mode may be selected. The competition index (*fc*) is calculated without a temperature increase.

Assign new height values to agents (Updatetreeheight)

Incorporates monthly growth into current tree height once the allocated resources have been calculated and plant growth has been performed.

B_{old} + gr = $B_{updated}$

Remove dead agents (Remove_dead_plant)

If the growth rate (*gr*) is 0 kill the agent and remove it.

If the growth rate (*gr*) is small ($gr <= B^{3/4} \times$ %death) kill the plant and remove it.

Plotting

Visualizes number of agents based on their location in the patch context. The patches are divided in 6 elevation zones over 100 units of elevation along the Y Ordinate. The number of agents is updated every month.

Generate new agents (Sproutall)

With a defined chance [sprout-probability] let new trees with initial parameters (Table 25) spawn on the map at a random location with the same base parameters used in the initialization process.

if (random-float 1 < sprout-probability) [sprout 1]

Competition mode working principle

We distinguish between five different modes for resource-mediated competition ranging from complete asymmetry (bigger takes all contested resources) and complete symmetric competition (even allocation of resources in their effective area independent of size). The different competition modes are labelled by the index fc. This in turn modulates the effective area (*Ae*) which can be used by the tree to allocate its resources towards growth.

fc Index for competition $\text{fc} = \frac{\text{n of shared patches}}{n\ of\ total\ patches}$

Ae Effective Area $Ae = B^{3/4} \times fc$

$$fc = \left(A_{no} + \sum_{k=1}^{n_o} \frac{B_i^p}{\sum_{j=1}^{n_j} B_j^p} A_{o,k} \right) / A$$

The index refers to the share of resources available in the area which tree 'i' could allocate to growth after competitive calculations due to overlapping areas.

A_{no} is not overlapping with any neighbours and is allocated full resources of the surrounding.

$A_{o,k}$ describes the shared area, overlapping with n_j different neighbours.

p describes the level of competition with the extremes being complete asymmetry (p = 0) and complete asymmetry (p approaching infinity, Figure 58)

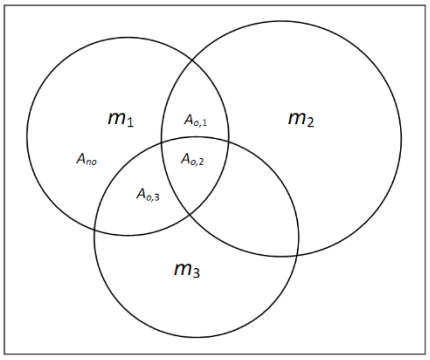

Figure 58: Illustration for calculating shared resources within the ZOI (adapted from Lin. et al., 2012). Three individuals with sizes m_1, m_2 and m_3 are interacting in this example. The area of the first one (m_1) either shows no overlap (A_{no}), overlaps with one neighbor (A_o,1; A_o,3) or both neighbors (A_o,2).

Then the actual area that individual one can allocate resources from $A_{o,1}$ is

$$A_{o,1}\frac{m_1^p}{\sum_{j=1}^{2} m_j^p} = A_{o,1}\frac{m_1^p}{m_1^p + m_2^p}$$

For $A_{o,2}$,

$$A_{o,2}\frac{m_1^p}{\sum_{j=1}^{3} m_j^p} = A_{o,2}\frac{m_1^p}{m_1^p + m_2^p + m_3^p}$$

And for $A_{o,3}$,

$$A_{o,3}\frac{m_1^p}{\sum_{j=1}^{2} m_j^p} = A_{o,3}\frac{m_1^p}{m_1^p + m_3^p}$$

therefore, the competitive index for the individual is the share of all four areas:

$$f_p = (A_{no} + A_{o,1}\frac{m_1^p}{m_1^p + m_2^p} + A_{o,2}\frac{m_1^p}{m_1^p + m_2^p + m_3^p} + A_{o,3}\frac{m_1^p}{m_1^p + m_3^p}) / A$$

C) Photo-oxidative stress mechanisms

Photo-oxidative stress in plants is expressed as the increased presence of reactive oxygen species (ROS) in the cellular membrane (Elstner & Osswald, 1994). These highly reactive compounds are usually a by-product of the photosynthesis or respirational processes within the plant (Foyer & Noctor, 2000). Even though high amounts of ROS can seriously damage the plant and impede germination success. Most plants do always have a relatively low amount of ROS in their cells as a normal byproduct of the above mentioned processes as well as corresponding antioxidative defense systems (Wieser & Tausz, 2007).

The outlining cause for the negative effects associated with photo-oxidative stress is an imbalance of absorbed light energy and the consumption of the reductant NADPH in the photosynthetic apparatus of the chloroplast. ROS are formed when the excess energy is either directly transferred to molecular oxygen or the over-reduction of the electron transport chain causes electrons to "leak" to molecular oxygen rather than NADP (Wieser & Tausz, 2007).

The creation of photo-oxidative stress can be caused by multiple environmental factors. They are usually linked to a combination of high solar radiation and drought conditions or low temperatures, limiting the stomatal CO2 uptake and hence carbon fixation rate or the enzymatic activity within the Calvin cycle. Cold ambient air temperatures do limit plant metabolism but not actively restrict light uptake, resulting in an imbalance of light and dark reaction in the photosynthesis (Wieser & Tausz, 2007).

The occurrence of excess excitation energy as well as presence and formation of ROS are often referred to as inescapable features of the photosynthesis. But so are the counteracting defense mechanisms of the plants as mentioned above. The complex responds can be excreting excess energy as heat, processing them by antioxidative compounds and enzymes within lipid membranes and repair functions.

Photosystem II can very quickly adjust the amount of light processed within the tissues. The drivers of the so called photoinhibition, the reduced efficiency after light exposure, is not fully understood but linked to pH gradients of the thylakoid membrane; longer, adjusted relaxation periods correlated to the xanthophyll cycle (Demmig-Adams, 2005) and longer recovery times resulting from a degradation of photosystem relevant proteins. The first two mechanisms are actively controlled by the plant itself and can be regarded as "photoprotective", however, the latter is a result of limited photosynthetic capacity due to damaged drivers and can therefore be referred to as "photodamage" (Wieser & Tausz, 2007).

The amount of excess excitation energy can be restricted by the mechanisms mentioned above within the plant cells. However, these safety responses are limited in itself, therefore other processes exist which actively reduce ROS: The Mehler-peroxidase reaction and the photorespiration (Asada, 1999; Niyogi, 2000). These alternate pathways enable scavenging of ROS within the glutathione-ascorbate-cycle (Mehler-Peroxidase) or via catalase contained specialized peroxisomes (Photorespiration).

Concentration of carotenoids and tocopherols within the thylakoid membrane also play an important role in regulating the amount of ROS within the plant tissues. The latter is abundant in green plant tissues and works as a powerful antioxidant as well as a protectant for plant membranes by scavenging lipid peroxides (Munné-Bosch & Alegre, 2002).

α-Tocopherol is regenerated by water-soluble ascorbate and therefore represents a bridge element between lipid and water based defense mechanisms of the plant (Wieser & Tausz, 2007). Ascorbic acid is abundant in most plant cells and plays an important role in scavenging ROS by serving as a substrate in the enzymatic degradation of H_2O_2, in the conversion of xanthophyll cycle and the regeneration of tocopherol (Smirnoff, 2000). By oxidation with ROS and regeneration by reduced glutathione in an enzymatic cycle (Foyer & Noctor, 2000). The interplay between ascorbic acid and the glutathione redox system is a requirement for the maintenance of ascorbate redox state (Grill et al., 2001)

Concentration of ascorbate within the plant tissues play high regulatory factors in metabolism and gene expression within the plant organism. Complete deficiency in ascorbate synthesized within parts of the plant system has been linked to increased lethality at the seedling stage (Dowdle et al., 2007). Cytosolic ascorbate peroxidase constitutes a key determinant of programmed cell death (Vacca et al., 2007). Glutathione has an important role as functioning as a regulatory redox buffer within the system. It is considered to be a key determinant of cell death and dormancy (Kranner et al., 2006) and interacts on a threshold-trigger based signal for programmed cell death and growth control (Foyer & Noctor, 2011). Above that, very high glutathione concentrations induced by overexpression of glutathione synthesis enzymes have shown, that high levels of glutathione within the cell are not sufficient enough in itself to trigger plant cell death and even can be tolerated by plants (Liedschulte et al., 2010). Hence, ascorbate and glutathione concentrations, whether mediated by ROS or other factors play an absolutely essential role in triggering and regulating communication cascades

that govern e.g. cell death, growth inhibition and excessive photooxidative stress (Foyer & Noctor, 2011).

Investigations into plant chlorophyll fluorescence are a powerful, non-invasive tool to derive quantitative information about the status of the leaves' photosystem II (Genty et al., 1989) without changing the ambient environmental conditions. In the following I briefly explain the theory behind the mechanisms behind chlorophyll fluorescence measurements and why they became an important tool to derive leaf tissue performance information non-destructively.

It is important to note that over-excitation of photosystem II due to high amounts of solar radiation occurs on a regular basis in plants (Demmig-Adams & Adams, 2006). Naturally the plant possesses pathways to de-excite activated chlorophyll molecules to prevent the formation of reactive oxygen species. In these mechanisms the excess energy gets stepwise passed on from the activated chlorophylls. We distinguish between three different pathways, all serving the same purpose:

Photochemical quenching (qP) is the enhanced re-oxidation of electron acceptors subsequent to PSII, essentially the photochemical light utilization. The other two pathways are part of a non-photochemical quenching component (NPQ, qN,) where the de-excitation is expressed as a spike in heat dissipation or by re-emittance of light called fluorescence. These 3 pathways are mediated by competitive interactions based on the generated yield, which in term means the magnitude and variation in these regulative pathways is strongly correlated. Hence changes in fluorescence will give an indirect info about shifts in photochemistry and thermal dissipation (Krause & Weis, 1991; Schreiber, 2004)

Due to a linear relationship between NPQ and the amount of xanthophyll-cycle pigments antheraxanthin and zeaxanthin at open reaction centres, the degree of heat dissipation can be derived by its correlation to the effective quantum yield of PSII at open reaction centres (Björkman & Demmig-Adams, 1995). The xanthophyll cycle and consequently the abundance of its respective molecules dictates the plants immediate response to the incoming light, with zeaxanthin being major player in the de-excitation of activated singlet chlorophyll (Jahns & Holzwarth, 2012).

Despite the relatively small portion of energy being emitted by the chlorophyll fluorescence pathway (3 - 4 %), the so-called saturation pulse method has proven to be a

reliable indicator for the assessment of general PSII health (Björkman & Demmig-Adams, 1995). In fact, optimal quantum yield for PSII calculated with previously dark-adapted leaves shows a remarkable consistency among many C_3 plants 0.832 ± 0.0004 (Björkman & Demmig, 1987). Assuming a light energy capture mechanism where translation and transfer of energy into the electron transport chain is perfect, the optimal quantum yield would equal 1. However, due to inefficiencies in the light energy transfer from the harvesting antennas towards the reaction centres the optimal quantum yield is reduced to 80% efficiency (Adams et al., 1990). This is the optimal state commonly experienced in pre-dawn conditions. In the early morning, once leaf tissues receive the first sunrays and the plant is experiencing photoinhibition, the generated ΦPSII decreases until a delicate balance between internal repair mechanism and experienced photodamage is achieved. Measuring PSII indirectly is therefore an ideal tool to provide a deep performance profile how the seedlings cope with extended periods of radiation exposure rather than just a momentary snapshot.

If incomplete utilization of the absorbed solar radiation occurs and the photo-protective mechanisms are not able to cope with that excess amount of energy in time, then reactive oxygen species start to form resulting in photo-oxidative stress. The de-excitation process is tightly coupled to the xanthophyll cycle. For instance, in periods of extended environmental stress the inflexible zeaxanthin mediated thermal energy dissipation can be temporarily limited (Demmig-Adams & Adams, 2006). Under high levels of radiation, the carotenoid Violaxanthin is converted over Antheraxanthin into Zeaxanthin in a process called de-epoxidation. This process is a rapid response and the molecular layout can change via minutes (Demmig-Adams & Adams, 1996). Recent knowledge supports the idea that Zeaxanthin is involved in the deactivation of excited singled oxygen and hence in the non-photochemical quenching component (Jahns & Holzwarth, 2012).

Under low light conditions epoxidation, the regeneration process from Zeaxanthin into Violaxanthin, occurs. This process takes minutes to hours and may even be further delayed by other stress factors (Demmig-Adams & Adams, 1996). Since Zeaxanthins is likely a key-component in the de-excitation process and the recycling process is oftentimes delayed, the abundance of the carotenoid can be seen as a stress-memory of recent periods of photoinhibition (Demmig-Adams & Adams, 1996). The kinetics of the xanthophyll cycle can be very dynamic, but in periods of rapid or extended stress exposure the Zeaxanthin pool can be exhausted, leading to a further decrease of the efficiency of the de-excitation process,

ultimately leading to photo-damage and a decreased in photosynthetic yield detected by the Mini-PAM fluorometer.

During colder periods in winter there is evidence that plants actively downregulate foliar carotenoid concentration to optimise their response to lower levels of solar radiation. Consequently, plants commonly show reduced NPQ capacity and are less prepared for a high fluctuation of light during winter. The quantum yield of PSII has been shown to become downregulated to approximately 40% during winter for *Yucca glauca* and remained constantly low throughout the day whereas in summer the photosynthetic yield generated typically shows a midday dip corresponding to the peak light intensity at noon (III Adams et al., 1995). The timing and extent of down regulated ΦPSII during the colder periods, particularly for more susceptive evergreen species is a field which deserves more attention. Zarter has provided valuable insights into the outlining mechanisms in his studies with Pine species and evergreen ground-cover bearberry *Arctostaphylos uva-ursi* in Colorado's high-altitude environments. Photosynthetically winter-active species reveal a Zeaxanthin retention, a decrease in oxygen evolution capacity and light-harvesting pigments which ultimately correlate with a depression in ΦPSII efficiency until the early spring (Zarter et al., 2006a,b,c). Sustained down-regulation of PSII performance is a particularly evident photoprotection mechanisms in extreme environments (Demmig-Adams & Adams, 2006) and the environmental factors triggering it are believed to be coupled to air & soil temperatures and moisture availability (Strand et al., 2002; Zarter et al., 2006c).

These insights gain further support when looking at relatives among the Nothofagaceae in Latin America. *Nothofagus dombeyi* and *Nothofagus nitidia* in Southern Chile and Argentina (Reyes-Díaz et al., 2005). Where *N. dombeyi* reveals a larger distribution range due to high daytime irradiance and night-time freezing temperature tolerance. However, both species revealed to be specifically susceptible to freezing in spring and summer but not during other seasons. This tendency was especially evident when comparing both species' performance during the seedling stage, where *N. nitidas* susceptibility to frost damage was significantly higher. It was summarized that this might be the potential reasons for *N. nitidia* limited distribution range compared to *N. dombeyi* (Reyes-Díaz et al., 2005).